Understanding soil water repellency under native vegetation in Australia: an empirical and molecular dynamics approach

This thesis is presented for the degree of

Doctor of Philosophy

in the

School of Veterinary and Life Sciences,
Murdoch University, Australia

2017

S. M. Mijan Uddin, BSc (Hons), MSc (Forestry), MSc (Environmental Science)

DECLARATION

I declare that this thesis is my own account of my research and contains as its main content work which has not previously been submitted for a degree at any tertiary education institution.

S. M. Mijan Uddin   Date: 02/10/2017

Abstract

Soil water repellency (SWR) is a major land management issue across southern Australia and inhibits the infiltration of water into soil with effects on the germination of crops and pastures and run-off in agricultural and forested land. SWR is a natural phenomenon and generally occurs in the surface layers of sandy soils where hydrophobic materials mostly of plant origin occur as particulate organic matter and as waxy coatings on soil particles. Although its incidence and severity have been anecdotally related to the previous native vegetation little is known about the specific organic compounds that may derive from this vegetation. Previous studies have concentrated on characterizing the contribution of soil organic matter, and this and the fact that soils are complex mixtures of a broad range of organic components may have obscured the contribution of a small concentration of compounds from the native species to SWR. Moreover, the precise distribution of these compounds (e.g., as coatings or in interstices between soil particles) and their contribution to SWR has not been quantified.

Although analysis of soil solvent extracts can identify the relative amounts of individual compounds, it is often difficult to determine the relative importance of all components in inducing SWR. It is even harder to determine synergistic effects from combinations of components. Experimental studies provide a broad understanding of the bulk effects of hydrophobic molecular coatings but do not provide a molecular level understanding of the coating structure or of its kinetic and/or thermodynamic stability. The molecular arrangement of those organic compounds on the soil particles have been shown to have implications for both the incidence and dynamics of SWR. Thus the present study

employed a range of approches to understand SWR in native vegetation: i) quantifying the contribution of canopy derived exudates from native tree species to SWR, ii) discerning the contribution of organic matter in different pools (e.g., on particle surfaces, as interstitial matter) to SWR and iii) examining the physical interaction of the organic molecules (without and with water) with soil mineral surfaces.

Canopy derived exudates were captured using an improvised technique, and organic compounds were extracted using nonpolar and polar solvents. In order to discern the contribution of different carbon pools to SWR, soils were separated into mineral and interstitial matter. Soils were extracted using a sonication technique. Individual and combinations of compounds were loaded onto acid washed sand (AWS) using a rotary evaporator. This experimental loading and measurement was complemented by fully atomistic molecular dynamics simulations with Materials Studio v 7.0 to understand the physical interaction of the molecules with mineral surfaces.

A range of different organic compounds that are widely reported in the incidence of SWR were detected in the canopy derived exudates and soil extracts. They were mostly long-chain alkanes, fatty acids, phytols, phytanols, amides, aldehydes, ketones, terpenoids, steroids, and some complex ring containing structures. Though there was similarity in the composition of both the nonpolar and polar compounds of exudates of *Banksia menziesii*, *Eucalyptus marginata*, *Xanthorrhoea preissii* and *Allocasuarina fraseriana*, the concentration level of the chemical species was found to be significantly different. The concentrations were found to differ over the sampling period. For example, docosanoic acid was found to be dominant in the summer for *B. menziesii* and *X. preissii*. while in *E. marginata* and *A. fraseriana* it was evident in the winter.

Moreover, the concentration level of the chemical species derived from the soil extracts were also found to be significantly different between the species of *A. fraseriana, E. marginata*, *E. wandoo* and *B. menziesii*. Notably, the main difference between *A. fraseriana* and the other three species (*E. marginata*, *E. wandoo* and *B. menziesii*) was the presence of long chain fatty acids and fatty alcohols. The concentration of the compounds was even different in different soil components (e.g., minerals and interstitial matter) of the soil matrix. For example, the concentration level of the individual compound derived from the bulk soil was similar to the total concentration level of the compound derived from both the coarse mineral materials and interstitial matters.

The molecular level arrangement of various hydrophobic molecules with mineral surfaces also varied. For example, amphiphilic molecules at surface density of 2.3 molecs/nm^2 were found in a tilted arrangement on kaolinite while on quartz surfaces they formed layered arrangements. However, silica did not favor a certain order of arrangement of the molecules due to its amorphous surface. The surface characteristics and polarity (abundance of OH groups) of the substrate (kaolinite > silica) were found to significantly modify the organo-mineral interactions. Different biogenic volatile organic compounds (BVOCs) or terpenoids commonly observed in vegetation smoke or forest fire, were not found to induce SWR. Moreover, the long chain amphiphilic molecules exhibited a balance between molecule-molecule and molecule-surface interactions on the quartz surface that supported surface adhesion, which in turn led to the formation of a hydrophobic layer. Furthermore, soil moisture or the addition of water molecules was found to significantly modify the conformation of molecules at the organo-mineral interfaces. For example, the polar kaolinite and silica surfaces were found to easily wet-up and reorganization of amphiphilic molecules on the surfaces took

place following aquation. The stronger interaction between water and organic molecules can thus be inversely correlated to organo-mineral interaction on soil particles.

Dedication

This noble work has been dedicated to the memory of my beloved father, Mr. M. Ashab Uddin Ansary, who left us forever just a couple of months before submission of my thesis.

Acknowledgements

Publications from this thesis

Uddin, S. M. Mijan., Daniel, N.R.R., Harper, R.J., Henry, D.J. 2017. Why do biogenic volatile organic compounds (BVOCs) derived from vegetation fire not induce soil water repellency? *Biogeochemistry* (2017) 134:147-161 (Chapter 4)

Conference papers:

Uddin, S. M. Mijan., Harper, R.J., Henry, D.J. 2017. Contribution of plant species and carbon pools to the severity of soil water repellency. Soil Science Society of America, Phoenix, United States, 6-9 November 2016: "Resilience Emerging from Scarcity and Abundance".

Henry, D.J.,**Uddin, S. M. Mijan**., Daniel, N.R.R., Harper, R.J., 2017. Effects of temperature on soil water repellence : Molecular dynamics and experiment. RACI 2017 Centenary Congress, 23-28 July 2017, Melbourne, Australia

Daniel, N.R.R., **Uddin, S. M. Mijan**., Harper, R.J., Henry, D.J. 2017. Fatty acid assembly on soil surfaces: soil water repellency study. RACI 2017 Centenary Congress, 23-28 July 2017, Melbourne, Australia

Uddin, S. M. Mijan., Harper, R.J., Henry, D.J. 2015. Soil water repellency under native vegetation of south-western Australia. Soil Science Society of Australia, Mandurah, WA. 6-7September 2015.

Report/Seminar

Henry, D.J., Daniel, N.R.R.,**Uddin, S. M. Mijan,** Harper, R.J., 2016. Soil Water Repellence: A Molecular Dynamics Study of Amphiphilic Compounds on Mineral Surfaces. RACI Physical Chemistry 2016 (PC16), Christchurch, New Zealand.

Acronyms and terms

AF   Appendix Figure

AT   Appendix Table

AWS   Acid Washed Sand

BVOC   Biogenic Volatile Organic Compound

DCM   Dichloromethane

DI   Deionized

E_{int} Interaction Energy

EDS   Energy Dispersive X-Ray Spectroscopy

EI   Electron Impact

GC-MS   Gas Chromatography-Mass Spectrometry

IOM   Interstitial Organic Matter

IM   Interstitial Materials

IPA   Isopropanol/Ammonia

KL   Kaolinite

MD   Molecular Dynamics

MED   Molarity of Ethanol Droplet test

NVT	N- constant number of atoms; V-volume; T-temperature
PA	Palmitic acid
RB	Round Bottom
RDF	Radial Distribution Function
SEM	Scanning Electron Microscopy
SWG	Standard Wire Gauge
SWR	Soil Water Repellency
TC	Total Carbon
TOC	Total Organic Carbon
TGA	Thermogravimetric Analysis
THF	Tetrahydrofuran
UHP	Ultra High Purity
vdW	van der Waals
WDPT	Water Drop Penetration Time

Table of Contents

Figures

xxii

xxvii

Tables

1 General Introduction

1.1 Preamble

Soil water repellency (SWR) is a major land management issue across a large tract of land in southern Australia and other parts of the world (Doerr et al., 2000). It occurs extensively on natural and agricultural lands with a severe impact on crop yields, surface and subsurface hydrology and can lead to the contamination of groundwater through finger flow (Blackwell, 2000; Doerr et al., 2000; Ma'Shum et al., 1988; Prats et al., 2012). Hydrophobicity induced finger flow can make a difference in soil moisture of up to 28% (vol.) between closely spaced samples (at 20 cm interval in depth) in water repellent sandy soils (Dekker & Ritsema, 1996). Such differences in soil moisture not only result in the disruption in soil water balance, but can also affect vegetation growth through limited nutrient mobilization.

The incidence and severity of SWR on farmland has been related to the previous native vegetation (King, 1981; McGhie & Posner, 1980). Native plants of Australia most commonly linked with SWR are evergreen trees and particularly eucalypts with a significant amount of resins, waxes or exudates (Doerr et al., 2000). Widespread SWR under *Eucalyptus globulus* and *Pinus pinaster* plantations in Portugal has been reported, particularly in dry summer conditions (Ferreira et al., 2000). Although the incidence and severity of SWR has been anecdotally related to the previous native vegetation of Australia, little is known about the specific organic compounds that may derive from this vegetation. This thesis sets out to explore these relationships.

Most of south-western Australia is underlain by the geological shield of the deeply weathered Yilgarn Craton and thus soils have inherently low fertility (Hopper, 2009; Moore, 2001). Along with poor fertility, soils in south-western Australia are often, but not exclusively, characterized by sand dominated surfaces and poor water holding capacity (McArthur, 1991). As the region has been extensively developed for agriculture, many of the reports on SWR come from agricultural areas.

SWR is generally associated with coarse-textured sandy soils because of their smaller surface area per unit volume in comparison with their finer counterparts (DeBano, 1981; Harper et al., 2000). It has also been related to the composition of soil organic compounds and molecular level interactions with soil particles (Doerr et al., 2000). However, the degree of repellence is often reported to vary with land use or vegetation types (Zavala et al., 2009b). Moreover, SWR is found with a marked seasonal pattern under the eucalypt stands of north-central Portugal (Keizer et al., 2008). Wetting and drying processes of the soil can considerably affect the severity of SWR (Jordán et al., 2008; Zavala et al., 2009b).

The specific role played by native plant species of Australia in inducing SWR has been partly established in Mediterranean soils, which form under a Mediterranean type climate characterized by warm to hot, dry summers and mild to cool, wet winters. For example, it has been closely associated with soils under natural vegetation of *Eucalyptus* and *Banksia* of south-western Australia (Garkaklis et al., 1998; Harper et al., 2000; Moore & Blackwell, 2004; Walden et al., 2015). Plant litter, resinous plant tissues and the activity of plant roots have all been considered as a source of hydrophobic substances to the soil (Doerr et al., 1998; Jordán et al., 2008; Mataix-Solera & Doerr, 2004; McFarlane et al., 1992; McGhie & Posner, 1981; McKissock et al., 1998; Ritsema & Dekker, 1994).

1.2   Methods of measurement

The severity and persistence of SWR can be measured through various methods including tension infiltrometer discs (Hunter et al., 2011), measurement of contact angles (Lamparter et al., 2010), low field nuclear magnetic resonance (Manalo et al., 2003), water drop penetration times (Dekker et al., 2009; Doerr et al., 1998) and molarity of ethanol droplet (King, 1981; Moody & Schlossberg, 2010). The most widely used methods for SWR measurement are i) water drop penetration time (WDPT) and ii) molarity ethanol droplet (MED) (Roy & McGill, 2002).

1.2.1   Water drop penetration time (WDPT) test

The persistence of SWR is measured using the WDPT test (Letey, 1969; Woudt, 1959). The WDPT test is carried out by placing a water drop on a smoothed soil surface and counting the time needed for its complete penetration. The test is used as it directly measures the absorption of water droplets on the soil surface. For example, in hydrophilic soil a water droplet would penetrate a porous material instantly, whereas in hydrophobic soil it remains on the surface until it is evaporated (Tschapek, 1984). The surface tension of the soil surface demonstrates the penetration time of the water droplet. For example, if the surface tension of the soil surface is higher than that of the water droplet (72.75 dynes cm^{-1} at 24 °C), it penetrates instantly. The Water drop penetration time (WDPT) varies from a few seconds to many hours and thus evaporation of droplets may influence results for very hydrophobic soil samples. A number of WDPT classes are recorded according to the following classification (Table 1.1) categories (Dekker et al., 2009; Stoof et al., 2011).

3

Table 1.1   A classification of SWR using the water drop penetration test (WDPT).

WDPT Class	Infiltration time	Description
0	<5 s	Not water repellent, wettable
1	5-60 s	Slightly water repellent
2	60-600 s	Strongly water repellent
3	600-3600 s	Severely water repellent
4	1-3 h	Extremely water repellent
5	3-6 h	Extremely water repellent
6	>6 h	Extremely water repellent

1.2.2   *Molarity of Ethanol Droplet (MED) test*

The MED test implies the known surface tensions of standardized solutions of ethanol in water. The degree or severity of SWR of soil surfaces can be assessed using the molarity of ethanol droplet (MED) test (King, 1981; Watson & Letey, 1970). The wettability of hydrophobic soil surfaces is increased by lowering the surface tension of the liquid, with different mixtures of water and ethanol. Small concentration increments are used to precisely estimate the surface tension at the time of initial contact. The higher the concentration of ethanol in a liquid droplet, the lower the liquid surface tension and thus the higher degree of SWR (Dekker & Ritsema, 1994). A detailed description of this test is given in the later Chapters and particularly in Chapter 4 (Uddin et al., 2017).

1.3   *Relationship of SWR to soil properties*

SWR is generally associated with coarse-textured, or sandy, soils because of their smaller surface area per unit volume (Giovannini & Lucchesi, 1983; McKissock et al.,

2000; Roberts & Carbon, 1972), but has also been reported on more clayey soils (McGhie & Posner, 1980). For example, a medium grained acid washed sand has a surface area of 102 cm^2 g^{-1} (Mainwaring et al., 2013) whereas, clay can have a surface area as large as 9×10^6 cm^2 g^{-1} (Rowell, 2014). An increased surface area of clay is thought to be effective in ameliorating SWR by masking hydrophobic surfaces in the soil matrix and exposing hydrophilic clay surfaces (Ward & Oades, 1993). In particular, specific minerals or aggregate surfaces have been widely recognized as a crucial factor in the induction of SWR (Doerr et al., 2000). Soil surface area, as measured by clay and silt contents, and the amount of organic carbon accounted for up to 63% of the variation in SWR (Harper et al., 2000) in a review of studies in south-western Australia. Thus, SWR is most likely to develop in soils with less than 10% clay content and in turn additions of clay to soil have been widely reported to reduce SWR (DeBano, 1991; Lichner et al., 2006; McKissock et al., 2000).

The coating of soil particles with organic substances that reduce the affinity for water is considered to be the primary mechanism for the induction of SWR (DeBano et al., 1970; Ma'shum & Farmer, 1985; Ma'Shum et al., 1988). SWR occurs primarily in the surface layers of sandy soils where hydrophobic materials, mostly of plant origin, exist as particulate organic matter and as waxy coatings on soil particles (Franco et al., 2000b). In many regions, trees with glaucous leaves accumulate waxy substances in the surrounding soil (Eglinton et al., 1962). However, the degree of SWR is often reported to vary with land use or vegetation type (de Blas et al., 2010; Zavala et al., 2009b). SWR under both native vegetation and farmland that has been deforested is widely reported in south-western Australia (Harper et al., 2000; McGhie & Posner, 1980; McKissock et al., 2000; Walden et al., 2015).

SWR is observed in long unburned soil and drier parts of different regions such as, Portugal (Leighton-Boyce et al., 2005), Spain (Mataix-Solera & Doerr, 2004), the US Northwest (Doerr et al., 2009), Germany (Greiffenhagen et al., 2006) and Netherlands (Dekker et al., 2000). It is considered to be significantly related to the composition and structural conformation of soil organic matter and it has been reported to have wider environmental implications (Doerr et al., 2000). It is mainly caused by the accumulation of long chain hydrophobic compounds on or between soil particles of the soil matrix. For example, if the pores between non-repellent coarse sand particles are filled with water-repellent matter, water penetration tends to be slow, whereas water-repellent sand with pores plugged with non-repellent fine material would allow water to penetrate the finer matter. Furthermore, the main soil properties that are considered to accelerate SWR include amount and type of organic matter, soil texture, soil water content and type of vegetation. For example, SWR in the surface horizon is found to increase following *Eucalyptus globulus* reforestation in south-western Australia (Walden et al., 2015).

1.4 *Molecular level interactions with soil particles*

The concentration of organic molecules required to produce maximum SWR also depends on their distribution in relation to other soil constituents, and in some cases there may be sufficient materials to allow the formation of multiple layers on soil particles (Mainwaring et al., 2013; McKissock et al., 2003). The precise nature of organo-mineral interfaces can significantly modify the extent of stabilization of organic compounds in soils (Petridis et al., 2013). For example, the presence of surface OH^- groups induces hydrophilicity of silica and kaolinite surfaces and provides a poor substrate for hydrophobic hydrocarbons (Nalaskowski et al., 2003; Tschapek, 1984).

In drier regions, polar ends of amphiphilic compounds associate and interact through hydrogen bonds with the mineral surfaces and non-polar ends oriented outwards, re-establishing SWR. During wetting, the displacement of organic compounds from soil particles can take place with the attraction of the polar ends of these molecules to water, ultimately resulting in a wettable soil (Doerr et al., 2000; McKissock et al., 1998). This suggests that the proposed re-orientation of amphiphilic molecules is not necessarily caused by the drying and wetting processes alone. This is presumably associated with the re-attachment of some organic molecules on soil particles through hydrogen bonding. Besides, SWR at different soil depths is varied following heating that helps organic molecules to form coatings and strong bonding to soil particles. The movement of hydrophobic organic substances downward may occur due to steep temperature gradients during hot summer conditions or vegetation fire (Crockford et al., 1991; DeBano, 2000). The continued heat movement downward through the soil may re-volatilize some of the hydrophobic substances resulting in thickening of the water repellent soil layer or fixing the hydrophobic substances *in situ* (DeBano & Krammes, 1966; Doerr et al., 1996).

The interaction of quartz and different layered silicates with hydrophobic organic molecules is of interest in several biogeochemical contexts. The complex nature of mineral-organic carbon interfaces can significantly influence the extent of stabilization of organic compounds in soils (Petridis et al., 2013). An amount of hydrophobic molecules equivalent to several monolayers may be required to result in a complete cover on a mineral surface (Ma'Shum et al., 1988). For example, 0.35 g of hydrophobic compounds in 1000 g of medium sized sand can induce severe SWR. The limiting area of 4.76 molecules nm^{-2} is attributed for a monolayer, which is observed for condensed films of straight chain fatty acids irrespective of chain length (Shaw & Costello, 1993).

Mainwaring et al. (2013) found that a loading of $0.1\text{-}0.2\times10^{-6}$ mol g^{-1} is required for monolayer coverage with octadecanoic acid. Morphological features (e.g. octahedral, tertrahedral, rhombohedral etc.) of soil particles can influence the arrangement and structure of monolayers (Miller et al., 2007; Tunega et al., 2004). For example, a low surface coverage of 2.35 molecules nm^{-2} of wax molecules was found to adopt a semi-ordered, tilted packing arrangement on the gibbsite like surface of kaolinite whereas on quartz it leads to a two layer arrangement (Walden et al., 2015). This suggests strong hydrogen bonding or van der Waal's dipole-dipole interaction affects in the layering and packing of wax molecules on soil particles (Horne & McIntosh, 2000; Ma'shum & Farmer, 1985; Wu et al., 2013). Teppen et al. (1998) suggested at least three distinct mechanisms coexist for the interaction of organic molecules on clay minerals in the environment: (i) full molecular contact, (ii) through single atom contact and (iii) never contact directly.

1.5   *Relationships of SWR to vegetation*

SWR is an extensively occurring phenomenon on natural and agricultural soils with a severe impact on crop yields, surface and subsurface hydrology and contamination of ground water (Blackwell, 2000; Doerr et al., 2000; Ma'Shum et al., 1988). The occurrence of SWR has been broadly associated with particular vegetation types (King 1981) though the specific contribution of many species to SWR is uncertain.

Leaf and trunk exudates from plant tissues of native species are usually a primary source of waxy compounds into the soil (Ma'Shum et al., 1988). The contribution of wax containing compounds namely, branched and unbranched C_{16} to C_{36} fatty acids and their esters, alkanes, phytanols, phytanes and sterols are reported to lead to the development

of SWR (Doerr et al., 2005; Franco et al., 2000b; Mainwaring et al., 2013; Morley et al., 2005).

Experiments conducted on natural decomposition and incorporation into the soil have been based on laboratory experiments with fresh plant material (McGhie & Posner, 1981; Roberts & Carbon, 1972). Native vegetation most commonly linked with the SWR is considered to be certain evergreen tree types (Doerr et al., 2000). For example trees with a significant amount of resins, waxes or exudates such as eucalypts and pines are widely reported to be implicated, both within natural and exotic environments (Table 1.2). Soils under Mediterranean heathlands are also reported as water repellent or nutrient impoverished (García et al., 2005; Lambers et al., 2010; Martínez-Zavala & Jordán-López, 2009; Mataix-Solera & Doerr, 2004).

1.5.1   *Reports from eucalypt forests*

The existing native forest and greater extent of eucalypt reforestation in south-western Australia and in other Mediterranean countries, and the association of this species with SWR there are growing concerns about the impact on agricultural lands. Anecdotal evidence from many farmers in south-western Australia suggested that farmland that was once covered with eucalypts was likely to develop SWR, with a marked increase in SWR from this reforestation quantified by Walden et al. (2015).

Eucalyptus is a native genus from Australia and comprises about 800 species (Ogunwande et al., 2003). Leaf extracts and exudates from plant tissues of native Eucalyptus are considered as a major source of waxy compounds into the soil (Ma'Shum et al., 1988). For example, Ferreira et al. (2000) observed the widespread existence of SWR under *Eucalyptus globulus* plantation soils in central and north littoral Portugal, particularly in summer dry conditions. Coelho et al. (2005) and Doerr et al. (2006)

observed that eucalypt stands appear to constitute a somewhat unusual case in that they have very high SWR levels in long unburned stands. Crockford et al. (1991) observed the fluctuation of SWR over the wet and dry periods of the year, and correlated SWR with the type of vegetative cover present. This fluctuation over extended periods of time under eucalypts can also be supported from the study conducted by Keizer et al. (2005a) and Leighton-Boyce et al. (2005). Santos et al. (2016) also observed the dynamic nature of SWR under eucalypts and that extreme SWR was found to enhance overland flow generation (Prats et al., 2012). Keizer et al. (2008) measured very strong to extreme severity of SWR under recently burnt eucalypt stands in north-central Portugal.

Table 1.2   Reports of SWR under native vegetation of Australia

Vegetation	Location	Rainfall (mm)[a]	Slope	Soil types/Soil texture	SWR	Source
Ulex europaeus	NW Spain	*1839*	~17°	Sandy loam	***	(Soto & Díaz-Fierros, 1998)
Eucalyptus globulus *Pinus pinaster*	Portugal	1300-1900	20°	Sand and silt	***	(Shakesby et al., 1996)
P. halepensis	E Spain	-	18°	Sandy loam	**	(Andreu et al., 2001)
Eucalyptus spp.	SW Sydney, Australia	900-1000	-	Loamy sands	***	(Shakesby et al., 2003)
Eucalyptus spp.	Canberra, SE Australia	640	>7°	Sandy	***	(Crockford et al., 1991)[b]
Native bush	SW Australia	-	-	Lateritic sand	*** ***	(McKissock et al., 1998)
E. astringens and Trifolium subterraneum Triticum aestivum	Western Australia	-	-	Fired sands	*** *	(McGhie & Posner, 1981)
Eucalyptus spp.	Western Australia	500-600	-	Lateritic sand	***	(Garkaklis et al., 1998)
E. globulus Pasture	Western Australia	574-1417		Lateritic sand	*** **	(Walden et al., 2015)

Medicago sativa *E. marginata*	SW Australia	-	-	Fired sands	***	(Roberts & Carbon, 1972)
E. leptopoda	WA	-	1-2%	Sandy loam	***	(McFarlane et al., 1992)
Eucalyptus spp. *Acacia* spp.	WA	-	-	Sandy loam	*** ** *	(Harper et al., 2000)
Eucalytus, Pinus, *fynbos*	South Africa	1296-2270	-	-	**	(Scott, 1993)

[a] mean annual rainfall is shown in upright font and measured rainfall for monitored period is shown in italics

[b] results obtained from Crockford and Richardson (1998)

*** Strongly repellent; ** repellent; * slightly repellent

1.5.2   Reports from dry land vegetation (with leaf glands)

Vegetation in the flammable ecosystems (Bond & Keeley, 2005) usually contains leaf glands that secrete exudates (Chaves et al., 1997) and accumulate on the soil and thus can be associated with the occurrence of SWR (Franco et al., 2000b). The composition and proportion of humic substances and free particulate SOM are also found to cause SWR that are associated with vegetation type and geological substrate (de Blas et al., 2010). For example, the extracted materials in some Australian hydrophobic soils is reported to restore SWR on acid washed sands at levels comparable to the original soils (Ma'Shum et al., 1988; McGhie & Posner, 1980). SWR is often reported under shrubs ranging from temperate heathland of NE Scotland (Mallik & Rahman, 1985) to semi-dessert chaparral of California (DeBano, 1991). Hansel et al. (2008) reported that biopolyesters from the lipid fractions of *P. taeda* were closely associated with SWR. Researchers from different regions have thus concluded that SWR is associated with a wide variety of vegetation types (Buczko et al., 2002; Cerdà & Doerr, 2007; Dekker & Ritsema, 1996; Doerr et al., 1998; Mataix-Solera et al., 2007; Zavala et al., 2009a) (Table 1.2). Despite this, even in SW Australia there are many other genera apart from the widely reported eucalypts that may have significant implications in affecting SWR (Harper et al., 2000).

1.5.3 Soil organic compounds reported to induce SWR

Hydrophobic compounds derived from soil organic matter and decomposed litter are closely associated with the induction of SWR in unburned soils (Atanassova & Doerr, 2010). The compounds extracted from different soils namely, components of wax containing organic compounds such as, branched and unbranched C_{16}-C_{36} fatty acids and their salts and esters, alkanes, phytanes, phytanols, and sterols are all suggested to cause SWR (Doerr et al., 2005). Besides, hydrophobic compounds of humic origin may contribute to SWR in sandy soils (Roberts & Carbon, 1972). Walden et al. (2015) noted strong variation in SWR in paired samples (eucalypt and pasture) despite similar total soil carbon content, and inferred that SWR is caused by variations in the composition of soil organic matter and suggested that this may be caused very small amounts of these compounds. Additionally, substantial changes in organic compound composition can be associated with heat induced increases in SWR. For example, heating at 300 °C resulted in a sharp absolute decrease of homologous aliphatic series of alkanols and alkanes, a shift of fatty acid signature to members $<C_{20}$ and an increase in total content of aromatic compounds to three Australian eucalypt-forest soils (Atanassova & Doerr, 2011).

Higher plants or native vegetation are considered as major sources of naturally occurring hydrophobic substances such as, n-alkanes, olefines, terpenoids, monoketones, β-diketones and polyesters of hydroxy-fatty acids that gradually accumulate in the soil environment (Horn et al., 1964; Tulloch, 1976). Eucalyptus waxes are very complex and major components of waxy compounds reported are β-dikeotones, hydrocarbons, unhydroxylated esters, free acids, free alcohols, flavone, triterpene γ-lactone acetate, triterpene γ-lactone alcohol, acetate of triterpene acid (Horn et al., 1964). Among them β-dikeotones and unhydroxylated esters are dominant.

14

Compounds of higher molecular weight namely, n-tritriacontan-16,18-dione, n-hentriacontan-14,16-dione and n-nonacosan-12,14-dione are closely associated with the species of *E. globulus*, *E. viminalis*, *E. cineria*, *E. behriana* and *E. pulverulenta* and *E. risdoni* (Pereira et al., 2005). They may also contain flavone and eucalyptin (5-hydroxy-4',7-dimethoxy-6,8-dimethylflavone) (Horn et al., 1964).

Moreover, eucalypt oils contain mainly monoterpenoids and small amounts of sesquiterpenoids whereas cineole (1,8-cineole) has been reported as a dominant component (Barton et al., 1989). Besides, α-pinene, γ-terpinene and p-cymene are also present as volatile fractions under most of the eucalypt species. However, both cineole and α-pinene are highly toxic terpenes and found to adsorb to colloidal soil particles of the litter and bare zones. These adsorbed terpenes are toxic to germinating seeds and seedlings and may affect the whole vegetation community. Moreover, water-soluble toxins found in the litter can inhibit herb growth due to allelopathic interferences. This interference is usually optimal on soils that are poorly drained, poorly aerated, shallow, and high in colloidal content and permit toxin concentrations to reach physiologically significant proportions. However, the release of phytotoxins and their activity depends on whether they are free or bound, and on their solubility.

1.6 Relationships of SWR to fire

Vegetation fires affect soil physicochemical properties including altering the total soil carbon content and the severity of SWR (DeBano & Rice, 1973; Heath et al., 2015; Sheridan et al., 2007). Higher temperatures during vegetation fire can also significantly modify physicochemical interactions between organic molecules and mineral surfaces (Uddin et al., 2017). Furthermore, it can alter the dynamics of SWR depending on fire temperature, duration and vegetation types (Doerr et al., 2004; Heath et al., 2015). For

example, moderate temperature burns (soil temperature of 175–300°C) on soils that already exhibit non-wetting characteristics, generally leads to an increase in SWR (Dlapa et al., 2008). The elimination of SWR in eucalypt stands during vegetation fire is also observed at a depth of 3-5 cm (Doerr et al., 2006; Scott, 1993). Nevertheless, SWR onset temperatures vary with post fire equilibration times, heating duration, physical and chemical attributes of soil particles (Arcenegui et al., 2007; Doerr et al., 2004). The variations in the severity of SWR can thus change soil hydrological properties (e.g., overland flow generation, infiltration), germination and the recruitment of seedlings (Coelho et al., 2005; Prats et al., 2012) and make the whole ecosystem non-resilient (Doerr et al., 2004).

Moreover, smoke derived biogenic volatile organic compounds (BVOCs) are known to collect in soil during vegetation fire and in fact are essential for the germination of some Australian native species as a seed pre-treatment (Dixon et al., 1995; Tieu et al., 1999). As a flammable compound, BVOCs again influence the intrinsic flammability of vegetation (Owens et al., 1998) and thus affect soil physicochemical properties. For example, when water repellent soil is exposed to fire, organic particles are heated to the extent that they coat and/or chemically bond to soil mineral particles (DeBano, 2000). The downward movement of heat through the soil even after vegetation fire can further intensify the hydrophobic layers (Savage, 1974).

1.7 *Ecological implications*

SWR is closely associated with climatic drought events (Muhr & Borken, 2009; Sowerby et al., 2008) and prolonged summer droughts are reported to reduce cumulative carbon mineralization through microbial activities (Borken & Matzner, 2009; Goebel et al., 2011). The lower soil moisture level hampers SOM mineralization

and develops semi-permanent SWR in certain soil domains during prolonged drought periods that revealed decreasing CO efflux rates with increasing SWR (Goebel et al., 2005). Low water availability and high temperature are considered to significantly retard plant growth and biomass production by leaf carbon fixation (Chaves & Oliveira, 2004). The subsequent soil environment is observed to favour a drought tolerant vegetation community in the Mediterranean region (Doerr et al., 2000). Furthermore, intensive drought is found to influence soil microbial community structure resulting in a gradual reduction of wax degrading actinobacterial communities (Roper, 2004) and increased fungal proliferation (Spohn & Rillig, 2012).

1.7.1   Germination

SWR is considered a major soil management issue to tens of millions of hectares of arable land in south-western Australia (Van Gool et al., 2008). Surface layers of sandy soils are usually affected by the accumulation of plant derived hydrophobic materials that account for coatings on them (Franco et al., 1995; Ma'Shum et al., 1988). Due to uneven wetting SWR affects seed germination, recruitment and crop production in vast areas of agricultural lands (Dekker & Ritsema, 2000; Ritsema & Dekker, 1994). Besides, preferential flow paths in water repellent soils are also reported to contaminate the groundwater through leaching of agro-chemicals (Bond & Harris, 1964; King, 1981). For example, reduced soil moisture is found to effectively reduce the growth of canola (*Brassica napus*) in Australia (King et al., 2006) and the average annual loss of lupin and wheat production due to SWR is about 30% and 10% respectively (Ghadim, 2000).

1.7.2   Water distribution

Soil moisture or water is an important means to accomplish all the physiological processes of plants and a major carrier to transporting metabolites. Water readily dissolves large quantities of ion and polar organic metabolites like sugars, amino acids and proteins that are critical to metabolism and life (Lambers et al., 2008). Water distribution on the surface soil is highly affected by the type of soil and vegetation it supports. For example, soils under eucalypt forest are reported to exhibit strong SWR even without any intervention of fire (Bond & Harris, 1964; Crockford et al., 1991; Doerr et al., 2006). Moreover, hydraulic lift of deep rooted plants may increase the chances of survival of neighbouring shallow rooted plants (Pang et al., 2013) and nutrient uptake (Prieto et al., 2012). Eucalypt forests in south-eastern Australia are subjected to catastrophic post-fire soil loss on slopes even with moderate rainfall (Shakesby et al., 2007). Loose and sandy water repellent soils are susceptible to rain splash detachment (Terry & Shakesby, 1993) and higher velocity overland flow to stream channels (Scott & Van Wyk, 1990). This overland flow generation can move spores of soil borne diseases and disrupt the vegetation type and soil properties in adjacent areas (Scott, 1993). Moreover, when the water repellent surface layer causes rainwater to pond, Hortonian (infiltration-excess) overland flow occurs (Doerr et al., 2000). For example, water repellent soil under an Australian eucalypt forest is reported to result in a threefold increase in overland flow following a drought period (Burch et al., 1989; Nyman et al., 2015).

During drier periods of the year soil macro-pores and dead roots are reported to play a vital role in soil moisture dynamics through preferential flow (Zhou et al., 2002). However, water repellent soils ultimately conserve soil moisture below the surface and preserve water against evaporation by a 'dry mulch' effect of the surface layers (Moore

& Blackwell, 2004; Yang et al., 1996). This may be an important mechanism for plant survival in water-limited regions.

1.7.3   Nutrient uptake

Soils are the product of different activities of plants that supply organic matter and restrict specific soil types (Lambers et al., 2009). Besides, soil properties also depend on the origin of the parent material. For example, the extreme infertility of most kwongan soils of Australia arises primarily due to the low nutrient content (e.g. P) of the parent material and to their old age and strong degree of weathering. (McArthur, 1991). In drier parts of the Mediterranean region plants are very sensitive to the nutrient deficiency after water and temperature (Lambers et al., 2009). This nutrient deficiency is more pronounced when soil particles are coated with hydrophobic organic matter and devoid of soil moisture (Blackwell, 2000).

1.7.4   Soil microbiology

Lower soil moisture directly affects communities of soil microorganisms that have interactions in the formation and modification of soil (Pate & Verboom, 2009). The ground vegetation and leaf litter help to increase water holding capacity of soil and encourage soil microbial proliferation (Roper, 2005). However, scarcity of soil moisture in water repellent soil greatly affects microbial community structure in mineralizing organic contents into nutrients and making them available into plant roots (Summers, 1987). Moreover, soil moisture deficiency reduces diffusion pathways for enzymes and solutes and leads to decreased accessibility of SOM to plant root systems (Goebel et al., 2011). For example, drought is reported to reduce plant productivity through decreasing the amount of available nitrogen (Borken & Matzner, 2009). Thus, available plant habitats are exploited by drought tolerant sclerophyll vegetation that compete for

available nutrients (Jon et al., 2012). However, organic compounds derived from decomposed eucalypts are reported to suppress soil microorganisms due to their biocidal properties (Senthil Nathan, 2007). For example, eucalyptus extracts have been found to inhibit the growth of gram-positive bacteria (Takahashi et al., 2004) and soils under *Pinus* directly affect bacterial growth and promote fungal intensification (Lebron et al., 2012).

Bioremediation of SWR thorough wax degrading bacteria has been suggested as a potential mechanism for its amelioration. Actinobacteria are reported to utilize waxes and break down the hydrophobic compounds (Roper, 2004). However, fungi are known to produce amphiphilic proteins called 'hydrophobins' that associate to form water repellent membranes to the soil particles (Spohn & Rillig, 2012). Paradoxically, basidiomycete fungi are reported to alter SWR of contaminated soil (Hallett et al., 2006).

1.8   *Conclusions*

Small amounts of soil moisture in the surface layers of water repellent soils limits the productivity of many natural vegetation ecosystems particularly in the Mediterranean region. How SWR affects vegetation growth and survival is likely to be closely associated with the availability of soil moisture in shallow horizons of the soil profile, root distribution and maximum root depth. Hydraulic lift may be of considerable benefit to shallow rooted plants in drier regions. However, water-wicking habits of trees or other deep rooted species can protect the top soil from severe desiccation and help to accomplish ecological processes such as, recruitment, nutrient cycling, organic matter dynamics and soil microbiology (Ehrenfeld, 2003).

1.9   Thesis research questions

A range of issues relating to SWR, on native and agricultural lands in south-western Australia, remain unexplained and these form the research questions in this thesis.

a)   Do exudates from different native species cause different levels of water repellence?

Walden et al. (2015) found that SWR varied between paired sites with pasture and Eucalypt plantations. These sites had identical soil characteristics including organic carbon content and particle size analysis.

Although SWR has been attributed to organic compounds from plants including cuticular waxes (Horn et al., 1964), alkanes (Ma'Shum et al., 1988), alkanols (Hansel et al., 2008), fatty acids and their salts and esters (Franco et al., 2000b; Ma'Shum et al., 1988), lipids and humic acids (de Blas et al., 2010; Roberts & Carbon, 1972) and phytanes, phytanols and sterols, the pathways into the soil are not well understood.

Plant leaves and their extracellular glands are also reported to secrete waxy compounds to the soil (Barton et al., 1989; Eglinton et al., 1962). These waxy compounds suggest small amounts of hydrophobic compounds from trees or canopy derived exudates can contribute to the incidence of SWR and these are examined in Chapter 2.

b)   Is there a difference in the nature of the carbon pools that contribute to SWR?

Different soil components and structures, including micro and macro aggregates of organic material, are distributed within sandy soils (Bisdom et al., 1993). Thus, organic material can both occur as coatings of grains and also as interstitial matter.

Analyses of repellent soils, however, is often undertaken on whole soil samples, with no discrimination of the contribution of different soil carbon pools. Chemical extraction of whole soil samples usually results in the total concentration of compounds instead of the concentration of different soil constituents. Identifying the contribution of organic matter composition from different soil pools (e.g., on particle surfaces, as interstitial matter, etc.) to SWR under different species is necessary to explain variations between species and this is explored in Chapter 3.

c)   Do biogenic volatile organic compounds (BVOCs) derived from vegetation fire induce SWR?

Smoke-derived compounds are known to collect in soil and in fact, are essential for the germination of some Australian native species as a seed pre-treatment (Dixon et al., 1995; Tieu et al., 1999). The heat during a fire is also widely reported to redistribute and alter the concentration of hydrophobic substances in the soil, and this is a major issue following forest fires in many areas (DeBano, 1981; Pierson et al., 2008; Sheridan et al., 2007). However, it is unknown whether fire-induced increases in SWR are due to the addition of smoke-related compounds to the ground or simply due to heat-induced rearrangement of the amphiphilic molecules (e.g., phytanols and fatty acids) already present in the soil. Therefore, a combined experimental and theoretical study (Chapter 4) will identify the role that smoke-related compounds may play in SWR.

d)   How do the physicochemical interactions of long-chain organic molecules with soil particles affect the severity of SWR?

Understanding both the chemical nature of the hydrophobic coating and its physical interaction with the soil particles is crucial to insights into SWR. Soils are complex mixtures containing a broad range of organic components. Although analysis of soil

solvent extracts can identify the relative amounts of individual compounds, it is often difficult to determine the relative importance of all components. It is even harder to determine synergistic effects from combinations of compounds. Experimental studies through different loading ranges on soil particles (e.g., acid washed sand (AWS)) (Mainwaring et al., 2013) provide a broad understanding of the bulk effects of hydrophobic molecular coatings but generally do not provide molecular level understanding of the coating structure or of its kinetic and/or thermodynamic stability on different soils. This can be achieved through developing the modeling framework for both the mineral surface and molecules, and molecular dynamics simulations can explore the nature of the organo-mineral interactions (Chapter 5). Moreover, the presence of water with the hydrophobic molecules on the soils may alter the coating structure or of its kinetic and/or thermodynamic stability, which is a typical scenario in a hydrophobic environment. Thus, understanding of the molecular level interactions with the simulated soil particles both in absence and/or presence of water may contribute to unlocking this land management issue (Chapter 6).

This thesis investigates the above questions (Table 1.3), resulting in a number of chapters, which form the majority of the thesis (Figure 1.1). Lastly, Chapter 7 provides the broader context of understanding SWR under native vegetation from the perspective of experimental and molecular dynamics outcomes.

Table 1.3   Research questions, associated research objectives, and thesis chapters.

Research question	Research objective	Thesis chapter
Do exudates from different native species cause different levels of water repellence?	1) To examine the contribution of canopy derived exudates of native vegetation to SWR.	Chapter 2: Contribution of canopy derived exudates under native vegetation of south-western Western Australia in the incidence of SWR
Is there any difference in the carbon pools that contribute to SWR?	2) To investigate the contribution of different soil carbon pools in inducing SWR.	Chapter 3: Contribution of organic carbon pools in inducing SWR
Do biogenic volatile organic compounds (BVOCs) derived from vegetation fire induce SWR?	3) To investigate the effect of BVOCs on SWR and compare them with long-chain aliphatic compounds.	Chapter 4: Role of BVOCs derived from vegetation fire in inducing SWR
How does the physicochemical interaction of long-chain organic molecules with soil particles affect the severity of SWR?	4) To determine the effects of different loading ranges of long-chain hydrophobic compounds and their mixtures in inducing SWR.	Chapter 5: Physicochemical interaction of long-chain hydrophobic compounds in the soil environment - an experimental and molecular dynamics approach.
	5) To examine molecular level interaction both in the absence or presence of water on various simulated soils.	Chapter 6: Physicochemical interaction of long- chain hydrophobic compounds in aqueous soil environment

```
┌─────────────────────────────────────────────────────────────┐
│                         Chapter 1                           │
│                    General introduction                     │
└─────────────────────────────────────────────────────────────┘
                              ⇩
┌─────────────────────────────────────────────────────────────┐
│                         Chapter 2                           │
│          Contribution of canopy derived exudates to SWR     │
└─────────────────────────────────────────────────────────────┘
                              ⇩
┌─────────────────────────────────────────────────────────────┐
│                         Chapter 3                           │
│            Contribution of organic carbon pools to SWR      │
└─────────────────────────────────────────────────────────────┘
                              ⇩
┌─────────────────────────────────────────────────────────────┐
│                         Chapter 4                           │
│                 Role of BVOCs in inducing SWR               │
└─────────────────────────────────────────────────────────────┘
                              ⇩
┌─────────────────────────────────────────────────────────────┐
│              Chapter 5            Chapter 6                  │
│                                                             │
│            Physicochemical interactions to SWR              │
└─────────────────────────────────────────────────────────────┘
                              ⇩
┌─────────────────────────────────────────────────────────────┐
│                         Chapter 7                           │
│                    General discussion                       │
└─────────────────────────────────────────────────────────────┘
```
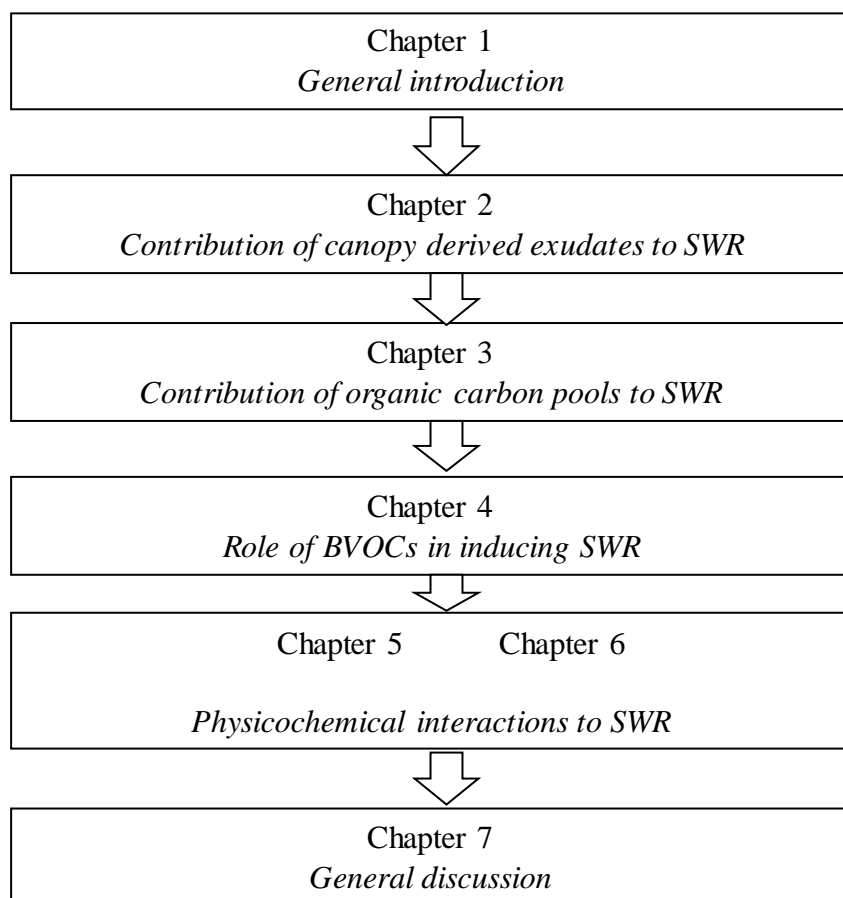
Figure 1.1   Roadmap of thesis chapters and interrelationships of research topics.

2 Contribution of canopy derived exudates under native vegetation of south-western Australia in the incidence of soil water repellency (SWR)

2.1 *Introduction*

Organic molecular assemblages are closely associated with inducing water repellency (SWR) in sandy soils (Jiménez-Morillo et al., 2016). Trees with glaucous leaves accumulate waxy substances in the surrounding soil, and SWR is attributed to these hydrophobic organic compounds coating soil particles or collecting in the soil environment. For example, despite there being no differences in soil characteristics including soil organic carbon content or particle size, between a pair of adjacent pasture and *E. globulus* plantation soils in the south-west of Western Australia, there was a difference in SWR suggesting a small contribution from the trees (Walden et al., 2015). The sites in the study were defined as a pair based on soil morphology and total nitrogen (N) and phosphorus (P) concentrations.

Composition of soil organic matter and molecular level interactions with soil particles can substantially modify the severity of SWR (Doerr et al., 2000). Organic carbon pools consisting of hydrophobic and amphiphilic molecules affect wetting properties through forming a film on mineral surfaces (Ellerbrock et al., 2005). However, the degree of SWR is often reported to vary with the type of vegetation (Zavala et al., 2009b). For example, SWR is found with a clear temporal pattern under planted eucalypt stands in north-central Portugal (Keizer et al., 2008). The general role played by native plant species in inducing SWR has been well established in Mediterranean soils that suggest, there may be a top-down contribution from the canopy of those species. For example,

SWR is reported in the soils under natural vegetation of *Eucalyptus* and *Banksia* of south-western Australia (Garkaklis et al., 1998; Harper et al., 2000; Moore & Blackwell, 2004; Scott, 1993; Walden et al., 2015); indigenous forest and pine, grassland and fynbos scrub of South Africa; pines and heathlands of Spain (García et al., 2005; Martínez-Zavala & Jordán-López, 2009; Mataix-Solera & Doerr, 2004; Scott, 1993). Plant derived materials from the vegetation are considered as a source of hydrophobic substances to the soil (Doerr et al., 1998; Jordán et al., 2008; Mataix-Solera & Doerr, 2004; McGhie & Posner, 1981; McKissock et al., 1998; Ritsema & Dekker, 1994). However, SWR can also be associated with fungal growth and soil microbes (Doerr et al., 2000). Moreover, variation in soil moisture in the soil can considerably affect the severity of SWR that is evident in Mediterranean shrublands or heathlands (Jordán et al., 2008; Zavala et al., 2009b). For example, it has been reported that the wetting and drying process forces the molecules to adopt a position in which their polar ends are attached to the mineral surface and the non-polar ends are oriented outwards (Doerr et al., 2000).

The effect of SWR on natural and agricultural soils is not only in crop production, also affects other environmental parameters namely, surface and subsurface hydrology and contamination of ground water (Blackwell, 2000; Doerr et al., 2000; Ma'Shum et al., 1988; Prats et al., 2012). Evergreen trees with a significant amount of resins, waxes or exudates, both within the indigenous and exotic environment can be substantially associated with SWR (Doerr et al., 2000). Due to the greater extent of *Eucalyptus* reforestation in Australia and other Mediterranean countries, and the association of this species with SWR, there are growing concerns about the residual impact of the species (Walden et al., 2015). Anecdotal evidence from many farmers in south-western Australia suggested that most farmland that was once covered with eucalypts are most

likely to develop SWR (Murty et al., 2002). The exudates from plant tissues of native species are usually a primary source of waxy compounds in the soil (Ma'Shum et al., 1988). The widespread existence of SWR in the *E. globulus* and *P. pinaster* plantation forest soils in Portugal is reported particularly in dry summer conditions (Ferreira et al., 2000). However, difference in the severity of SWR is evident over extended periods of the year including recently burned and long unburned stands (Coelho et al., 2005; Crockford et al., 1991; Doerr & Shakesby, 2006; Keizer et al., 2005a; Keizer et al., 2005b; Leighton-Boyce et al., 2005; Santos et al., 2016).

Although the eucalypts and other native species that occupy significant portions of Australia's native and plantation forest estate are widely accepted to cause SWR (King, 1981; McGhie & Posner, 1980), little is known about the specific organic compounds derived from the native species that are responsible. Furthermore, nothing is known about how this may relate to the patterns of SWR in croplands, where it is a major problem.

It is therefore postulated that SWR is the result of complex organo-mineral interactions where the molecular composition of these fractions could play a substantial role. Because SWR is a soil property, previous studies have concentrated on characterizing the contribution of soil organic matter. Soil, however, is a complex material, and this is likely to have obscured the top-down contribution of small concentrations of compounds of the native species to SWR. Thus, this chapter investigates canopy derived exudates from native tree species and their association with the induction of SWR.

2.2 Materials and methods

2.2.1 Selection of the site

A pilot experiment was set up at Murdoch University campus under a small stand of *Eucalyptus globulus* to assess a number of exudates over a given period and develop a collection technique. This involved capturing exudates from the canopies using mounted glass beakers and comparing the amount of exudates with the control.
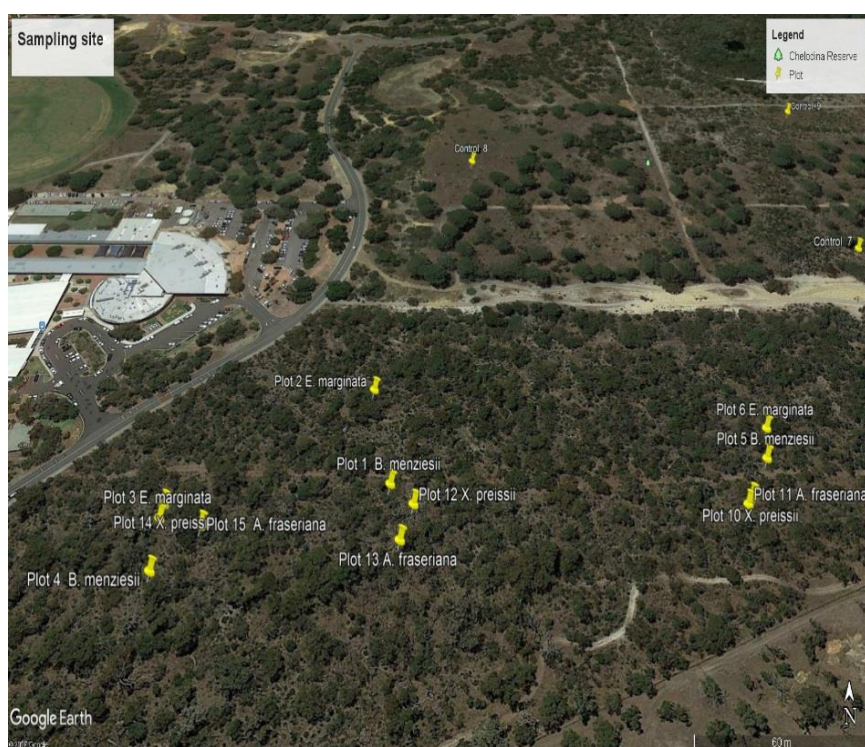
Figure 2.1   Sampling plots of the investigated species and the control site at Murdoch University campus to capture exudates.

Based on the pilot experiment, an experimental field site was selected in the Chelodina Reserve of Murdoch University (Figure 2.1). To set up the experiment the site was divided into three blocks, and in each block, four plots were selected such that each plot contained a specific species. The species selected were *Eucalyptus marginata*, *Banksia menziesii*, *Xanthorrhoea preissii* and *Allocasuarina fraseriana* (Figure 2.2).

29
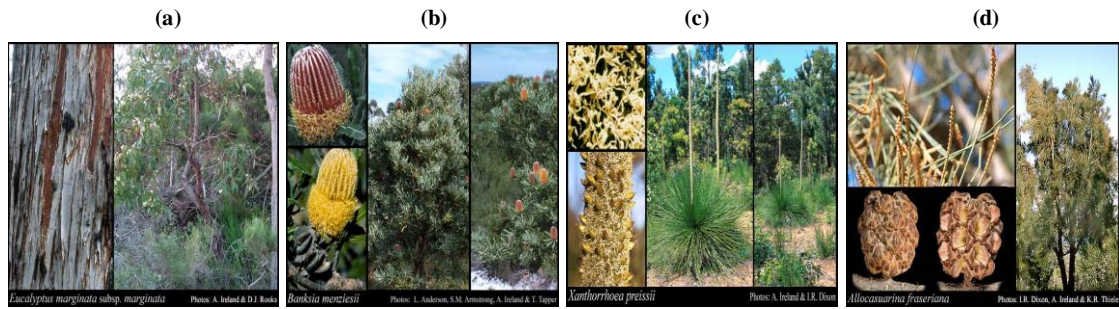
Figure 2.2   Images of the species (a) *Eucalyptus marginata*, (b) *Banksia menziesii*, (c) *Xanthorrhoea preissii* and (d) *Allocasuarina fraseriana*, Source: WA FloraBase.

Control plots were selected just outside the boundary of the reserve in cleared land in the spaces free from canopies. The species were selected as they were from quite different families. Nonetheless, they are all well represented in the flora of the Perth region.

2.2.2   Capturing canopy exudates

Exudates from the different trees were collected in beakers set up under the canopy of the individual species. Three glass beakers (600 ml) were set up under the canopy of each species, with sampling occurring over a series of 2 month periods/ intervals from June 2015. The samples were collected at eight weekly (56 days) intervals. The time for capturing exudates was designated as June-July (J-J), Aug-Sep (A-S); Oct-Nov (O-N), Dec-Jan (D-J), Feb-Mar (F-M) and Apr-May (A-M) of 2015-2016.

Beakers were fixed around a metre above the forest floor and fastened against an iron stake using cable ties (Figure 2.3a,b). The beakers were replaced every eight weeks, with extra-caution to avoid spillage during winter because that is when rainfall is more likely.

Figure 2.3　　Capturing exudate under the canopies in the mounted glass beakers and aluminum mesh fitted on top of the beakers.

In addition, a 600 ml beaker was covered with a fine mesh on the top in such a way that it can hold a 100g of acid washed sand (AWS) of 300-350m diameter range that was collected from Perth Scientific Pty Ltd (Figure 2.3c, d), to test for induction of SWR over the sampling periods. Commercial grade mesh (size 120; SWG (standard wire

gauge) 44; nominal aperture 0.132mm; wire diameter 0.08mm; approx. % open area 39) made of aluminum was used to release the soaked water during winter.

2.2.3 Soil sample collection

Surface soil samples were collected from under the canopy of the individual species (e.g. 3 replicates with 4 treatments or species). Samples were taken randomly to depths of 0-5 cm (topsoil) during winter and autumn 2016. Three replications of each sample were made and these samples were bulked for analysis. Collected soils were air dried, and coarse particles and debris were removed by a very gentle sieving using a 2-mm sieve.

2.2.4 Soil extraction

30 g of dried and sieved soil (AWS) was placed in a 100 ml Schott bottle, and 50 ml of IPA/NH_3 (70:30) solvent added and shaken gently for about a minute. The mixture was then placed into a sonication bath at a set temperature of 10°C. The sample was sonicated for 30 minutes and left for 24 hours; the mixture was then sonicated again for another 30 minutes (McCready et al., 2000). 30 ml of the supernatant aliquot was placed into a tarred glass jar. The lid of the jar was left open for 24 hours under a fume hood to evaporate excessive NH_3, and in case of excess ammonia, a solvent trap was used. The concentrated sample was then dried using a Labconco Centri Vap Concentrator System 78100 series at 1725 rpm rotation and 45^0 C temperatures for about 12 hours. The weight of solid material was determined by subtracting the weight of empty vial from that of the vial plus dried material. The weight (g/kg) of the solid material was converted to g/m^2 considering bulk density of 1.5t/m^3.

A DCM/MeOH (2:1) solution was prepared and spiked with dodecane at a compatible concentration with the analyte to make a concentration of approximately 10,000-50,000

ppm. An aliquot of the redissolved sample with the solution was transferred from the glass jar into a GC-MS vial filtered through a Pasteur pipette using $MgSO_4$ as a drying agent.

2.2.5   Extraction of canopy exudates

The captured exudate from the three blocks was analyzed separately and it was filtered through a glass sintered funnel and then the nonpolar and polar components extracted using $CHCl_3$ (nonpolar) and MeOH (polar) solvents, respectively. The exudate in the walls of the beakers was dissolved with the solvents using a Pasteur pipette. The filtered nonpolar fraction was dried in a rotary evaporator, and the solvent was removed under reduced pressure at 45°C temperature. The polar fraction was dried through Labconco Centri Vap Concentrator System 78100 series at 1725 rpm rotation and 45^0 C temperature for about 20 hours. The dried polar fraction was then redissolved in IPA/NH_3 to extract the analyte as efficiently as possible and filtered using glass wool. This redissolved analyte was then dried again in a Labconco Centri Vap Concentrator at the same rotation speed and temperature for around eight hours. After removing the solvents, a tiny amount of solid mass was detected in both the polar and nonpolar fractions. The weight (µg) of the solid was converted to g/m^2 considering surface area of the capturing beakers.

An internal standard for nonpolar extracts was prepared from $CHCl_3$ spiked with dodecane while, MeOH spiked with 1-chorododecane was used for polar extracts at a compatible concentration with the analyte, to make a concentration of approximately 10,000-50,000 ppm. This was calculated using the formula given hereunder,

$$\text{Concentration of analyte (ppm)} = \frac{\text{mass of dried analyte (g)} \times 10^6}{\text{Volume of solvent (ml)}}$$

A vortex mixer was used to mix the internal standard with the analyte thoroughly. An aliquot of the redissolved sample was transferred from the centrifugal vial into a GC-MS vial filtered through a Pasteur pipette using $MgSO_4$ as a drying agent.

2.2.6 Water repellency (SWR) measurement

The severity of SWR of the collected soil sample was assessed using the molarity of ethanol droplet (MED) test (King, 1981) both under standard laboratory conditions and after drying the soil at 105°C and allowing to cool to room temperature. 105°C was chosen as it gives the potential SWR of the sample (Dekker et al., 2001). To measure at standard lab temperature, each sample (~ 20 g) was placed in a petri dish (50 ×10 mm) and put into an oven at 40°C for 48 hours. Another batch of the sample (~ 20g) was put into the oven at 105°C for 24 hours to measure its potential SWR. MED tests were conducted on each of the samples following desiccation for around 4 hours to reduce the effect of humidity.

The surface of the samples was leveled by gentle tapping on the bench, and in some cases, a light pressure was applied by a flat bottom beaker to make the surface smooth and uniform.

The wettability of a hydrophobic soil surface is usually increased by lowering the surface tension of the liquid, using a range of different concentrations of ethanol solution. A stock solution of 4 M ethanol was prepared, and a number of 50 ml solutions were made at concentrations between 0 and 4 M with increments of 0.2 M. A droplet (50-µl) of the prepared ethanol solutions were then applied onto the surface of the samples from 5-mm height, starting from the lowest ethanol concentration. The time required for each drop to penetrate the surface was recorded. The minimum concentration for which the infiltration time was <10 s was considered as the MED value for that sample (King, 1981). On each sample, the test was repeated at least three

times, and the mean value was taken for the analysis. Repellency of the samples was then classified according to a scheme similar to that proposed by Mao et al. (2015), where a MED of < 0.5 M corresponded to wettable and a MED > 3.5 M to extreme repellency.

2.2.7 GC-MS analysis

All GC–MS analyses were conducted on a Shimadzu 2010GC–MS instrument using a splitless injector and a 30 m × 0.25 mm BPX5 fused silica column with 5% phenyl polysilphenylene-siloxane. The temperature program was 60^0C held for 1 min then ramp to 100^0C at 30^0C per minute, stay for 1 min then ramp to 300^0C at 4^0C per minute, then hold for a further 5 minutes with UHP helium as the carrier gas. The GC was connected to a Shimadzu QP2010S single quadrupole mass spectrometer.

The mass spectrometer was operated in electron impact (EI) mode. The ion source was maintained at 200^0C and the electron energy at 70 eV. Identification of compounds was based on interpretation of the mass spectroscopy fragmentation, comparison with spectra published in the literature and those available in the computerized database of the instrument, and relative GC-retention times.
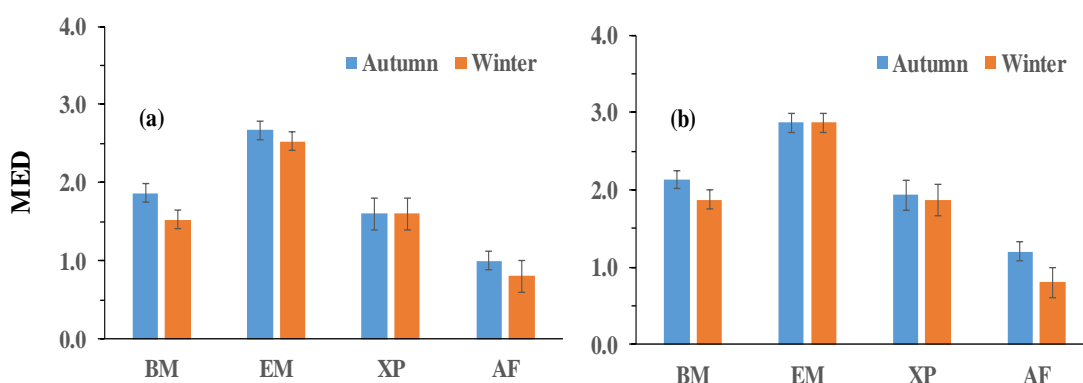
Figure 2.4   MED of soil collected from different species following drying at a) 24°C and b) 105°C.

2.3   Results

2.3.1   Water repellency (SWR) of the collected soil sample

The severity of SWR of the collected soil samples were measured with molarity of ethanol droplet test (MED). It was found with 1.87, 2.67, 1.6, and 1.0 M at 24°C during autumn while the values were slightly lower in the winter as evident to 1.53, 2.53, 1.6, and 0.8 for the species of *Banksia menziesii* (BM), *Eucalyptus marginata* (EM), *Xanthorrhoea preissii* (XP) and *Allocasuarina fraseriana* (AF), respectively (Figure 2.4 a). The potential SWR after heating at 105°C was found slightly higher than the values observed at 24°C (Figure 2.4 b). Notably, the SWR was found to be insignificant on the collected acid washed sand (AWS), put on the aluminum meshes that were fixed in top of the beakers under the canopy at the experimental site. The wettability of AWS indicates that the time of sampling interval (8 weeks) may not enough to coat the soil particles with the exudates and thus to induce SWR.

2.3.2   Composition of soil organic pools

The material extracted from soil using isopropanol and aqueous ammonia (7.3 v/v) as solvent, revealed the amount of the material was higher in the autumn compared to that of the winter. The autumn and winter were only chosen in order to get a significant temporal variation in the severity of soil water repellency. The amount of the material was found around 410, 480, 394, and 370 g/m^2 in the autumn while the extracts were 275, 160, 195, and 188 g/m^2 in the winter for the species of BM, EM, XP, and AF, respectively (Figure 2.5). The decreasing amount of extracts in winter suggest that the downward movement of rainfall through trunk and canopy of the plants may affect the top soil carbon pools.
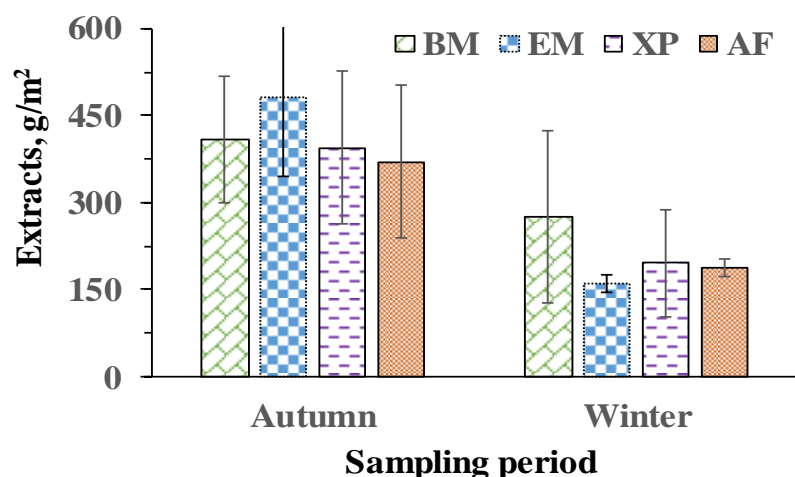
Figure 2.5   Amount of material extracted by sonication using isopropanol and aqueous ammonia (7.3 v/v) from different species.

As described in the methods section, both polar and nonpolar compounds were characterised from soil extracts using DCM/MeOH (2:1). A range of polar and nonpolar compounds were found in the soil samples examined (Appendix Table 2.1). From the characterized compounds, abundant hydrophobic and amphiphilic compounds were identified based on the concentration of individual compounds usually observed in the hydrophobic soil (Figure 2.6).

The individual concentration of the abundant compounds was compared between the seasons, considering a base concentration of $\geq$ 0.0375 g/m^2 (0.001g/kg). This concentration was used due to the reported individual compound (octadecanoic acid) concentration level in hydrophobic soil of 0.003 g/kg (0.01×10^{-6} mol g^{-1}) by GC-MS (Mainwaring et al., 2013). Considering the concentration level in hydrophobic soil, loading experiments with the pure compounds will be presented in Chapter 4 and 5.
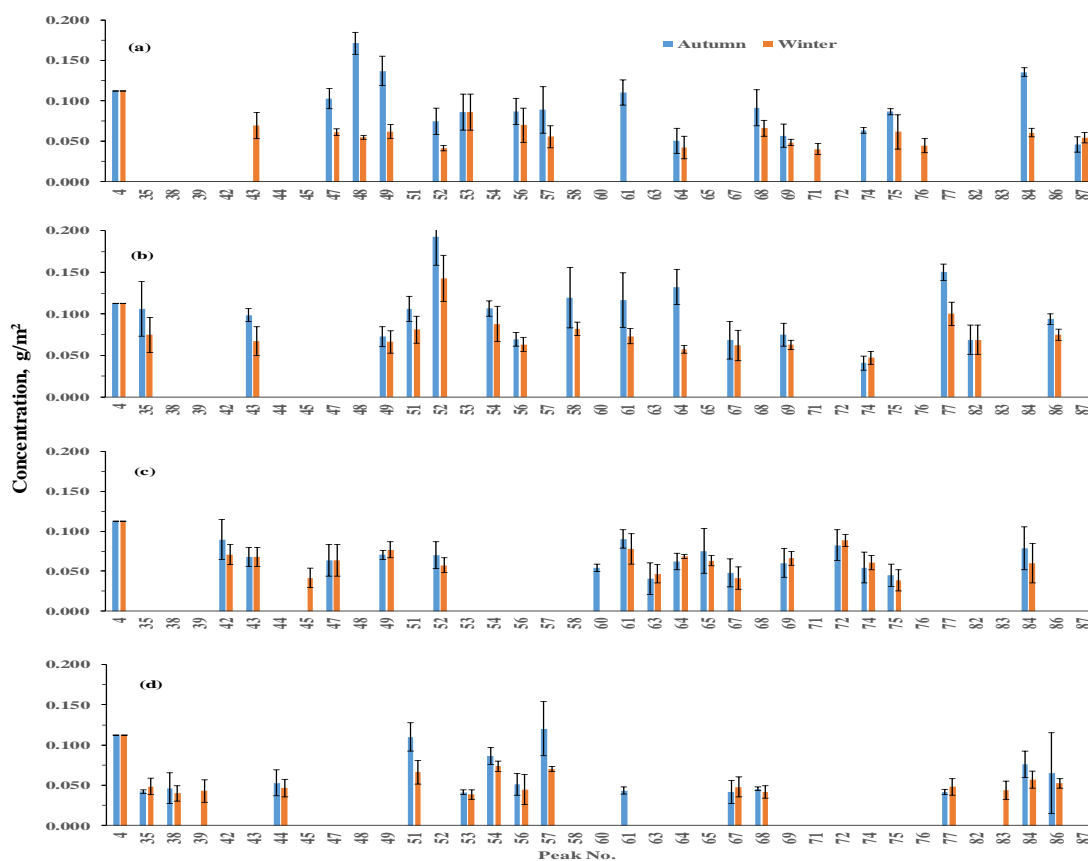
Figure 2.6   Composition of abundant soil organic pools (a) *Banksia menziesii*, (b) *Eucalyptus marginata*, (c) *Xanthorrhoea preissii*, and (d) *Allocasuarina fraseriana*. Peak 4 was an internal standard of dodecane. The error bars shown are based on standard deviation.

A range of even numbered and long chained alkanes (C_{24} – C_{44}) were detected in the soil samples. C_{24} and C_{28} alkanes were detected under all the investigated species but C_{24} alkane (peak 44) was only abundant in AF while C_{28} alkane (peak 56) in BM, EM and AF (AT 2.1 of the Appendix). C_{34} (peak 64) were observed in all the soil samples except that of AF (Figure 2.6 d). C_{44} alkanes (peak 75) were only observed in BM and XP. Moreover, C_{36} alkane (peak 67) was not detected in the soil samples collected from BM (Figure 2.6 a).

Long-chain fatty acids ($C_8 - C_{26}$) were found in the soil extracts whereas, $\geq C_{16}$ carbon acids are already reported to have a significant effect in inducing SWR (Uddin et al., 2017). C_{20} and C_{24} fatty acids were only observed in the samples collected from the soil under BM and XP, respectively (Figure 2.6 a, c). Moreover, C_{22} and C_{26} acids were evident in all the species except AF. The abundance of long chain fatty acids suggests they can significantly influence the incidence of SWR in the soil as it was evident substantially less SWR under AF compared to other three species.

A number of long-chain fatty alcohols ($C_{10} - C_{27}$) with almost similar chain lengths to fatty acids were detected. For example, C_{16} and C_{22} - alcohols (peak 43 and 49) were observed in all the samples except those collected from the soil under AF (Figure 2.6 d). However, fatty alcohol with 27 carbon atoms (peak 60) was only observed in XP. Phytols with 10 and 20 carbon atoms (C_{10} and C_{20}) (peak 13 and 37) were found in all the species except AF and XP, respectively. Moreover, both of C_{10} and C_{20} –phytols (peak 10 and 27) were only detected in AF (AT 2.1 of the Appendix).

Furthermore, a range of esters ($C_8 - C_{35}$) and amides ($C_6 - C_{22}$) were identified. C_{23} and C_{35} esters were evident in the entire samples under all the species examined. Esters with 19 and 21 carbon atoms (peak 45 and 52) were found in all the samples except collected from the soil under AF (Figure 2.6 d). Moreover, isopropyl myristate (peak 35) and hexadecanoic acid, methyl ester (peak 42) was not identified in XP and BM, respectively. However, C_{28} ester (peak 77) was found under all the species except XP (AT 2.1 of the Appendix). Notably, an acetate ester (peak 63) was found abundant only in XP (Figure 2.6 c), though it was observed in BM.

Amides were observed with the concentration level noted in the previous section in soil samples under different species. Among those compounds, tetradecanamide (peak 47)

and hexadecanamide (peak 51) were abundant in (BM and XP) and, (EM and AF) respectively. Besides, octadecanamide (peak 54) was abundant in EM and AF (Figure 2.6 b, d) while 13-docosenamide (peak 68) was dominant in both BM and AF (Figure 2.6 a, d).

In addition to the organic compounds mentioned above, a range of other compounds under different classes were observed including alkenes, aldehydes, ketones, glycerides, pyranones, terpenoids, steroids, and some ring containing compounds (AT 2.1 of the Appendix).

The nature of compounds identified indicates the need for further investigation of the molecular level interactions of individual and combination of the pure compounds on different mineral surfaces to understand their potential in coating the soil particles. This will be presented in Chapters 4, 5 and 6.

Table 2.1   Compounds selected from abundant soil carbon pools based on an a priori likelihood of inducing SWR.

Class	Peak #	Formula	Assignment	Concentration (g/m^2)			
				BM	EM	XP	AF
Fatty acids	48	$C_{20}H_{40}O_2$	Eicosanoic acid	0.171	0.000	0.000	0.000
	69	$C_{22}H_{44}O_2$	Docosanoic acid	0.057	0.075	0.060	0.000
	72	$C_{24}H_{48}O_2$	Tetracosanoic acid	0.000	0.000	0.083	0.000
	74	$C_{26}H_{52}O_2$	Hexacosanoic acid	0.063	0.041	0.055	0.000
Alcoh-ols	43	$C_{16}H_{34}O$	1-Hexadecanol	0.000	0.099	0.068	0.000
	49	$C_{22}H_{46}O$	1-Docosanol	0.137	0.073	0.070	0.000
	60	$C_{27}H_{56}O$	1-Heptacosanol	0.000	0.000	0.054	0.000
Amides	54	$C_{18}H_{37}NO$	Octadecanamide	0.000	0.107	0.000	0.086
Alkane	44	$C_{24}H_{50}$	Tetracosane	0.000	0.000	0.000	0.053
	56	$C_{28}H_{58}$	Octacosane	0.087	0.070	0.000	0.051
	64	$C_{34}H_{70}$	Tertratriacontane	0.050	0.132	0.062	0.000
	67	$C_{36}H_{74}$	Hexatriacontane	0.000	0.068	0.048	0.042
	75	$C_{44}H_{90}$	Tetratetracontane	0.087	0.000	0.045	0.000

Considering the reported loading experiments with the pure compounds that have a prori likelihood of inducing SWR, several compounds were selected (Table 2.1) from the abundant soil carbon pools for further analysis particularly, comparison with the exudates and their seasonal fluctuations in terms of individual concentration. For example, straight chain fatty acids and alcohols of $\geq C_{16}$ chain length were considered because, palmitic acid (C_{16}) and 1-hexadecanol (C_{16}) was found to significantly induce SWR at normal temperature (24°C) in both experimental and molecular dynamics study (Uddin et al., 2017). Moreover, straight chain amides of $\geq C_{18}$ were also chosen as they are reported to induce SWR onto acid washed sand (AWS) (Mainwaring et al., 2013). Alkanes of $\geq C_{18}$ chain length were selected for comparison as they are found with enhancing effect in inducing SWR in a binary mixture with the amphiphilic compounds of octadecanoic acid (Mainwaring et al., 2013). Moreover, the effect of alkane in combination with palmitic acid 1-docosanol will be examined in Chapter 5.

2.3.3 Seasonal fluctuation of soil organic pools

It was revealed that most of the compounds detected were present in both in samples collected in autumn and winter but with different concentrations. As noted in the previous section, a range of compounds was observed above the mentioned concentration level (0.0375 g/m^2) for the entire soil samples. Long-chain alkanes in *Banksia menziesii* (BM) were found slightly higher concentration in the autumn compared with winter (Figure 2.7 a). Moreover, tetracosane was only observed in *Allocasuarina fraseriana* (AF) with almost similar concentrations both in the summer and winter (Figure 2.7d). Importantly, tetratriacontane in *Xanthorrhoea preissii* (XP) (Figure 2.7c) and hexatriacontane in AF were found with slightly higher concentrations in the winter. The somewhat higher concentration in winter suggests that the canopy structure and phenological traits of the vegetation can substantially modify the chemical properties of soil. Notably, the alkanes in AF were mostly of shorter chain length and with lower concentration (~0.05 g/m^2) compared with the other species. The dominant (~0.15 g/m^2) alkane (e.g., tretratriacontane) was observed in autumn under EM (Figure 2.7 b). The higher concentration of the compounds in EM suggest that compounds concentration can substantially modify the SWR.
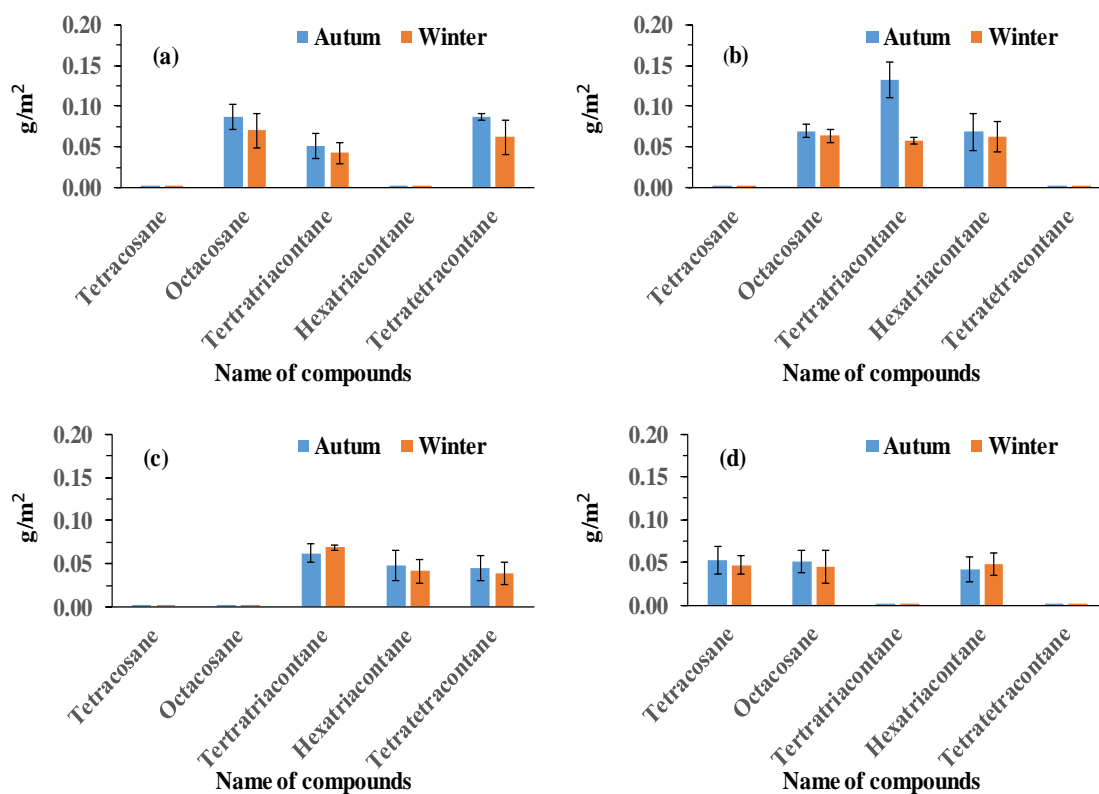
Figure 2.7   Soil nonpolar compounds from (a) *Banksia menziesii*, (b) *Eucalyptus marginata*, (c) *Xanthorrhoea preissii*, and (d) *Allocasuarina fraseriana*. The error bars shown are based on standard deviation.

All the fatty acids were found with higher concentrations in autumn in the entire soil samples except the XP (Figure 2.8c). Interestingly, in soil samples under XP the tetracosanoic acid (peak 72) acid was found with higher concentration (~0.083 g/m^2) both in autumn and winter. The higher concentration in winter suggested dense canopies with thatching like materials of *X. preissii* might inhibit the effect of rainfall on the soil. Notably, no long-chain fatty acids were observed in AF (Figure 2.8 d) compared with the other three species. However, the composition and concentration of the compounds were different between BM, EM and XP (Figure 2.8 a-c).
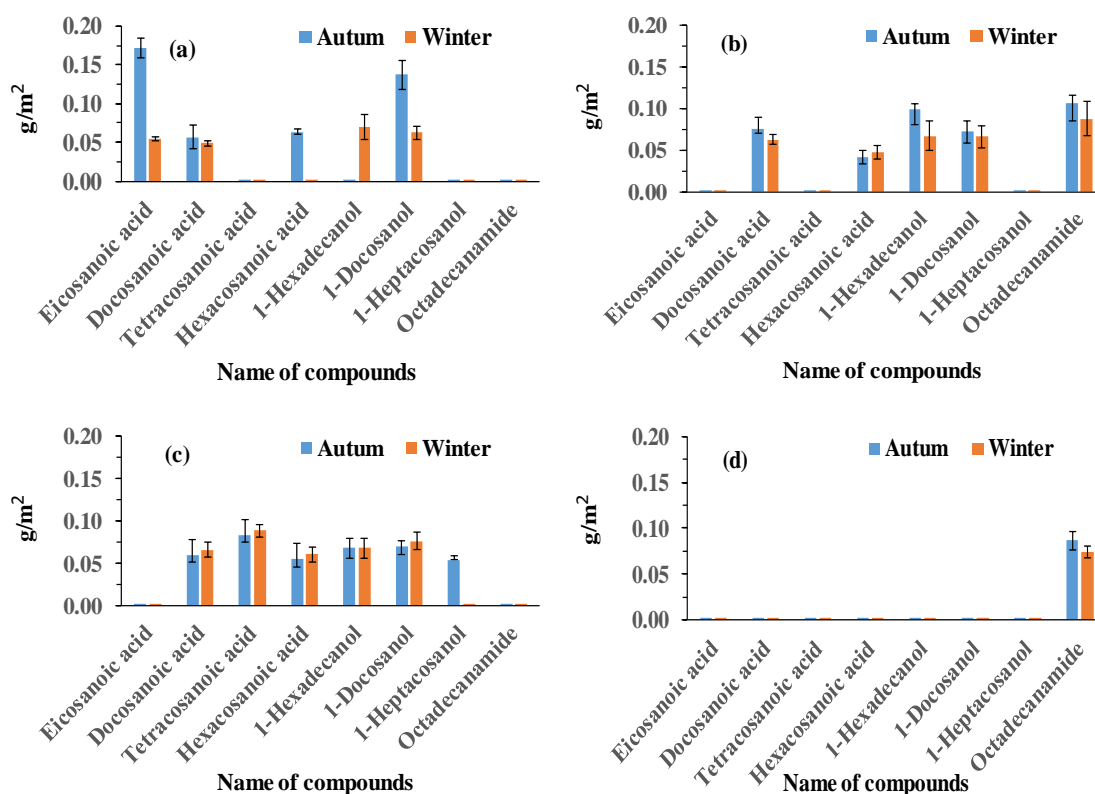
Figure 2.8   Soil polar compounds from under (a) *Banksia menziesii*, (b) *Eucalyptus marginata*, (c) *Xanthorrhoea preissii*, and (d) *Allocasuarina fraseriana*.

Moreover, among the long-chain fatty alcohols, 1-hexadecanol was only observed in winter under BM (Figure 2.8 a) while 1-heptacosanol was only found in autumn under XP (Figure 2.8 c). Notably, 1-hexadecanol was evident with similar concentration while 1-docosanol was observed with a slightly lower concentration during autumn under XP. Both of the 1-hexadecanol and 1-docosanol were only observed in EM and XP. However, 1-hexadecanol concentration (> 0.100 g/m^2) was found higher in EM compared with the XP during autumn. Furthermore, octadecanamide (~ 0.100 g/m^2) was only observed in EM and AF. Characterization of octadecanamide suggests the existence of octadecanoic acid in the soils under EM and AF.

2.3.4   Composition of canopy-derived organic pools

The nonpolar and polar materials (g/m^2) were extracted from exudate captured under the canopies. It was found that the amount of both nonpolar (Figure 2.9 a) and polar (Figure 2.9 b) materials were higher in *Eucalyptus marginata* (EM) compared with the other three species of *Banksia menziesii* (BM), *Xanthorrhoea preissii*, (XP), and *Allocasuarina fraseriana* (AF) over the sampling period (Figure 2.9 a-b).
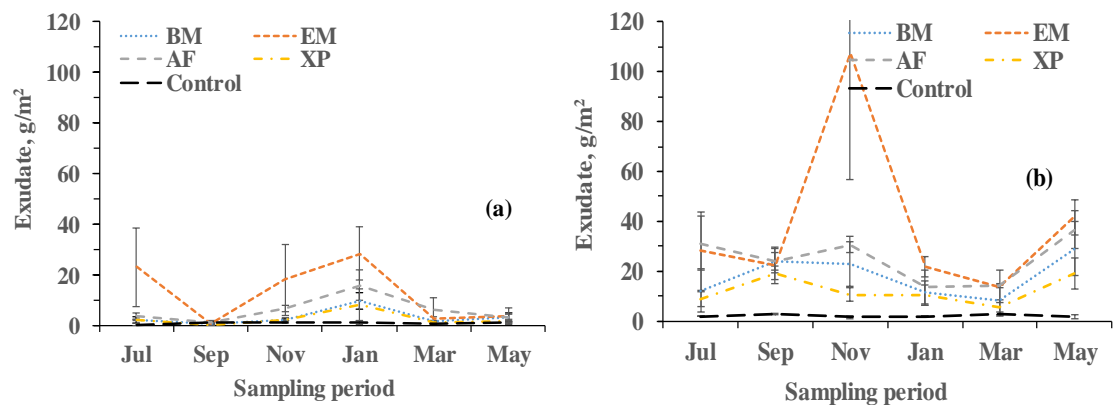
Figure 2.9   Captured exudates of both a) nonpolar and polar fraction over the sampling period for each of the four species.

The seasonal fluctuation in the amount of exudates suggests not only phenological implications of the investigated native species but also could be due to build up and wash off during random rainfall events.
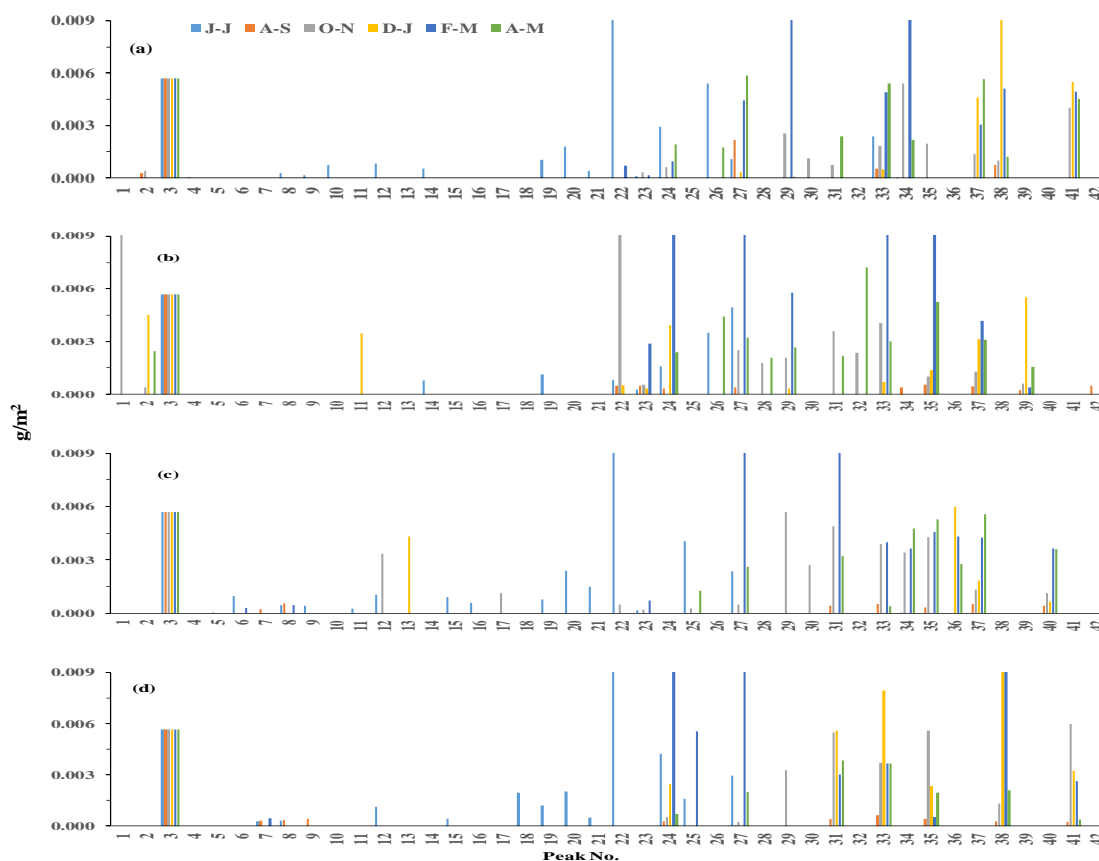
Figure 2.10   Nonpolar compounds of canopy derived exudate for a) *B. menziesii*, b) *E. marginata* c) *X. preissii* and d) *A. fraseriana* for different time periods (June-July (J-J), Aug-Sep (A-S); Oct-Nov (O-N), Dec-Jan (D-J), Feb-Mar (F-M) and Apr-May (A-M)). Peak 3 was an internal standard of dodecane.

Compounds were characterized in GC-MS using both nonpolar ($CHCl_3$) and polar (MeOH) solvents. A range of different nonpolar and polar compounds in the entire exudate samples of BM, EM, XP, and AF was identified (AT 2.2, 2.3 of the Appendix). However, the concentration (g/m^2) of the compounds was too small to coat the soil particles. The primary compounds were long- chain alkanes (Figure 2.10), fatty acids, alcohols, amides, and esters (Figure 2.11). Furthermore, there were also compounds containing ketone, aldehyde, phenol functional groups as well as some cyclic compounds. Several terpenoids, phytols, steroids, ketones, and aldehydes were detected

46

in both nonpolar and polar extracts. However, the similar compounds in both nonpolar and polar extracts were not compared with the soil derived compounds as they were not unequivocally reported to induce SWR at normal temperature. Notably, a number of terpenoids that are usually found in the smoke composition derived from vegetation fire were detected and they will be examined in Chapter 4 whether inducing SWR or not on sandy soils.
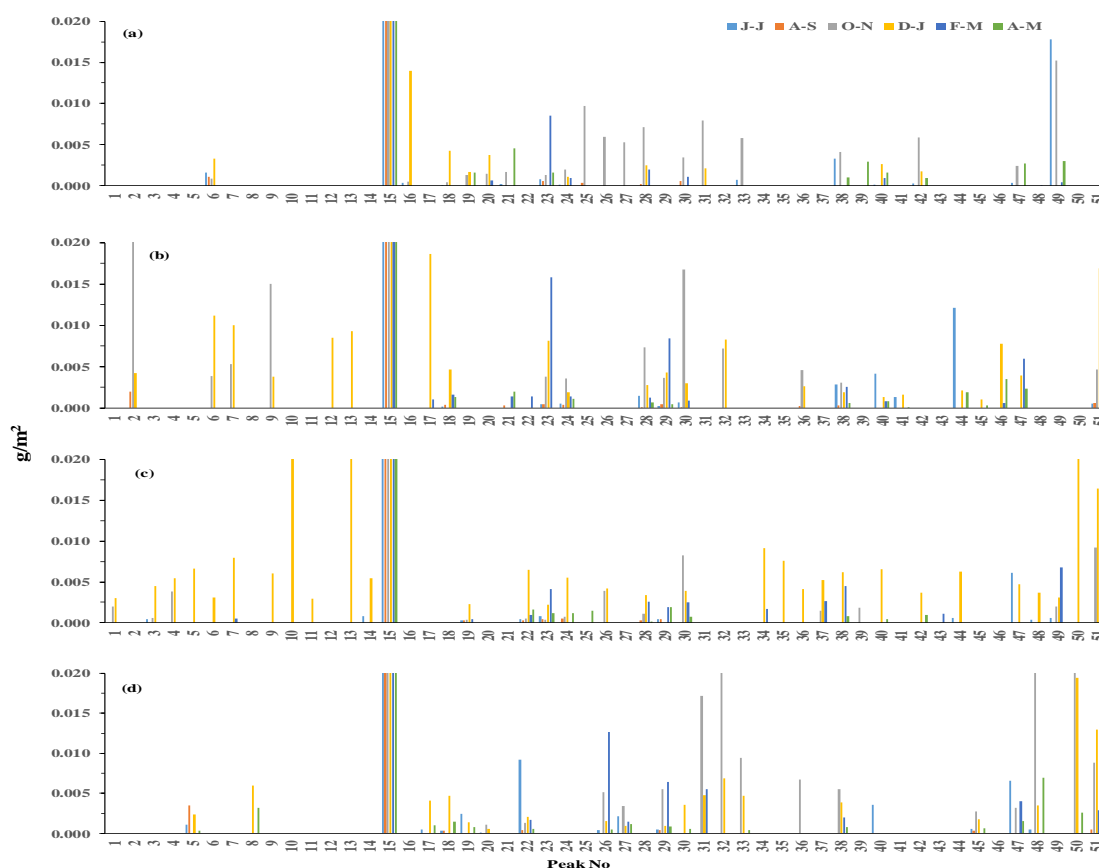
Figure 2.11   Polar compounds of canopy exudate for a) *B. menziesii*, b) *E. marginata* c) *X. preissii* and d) *A. fraseriana* for different time periods (June-July (J-J), Aug-Sep (A-S); Oct-Nov (O-N), Dec-Jan (D-J), Feb-Mar (F-M) and Apr-May (A-M)). Peak 15 was an internal standard of 1-chlorododecane.

A number of long chain alkanes mostly with odd-numbered (C_{25}, C_{29}, C_{35}, C_{37} and C_{55}) carbons were identified (Table 2.2) based on a priori likelihood of inducing SWR as

noted in the previous section. The compounds found in the nonpolar canopy derived exudate, are consistent with the findings of Eglinton et al. (1962) that most plant hydrocarbons derived from leaf waxes are odd-numbered (C_{21} -C_{27}) carbon atoms. However, the detected even-numbered alkanes in the soil may be subjected to decay by different microbes through their nutritional requirements.

Table 2.2   Selected long chain alkanes of exudate that were found closer in chain length to the soil derived compounds and have an a priori likelihood of inducing SWR.

Class	Peak #	Formula	Assignment	Concentration (g/m^2)			
				BM	EM	XP	AF
Alkane	27	$C_{25}H_{52}$	Pentacosane	0.014	0.062	0.034	0.096
	33	$C_{29}H_{60}$	Nonacosane	0.016	0.111	0.009	0.020
	34	$C_{35}H_{72}$	Pentatriacontane	0.040	0.060	0.012	0.000
	35	$C_{37}H_{76}$	Heptatriacontane	0.002	0.115	0.015	0.011
	37	$C_{55}H_{112}$	Pentapentacontane	0.015	0.012	0.014	0.000

Furthermore, a range of polar compounds were also detected in the polar extracts, mostly of long chain fatty acids, alcohols, esters, amides, and steroids. However, the compounds that have a priori likelihood of inducing SWR were observed both in the exudates and in soil extracts and were selected for further analysis (Table 2.3).

Table 2.3 Selected amphiphilic compounds from exudates that were similar to the soil derived compounds and have an a priori likelihood of inducing SWR.

Class	Peak #	Formula	Assignment	Concentration (g/m^2)			
				BM	EM	XP	AF
Fatty acids	27	$C_{20}H_{40}O_2$	Eicosanoic acid	0.006	0.000	0.000	0.009
	40	$C_{22}H_{44}O_2$	Docosanoic acid	0.005	0.007	0.007	0.004
	43	$C_{24}H_{48}O_2$	Tetracosanoic acid	0.000	0.000	0.002	0.000
	44	$C_{26}H_{52}O_2$	Hexacosanoic acid	0.000	0.016	0.007	0.000
Alcohols	23	$C_{16}H_{34}O$	1-Hexadecanol	0.013	0.029	0.009	0.000
	28	$C_{22}H_{46}O$	1-Docosanol	0.012	0.014	0.008	0.000
	34	$C_{27}H_{56}O$	1-Heptacosanol	0.000	0.000	0.011	0.000
Amides	32	$C_{18}H_{37}NO$	Octadecanamide	0.000	0.016	0.000	0.043

2.3.5 Seasonal fluctuation of canopy derived organic pools

The compounds identified through GC-MS were found to vary both in composition and concentration over the sampling period. The variation in the amount of exudates has already been shown in Figure 2.9.

The number of compounds was higher in the autumn compared with winter which suggests phenological control of the secretion of exudates from the extracellular glands of leaves of the investigated species. As noted in the previous section, long chain alkanes are effective in enhancing the SWR in combination with the amphiphilic compounds. However, they were found to vary in concentration over the sampling period. For example, the concentration of pentacosane was higher in March for the species XP, EM, and AF, with values from 0.034, 0.062, and 0.096 g/m^2, respectively (Figure 2.12 b-d). This suggests vegetation types and phenological traits are closely associated with the secretion of hydrophobic compounds into the soil. C_{29}-alkane (nonacosane) was detected in almost every sampling period for BM and AF (Figure 2.12 a, d) and it was substantially observed in November-March for EM and XP (Figure 2.12 b, c). Moreover, C_{35}-alkane (pentatriacontane) was abundant in BM in March

49

compared to November. However, pentatriacontane in XP was found with a small concentration in the same period (Figure 2.12 c). In BM, C_{37}-alkane (heptatriacontane) was only evident in Nov (Figure 2.12 a) while in the other three species it was found in several periods of sampling. Furthermore, C_{55}-alkane (pentapentacontane) was evident in all the species over the sampling year except in AF (Figure 2.12 d).
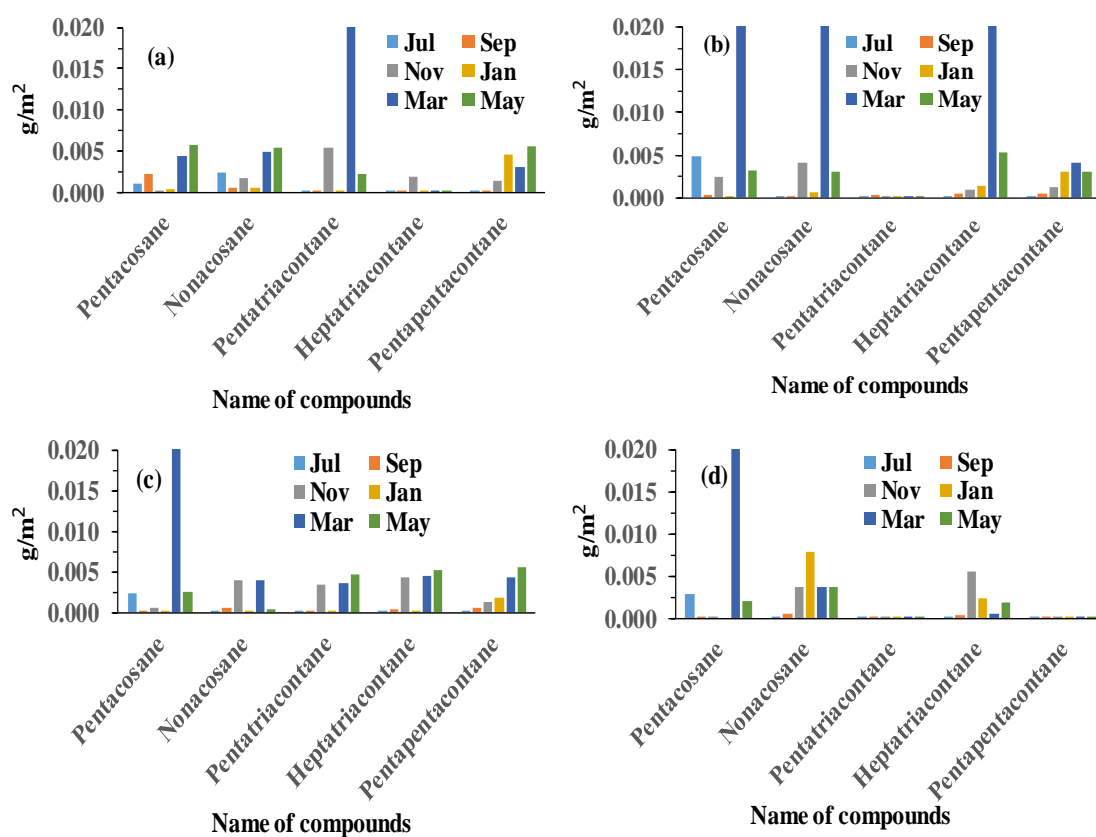
Figure 2.12   Seasonal variation of nonpolar compounds derived from exudate of (a) *Banksia menziesii*, (b) *Eucalyptus marginata*, (c) *Xanthorrhoea preissii*, and (d) *Allocasuarina fraseriana*.

A number of polar compounds were detected in the polar extracts, and as noted in the previous section, some of them have priori likelihood of inducing SWR. The important classes of compounds detected were long chain fatty acids, alcohols and amides but

with smaller amounts (0.004-0.043 g/m^2) (Figure 2.11). For example, docosanoic acid was found in all the species with the higher concentration in Jan for all the species except AF. However, in AF it was observed in Jul. Eicosanoic acid was only observed in BM and AF, but with a tiny concentration (Figure 2.13 a,d) and it was mostly visible in AF over the sampling period. C$_{24}$ -acid (tetracosanoic acid) was only evident in XP with a tiny concentration (0.002 g/m^2) in Mar. Moreover, hexacosanoic acid (C$_{26}$) was observed mostly in Jul and Jan for EM and XP, respectively (Figure 2.13 b,c).
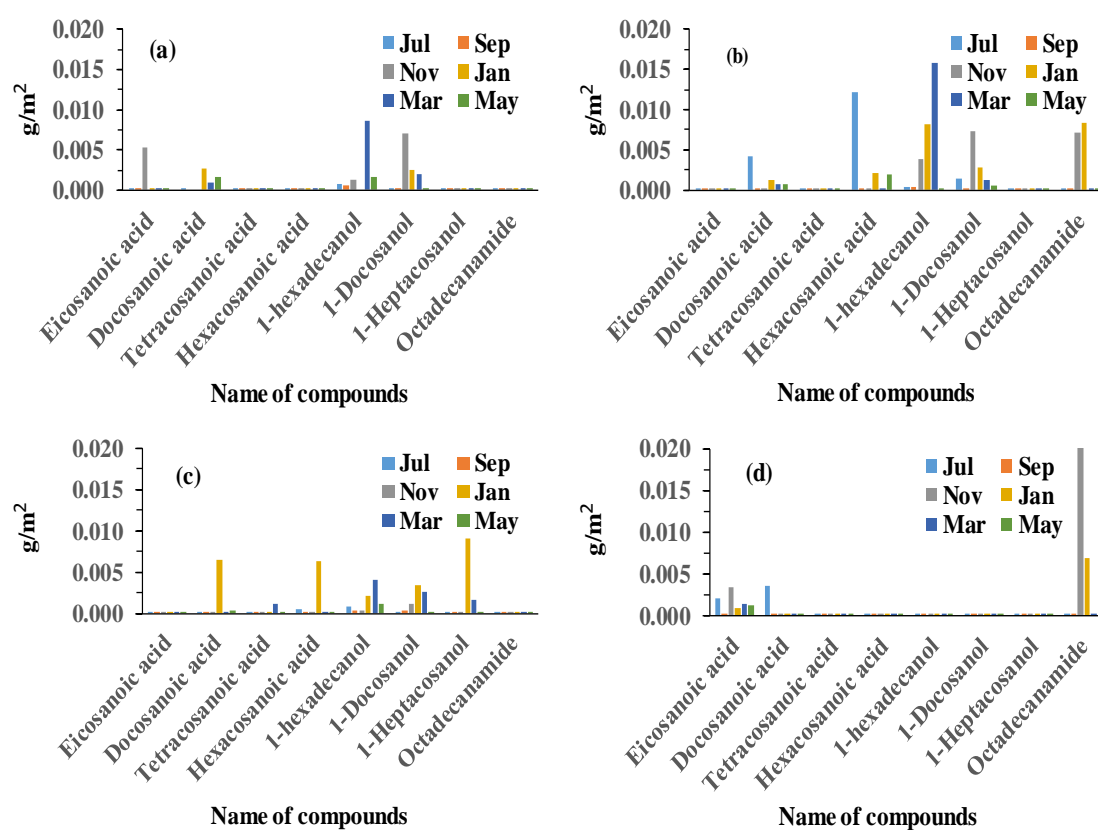
Figure 2.13   Seasonal variation of amphiphilic compounds derived from exudate of (a) *Banksia menziesii*, (b) *Eucalyptus marginata*, (c) *Xanthorrhoea preissii*, and (d) *Allocasuarina fraseriana*.

The long-chain alcohols (C$_{16}$ and C$_{27}$) were found in all the species except AF, and they were mostly evident over the sampling period (Figure 2.13 a-c). 1-Docosanol was also

not detected in AF and in the other three species it was evident with lower concentration. Moreover, C_{27} alcohol (1-Heptacosanol) was only evident in the XP mostly evident in Jan with a concentration of 0.0112 g/m^2. Furthermore, octadecenamide was detected in the species of EM and AF and was evident in Jan and Nov. The detection of octadecanamide suggests the soil contains octadecanoic acid and presumably the compound played substantial role in the incidence of SWR in AF.

2.3.6 *Contribution of canopy derived organic pools to substratum*

Because of very low concentration of nonpolar compounds, a comparison was made for the cumulative concentration of individual compounds derived from exudates with the concentration of soil derived compounds that were evident in the autumn to get insights of the overall contribution of canopy derived organic pools on the SWR. It was compared with the compound composition of soil found in the autumn due to the abundance of the carbon pools in the sampling period. It was revealed that the composition and concentration of compounds were varied between the species (Figure 2.14).
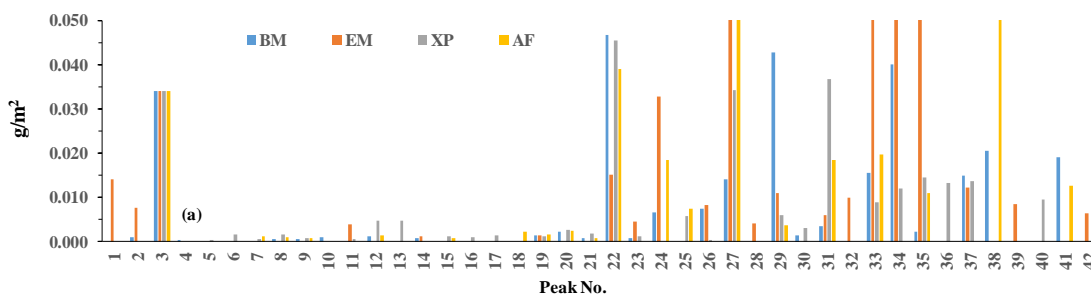
Figure 2.14   Cumulative amount of nonpolar compounds in exudates for the species of (a) *Banksia menziesii*, (b) *Eucalyptus marginata*, (c) *Xanthorrhoea preissii*, and (d) *Allocasuarina fraseriana* over the course of one sampling year. Peak 3 was an internal standard of dodecane.

As noted in previous section that long chain alkanes were found with even numbered C atoms in the soil. It was found that cumulative concentration of nonpolar compounds particularly long chain alkanes was higher in exudates derived from EM (~0.12 g/m^2) compared with other species. Moreover, the concentration of soil derived alkanes was also higher in EM followed by BM. (Figure 2.15 a,b). However, pentacosane was found with higher concentration in exudates derived from AF (Figure 2.15 d) compared with the other species.
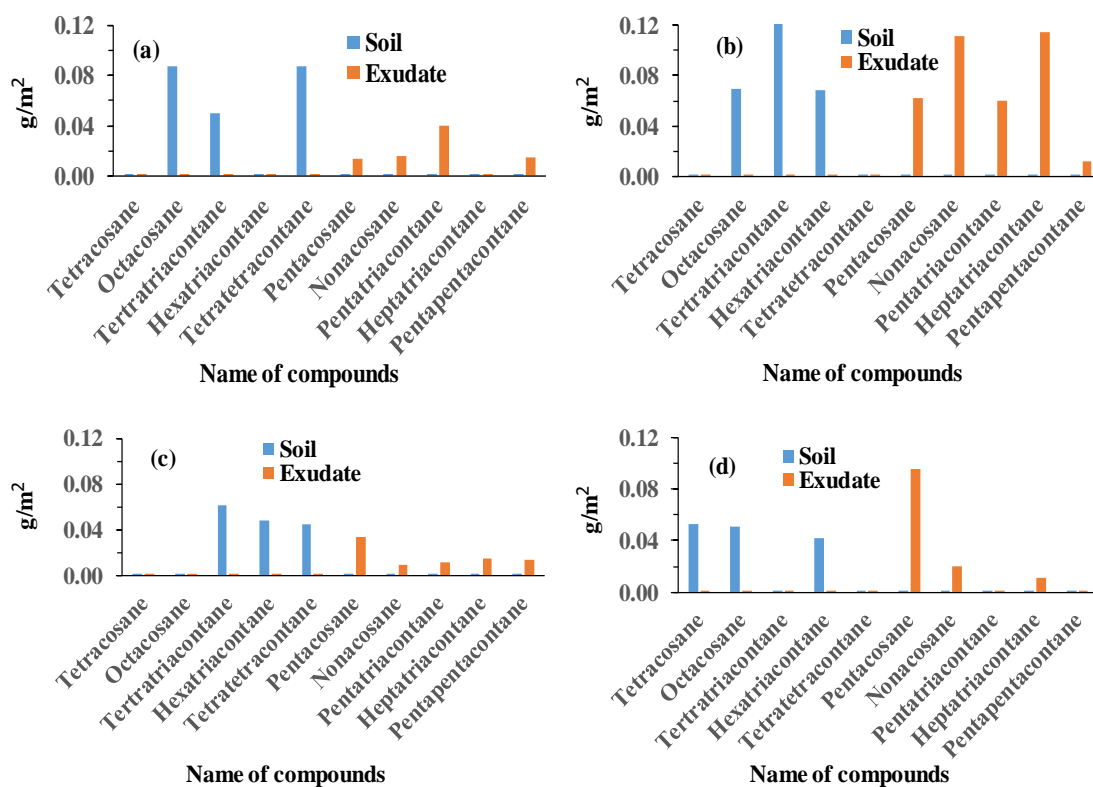
Figure 2.15   Contribution of nonpolar exudate compared with the compounds found in soil for (a) *Banksia menziesii*, (b) *Eucalyptus marginata*, (c) *Xanthorrhoea preissii*, and (d) *Allocasuarina fraseriana*.

Furthermore, cumulative amounts for all polar compounds were determined, and it was revealed that the total contribution was very low, with values ranging from ~0.004 g/m2 for docosanoic acid (peak 40) to 0.045 g/m2 for octadecanamide (peak 32) in AF (Figure 2.16). Moreover, docosanoic acid was found with a similar concentration over the year in both EM and XP followed by BM and AF.
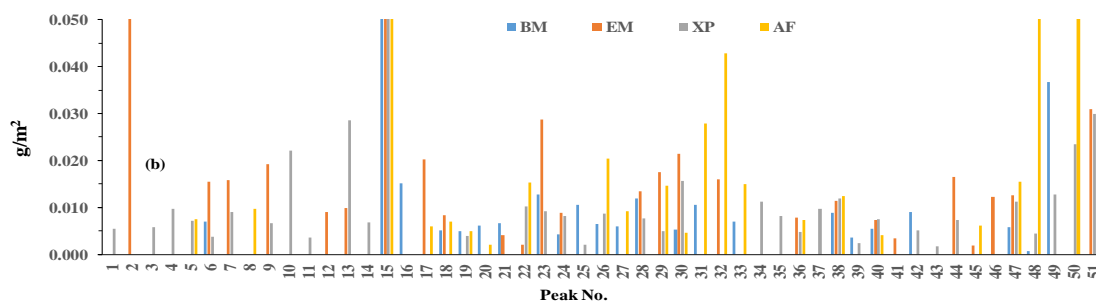
Figure 2.16   Cumulative amount of polar compound (g/m²) in leaf exudates of the different species of (a) *Banksia menziesii*, (b) *Eucalyptus marginata*, (c) *Xanthorrhoea preissii*, and (d) *Allocasuarina fraseriana* over the course of one sampling year. Peak 15 was an internal standard of 1-chlorododecane.

However, there were other similar amphiphilic compounds that were evident both in the soil and exudate and have a priori likelihood of inducing SWR (Figure 2.17). For example, eicosanoic acid was found with higher concentration (~0.15 g/m²) in soil for BM compared to a small concentration in the exudate (~0.008 g/m²) (Figure 2.17a). Moreover, tetracosanoic acid and hexacosanoic acids were found with higher concentration in the soil (~0.100 g/m²) compared to that of exudate (~0.002 g/m²) in XP (Figure 2.17c). Notably, the long-chain fatty acids were not observed in the soil of AF, while a tiny concentration of eicosanoic acid (~0.009 g/m²) and docosanoic acid (~0.004 g/m²) were evident in the exudate (Figure 2.17 d).
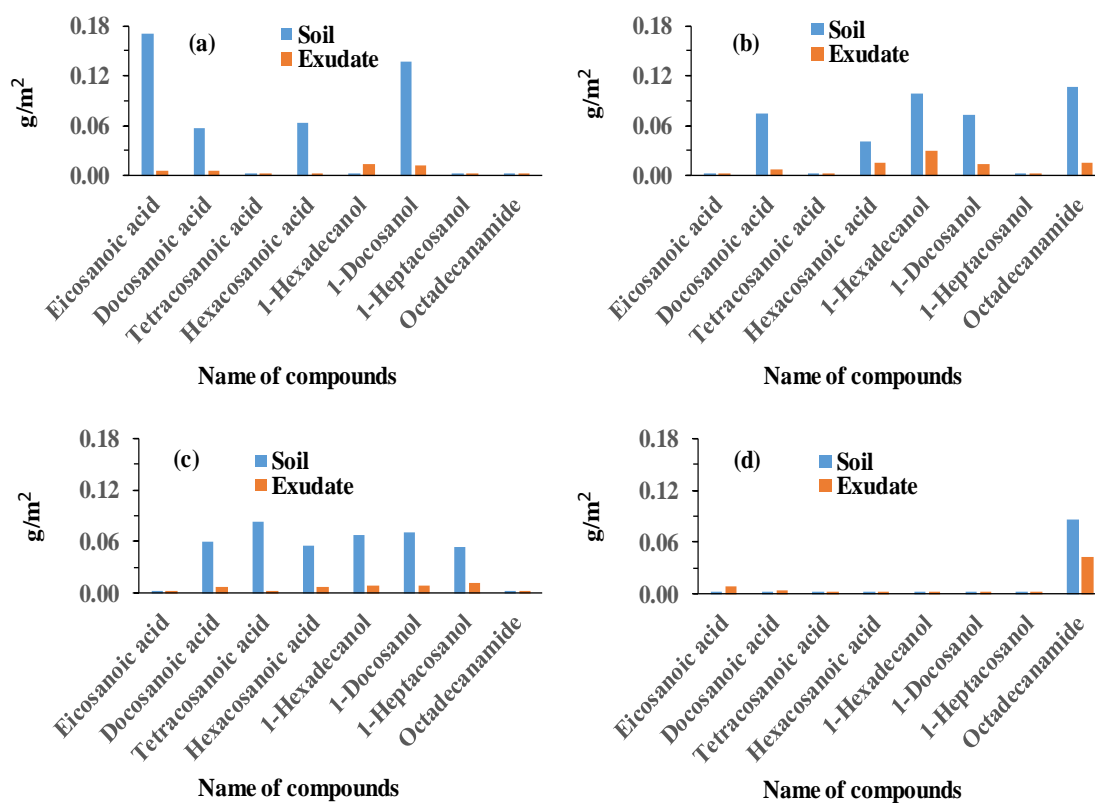
Figure 2.17   Contribution of polar exudate compared with the compounds found in soil in (a) *Banksia menziesii*, (b) *Eucalyptus marginata*, (c) *Xanthorrhoea preissii*, and (d) *Allocasuarina fraseriana*.

Long-chain (C_{16} - C_{27}) alcohols were found both in the soil and exudate. However, the concentration was lower compared to that of the soil. For example, 1-Docosanol in the soil and exudate of BM was higher with a concentration of ~0.137 g/m^2 and 0.012 g/m^2, respectively, followed by EM and XP. Moreover, a substantial amount of 1-Heptacosanol (C_{27}) was only evident in XP (Figure 2.17c) with a concentration of 0.054 g/m^2 and 0.011 g/m^2 in the soil and exudate, respectively. Notably, the long-chain alcohols were not observed both in the soil and exudate of AF. Furthermore, the octadecanamide was found both in the soil and exudate of EM and AF, with a concentration of (0.107 & 0.016 g/m^2) and (0.086 & 0.043 g/m^2), respectively (Figure 2.17b, d).

2.4 Discussion

2.4.1 Composition of organic pools

The amount of material extracted by sonication from soil was even greater than the cumulative amount of both non-polar and polar exudates of the investigated species. For example, amount of material extracted from soil (~480 g/m^2) in autumn was higher compared to that of both polar (235 g/m^2) and nonpolar (77 g/m^2) exudates in EM. A heterogeneous mixture of compounds with different functional groups were detected both in the canopy derived exudates and soil extracts of *Banksia menziesii* (BM), *Eucalyptus marginata* (EM), *Xanthorrea preissii* (XP) and *Allocasuarina fraseriana* (AF) (AT 2.1, 2.2 and 2.3 of the Appendix). Among them a range of long-chain alkanes, fatty acids, alcohols, amides, ketone, steroids, compound with a ring containing structure, and an unknown compound were found abundant with a substantial concentration.

The major classes of compounds reported to be implicated in the incidence of SWR are observed both in the canopy derived exudates and soil extracts. Odd-numbered alkanes (C_{25}, C_{29}, C_{35}, C_{37}, and C_{55}), mostly of plant derived exudates, were detected. Eglinton et al. (1962) also found odd-numbered (C_{21} -C_{37}) alkanes as a major constituent of leaf waxes. However, there was a predominance of an alkane with even-numbered carbon atoms in the soil samples, suggesting a microbial association of the soil samples and changes of organic pools in the soil. Each chain length between 24-44 carbon atoms could also indicate that not all the alkanes were of plant origin, rather they may have been subjected to decay or microbial or fungal attack (Morley et al., 2005). Notably, the existence of C_{24}, C_{28}, C_{34}, C_{36}, and C_{44} alkanes in the soil compared to the odd-numbered alkanes (C_{25}, C_{29}, C_{35}, C_{37}, and C_{55}) of exudates suggest there might be a significant

correlation of the compounds between soil and exudate. Franco et al. (2000b) also found the presence of alkanes in litter beneath eucalyptus trees in South Australia.

GC-MS analyses also indicated the presence of amphiphilic compounds both in the canopy derived exudates and in soil extracts. Among them, long-chain alcohols (Uddin et al., 2017), fatty acids and amides are reported with a priori likelihood of inducing SWR onto acid washed sand (AWS) at normal temperature (20°C) (Mainwaring et al., 2013). Ma'Shum et al. (1988) observed a similar distribution of apparently even-numbered long chain fatty acids (16-24 carbon atoms) in the hydrophobic soils of Australia. The similarity of compounds between exudates and soil extracts suggests the paucity of degradation of these acidic substances in the soil. Hayes and Graham (2000) also reported reduced degradability of fatty acids into humic substances. The ratio of the compound concentration between exudate and soil also revealed an indication of the accumulation of the compounds. Previous studies also reported the presence of fatty acids both in plant cuticles (Hayes, 1998) and hydrophobic soils (Franco et al., 1995; Horne & McIntosh, 2000).

A similar chain-length distribution of alcohols was observed both in the polar extracts of exudates and soil. For many of the long chained acids, there appeared to be an alcohol of the same chain length (e.g., C_{22}), which supports our hypothesis that top down contribution from vegetation can affect the chemical properties of soil. The identification 1-Docosanol is also consistent with Franco et al. (2000b) who noted long-chain alcohol can significantly modify the wetting properties of soil.

Moreover, octadecanamide was found similar both in the soil extracts and in exudates. The detection of octadecanamide indicates the presence of octadecanoic acid in the extracts, presumably derived during analysis with aqueous ammonia. However, it could

not be unequivocally determined whether the amides were initially present in the soils or were formed as a result of heating at a lower temperature for shorter periods in the presence of ammonia.

A number of terpenoids were observed both in the exudates and soil extracts that are widely reported to emit during vegetation fire. However, their emission can be affected by environmental parameters (Kesselmeier et al., 1997). This suggests naturally occurring terpenoids (Horn et al., 1964) may also contribute to hydrophobic substances in the soil. However, the role of their contribution in inducing SWR will be examined in Chapter 4 using an experimental and molecular dynamics approach. Giovannini and Lucchesi (1997) observed modifications in physicochemical parameters in soil at different fire intensities.

Finally, we can conclude that severity of SWR is not only related to the amount of exudates, also closely associated with the composition and concentration of certain compounds. However, the particular role of the pure compounds and their concentration in physicochemical interaction with soil particles will be discussed in Chapter 4, 5 and 6.

2.4.2   Seasonal fluctuation

The amount of material extracted in soil was found higher in autumn compared with winter. Rainfall again not only be an explanation for this variation, type of vegetation including canopy and trunk size can modify the top soil carbon pools, and consequently the amount of material was reduced. For example, the amount of materials in *Banksia menziesii* (BM) was   ~410 g/m^2 in autumn compared to ~275 g/m^2 in winter. Besides vegetation type, age of the trees are reported to have profound implication in the quantitative variations of terpenoids (Kim et al., 2005). However, the contribution of

carbon pools can be different in different soil components that will be discussed in Chapter 3. Moreover, both the polar and nonpolar compounds detected in canopy derived exudates were found to fluctuate over the sampling periods. For example, the higher concentration long-chain alkanes of exudate were found in March of the sampling period. However, most of the alkanes were varied in concentration between the species over sampling period. For example, concentration of pentatriacontane in BM (~0.20 g/m^2) was evident with higher concentration compared to XP (0.005 g/m^2) in March. Moreover, most of the amphiphilic compounds were abundant during January and March of the sampling period. For example, docosanoic acid was found with higher concertation in January for *Banksia menziesii* (BM) and *Xanthorrhoea preissii* (XP) with a concentration of ~0.005 and ~0.007 g/m^2, respectively. However, in EM and AF (*Allocasuarina fraseriana*) it was evident in July with a concentration of ~0.007 and ~0.004 g/m^2 respectively. This suggested phenological stages (e.g., leaf flushing, flowering, and fruiting) of tree species can affect the secretion of exudates from the extracellular glands of their leaves (Rapparini et al., 2001). Canopy structure of the tree species are also attributed to modify the physicochemical properties of the soil (Gerrits et al., 2010). For example, in the Mediterranean climate of Portugal, canopy interception is reported as 48.7 ± 17.8% in the winter season (Stoof et al., 2011). Moreover, 1-Hexadecanol and 1-Docosanol were detected in all the species except AF. The higher concentration of 1-Hexadecanol was found in March for EM (~0.015 g/m^2), whereas, 1-Docosanol was observed with a higher concentration of ~0.007 g/m^2 in November for both of BM and EM. Interestingly, octadecanamide was only evident during November and March for the species of EM (~0.007 g/m^2) and AF (~0.007- 0.020 g/m^2). The study carried out by Kamatou et al. (2008) revealed mostly quantitative rather than qualitative seasonal variations in the essential oil composition of three South African *Salvia*

species. Moreover, concentration of isoprene are also reported to fluctuate in different months of the year measured in the boreal coniferous forest of Finland (Hakola et al., 2003). Finally, we can conclude that composition and concentration of compounds both in the exudates and soil extracts are varied in different periods of the year. This variation may even lead to differences in SWR in the substratum and also in different components of soil that will be presented and discussed in the next Chapter.

3 Contribution of organic carbon pools in inducing soil water repellency (SWR)

3.1 Introduction

Soil water repellency (SWR) is a major land management issue across farmland in southern Australia, through its close association with crop production. Although its incidence and severity have been anecdotally related to the previous native vegetation (McGhie & Posner, 1980) little is known about the specific organic compounds that may derive from this vegetation. Different plant species may make various contributions to SWR (Doerr et al., 1996; Roberts & Carbon, 1972); indeed Chapter 2 demonstrated the differences in the composition of organic inputs from different native plant species which are found to secrete as exudates from their extracellular glands to the soil.

SWR is considered to be the result of the coating of soil particles with organic substances that reduce the affinity for water (DeBano et al., 1970; Ma'shum & Farmer, 1985; Ma'Shum et al., 1988). It's a natural phenomenon and occurs in the surface layers of sandy soils where hydrophobic materials mostly of plant origin occur as particulate organic matter and as waxy coatings on soil particles (Franco et al., 2000b). In many regions, trees with glaucous leaves accumulate waxy substances in the surrounding soil. However, the precise distribution of these compounds (e.g., as coatings or in interstices between soil particles) and their contribution to SWR is not quantified.

Furthermore, there are reports of a correlation between total organic carbon (TOC) and SWR, but these are often in narrow ranges or unpaired samples. Although SWR is closely related to organic carbon content (Bisdom et al., 1993) and soil texture or surface

area (Roberts & Carbon, 1972), there may also be a contribution from organic matter composition (Harper et al., 2000; McGhie & Posner, 1981; McGhie & Posner, 1980; McKissock et al., 2003). McGhie and Posner (1981) for example, suggest that different plant species contribute differently to the induction of SWR through the production of different (uncharacterized) compounds. Thus, the contribution of organic matter composition in inducing SWR is an important consideration in this natural phenomenon (Doerr et al., 2000; Ellerbrock et al., 2005).

SWR is associated with coarse-textured sandy soils because of their smaller surface area per unit volume (McKissock et al., 2000; Roberts & Carbon, 1972). However, the degree of SWR is often reported to vary with land use or type of vegetation (de Blas et al., 2010; Zavala et al., 2009b). For example, SWR under dominant native vegetation is widely reported in south-western Australia (Harper et al., 2000; McGhie & Posner, 1980; McKissock et al., 2000; Walden et al., 2015), as described in Chapter 1. Plant litter, resinous plant tissues and activity of plant roots are usually considered as a source of hydrophobic substances to the soil (Doerr et al., 1998; Jordán et al., 2008; Mataix-Solera & Doerr, 2004; Ritsema & Dekker, 1994). In hydrophobic soils, it is thought that polar ends of the amphiphilic compounds are attached to the mineral surface, and the nonpolar ends are oriented outwards. Moreover, soils under this native vegetation are considered to be water repellent due to the presence of hydrophobic skins of a very stable humic fraction (Roberts & Carbon, 1972).

Soils in south-western Australia are often, but not exclusively, characterized by sandy surfaces and poor water holding capacity (McArthur, 1991). As the region is extensively developed for agriculture, many of the reports on SWR come from agricultural areas. Though a significant aspect of the agricultural soils is SWR or non-wetting, how this

soil property can be related to prior major native species is often overlooked or treated in a non-quantitative, anecdotal fashion (e.g. King, 1981). However, soil is complex, and substantial functional differences in organic matter composition between different native species may contribute to differences in the severity of SWR. For example, despite similar soil characteristics, small amounts of hydrophobic compounds from the trees may be responsible for the variation in SWR (Doerr et al., 2000).

The contribution of wax containing compounds namely, branched and unbranched C_{16} to C_{36} fatty acids and their esters, alkanes, phytanols, phytanes and sterols are widely reported as contributing to the development of SWR (Doerr et al., 2005; Franco et al., 2000b; Mainwaring et al., 2013; Morley et al., 2005). The hydrophilic head groups of amphiphilic molecules should have a natural affinity for the polar surfaces of mineral particles and thus align them differently relative to nonpolar surfaces of soil particles. For example, 2.35 wax molecules nm^{-2} on a kaolinite (clay) surface adopt a semi-ordered, tilted packing arrangement whereas, on quartz (sand) surface adopt a multi-layered arrangement (Walden et al., 2015). Apart from biological and physical factors, environmental parameters affect the severity of SWR through redistribution of compounds. For example, vegetation fires can significantly modify soil physicochemical properties through altering total soil carbon content and inducing SWR (Atanassova & Doerr, 2011; DeBano & Rice, 1973; Heath et al., 2015; Sheridan et al., 2007).

Although many papers suggest that SWR is induced by the coating of soil mineral particles, organic material in soils also occurs as particulate matter that can occupy pores or interstices between particles. Moreover, by holding strategic positions such as

at the beginning or end of elongated pores, organic compounds can be very effective in decreasing wettability even with small quantities in the soil matrix (Ellies et al., 2005).

This chapter is about the separation of soil organic matter into different pools, based on a physical separation process. Different soil components and soil structures, namely, micro and macro aggregates and coated plant remains are differently distributed over the wettable to extremely water repellent sandy soils (Bisdom et al., 1993). SWR analyses are often undertaken on whole soil samples, with no discrimination of the contribution of different soil pools. Thus, this Chapter examines two interconnected ideas, (1) discerning the contribution of organic matter composition to SWR and (2) determining how organic matter in different pools (e.g., on particle surfaces, as interstitial matter) contributes to SWR.

3.2   Materials and methods

3.2.1   Sample collection and preparation

Surface soil samples were collected under four native species *(Eucalyptus marginata, E. wandoo, Banksia menziesii* and *Allocasuarina fraseriana)* in southwestern Western Australia. The locations of the sample sites are given in Table 3.1. In each case, the natural vegetation was relatively undisturbed and considered to be close to a natural state. The species were selected due to their close association to SWR, which have been noted in the previous chapters. Despite the similar sand dominated surfaces and scanty undergrowth on the substratum, organic carbon content (given hereafter) of the top soil were different under the investigated species.

Table 3.1   Location of the sample sites.

Species name	Location
Banksia menziesii	Murdoch University campus, (-32.07°, 115.83°)
Eucalyptus marginata	Bowelling, (-33.46°, 116.58°)
Eucalyptus wandoo	Bowelling (-33.45°, 116.60°)
Allocasuarina fraseriana	Worsley (-33.28°, 115.96°)

Samples were taken randomly from an area of around 100 m^2, from under the canopies of the respective species, in February-2016 when the soils were dry, at a depth of 0-5 cm (topsoil), using a 50 mm diameter corer. Each sample comprised 15 subsamples which were bulked. Three replications for each species were taken. Collected soils were air dried, and coarse particles were eliminated by gentle sieving using a 2 mm sieve.

3.2.2   Separation of different soil components through winnowing

Soils are usually comprised of different components, namely, macro aggregates, plant fragments and coatings on sand grains. An attempt was made to separate soils into the coarse mineral particulate matter (CM) and finer interstitial organic and mineral materials (IM) through winnowing (Figure 3.1a) in an air-stream. Each of the sampled sites had sandy soils.

For the winnowing treatment, a technique was designed for physical removal of interstitial matter (IM) from the soil matrix. In order to remove IM, two larger conical flasks with an outlet were joined by a plastic tube, and one of them was filled with untreated soil (~200g) while another was fixed to capture the blown out IM. Air was

blown from the top to the soil matrix, and a magnetic stirrer was placed inside to agitate the soil so that it could release the interstitial matter. A fine filter paper was placed on top of the capturing flask in order to stop finer particles escaping.

a) Separation by winnowing   **b) Extraction by sonication**

Figure 3.1   Separation of different soils components (a), and Extraction of soil and coarse mineral materials (b).

The interstitial matter (IM) may contain mineral material along with particulate organic matter. However, the content of carbon is usually higher in IM relative to bulk soil and winnowed coarse mineral materials alone.

3.2.3 Determining the contribution of organic matter composition to soil water repellency (SWR)

Invariably, it is difficult to separate the contribution of organic matter composition to SWR as the measured values are obscured by variations in organic carbon content and soil particle size. Thus, a technique to develop response curves comparing organic carbon content with SWR was developed. Organic carbon content was manipulated by adding an inert medium; acid washed sand (AWS). The assumption was that the effect

of organic matter composition on SWR would be reflected in differences in the resultant response curve.
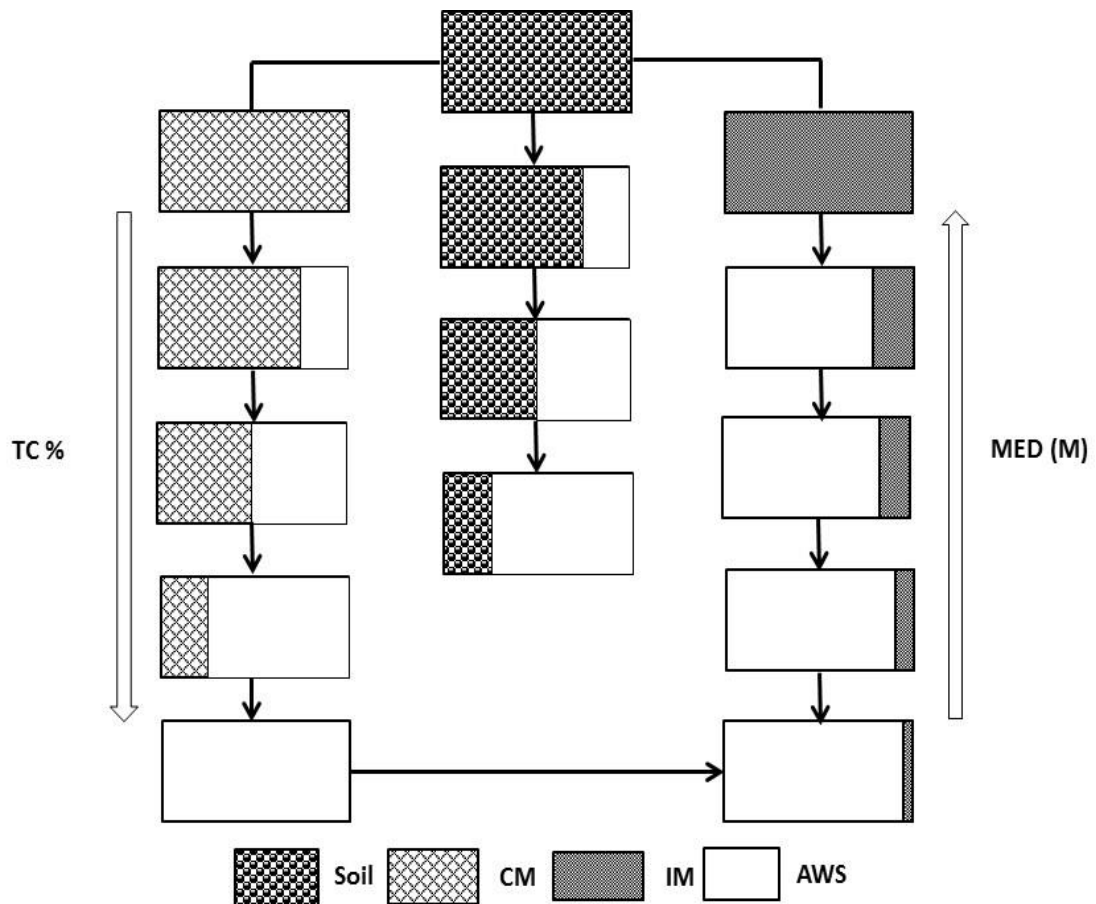
Figure 3.2   A conceptual model depicting the separation of soil into different components that may affect SWR (Soil- dried and sieved field sample; CM- coarse mineral materials; IM- interstitial matter; TC-total carbon; MED-molarity of ethanol droplet) and subsequent dilution of derived fractions with acid washed sand (AWS).

This approach was used in two ways:

1. Untreated soil and winnowed coarse materials were diluted by adding different proportions (25, 50 and 75%) of acid washed sand (AWS).

2. The interstitial particulate matter was added onto AWS in different proportions (5, 10, 15, and 20%) to examine the effect of carbon pools in the incidence of SWR as suggested by the model developed (Figure 3.2).

3.2.4 Treatment of mineral component

Winnowed coarse materials were washed with deionized water. For, example, 120 g of coarse materials were washed with 100 ml of DI water. The mixture of coarse materials and water was stirred gently with a glass bar and the excess water was poured off after couple of minutes. The process was repeated three times in order to remove all the water soluble compounds as best as possible. The washed soil sample was then split into two and heated in the oven at 50 ^{0}C, and 105 ^{0}C, respectively, to measure the potential SWR following desiccation.

3.2.5 Sample extraction and analysis

30 g of different soil components were placed in a 100 ml Schott bottle. 50 ml of IPA/NH$_3$ (70:30) solvent was added to the soil and the mixture was shaken gently for about a minute. The mixture was then put into a sonication bath at a set temperature of 10°C (Figure 3.1b). The mixture was sonicated for 30 minutes and left for 24 hours, and then sonicated again for another 30 minutes (McCready et al., 2000). It's noteworthy that the water level inside the sonication bath should be above the solvent level of the beaker that is put into the bath, to get the desired concentration of the analyte.

Then 30 ml of supernatant aliquot was taken into a tarred glass centrifugal vial. The lid of the vial was left open for 24 hours under the fume hood to evaporate excess NH$_3$ and in case of excess ammonia production a solvent trap was used. The concentrated sample was then dried using a Labconco Centri Vap Concentrator System 78100 series at 1725 rpm rotation and 45^0 C temperature for about 12 hours. The weight of solid material

was determined by subtracting the weight of the empty vial from that of the vial with dried material. DCM/MeOH (2:1) solution was prepared and spiked with dodecane at a compatible concentration with the analyte to make a concentration of approximately 10,000-50,000 µg/ml (ppm). An aliquot of the redissolved sample was transferred from the centrifugal vial into a GC vial filtered through a Pasteur pipette using $MgSO_4$ as the drying agent.

Furthermore, 0.05 g of interstitial matter (IM) was placed in a centrifuge vial, and 1.0 ml of DCM/MeOH (2:1) solution spiked with dodecane was added to determine the most abundant compounds of the IM. The mixture was shaken gently for 1 min and put on the vortex mixture to make the solution homogeneous.

3.2.6 SWR assessment

The severity of SWR of each of the samples was assessed using the molarity of ethanol droplet (MED) test (King 1981). A stock solution of 4M ethanol was prepared, and the solutions were made at concentrations between 0 and 4M with increments of 0.2M. Approximately ~ 20g of soil sample was placed in a petri dish (50×10 mm) and put into a desiccator for around four hours to make the sample free from humidity and to eliminate any effects of pH (Smith & Tanford, 1973).

A second sample of the same species was placed in an oven at 105°C for 24 hours. The oven-dried sample was then cooled to room temperature in a desiccator.

The surfaces of the samples were leveled by gently tapping on the bench, and in some cases, a light pressure was applied with a small flat bottom beaker to make the surface smooth and uniform.

At least three droplets (50 µL) of the prepared ethanol solutions were then applied to the surface of the samples from 5 mm height, starting from the lowest ethanol

concentration. The time required for each drop to penetrate the surface was recorded. The lowest concentration for which the infiltration time was <10 s, considered as the MED value for that sample (King, 1981).

3.2.7 Loading of IM onto acid washed sand

Interstitial matter (IM) was applied onto AWS at different loadings (%). (i) The MED was also measured on the samples made through mixing IM physically onto AWS. (ii) a mixture of IM with AWS (120 g) was placed in a larger RB flask (250 ml) and 100 ml of tetrahydrofuran (THF) was added to the sample. The mixture was thoroughly mixed in a rotary evaporator for 10 min and the solvent was then evaporated under reduced pressure at 45°C and 120 revolutions per minute. The sample was then prepared for SWR assessment as described in section 3.2.6.

3.2.8 Distribution of compounds through wetting and heating

To distribute compounds, all the untreated and winnowed coarse mineral samples with their diluted subsamples were wetted up and dried at 50°C for 48 hours in the oven and then SWR was measured following desiccation. The severity of SWR was also measured following desiccation after heating at the higher temperature of 105°C.

A 20 ml of DI water was added to 120 g of soil and stirred gently with a glass bar to uniformly wet up the sample. Moreover, interstitial matter loaded (10%) samples were also heated at a range of temperatures namely, 50, 100, 150 and 200°C for 24 hours to investigate heat induced distribution of compounds in the sample and consequent changes in the severity of SWR.

3.2.9   GC-MS analysis

GC–MS analysis was conducted on a Shimadzu 2010GC–MS instrument using a splitless injector and a 30 m × 0.25 mm BPX5 fused silica column with 5% Phenyl polysilphenylene-siloxane. The temperature program was 60^0 C, held for 1 min then ramped to 100^0 C at a rate of 30^0 C min^{-1}. Again, it was held for 1 min then ramped to 300^0C at 4^0C min^{-1}. Then again it took place for a further 5 minutes under UHP helium as the carrier gas. The GC was connected to a Shimadzu QP2010S single quadruple mass spectrometer.

The mass spectrometer was operated as an electron impact (EI) ionizer. The ion source was maintained at 200 ^{0}C with the electron energy at 70 eV. Identification of compounds was based on interpretation of the mass spectroscopy fragmentation, comparison with spectra published in the literature, those available in the computerized database of the instrument and relative GC-retention times.

3.2.10 Measurement of soil carbon

Soil carbon (%) was measured by Rayment and Lyons (2010) Method 6B2 (Leco Analyzer). Samples were loaded into a combustion tube, taken to 1350 ^{0}C and flushed with oxygen. Gases generated from this process are measured using an infra-red detector for carbon. The total carbon (%) content was measured for Soil, winnowed coarse material (CM), winnowed interstitial matter (IM) and AWS by CSBP Laboratories, WA.

3.2.11 SEM and TGA analysis

Scanning electron microscopy (SEM) was used to take images of untreated soil sample, winnowed coarse material (CM), winnowed interstitial matter (IM) and ash contents derived through TGA analysis.

SEM and EDS analyses were performed in JEOL JCM-6000 SEM/EDS analyzer.

TGA analysis was also performed in Simultaneous Thermal Analyser (STA 6000) of Perkin Elmer.

3.3   Results

3.3.1   Composition of compounds

GC-MS identified a range of different types of compounds in all the samples investigated, including long chain fatty acids, amides, alkanes, acetates or ketones and more complex ring-containing structures. There were also alkenes, alcohols and benzene derived compounds in the total compound composition. In order to compare the results, the main peaks in all the species have been numbered 1-104. The assignments of these peaks are listed in AT (Appendix Table) 3.1 of the Appendix.

GC-MS analysis denoted the presence of mostly long-chain fatty acids with 18-26 carbon atoms (C_{18}, C_{20}, C_{22}, C_{26}). Even-chain acids predominated while an unsaturated oleic acid occurred in the untreated sample of *E. wandoo*. The chain length distribution of amides was also found to be similar to many of the long- chain acids. The amides appeared to be long chain structures with 18-22 carbon atoms. Unsaturated amides were also observed. However, further work is needed (e.g., using chemical ionization mass spectrometry) before unambiguous identifications (cis- and trans- orientations) of these compounds can be determined.

Alkanes were found with a slightly higher chain length distribution than that of the acids and amides. There was a predominance of compounds having an even number of carbon atoms. Moreover, alcohols having long chain carbons (16-30) were detected and ring containing phytols and phytanols were found to be predominantly triterpenoid. The predominant esters detected in these samples were derived from fatty acids and alcohols

with carbon atoms ranging from 21-35. Moreover, acetate or ketones having 27-32 carbon atoms were identified. The ring-containing compounds observed were predominantly cholesterol and stigmasterol derivatives.

The diisooctyl phthalate (1,2-Benzenedicarboxylic acid, diisooctyl ester) detected (peak 77) is most likely due to contamination from the plastic bags that were used for storing the samples. Moreover, few benzene-derived compounds with lower molecular weights were evident.

3.3.2 Concentration profiles between species and treatments

The abundance of organic compounds from the different species and treatments were determined on the basis of an absolute concentration value of ≥ 15 µg (0.001g/kg). Mainwaring et al. (2013) determined octadecanoic acid loadings of 0.003 g/kg induced SWR on AWS, based on organic compound loadings found on a range of sandy soils (see Morley et al. (2005) and Doerr et al. (2005) for details).

The number of most abundant compounds (including IS, peak 5) for untreated soil were 14, 29, 27 and 14 for the species *E. marginata*, *E. wandoo*, *B. menziesii* and *A. fraseriana*, respectively (Figure 3.3). The abundant compounds were observed from peaks 1, 2, 16, 62, 65, 66, 77, 85, 86, 91, 94, 101 and 104 for the species of *E. marginata* (AT 3.1 of the Appendix). In *E. wandoo* the most abundant organic species were evident by the peaks of 4, 5, 30, 32, 34, 35, 39, 42, 44, 45, 53, 54, 55, 59, 61, 62, 63, 65, 67, 68, 69, 72, 85, 86, 91, 98, 99, 101 and 104 (AT 3.1 of the Appendix). Interestingly, the abundant compounds for *B. menziesii* were not exactly the same as the previous two species and the peaks were 5, 23, 24, 29, 33, 55, 59, 62, 63, 67, 68, 72, 75, 77, 85, 88, 91, 94, 96, 97, 98, 99, 100, 101, 102, 103 and 104 (AT 3.1 of the Appendix). Moreover,

abundant compounds were shown by the peaks of 2, 5, 54, 57, 60, 62, 65, 70, 74, 75, 79, 98, 99 and 101 for *A. fraseriana* (AT 3.1 of the Appendix).

As noted in the previous section, untreated soil (UT) was separated into the winnowed coarse mineral material (CM) and interstitial matter (IM). The concentrations of the compounds found in each of these fractions (CM, IM) were compared with that of untreated soil (UT) (Figure 3.3).

Importantly, the concentration of the compounds in the UT sample were found to be similar to the total amount from CM and IM. For example, the concentration of benzene, 1-methyl-2-(1-methylethyl)- (peak no. 1), Glycerin (2), benzenemethanol, 4-(1-methylethyl)- (16), isopropyl stearate (62), octadecanamide (65), hexanoic acid, pentadecyl ester (66), 1,2-benzenedicarboxylic acid, diisooctyl ester (77), hexacosanoic acid (85), hexatriacontane (86), cholesta-4,6-dien-3-ol, (91), beta.-sitosterol acetate (94), cholesta-4,6-dien-3-one (101) and benzenepropanoic acid, octadecyl ester (104) extracted from the untreated sample of *E. marginata* was found to be close to the total amount of the same compounds from CM and IM fractions (Figure 3.3a).

The number of compounds detected with concentration level ≥ 0.001g/kg was highest in *E. wandoo* (29) followed by *B. menziesii* (27)*, E. marginata* (14) *and A. fraseriana* (14) (Figure 3.3a-d). This suggested that the carbon content and concentration of compounds were different for the different species and thus can be associated with variation in SWR. Interestingly, for species *A. fraseriana* no peaks of long chain fatty acids and fatty alcohol like waxy compounds (e.g., peaks 59, 61, 85, 86) were detected in the extracts of any of the different treatments (Figure 3.3d).
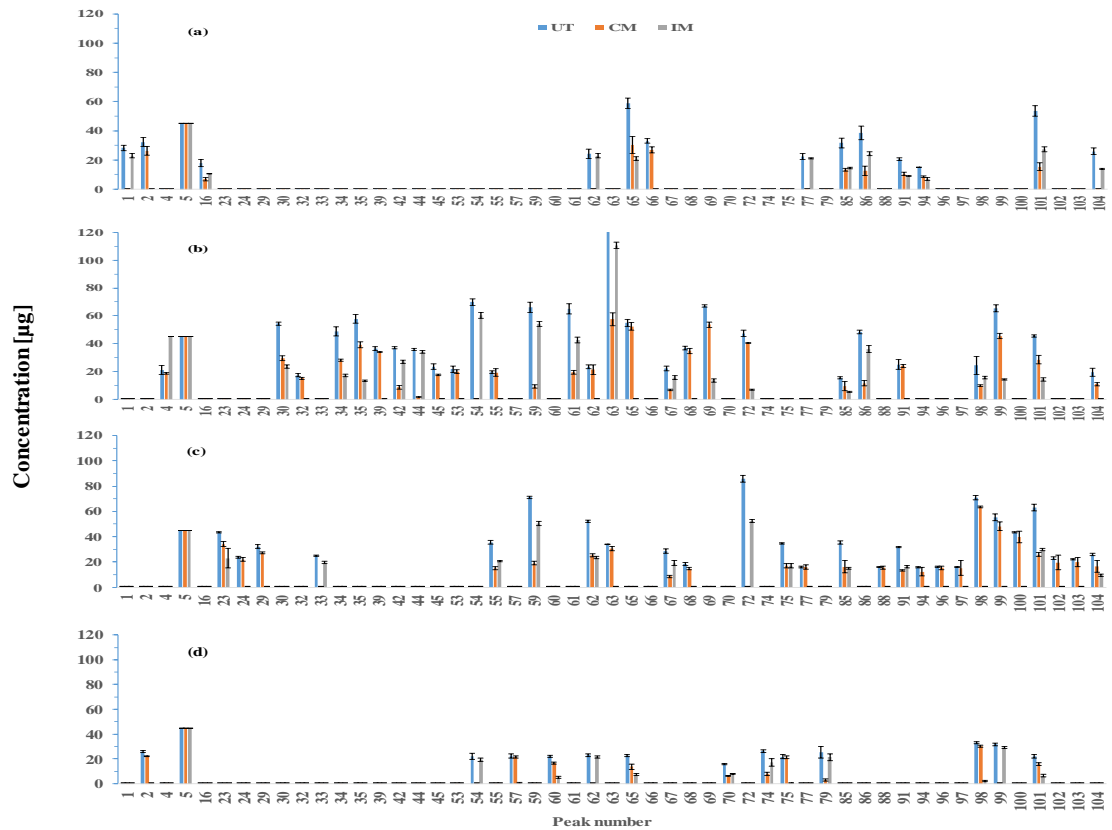
Figure 3.3   Distribution of compounds for different treatments (UT-untreated, CM-winnowed coarse material, IM winnowed interstitial matter) of a) EM (*E. marginata*), b) EW (*E. wandoo*), c) BM (*B. menziesii*) and d) AF (*A. fraseriana*). A minimum concentration of 0.001 g/kg was considered for comparison between the species.

3.3.3   Contribution of carbon pools to SWR

3.3.3.1   Effect of winnowing on SWR

The severity of SWR was assessed in different treatments, and it was observed that winnowing separates the soil into different components namely coarser mineral materials and finer interstitial matter, resulting in different carbon pools. For example, carbon content (TC) was higher in the winnowed interstitial matter (IM), followed by untreated soil (UT) and winnowed coarse material (CM). Moreover, washed coarse

mineral material (WS) was found both with the lowest SWR and TC values (Figure 3.4).

It was evident that the soil under different tree species had different SWR values and they were also different in different soil components. However, SWR is closely associated with the total carbon content (TC), and thus substantial contribution from the IM was identified in inducing SWR.
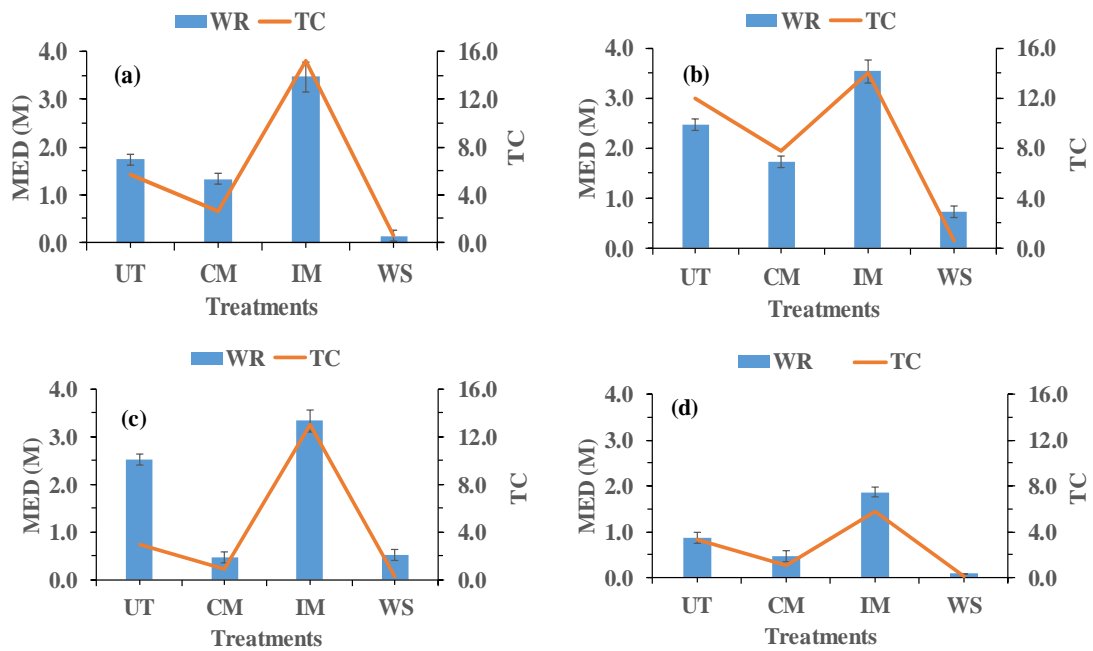
Figure 3.4   SWR and TC values under different treatments of a) *E. marginata* b) *E. wandoo* c) *B. menziesii* d) *A. fraseriana* (UT-untreated, CM-winnowed coarse material, IM- winnowed interstitial matter, WS- washed coarse mineral material, TC- carbon content, WR-water repellency).

3.3.3.2   Untreated soil (UT)

As noted in Section 4.2.3 the air dried field sample (UT) was diluted adding different proportions of AWS for each of *E. marginata*, *E. wandoo*, *B. menziesii* and *A. fraseriana*. SWR was measured both at standard laboratory temperature of 24°C and

following treatment with a higher temperature of 105°C. It was found that SWR was the greatest (2.53 M) under *B. menziesii*, compared to the other species whereas, the lowest was found under *A. fraseriana* (0.87 M) (Figure 3.5). SWR disappeared with the addition of 75% AWS for all the samples. Moreover, it disappeared with the addition of 50% AWS to the samples from *A. fraseriana*.
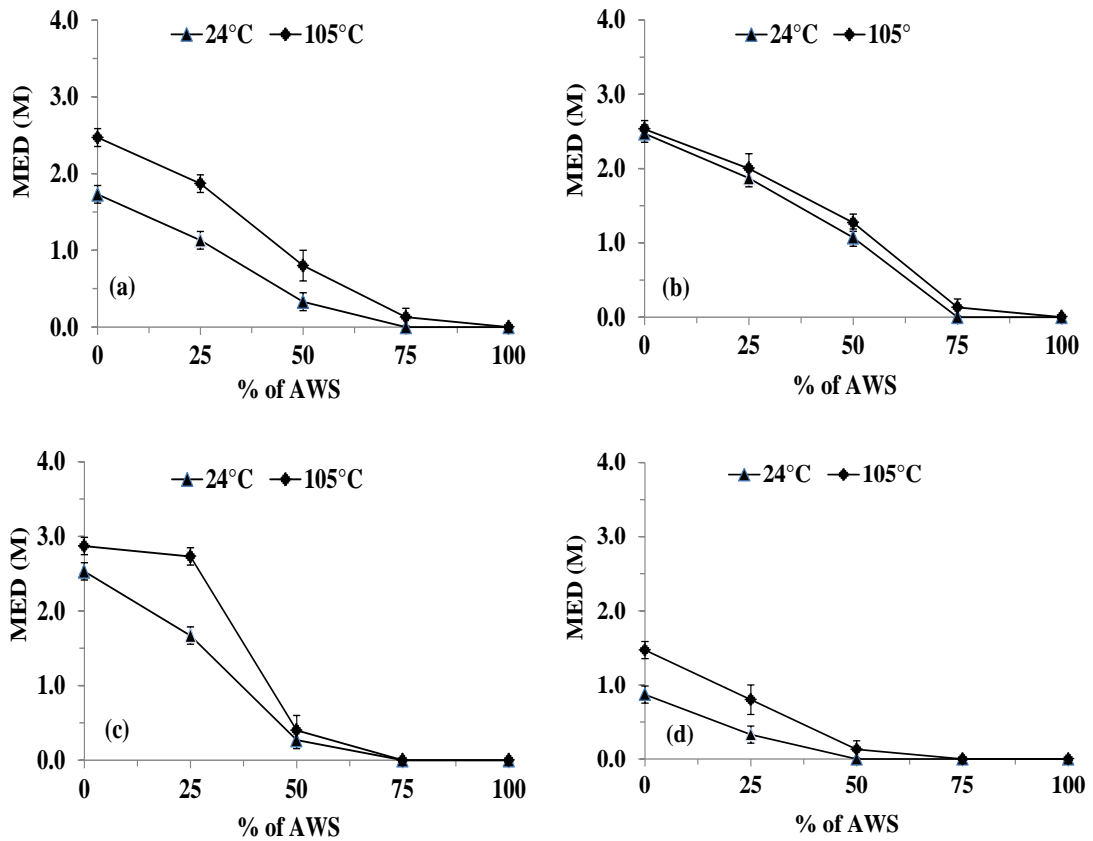
Figure 3.5   Dilution response of untreated (UT) sample a) *E. marginata* b) *E. wandoo* c) *B. menziesii* d) *A. fraseriana*.

The SWR value was found to be 1.73 M and 2.47 M for the samples collected from *E. marginata* and *E. wandoo,* respectively. The decreasing rate of the severity of SWR, with the addition of AWS for all the species, suggested that the carbon concentration makes a significant contribution to the incidence of SWR.

Moreover, when the untreated and diluted samples were heated at the higher temperature of 105°C, the severity of SWR increased. The SWR of all control samples at the higher temperature was found to be 2.47, 2.53, 2.87 and 1.47 M for the species of *E. marginata*, *E. wandoo*, *B. menziesii* and *A. fraseriana*, respectively (Figure 3.5). Interestingly, although SWR had disappeared with the addition of 75% AWS, it reappeared at higher temperature for the species of *E. marginata* (0.13 M) and *E. wandoo* (0.13 M).
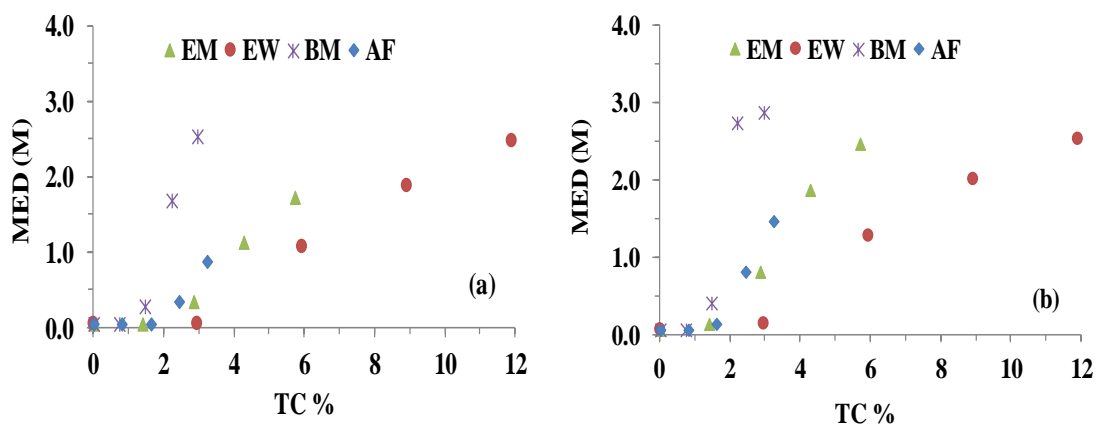
Figure 3.6   SWR against total carbon for untreated (UT) sample at a) 24°C b) 105°C, EM- *E. marginata;* EW-*E. wandoo;* BM- *B. menziesii;* AF- *A. fraseriana.*

Figure 3.5 shows the response to SWR with different proportions of AWS, the initial carbon concentrations are different for the four species. Thus, for Figure 3.6, SWR is compared to the final carbon content, this allowing comparison of the effect of carbon in inducing SWR for the different species.

It is clearly apparent that there are differences in the effectiveness of carbon in inducing SWR between species. SWR rapidly increased for *B. menziesii* with the increasing carbon content at 24°C (Figure 3.6a). Though the carbon content of the untreated sample under *E. wandoo* was higher than other species, the SWR only slowly increased with

increasing carbon content. The rate of increase in SWR with increasing carbon content was similar for *E. marginata* and *A. fraseriana*.

Interestingly, at the higher temperature of 105°C, the values of SWR were increased for all the species in comparison with that of 24°C (Figure 3.6b). The increasing severity of SWR suggested that as a result of heating at 105°C, the organic molecules rearranged themselves in the different soil components or the samples reached at hyper-dry conditions (Moody & Ebel, 2012).

There appeared to be a threshold amount of carbon, below which SWR did not occur. Based on the individual compound concentration usually found in hydrophobic soil, 0.001g/kg (0.01×10^{-6}mol/g) was considered for all the species, below which SWR did not occur (AT 3.1 of the Appendix). In Chapter 4 and 5, $0.25\text{-}20 \times 10^{-6}$ mol/g loadings of the individual and binary mixtures of the compound have been used for inducing SWR.

The threshold amount of carbon detected for the untreated samples for the 4 species investigated was 1.43, 2.98, 0.75 and 0.82%, respectively. However, for winnowed coarse materials the values were found as 1.29, 1.94, 0.70 and 0.80, respectively (Figure 3.6, 3.8).

3.3.3.3 Winnowed coarse mineral material (CM)

Winnowed coarse mineral materials (CM) were derived by removing interstitial matter from the soil matrix through winnowing. Given the sandy nature of the soils, these coarse materials were predominantly quartz.

The samples of winnowed coarse materials were then diluted with different proportions of AWS, using the same approach as for the untreated soil. It was found that the SWR

for the winnowed coarse materials of *E. marginata*, *E. wandoo*, *B. menziesii* and *A. fraseriana* were 1.33, 1.73, 0.47 and 0.47 M, respectively (Figure 4.7).

The SWR again disappeared at 75% addition of AWS for *E. wandoo* while it vanished with 50, 25, and 25% addition of AWS for *E. marginata*, *B. menziesii* and *A. fraseriana,* respectively. However, as for the untreated soil sample, the severity of SWR of winnowed coarse materials was enhanced after heating at the higher temperature of 105°C.
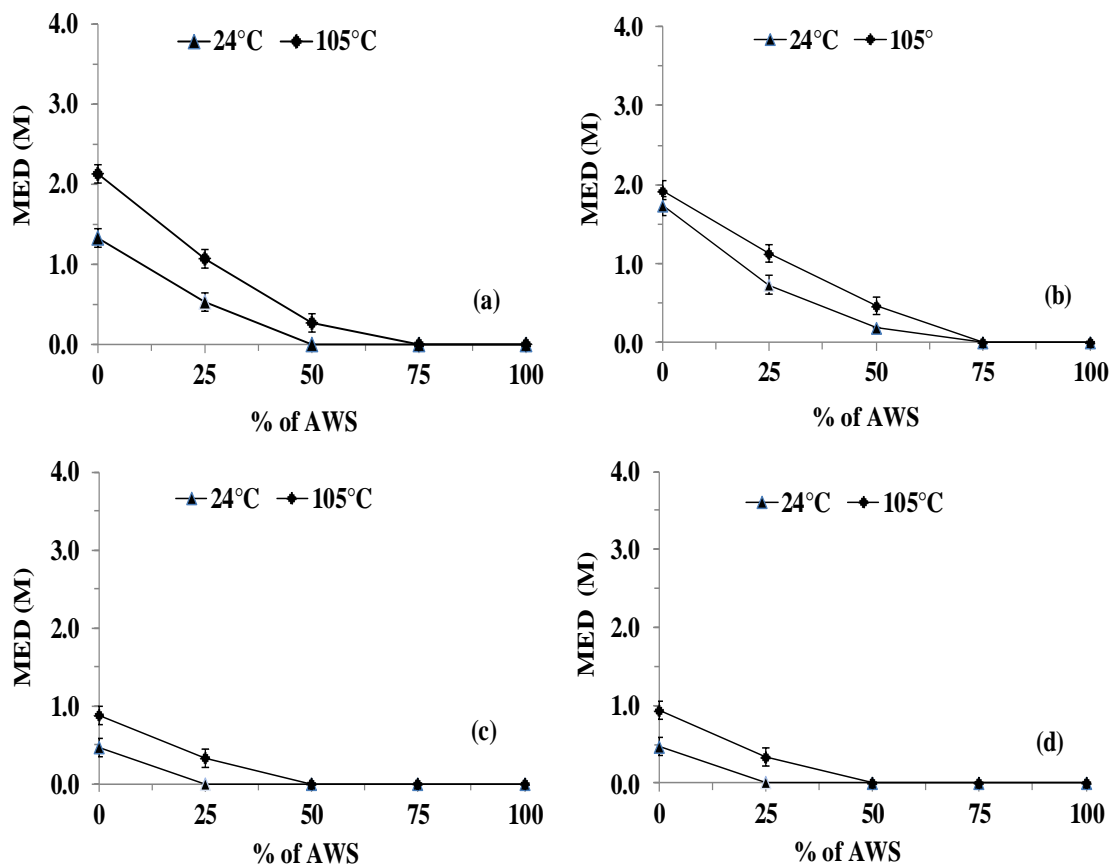
Figure 3.7   Dilution response of winnowed coarse material (CM) a) *E. marginata* b) *E. wandoo* c) *B. menziesii* d) *A. fraseriana.*

In particular, MED values of 2.13, 1.93, 0.87 and 0.93 M were found for *E. marginata*, *E. wandoo*, *B. menziesii* and *A. fraseriana*, respectively, after heating at this higher temperature (Figure 3.7). This suggests that heating provided the molecules sufficient

kinetic energy to reorient themselves on the soil particles and thus the severity of SWR was increased. This organo-mineral interaction at the molecular level is discussed in chapters 4 and 5.

The severity of SWR was investigated against the total carbon content across the entire dataset. Again, there were differences in the rate of increase in SWR with increasing increments of organic carbon between species.

It was revealed that SWR started to increase from < 2% TC for the winnowed coarse material (CM) samples derived from *B. menziesii* and *A. fraseriana* (Figure 3.8). However, it rapidly started to increase from ~2% TC of *E. marginata* while it was found to increase from ~4% TC for E. wandoo gradually. Importantly, the carbon content of the samples from *E. wandoo* was higher in comparison with that of other species, across all the samples investigated. The SWR in the coarse material of *E. wandoo* was 1.73M and 1.93M at 24°C and 105°C, respectively, with a carbon content of ~8%. However, it was found to be 1.33 (24°C) and 2.13M (105°C) for *E. marginata* with a carbon content of <3% TC (Figure 3.8).

After washing the winnowed coarse materials, the severity of SWR dropped to 0.13, 0.73, 0.53 and 0.09 M for *E. marginata*, *E. wandoo*, *B. menziesii* and *A. fraseriana*, respectively. The residual compounds detected in the washed sample were mostly long chained alkanes and some steroids (AF 3.1 of the Appendix).
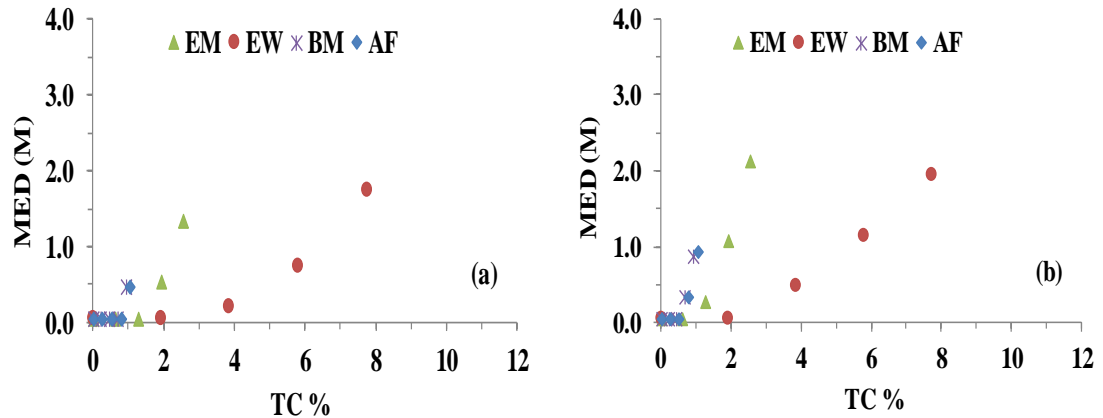
Figure 3.8 SWR against total carbon content for winnowed CM sample at a) 24°C b) 105°C, EM- *E. marginata;* EW-*E. wandoo;* BM- *B. menziesii;* AF- *A. fraseriana.*

3.3.3.4 Interstitial matter (IM)

Different proportions (w/w) of winnowed interstitial matter (IM) were added to AWS to examine the effect of carbon pools in inducing SWR. It was revealed that the addition at <5% of IM the severity of SWR started to develop for *E. marginata*, *E. wandoo* and *B. menziesii*. For those three species it was found that with the addition of 20% IM, the severity of SWR was found to increase to values greater than for the untreated (UT) soils (Figure 3.9 a, b, c).

However, when the winnowed IM from *A. fraseriana* was added to AWS there was a less marked increase in SWR, relative to the other species investigated. For example, the SWR only started to increase at >5% while the highest loading (20%) produced an MED of around 1.0M (Figure 3.9d).
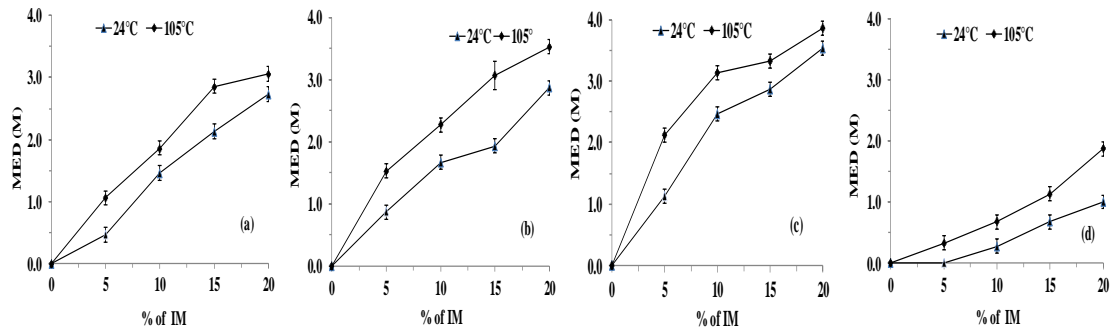
Figure 3.9   Effect of winnowed interstitial matter (IM) derived from a) *E. marginata* b) *E. wandoo* c) *B. menziesii* d) *A. fraseriana* on SWR.

It was evident that SWR increased with increasing carbon content for all species (Figure 3.10a). However, the responses of *E. marginata, E. wandoo*, and *A. fraseriana* were very closed to each other compared to that of *B. menziesii* , suggesting the importance compound composition in the incidence of SWR.

Importantly, the carbon content of the added IM was found to be ~3% for all the species except *A. fraseriana.* At the higher temperature of 105 °C the severity of SWR was slightly increased, and this supports our previous findings of enhanced severity of SWR following drying at higher temperature (Figure 3.10b).
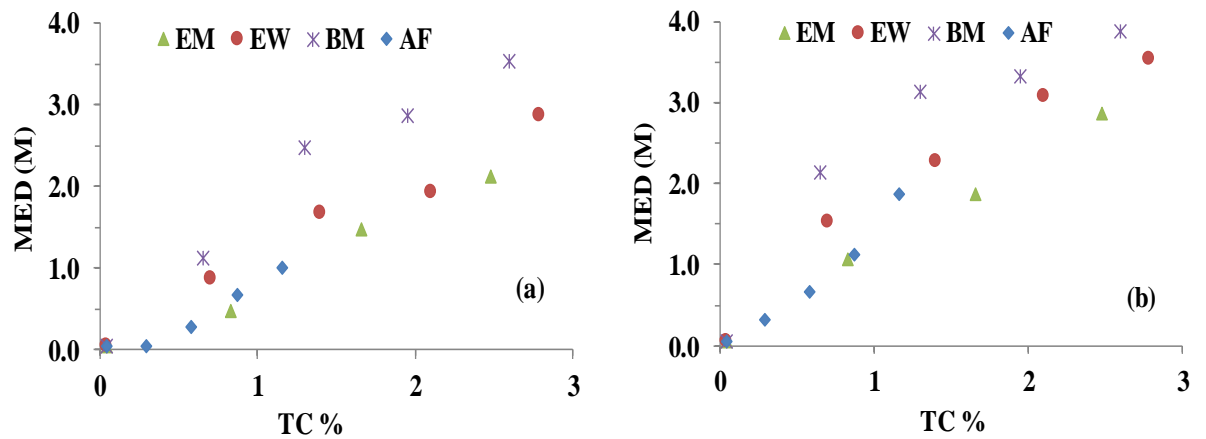
Figure 3.10   Effect on repellency (MED) of increasing total carbon of interstitial matter (IM) at a) 24°C b) 105°C, EM- *E. marginata;* EW-*E. wandoo;* BM- *B. menziesii;* AF- *A. fraseriana.*

The SEM images of untreated, winnowed coarse material and winnowed interstitial matter of *A. fraseriana* revealed the dominance of quartz like particle (Figure 3.11a, b, c). Moreover, the image of the ash content (Figure 3.11d) derived through TGA analysis was found to be similar in shape with that of the acid washed sand (Figure 3.11e). This implies quartz dominated soil particles of the collected samples from *A. fraseriana*.

85

| (a) UT | (b) CM | (c) IM | (d) Ashes of IM | (e) AWS |
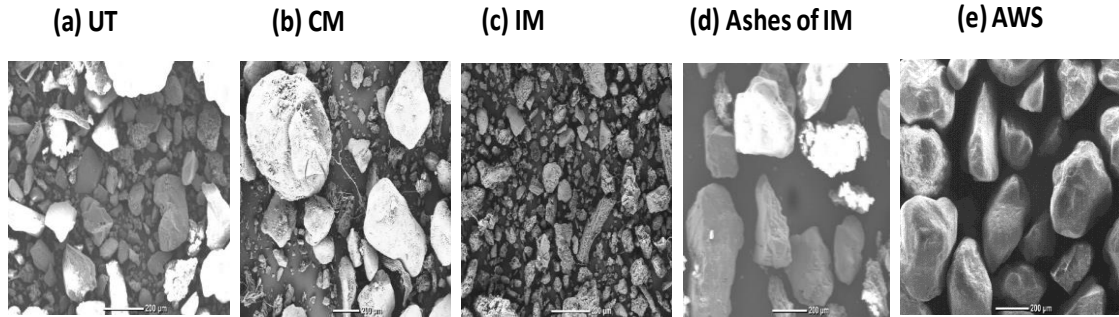
Figure 3.11   SEM images for the samples of A. fraseriana a) untreated (UT) soil, b) winnowed coarse material c) winnowed interstitial matter (IM), d) ash content of IM after TGA, and e) acid washed sand (AWS). All these images are at the same scale (200μm).

3.3.4   *Effect of a wetting and drying cycle on SWR*

The untreated soils were wetted up and dried at 50°C to examine the distribution of compounds and consequent changes in the severity of SWR. Moreover, entire diluted samples after adding different proportions of AWS to untreated soils, were treated in the same way for each of *E. marginata*, *E. wandoo*, *B. menziesii* and *A. fraseriana*. Importantly, it was found that after wetting up with DI water and drying, the severity of SWR decreased. For example, the intensity of SWR was reduced from 1.73 to 0.73 M for the untreated (UT) control of *E. marginata*. The SWR values for other species were also found to decline relative to their control samples with values of 0.0, 1.47 and 0.47M for *E. wandoo*, *B. menziesii* and *A. fraseriana*, respectively (Figure 3.12). However, at the higher drying temperature of 105 °C the severity of SWR was found to increase for all species gradually.
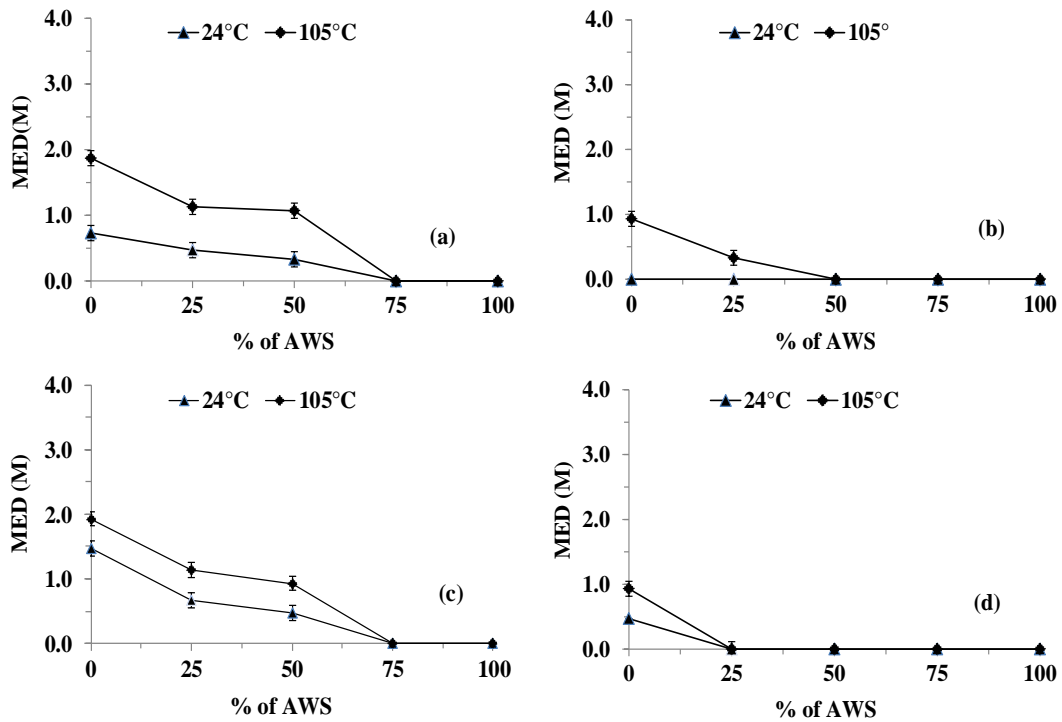
Figure 3.12   Change in SWR for untreated (UT) samples of a) *E. marginata*, b) *E. wandoo*, c) *B. menziesii* and d) *A. fraseriana* following wetting and then drying at 24°C and 105°C.

Moreover, when the winnowed coarse materials (CM) were wetted up and dried, the severity of SWR was changed. For example, the severity of SWR for all control samples of the species of *E. marginata*, *E. wandoo*, *B. menziesii* and *A. fraseriana* was found as 0.53, 0.0, 0.0 and 0.2 M, respectively (Figure 3.13). However, at the higher temperature the severity of SWR was slowly increased, but not to the values of the samples that had not been subjected to a wetting and drying cycle (Figure 3.7).
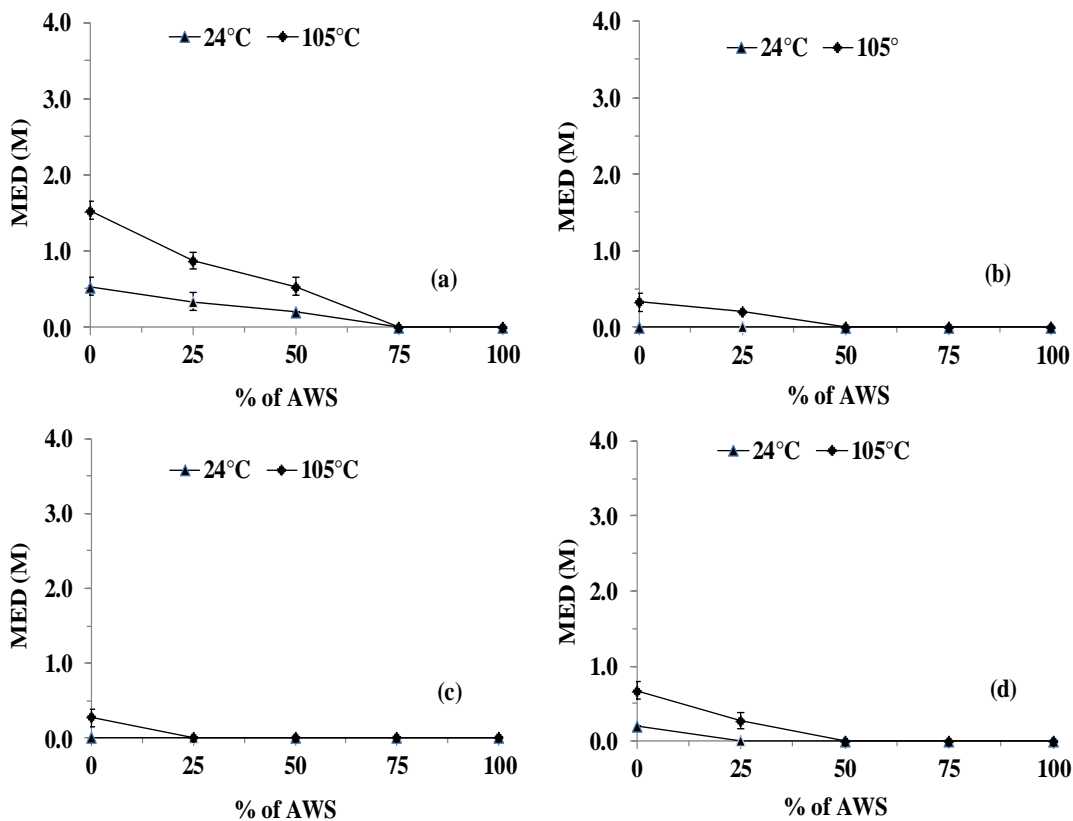
Figure 3.13   Redistribution of compounds for winnowed CM of a) *E. marginata* b) *E. wandoo* c) *B. menziesii* d) *A. fraseriana* after wetting and drying.

3.3.5 *Effect of an increasing temperature on SWR of interstitial matter (IM)*

The samples made with the mixture of AWS and 10% interstitial matter (IM), were directly heated to a range of temperatures to investigate the changes in the severity of SWR after heating. As noted in the previous section, untreated (UT) and winnowed coarse materials (CM) had larger SWR values at 105°C, therefore, the samples of AWS with the loaded interstitial matter (IM) were also heated at the higher temperature. However, in this case the samples were heated at a range of temperatures (50, 100, 150, and 200°C) in order to examine if there were differences in the distribution of compounds from the loaded IM. A gradual increase in the severity of SWR was observed up until ~150°C then there was an evident decrease at 200°C (Figure 3.14a).

88

TGA analysis of the winnowed interstitial matter (IM) found the lowest deviation in weight for *A. fraseriana* compared with the other species, over the increasing temperature of 25-1000°C (Figure 3.14b). The low mass loss (~12%) suggested a lower carbon pool, which corresponds with the lower severity of SWR .
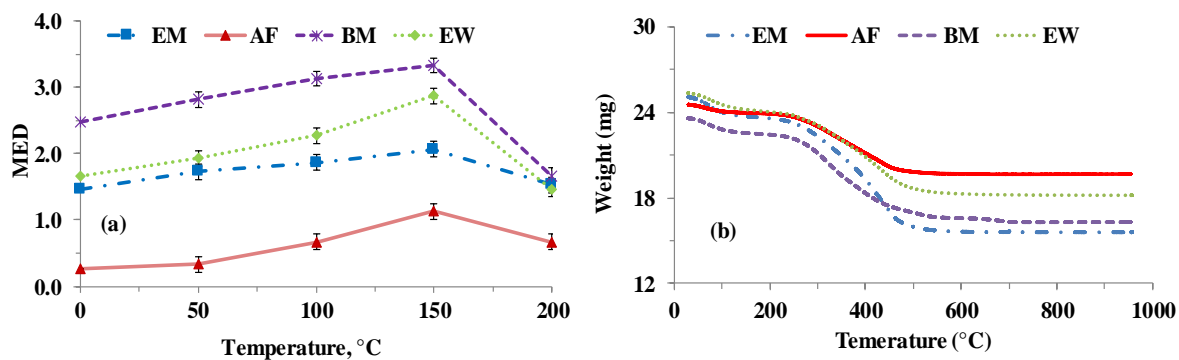
Figure 3.14   Distribution of compounds after heating a) loadings with 10% IM on AWS and b) TGA analysis of IM, where EM- *E. marginata*, EW-*E. wandoo*, BM-*B. menziesii* and AF-*A. fraseriana*.

3.4 Discussion

3.4.1 Compounds causing SWR

This study has shown that the composition of organic matter and different levels of carbon pools can significantly modify the severity of SWR under native plant species in the south-west of Western Australia. The predominant compounds detected in the entire soil samples were straight and branched chain fatty acids and esters, phytols, phytanols, sterols, alkanes, amides, acetates and aldehydes or ketones. All the soil samples except those collected from *A. fraseriana*, contained long chain fatty acids (C_{18} -C_{26}) and phytanols (C_{16} - C_{22}). The chain length distribution of fatty acids is similar to the study of Ma'Shum et al. (1988) with mostly even-numbered long chain fatty acids present, but with chain lengths of 16-32 carbon atoms. Long chain fatty acids and alkanes were also detected in the previous studies as the dominant cause of inducing SWR (Franco et al., 1995; Horne & McIntosh, 2000; McKissock et al., 2003). Moreover, long chain fatty acids and alkanes are also reported to originate from exudates derived from plant cuticles (Hayes, 1998).

Besides, a range of amides (C_6 - C_{22}), mostly of similar chain lengths to the acids, higher chain length alkanes ($C_{24} - C_{44}$), esters ($C_{17} - C_{35}$), ketones ($C_{19} - C_{29}$) and more complex acetate and a ring containing structures were also detected. Franco et al. (2000b) also found the distribution of even-numbered alkanes with 20-26 carbons, in the organic fractions, responsible for SWR in some Australian sandy soils. It is noteworthy that all samples collected from beneath 4 native species contained hydrophobic compounds (e.g., alkanes), which are closely associated with the incidence of SWR. Baldock et al. (1992) reported that the presence of the polymethylenic moieties is characteristic of the decomposition sequence of plant materials in soils. Most plant

hydrocarbons are usually straight chain, saturated compounds with long chain carbon atoms (Eglinton et al., 1962).

The significant difference between *A. fraseriana* and the other three native species (*E. marginata*, *E. wandoo* and *B. menziesii*) was the presence of long chain fatty acids and fatty alcohols. Capriel et al. (1995) reported that hydrophobic soils are found to contain relatively higher ratios of alkyl C that is accountable for the incidence of SWR. However, these dominant waxy compounds were mostly absent in the *A. fraseriana* and it can be assumed that their presence in significant amounts is necessary to get the enhanced severity of SWR into the soil. The particular compound composition of the investigated species is consistent with the study of Mainwaring et al. (2013) that the extent of SWR induced on AWS depends on the presence of specific compounds.

3.4.2   Contribution of carbon pools

The variations in the concentration profile of different treatments indicate that coating around soil particles as well as interstitial organic matter within soil pores have combined effects on the incidence of SWR. Doerr et al. (2000) have also suggested that accumulation of the small amount of hydrophobic particulate matter within the soil pores, rather than coating individual grains, can modify the level of SWR. For example, due to the difference in the degree of carbon pools between the treatments, similar compounds were found with different concentrations. Franco et al. (2000b) suggested that constituents present in all of the plant derived materials have very similar chemistry and are often homologous series of constituents but with different concentrations.

The physical dilution of untreated and winnowed samples with AWS was found to reduce SWR, suggesting the level of carbon pools has implications on the development of SWR. Interestingly, the SWR disappeared at 75% dilution with AWS but once again

91

reappeared after heating at 105°C for the species of *E. marginata* (0.13M) and *E. wandoo* (0.13M). SWR has also been previously reported to fluctuate both spatially and temporally in samples collected from beneath the *E. globulus* plantations even in other regions with Mediterranean climate (Coelho et al., 2005; Doerr et al., 1998; Ferreira et al., 2000; Rodríguez-Alleres & Benito, 2011).

The response of SWR with increasing carbon content in the untreated samples varied between the species, suggesting relative importance of particular compounds, combination or composition of compounds and particle size distribution to the development of SWR. Importantly, at a higher temperature of 105°C, the severity of SWR was increased for all the species. The increased severity of SWR in the untreated samples is consistent with the previous study of Franco et al. (1995) that during heating, waxes from particulate organic matter migrate onto soil particle surfaces, thereby increasing SWR. Moreover, the changing severity of repellency can be associated with the moelcular arrangement on the soil surafces, which is in agreement with the suggestion of Doerr et al. (2000) that upon drying amphiphilic molecules reorient with their polar ends attached to the mineral surface, and the nonpolar ends are oriented outwards. The severity of SWR for the winnowed coarse materials of *E. wandoo* was MED- 1.73M at 105°C, with ~8% TC. Thus the association of SWR with carbon content again suggests compound composition has greater implications in the incidence of SWR. Interestingly, the MED was 2.13M with the addition of ~2% TC from *E. marginata*. Thus it suggests that OC beneath *E. marginata* has more hydrophobic compounds per unit than that of *E. wandoo.* However, the amount of hydrophobic materials might affect the severity of repellency by not only covering the coarser, but also much of the finer-sized particles with an organic coating (Doerr et al., 1996).

With increased loadings of winnowed interstitial matter onto AWS, the severity of SWR sharply increased for *E. marginata*, *E. wandoo* and *B. menziesii*. However, it was found to only slowly increase for *A. fraseriana*. The slower rate suggests that carbon content and composition for *A. fraseriana* differ from the other species. For example, there were not any long-chain fatty acids and alcohols observed at or above the minimum concentration level (0.001g/kg) considered. However, soil texture and particle size distribution can also modify the severity of SWR as evident through the response in the dilution experiments. For example, amphiphilic molecules usually have lower surface interaction to the nonpolar surface of quartz in comparison with polar like kaolinite surfaces.

The ash content derived from TGA analysis did not contain any elements like Ca and K in the winnowed interstitial matter of *A. fraseriana*, suggesting quartz dominated the soil, which again implied the importance of soil particles in the severity of SWR. Furthermore, when SWR was examined against corresponding carbon content of IM, the severity of SWR of *B. menziesii* was found higher, compared to other species. The close association of SWR with carbon content suggests that small amount of hydrophobic compounds and their arrangement on soil particles can significantly modify the incidence of SWR. Importantly, despite the closer carbon content between *E. wandoo* and *B. menziesii* at the highest loadings, the severity of SWR was different. Moreover, at the highest loading of interstitial matter, the severity of SWR was similar for different carbon contents between *E. marginata* and *E. wandoo*. This discrepancy again suggests, SWR is either affected by small amounts of hydrophobic compounds or that the composition of the organic matter is causing SWR. This difference in the severity of repellency is also consistent with the previous findings (Doerr et al., 2000; Franco et al., 2000b).

Water is considered to move freely as vapor in a water repellent soil allowing soil water to be redistributed (Barrett & Slaymaker, 1989). The untreated and winnowed samples were wetted up and dried at 50°C. The consequent severity of SWR was found to be reduced from their original counterparts. The difference in SWR suggests, the molecules were redistributed within the samples or possibly due to rearrangement on the soil particles. Soil moisture was also found to be closely associated with SWR in the study of King (1981). Moreover, heating the mixture of AWS with interstitial matter (10%) at a range of temperatures (e.g., 50, 100, 150, and 200°C) was found the change in the severity of SWR. A gradual increase in the severity of SWR was observed for all species up to 150°C while at 200°C there was an evident drop. The changing severity of SWR suggests that after having sufficient kinetic energy at a higher temperature, the molecules reorganize themselves on soil particles. The temperature effect on SWR was also evident for *E. wandoo* and *B. menziesii* after heating the winnowed coarse material at 105 °C. Apart from redistributing and concentrating in the soil, heating can improve the bonding of hydrophobic substances to soil particles (Savage et al., 1972). TGA analysis of the winnowed interstitial matter also indicated the level of carbon pools and their distributions can significantly modify the severity of SWR.

Finally, SWR is very dynamic, and the severity of SWR can be changed due to the compound composition and particle size distributions. The relative importance of compounds and their concentrations is also crucial in causing SWR. This organo-mineral interaction at the molecular level will be presented in the next chapters.

4 Role of biogenic volatile organic compounds (BVOCs) derived from vegetation fire in inducing soil water repellency (SWR)[1]

4.1 *Introduction*

Biogenic volatile organic compounds (BVOCs) are non-methane hydrocarbons generally produced by plants (Ciccioli et al., 2014). Although they are continually emitted from almost all types of plants, substantial amounts are also released during vegetation fires (Maleknia et al., 2007). The eucalypt-dominated vegetation of Australia produces and emits a large number of BVOCs including plant specific isoprenoids (isoprene (C_5H_8), monoterpenes ($C_{10}H_{16}$), sesquiterpenes ($C_{15}H_{24}$)), and a range of other classes of compounds (organic acids, aldehydes, ketones and alcohols) into the ambient atmosphere (Maleknia et al., 2009).The annual release of BVOCs in Australia is estimated to be at the teragram scale (10^{12} g) (He et al., 2000).

In addition to releasing BVOCs, different types of vegetative cover (*Eucalyptus*, *Pinus*) are also found to release less volatile compounds such as phytanols and fatty acids that induce SWR (Crockford et al., 1991; Ferreira et al., 2000; Keizer et al., 2005a). Consequently, long unburned eucalypt stands are often associated with very high SWR levels under dry summer conditions in Australia, South Africa and Portugal (Doerr et al., 2006; Doerr et al., 1998; Scott, 2000). Soil mineral or aggregate surfaces are also

---

[1] **Uddin, S.M.M.**, Daniel, N., Harper, R.J. and Henry, D.J. (2017). Why do biogenic volatile organic compounds (BVOCs) derived from vegetation fire not induce soil water repellency? *Biogeochemistry* **134**, 147-161.

widely recognized as being a crucial factor in the expression of SWR (Doerr et al., 2000). In particular, soils with coarser particles are usually more susceptible to coating with hydrophobic compounds, due to their smaller surface area per unit volume, in comparison with their finer counterparts (Giovannini & Lucchesi, 1983). SWR is thus most likely to develop in sandy soils but the severity of SWR can be influenced by very small changes in clay content (Harper et al. 2000). SWR is generally quantified using the Molarity of an Ethanol Drop (MED) test. This test involves adding water/ethanol drops with increasing ethanol concentration, and thus lowering surface tension, until a mixture is identified that enables the drop to penetrate the soil surface within a specified time. The molarity of the ethanol drop is then reported as a measure of SWR (King, 1981).

Vegetation fires can significantly modify soil physicochemical properties including altering the total soil carbon content and altering the level of SWR (DeBano & Rice, 1973; Heath et al., 2015; Sheridan et al., 2007). Specialized post fire persistence traits (e.g., re-sprouting and seed banking in the soil and canopy) make plant communities resilient to periodic vegetation fires (Syphard et al., 2009). However, large increases in SWR can make the whole ecosystem non-resilient (Doerr et al., 2004) because variations in severity of repellence can significantly alter soil hydrological properties, such as overland flow generation and infiltration (Coelho et al., 2005; Prats et al., 2012). Furthermore, vegetation fire can alter the dynamics of SWR depending on fire temperature, duration and vegetation types (Doerr et al., 2004; Heath et al., 2015). For example, moderate temperature burns (soil temperature 175 – 300°C) on soils that already exhibit non-wetting characteristics generally leads to an increase in SWR. However, high temperature (>300°C) can reduce or eliminate SWR due to combustion of hydrophobic organic coatings on soil particles (DeBano, 2000). It has also been found

that pyrolytic compounds in volatilized fractions released above 350°C from chapparal soils from California, induced slight SWR to wettable sand, but the treated sand became highly repellent when heated at 300°C for 10 min (Savage et al., 1972). Furthermore, SWR of sandy forest soils from Slovakia was found to increase as the soil temperature reached 175°C (Dlapa et al., 2008), but was largely eliminated at higher temperatures (280-400°C) (DeBano & Krammes, 1966). The elimination of SWR in eucalypt stands during vegetation fire has also been observed at a depth of 3-5 cm (Doerr et al., 2006; Scott, 1993). Nevertheless, SWR also varies with heating duration, the physical and chemical attributes of the soil particles and the time after cooling (equilibration time) that the SWR measurement is made (Arcenegui et al., 2007; Doerr et al., 2004). The downward movement of heat through the soil even after vegetation fire can re-volatilize some of the hydrophobic substances that can further intensify the hydrophobic layers (Savage, 1974).

Smoke-derived compounds are known to collect in soil and in fact are essential for the germination of some Australian native species as a seed pre-treatment (Dixon et al., 1995; Tieu et al., 1999). The heat during a fire is also widely reported to redistribute and alter the concentration of hydrophobic substances in the soil. However, it is unknown whether fire induced increases in SWR are due to addition of smoke-related compounds to the soil or simply due to heat induced rearrangement of the amphiphilic molecules (e.g. phytanols and fatty acids) already present in the soil. Therefore, we have undertaken a combined experimental and theoretical study to identify the role that smoke-related compounds may play in SWR. Accordingly, we have identified from the literature a selection of common non-pyrolytic smoke-related compounds (terpenes and alcohols) that have significant atmospheric lifetimes (~1.5 to 24 h). For comparison, we have also included a fatty acid known to induce SWR. Experimental loadings of the

compounds onto acid washed sand (AWS), and molecular dynamics simulations were performed in order to determine (a) the potential of each compound to induce SWR under identical conditions (25 °C), (b) to investigate the effects of heating (105°C) on SWR for different loadings of these compounds and (c) to identify the molecular level interactions of the different compounds with sand particle surfaces using molecular dynamics.

4.2 Methods

4.2.1 Experimental assessment of water repellency (SWR)

Many of the organic compounds selected for this study have previously been identified as components of smoke from vegetation fire e.g. terpenoids (cis-3-hexen-1-ol (3HexOH), levoglucosenone, 2-methyl-3-buten-2-ol (2MBuOH), cineole, α-phellandrene and α–terpinene) (Ciccioli et al., 2014; Maleknia et al., 2009; Zini et al., 2001). Furthermore, palmitic acid is commonly identified in hydrophobic soils both before and after fire events (Atanassova & Doerr, 2011; Doerr et al., 2005; Franco et al., 2000b; Morley et al., 2005).

The selected compounds were applied on medium grained acid washed sand (AWS) (300-350 µm diameter range) with different loading ranges of 1 to 20×10^{-6} mol g^{-1}, commensurate with previous studies (Mainwaring et al., 2013). The loading range chosen was comparable to previous studies and is based on average loadings of organic compounds identified from a range of sandy soils before a fire event (Doerr et al. 2005; Morley et al. 2005). The standard procedure involved preparing a stock solution of the selected compound in tetrahydrofuran (THF) (4×10^{-4} M), followed by preparing standards to achieve specific loadings. The solutions (50 mL) were then applied to AWS (40 g) in a round bottom (RB) flask and thoroughly mixed for 10 minutes without

reduced pressure. The loaded AWS samples were then separately dried in a rotary evaporator at 45°C under reduced pressure.

For each compound ~ 20g of loaded AWS was placed in a petridish (50 × 10mm) and put into a desiccator for around four hours following rotary evaporation, in order to make the sample free from humidity and thereby eliminate any effects of pH (Smith & Tanford, 1973). A second sample with the same loading of compound was placed into oven at 105°C for 24 hours. The oven-dried sample was then cooled to room temperature in a desiccator. The surfaces of the samples were levelled by gently tapping on the bench and in some cases a light pressure was applied with a small flat bottom beaker in order to make the surface smooth and uniform. The severity of SWR of each of the loaded samples was assessed using the molarity of ethanol droplet (MED) test (King 1981). A stock solution of 4M ethanol was prepared and solutions were made at concentrations between 0 and 4M, with increments of 0.2M. Starting from the lowest ethanol concentration, at least three droplets (50µL) of the prepared solutions were then applied to the surface of the loaded samples, from 5mm height. The time required for each drop to penetrate the surface was recorded. The lowest concentration for which the infiltration time was <10 s was considered as the MED value for that sample (King, 1981). SWR of the samples was then classified according to a scheme similar to that proposed by Mao et al. (2015), where a MED of <0.5 M corresponded to wettable and a MED >3.5 M to extreme SWR.

4.2.2 Computational methods

Molecular dynamics simulations were performed to explore the nature of the interactions for a selection of the compounds on the quartz surface. The modelling framework for both the surface and molecules was developed using Materials Studio v

99

7.0 (Accelrys, 2013). The surface of a sand particle was represented by a cleaved quartz surface. Models of BVOCs included cis-3-hexen-1-ol (3HexOH), levoglucosenone, 2-methyl-3-buten-2-ol (2MBuOH) and cineole. We also constructed a model of palmitic acid (1-hexadecanoic acid). Furthermore, since none of the BVOCs contain an acid functional group, 1-hexadecanol was included in the modeling studies to identify any differences in the interactions of acid and alcohol functionalized molecules. Different loadings of compounds (0.1 – 5.0 molecules nm^{-2}) were achieved by placing different numbers of molecules on the quartz surface. Each simulation was placed in a unit cell with dimensions 30.7 x 37.3 x 70.0 Å. The large z-dimension ensures that adjacent cells do not interact along the z-axis when periodic boundary conditions are applied, resulting in a quasi-2D interface.

The potential energy for each simulation was calculated using the COMPASS force field (Sun, 1998), which has previously been shown to perform well for describing the interactions between condensed hydrophilic and hydrophobic surfaces (Henry et al., 2006; Henry et al., 2005; Shaw et al., 2013). Electrostatic interactions were calculated using the Ewald procedure, while van der Waal's interactions were calculated with an atom-based procedure using a 12.50 Å cutoff, a spline width of 1.00 Å, a buffer of 0.50 Å and a long-range tail correction. The modelled interfaces were initially energy minimized using the conjugate-gradient procedure, with a convergence criterion of 0.04 kJ mol^{-1}. Molecular dynamic simulations were performed in the canonical ensemble (NVT, constant number of atoms (*N*), volume (*V*) and temperature (*T*)), equilibrated for 500 picoseconds (ps), followed by data acquisition for 4500 ps using 1.0 femtosecond (fs) time steps. The temperature was maintained at 298 K using the Andersen thermostat (Andersen, 1980) with a collision ratio of 1.0.

Concentration profiles of the quartz and BVOCs components were found by averaging the number of atoms in strips (parallel to the x-y plane) over the course of the molecular dynamic simulations. The interface region of each simulation is arbitrarily considered as the region of coexistence of the two components (surface/BVOCs) and is quite narrow (~0.05 Å), due to the rigidity of the quartz surface. Interactions between surface atoms and BVOCs in our study were investigated using radial distribution functions (RDFs) ($g(r)$) (Chandler, 1987).

The average interaction energy (E_{int}) was determined over the final 500 frames of the molecular dynamics (MD) trajectories as:

$$E_{int} = (E_{quartz} + E_{molecules} - E_{total})/n \qquad (1)$$

where E_{quartz} is the potential energy of the quartz surface, $E_{molecules}$ is the potential energy of the molecules, E_{total} is the total potential energy of the simulation and n is the number of organic molecules in the simulation cell. The interaction energy therefore quantifies the strength of the non-bond interactions (electrostatic and van der Waals (vdW)) between the molecular layer and the quartz surface. The van der Waals contribution ($W_v(d)$) was interpreted using the Hamaker relationship for two surfaces (quartz and organic molecular layer) (Hamaker, 1937):

$$W_v(d) = A_{12}/12\pi d^2 \qquad (2)$$

where A_{12} is the Hamaker constant and d is the interfacial separation. The Hamaker constant is determined by the properties of the materials in the two surfaces according to:

$$A_{12} = \pi^2 C_{12}\rho_1\rho_2 \qquad (3)$$

where ρ_1 and ρ_2 are the density of atoms in the quartz and molecular layer, respectively, and C_{12} is the coefficient of the interatomic pair potential of the atoms in the layers, which is related to the chemical composition.

4.3 Results and Discussion

4.3.1 Experimental water repellency (SWR) assessment
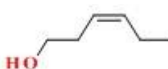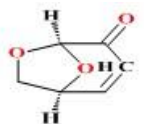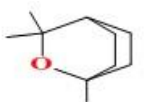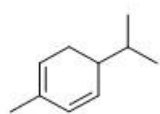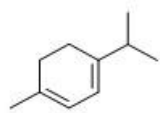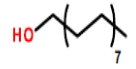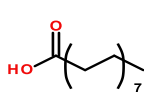
The 6 smoke related BVOCs selected for this study (cis-3-hexen-1-ol (3HexOH); levoglucosenone; 2-methyl-3-buten-2-ol (2MBuOH); cineole; α-phellandrene; α–terpinene) were chosen because they are non-pyrolytic species that have significant atmospheric lifetimes (~1.5 to 24 hours) and represent a range of different classes including terpenes and alcohols. Within this group, the variations include linear (cis-3-hexen-1-ol), branched (2-methyl-3-buten-2-ol), cyclic (α-phellandrene and α–terpinene) and bicyclic (levoglucosenone and cineole) structures with alcohol, alkene, carbonyl, and ether functional groups (Table 4.1).

Cineole, α-phellandrene and α-terpinene are all hydrophobic hydrocarbons with melting points less than 100 °C and boiling points of ~175 °C. Therefore, these compounds should have similar levels of intermolecular interactions and be present as oil or wax-like phases (Horn et al., 1964). However, when Cineole, α-phellandrene and α-terpinene were applied to AWS they were found to have an insignificant effect on SWR (Figure 4.1a).

Cis-3-hexen-1-ol (3HexOH), levoglucosenone and 2-methyl-3-buten-2-ol (2MBuOH) are amphiphilic compounds and the polar functional groups in these molecules should be attracted to the mineral surface, with the non-polar portion creating a hydrophobic layer that might be expected to induce SWR (Horne & McIntosh, 2000). However, cis-3-hexen-1-ol, levoglucosenone and 2-methyl-3-buten-2-ol made no significant change

to the wettability of AWS (Figure 4.1a) at loadings of 1 to 20×10^{-6} mol g^{-1}. Additional loadings were investigated up to 500×10^{-6} mol g^{-1} but there remained no significant change in the wettability, confirming the inability of these compounds to induce SWR. Palmitic acid (PA) was found to significantly induce SWR, even at low loading levels (1 x 10^{-6} mol g^{-1}) (Figure 4.1a), consistent with previous studies (Mainwaring et al., 2013).This induction of SWR has generally been attributed to the strong attachment of the polar head groups (-COOH) to the surface of the sand particles, combined with alignment of the long non-polar tails to give hydrophobic condensed films (Mainwaring et al., 2013; Shaw & Costello, 1993). Although the inter-molecular interactions in the pure compounds may be similar across the series of molecules, the above results suggest that the interactions with the sand particles differ significantly.

Table 4.1   Chemical structure of BVOCs (1-6) and long-chain hydrophobic compounds (7-8) applied and respective application rates to acid washed sand (AWS).

	Compound	n* (molec. wt)	Structure	Melting point, m.p. (°C)	Boiling point, b.p. (°C)	SWR class at 105°C
1	2-methyl-3-buten-2-ol	5 (86.13)		-28	99	Wettable
2	Cis-3-hexen-1-ol	6 (100.16)		-61	156.5	Wettable
3	Levoglucosenone	6 (126.11)		0	115 (at 10 mm Hg)	Wettable
4	Cineole	10 (154.25)		1.5	176	Wettable
5	α-Phellandrene	10 (136.23)		55	175	Wettable
6	α-Terpinene	10 (136.23)		61	174	Wettable
7	1-Hexadecanol	16 (242.45)		49.3	344	Extreme
8	Palmitic acid	16 (256.42)		63	351	Extreme

* n is the number of carbon atoms per molecule
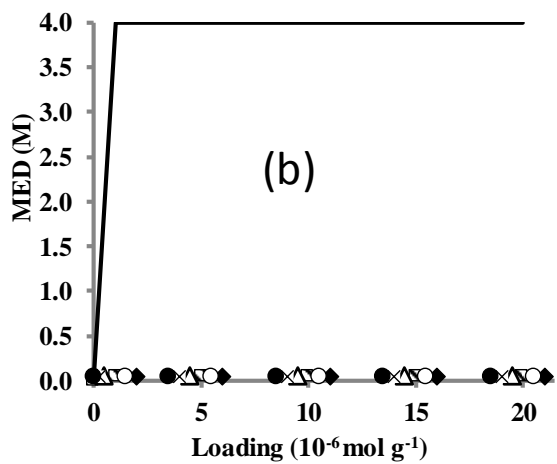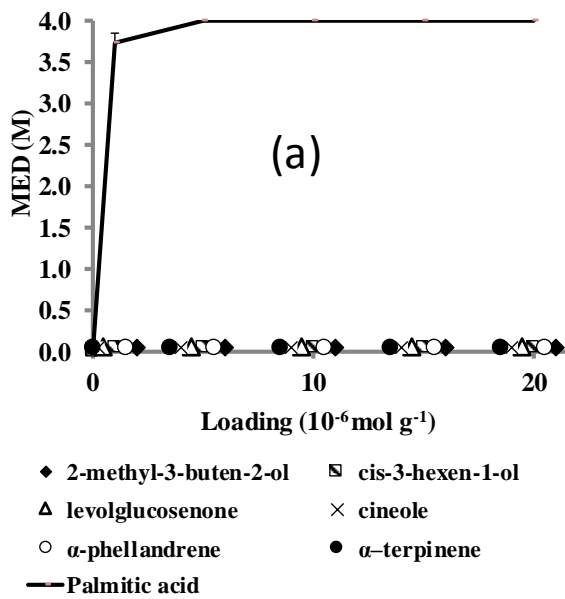
Figure 4.1   Effect of selected organic compounds on the wettability of acid-washed

sand (AWS) at a) 25 °C and b) 105°C following desiccation.

Heating was found to have no effect at all on the SWR of the BVOCs, which remained

non-repellent. SWR was enhanced for low concentrations of applied palmitic acid

following treatment at 105°C (Figure 4.1b). This enhancement of SWR may be the

result of the thermal rearrangement of organic molecules on the sand grain surfaces

(Mainwaring et al., 2013). Heating may also have melted the long-chain compounds

resulting in a better coating on the sand surface (Savage et al., 1972). For the higher

concentrations (5-20 x 10^{-6} mol g^{-1}), the palmitic acid samples were already at

maximum SWR values. The difference in SWR of the palmitic acid sample compared with the BVOC samples implies differences in the molecular level interactions at the sand particle surfaces.

(a) cineole

1.0 molecs nm^{-2} 2.3 molecs nm^{-2} 5.0 molecs nm^{-2}

(b) palmitic acid

1.0 molecs nm^{-2} 2.3 molecs nm^{-2} 5.0 molecs nm^{-2}
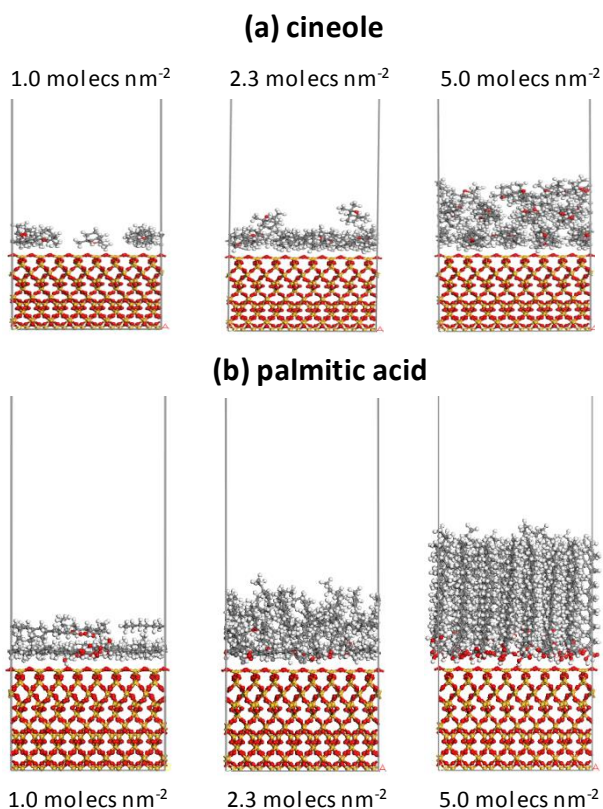
Figure 4.2   Modelled cross sections of molecule/quartz interfaces at 298 K for (a) cineole and (b) palmitic acid after equilibration.

4.3.2   *Computational modeling*

Molecular dynamics simulations reveal that when a single molecule (0.1 molecules nm^{-2}) of any of the selected compounds was placed on the quartz it moves about freely on the surface at 298 K. Importantly, the intermolecular forces were sufficient to hold the molecules close to the surface. The molecules adopted orientations to maximise the contact and interaction with the quartz surface. The compact BVOC molecules were found to move around randomly and interact with the surface through their polar head

groups (Figure 4.2a). In comparison, the long-chain molecules adopted a lateral arrangement in which both the polar head group and the non-polar tail were in contact with the mineral surface (Figure 4.2b).

As the surface density of molecules was increased (1.0 molecule nm^{-2}) the molecules scattered randomly across the surface to initially forming a monolayer. This monolayer arrangement is also evident by the presence of a single peak in the concentration profiles (Figure 4.3). The interface region (the region of overlap) was quite narrow (~0.05 Å) due to the rigidity and smoothness of the quartz surface.
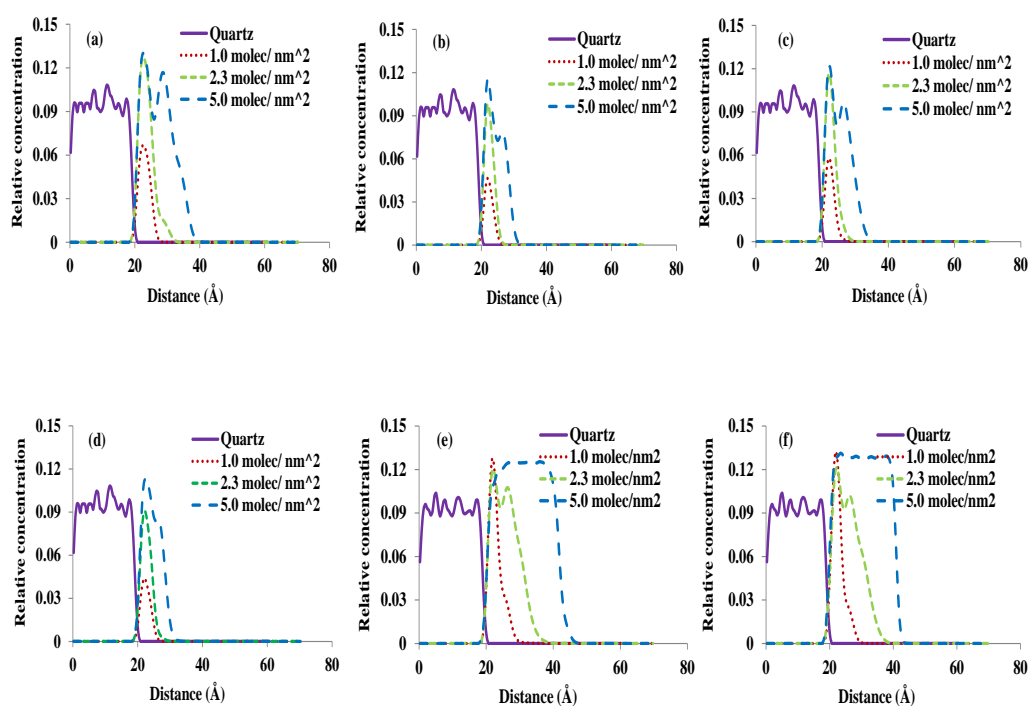
Figure 4.3   Concentration profiles at 25°C for (a) cineole, b) levoglucosenone, c) cis-3-hexen-1-ol d) 2-methyl-3-buten-2-ol e) palmitic acid and f) 1-hexadecanol with quartz.

Further increases in the surface density of the compounds led to the layering of the molecules. The thickness of the adsorbed layer was similar for surface densities of 1.0 and 2.3 molecules nm^{-2} and suggested that only a monolayer of molecules was present.

For cineole, there was a small shoulder on the peak of 2.3 molecule nm^{-2} that indicated the initial stages of formation of the second layer (Figure 4.3a). This may be due to difficulty in packing these bicyclic molecules efficiently on the quartz surface. The second layer is fully formed by 5.0 molecules nm^{-2} and the subsequent shoulder on the second peak of the concentration profile suggests that there was a partial third layer at this density. In comparison, for levoglucosenone, 3HexOH and 2MBuOH, a second peak and therefore a second layer of molecules only appeared at a surface density of 5.0 molecule nm^{-2} (Figure 4.3b – d). This later formation of the second layer implies that these molecules pack more efficiently on the quartz surface. The concentration profiles for palmitic acid and 1-hexadecanol (Figure 4.3e, f) suggested that a second layer was fully formed and a third layer had already begun to form at a surface coverage of 2.3 molecule nm^{-2}, which was consistent with the molecular conformation of wax molecules on quartz (Walden et al., 2015). However, the molecules were not completely lateral in these layers, which may be evidence of a transition from lateral layering to a tilted monolayer as might be expected on water or a highly polar surface (Henry et al., 2010; Plazzer et al., 2011). The palmitic acid and 1-hexadecanol simulations at high surface coverage started with a vertically aligned arrangement of molecules. This arrangement corresponded to a uniform monolayer of molecules, with the polar head groups close to the quartz and the non-polar tails aligned away from the mineral. This orientation is in agreement with the predictions of Zisman (1964) that a single layer of hydrophobic molecules can render a neutral hydrophilic mineral surface water-repellent. We note that both palmitic acid and 1-hexadecanol retained this alignment of the molecules within the timeframe of the simulations.

Physicochemical interactions determine the spatial order of organic molecules on the surface of minerals (Petridis et al., 2013). Radial distribution function analysis was used

to determine if there is any affinity of the carbon atoms of the molecules (C^{molec}) for the oxygen (O^{surf}) and silicon (Si^{surf}) atoms of the quartz surface. The C^{molec}–O^{surf} RDF for the cineole simulation (Figure 4.4a) was representative of the interactions in the levoglucosenone, cis-3-hexen-1-ol and 2-methyl-3-buten-2-ol simulations (AF 4.1 of the Appendix). The C^{molec}–O^{surf} RDFs indicated that the minimum separation between the molecules and the surface was ~2.7Å and did not exhibit strong correlations for any of the BVOC molecules investigated. A previous study (Shevchenko & Bailey, 1998) demonstrated that low-molecular-weight organic molecules also have relatively low affinity for mica surfaces.

The corresponding C^{molec}–O^{surf} RDFs for PA and 1-hexadecanol indicated that the closest approach of the hydrophobic tails of these molecules to the surface was also 2.7 Å, but overall the RDFs exhibited more distinct features than the BVOCs (Figure 4.4b, c). In particular, at a surface density of 1.0 molecules nm^{-2} there were broad peaks at 4.1 Å and 4.2 Å, respectively, which corresponded to the lateral layering of the long tails of these molecules. As noted earlier, at 5.0 molecules nm^{-2} there was vertical alignment of the tails and the peaks now correspond to alignment of corresponding carbon atoms (C1, C2, C3, …C16) of the respective molecules in the layer, consistent with all-trans conformations. The similarity in the C^{molec} – O^{surf} and C^{molec} – Si^{surf} RDFs revealed that the principal interaction between the hydrophobic tails and the surface was vdW forces.
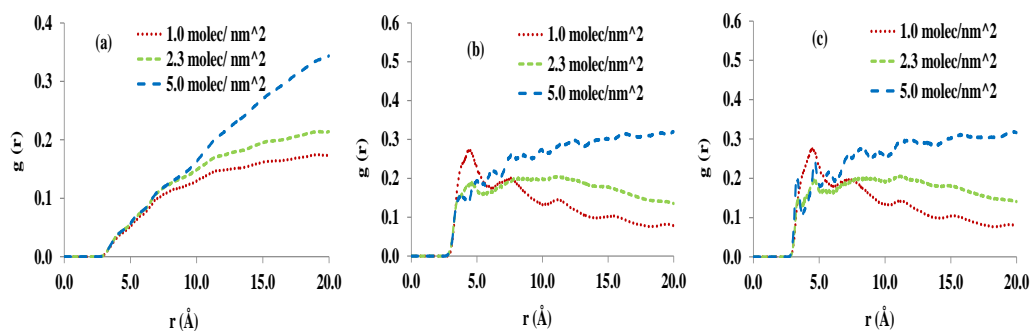
Figure 4.4   Radial distribution functions for C ^{molec}- O ^{surf} in a) cineole, b) palmitic

acid c) 1-hexadecanol with quartz.
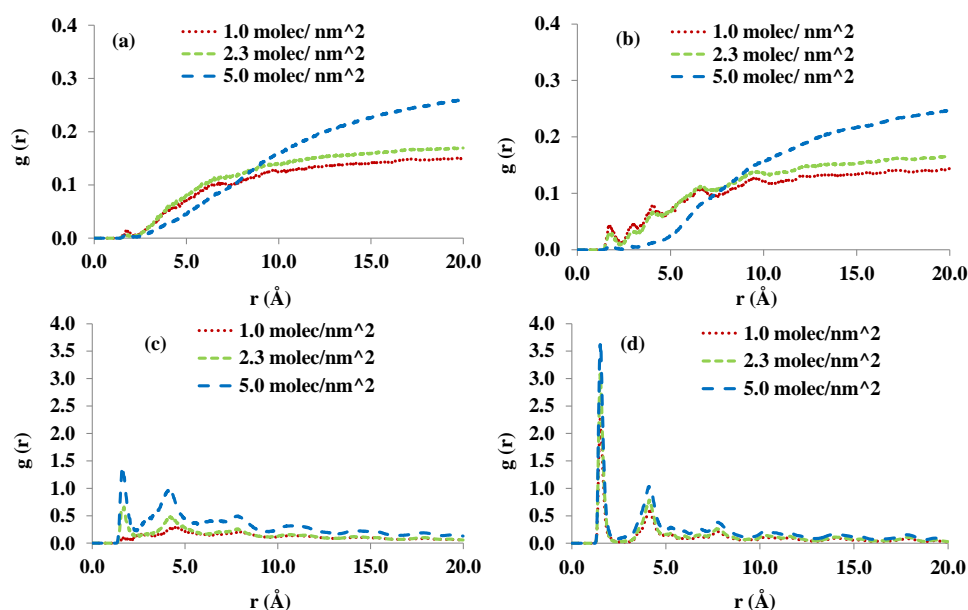
Figure 4.5   Radial distribution functions for H^{molec}- O^{surf} in a) cis-3-hexen-1-ol b) 2-

methyl-3-buten-2-ol c) palmitic acid d) 1-hexadecanol with quartz.

Cineole and levoglucosenone do not contain acidic hydrogen atoms and therefore did

not exhibit specific H-bond donor interactions with the quartz surface (AF 4.2 of the

Appendix). For the simulations with alcohol or acidic groups there were varying degrees

of H-bonding with the quartz surface RDF (H^{molec} – O^{surf}) (Figure 4.5). For example,

the interaction between H^{molec} – O^{surf} for cis-3-hexen-1-ol was extremely weak (g(r)

~0.01Å) (Figure 4.5a) at all surface coverages which indicated there was negligible H-

bonding between the molecules and the surface. In comparison, the H^{molec} – O^{surf} RDF

for 2-methyl-3-buten-2-ol layer had a peak at ~1.6 Å that revealed moderate H-bonding interactions (g(r) ~0.04Å) between the alcohol groups of these molecules and the oxygen atoms of the quartz surface. However, these H-bonding interactions were only evident for the layered arrangement with a surface coverage of 1.0 and 2.3 molecules nm^{-2}, while at the highest surface coverage (5.0 molecules nm^{-2}) the interactions were found to be insignificant (g(r) ~0.0Å) (Figure 4.5b).

The interaction between the acidic hydrogen of palmitic acid (PA) and oxygen of quartz was stronger than the alcohol interaction of 2-methyl-3-buten-2-ol. However, unlike 2-methyl-3-buten-2-ol, the palmitic acid increased with surface density (Figure 4.5c). Strong H-bonding was observed between the alcohols of 1-hexadecanol and the oxygen atoms of quartz, even at low surface coverage, as revealed by the intense peak at 1.8 Å (Figure 4.5d). This peak indicated that 1-hexadecanol was a better H-bond donor to quartz than palmitic acid. Secondary peaks in the RDFs reflected the uniform arrangement of the oxygen atoms in the quartz surface rather than any specific mid-range ordering of the organic molecules.
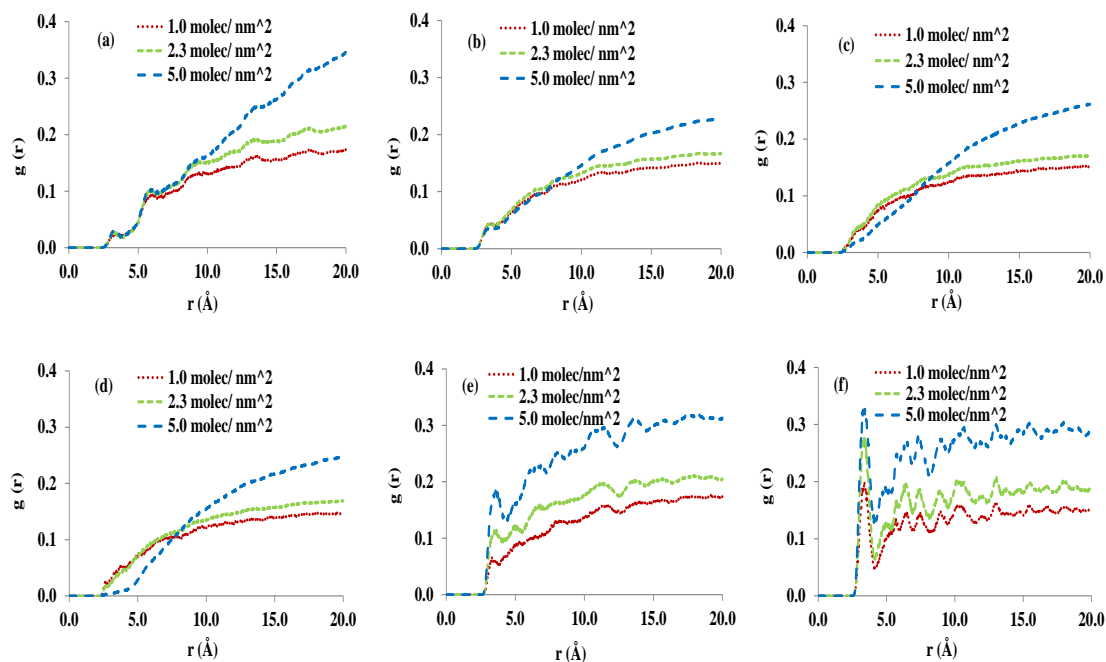
Figure 4.6   Radial distribution functions for O^{molec} – Si^{surf} in a) cineole, b) levoglucosenone, c) cis-3-hexen-1-ol d) 2-methyl-3-buten-2-ol e) palmitic acid and f) 1-hexadecanol with quartz.

Potential electrostatic interactions between the molecules and the quartz surface were investigated by analysing the RDFs for oxygen atoms of the molecules with the silicon atoms of the quartz. Cineole and levoglucosenone had small peaks at ~3.0Å (g(r) ~0.03Å) in the O^{molec} – Si^{surf} RDFs that could be due to a weak electrostatic interaction and definite orientation of the molecules towards the surface (Figure 4.6a, b). The corresponding RDFs for 3HexOH and 2MBuOH indicated that the nearest approach of molecular oxygen atoms to the surface was 2.3 Å, but there were no specific features in the RDFs (Figure 4.6c, d). The RDFs for palmitic acid and 1-hexadecanol indicated that at all surface densities there were sharp peaks at ~3.0Å indicating strong interaction with the surface (Figure 4.6e, f). However, the RDF between molecular oxygen and surface oxygen exhibited an identical pattern that indicates there were non-specific

interactions between molecular oxygen atoms and the quartz surface (AF 4.3 of the Appendix).
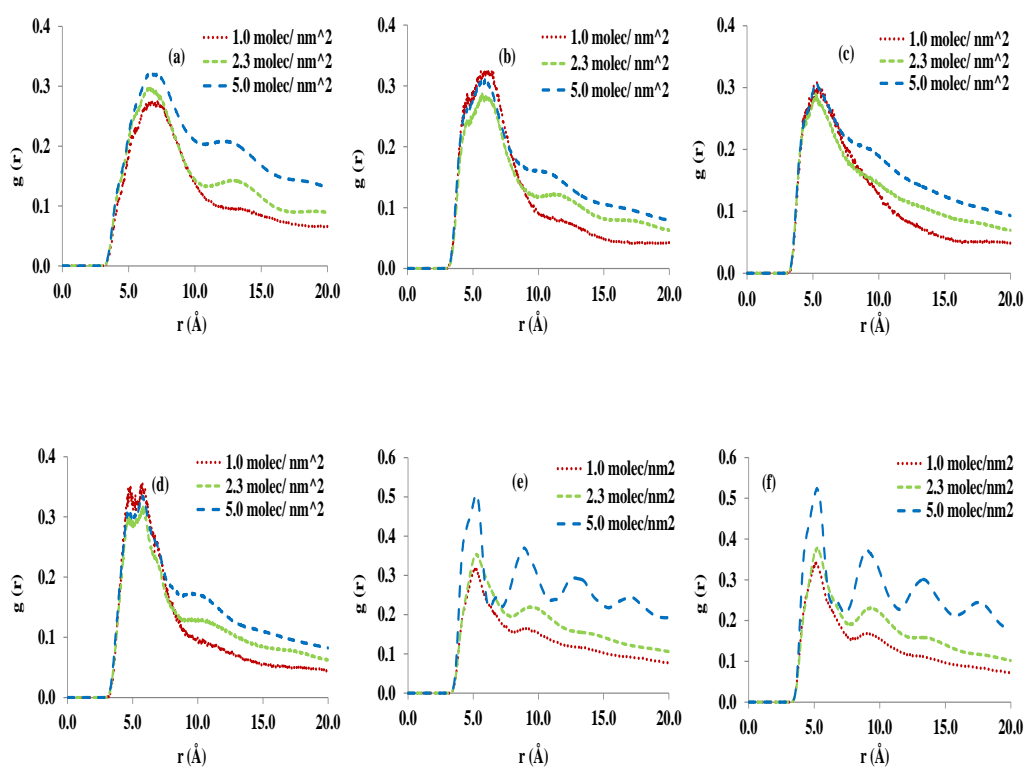
Figure 4.7   Intermolecular C ^{molec} – C ^{molec} RDFs for a) cineole, b) levoglucosenone, c) cis-3-hexen-1-ol d) 2-methyl-3-buten-2-ol e) palmitic acid and f) 1-hexadecanol with quartz.

The stability of surface monolayers is not only dependant on the interactions of the molecules with the surface but also on the interactions between the molecules in the layer. These interactions were investigated by analysing the intermolecular carbon – carbon RDFs (C^{molec}– C^{molec}). For the cyclic compounds, cineole and levoglucosenone, the C^{molec} – C^{molec} RDFs exhibit peaks at ~6.4 and ~5.5Å, respectively (Figure 4.7a, b). The broad nature of these peaks suggests that there are no specific packing arrangements in the layers formed from these molecules, even as the surface density of these species was increased. For the non-cyclic BVOCs, cis-3-hexen-1-ol and 2-methyl-3-buten-2-ol, the first peak appeared at ~5.0 and ~4.5 Å, respectively, suggesting stronger

113

interatomic interactions and a more intimate packing arrangement, independent of surface density. The RDFs for palmitic acid and 1-hexadecanol indicated much greater packing order of the long tail amphiphilic molecules, both in the lateral arrangement (1.0 and 2.3 molecules nm^{-2}) and in the vertical Langmuir monolayer arrangement (5.0 molecules nm^{-2}). These results suggest that the molecules sorb to the mineral surface in a discrete zonal structure as proposed by Kleber et al. (2007).
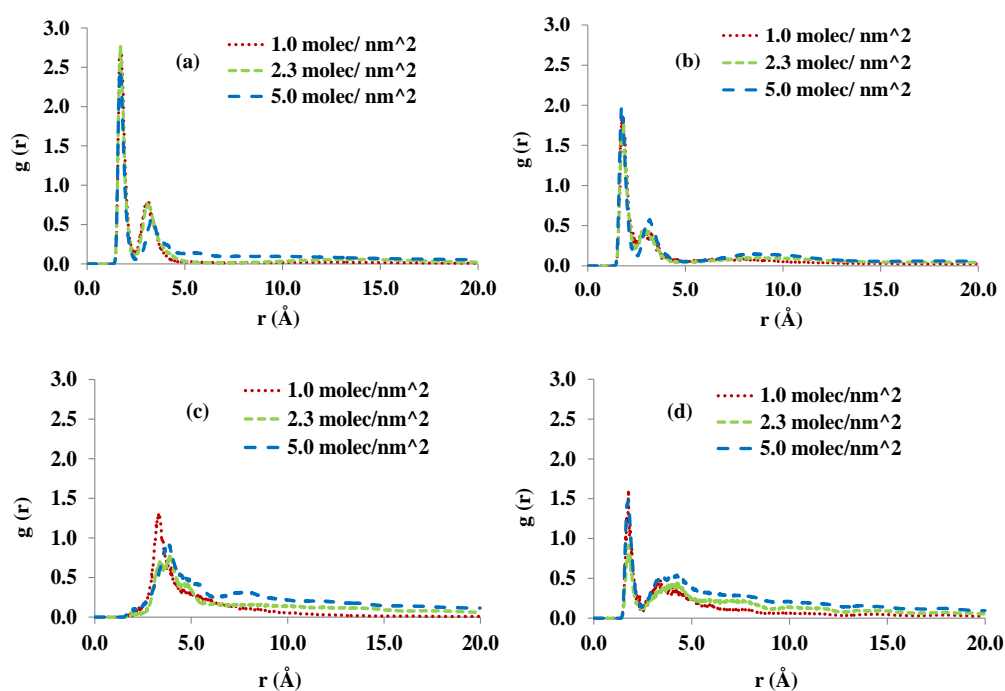
Figure 4.8   O^{molec}- H^{molec} RDFs in a) cis-3-hexen-1-ol b) 2-methyl-3-buten-2-ol c) palmitic acid and d) 1-hexadecanol with quartz.

The RDFs for molecular oxygen with molecular hydrogen (O^{molec}- H^{molec}) showed that cineole and levoglucosenone did not exhibit any significant H-bond type interactions between molecules (AF 4.4 of the Appendix). However, cis-3-hexen-1-ol and 2-methyl-3-buten-2-ol had strong H-bonding between neighbouring molecules, as shown by primary peaks at ~1.7Å and second peaks at 4.0 Å (Figure 4.8a, b). The interaction between the hydrogen and oxygen atoms of 3HexOH and 2MBuOH molecules inversely correlated with the weak interactions with the surface. Sharp peaks were also

observed in the RDFs for palmitic acid and 1-hexadecanol molecules indicating significant intermolecular H-bonding between the molecules. However, the intensity of these peaks was lower than that observed for 3HexOHand 2MBuOH. This change was consistent with the observation that palmitic acid and 1-hexadecanol have stronger H-bonding to the surface and weaker intermolecular H-bonding.

Table 4.2   Interaction energies (KJ mol^{-1}) per molecule of different surface densities (1.0, 2.3 and 5.0 molecules nm^{-2}) at two different temperatures.

Compound	Interaction energy (per molec) at 25 °C			Interaction energy (per molec) at 175°C
	1.0 molec nm^{-2}	2.3 molec nm^{-2}	5.0 molec nm^{-2}	2.3
2-Methyl-3-buten-2-ol	23.6	21.4	12.0	16.5
Cis-3-hexen-1-ol	27.7	24.1	12.8	18.2
Levoglucosenone	29.7	28.4	16.9	22.8
Cineole	30.0	25.8	12.6	21.1
1-Hexadecanol	67.4	35.5	16.5	24.9
Palmitic acid	57.8	32.7	18.9	24.6

The average interaction energy per molecule was calculated for all of the simulations (Table 4.2). The BVOCs are small molecules and therefore have low molecular weight and are composed of a small number of atoms. Therefore, for a given number of molecules per unit area, the density of atoms (ρ_2) within a layer of BVOCs was low. As shown by the Hamaker relationship, a low value for ρ_2 leads to a small van der Waals contribution to the interaction energy, resulting in a low interaction energy per molecule. At low surface coverage (1.0 molecules nm^{-2}) the long alkyl chain molecules exhibited the highest interaction energies with the quartz surface. These high energies

could be attributed to the high molecular weight and lateral arrangement of the molecules that facilitated the formation of a layer with a high density of atoms (ρ_2) and therefore a large vdW contribution to E_{int}. The lateral arrangement also accommodated H-bonding of the head group to the surface that added to the strength of the interaction and increased E_{int}. However, as the surface density was increased the additional molecules were further from the surface and therefore had a weaker interaction and consequently a lower interaction energy. In the vertically aligned Langmuir monolayer arrangement (5.0 molecules nm^{-2}), only the head groups had a close interaction with the surface, so the vdW interaction with the tails was weaker and the average E_{int} dropped further. For the small BVOC molecules, layer formation was a more gradual process, and the E_{int} decreased more slowly. Nevertheless, at the highest surface coverage, the E_{int}s for 1-hexadecanol and palmitic acid were still slightly higher (4-7 kJ mol^{-1}) than the corresponding values for the BVOCs, reflecting the stronger attraction of these molecules to the surface. Therefore, the strong water-SWR induced by 1-hexadecacnol and palmitic acid appears to be due to a combination of the orientational preference (i.e. polar head group to the surface and hydrophobic tail away from the surface) and the stronger interaction energies. In comparison, the BVOCs had weaker interaction energies and less uniform orientation, which inhibited the formation of a densely packed hydrophobic layer.

It is important to note that soils contain a large mixture of different organic molecules and the expression of SWR arises from the net effect of these compounds. In addition to individual compounds inducing SWR, there may be combinations of compounds that enhance SWR through synergistic effects. For example, it has been shown that loadings of octadecanoic acid with octadecane produce greater SWR than the acid or alkane alone (Mainwaring et al., 2013). Therefore, although both the simulations and the

loading experiments demonstrate that the BVOCs individually do not induce SWR, specific combinations of these compounds with other soil organic compounds may lead to synergistic effects that contribute to SWR. Vegetation fire can further alter the composition and structure of soil organic matter through volatilization, pyrolysis, rearrangement and condensation of molecules, which is evident from the reported changes in SWR between pre- and post-fire events (Dlapa et al. 2008; Doerr et al. 2004).

4.3.3   Simulations at higher temperature

Thermal energy input has previously been found to induce increases in SWR, as measured by the water drop penetration time (WDPT) test in sandy forest soils from Slovakia (Dlapa et al., 2008). Savage et al. (1972) proposed that heating facilitates the movement of organic compounds "fixing" some of the more polar hydrophobic substances and revolatilizing the less polar substances, thereby broadening the water-repellent layer. Molecular dynamics simulations were also performed at 175°C (448 K) on each compound with a surface density of 2.3 molecules nm^{-2}, to explore the effect of increased temperature. At this higher temperature, the organic molecules had much greater kinetic energy and explored a range of different conformations during the simulation. In particular, for the 3HexOH and 2MBuOH, several molecules were observed to "escape" from the quartz surface into the vacuum space within the timeframe of these simulations. The palmitic acid and 1-hexadecanol molecules also exhibited greater kinetic energy. However, none of these molecules escaped from the molecular layers, which implied stronger interactions with the surface.
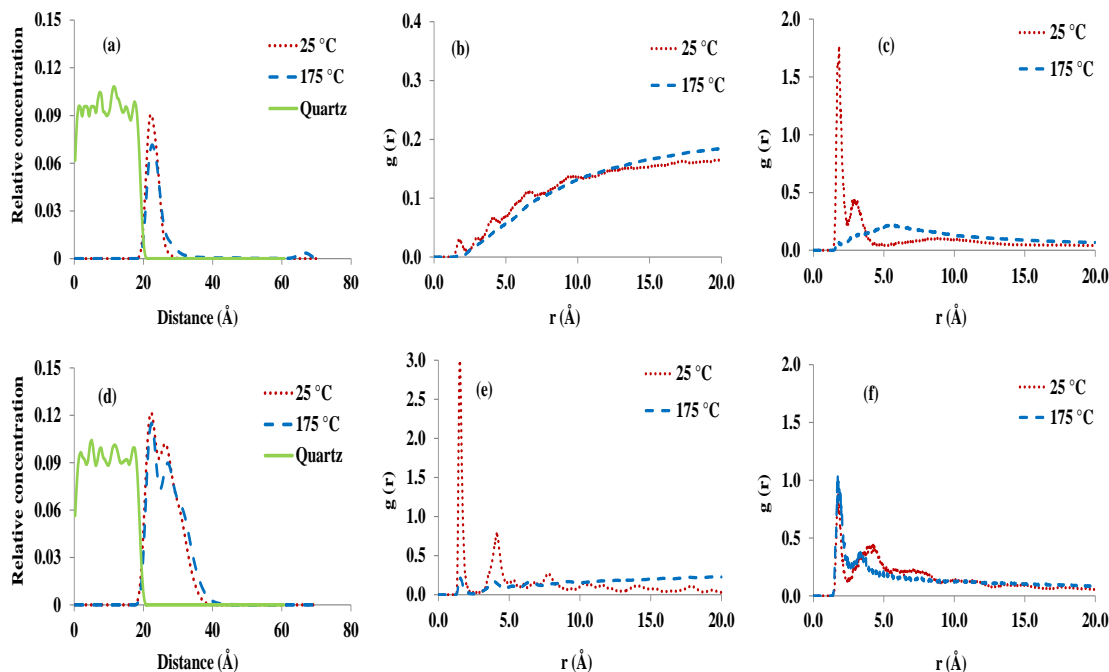
Figure 4.9   Concentration profile, H^{molec}-O^{surf} RDF and H^{molec}-O^{molec} RDF of 2-methyl-3-buten-2-ol (a-c) and 1-hexadecanol (d-f) at two different temperatures of 25°C and 175°C.

Figure 4.9a reveals there was an expansion (~4 Å) of the thickness of the molecular layer of 2MBuOH at 175°C compared to 25°C. The RDF for C^{molec} to Si^{surf} for each of the BVOCs exhibited a shift from ~2.5 Å at 25°C to ~3.0 Å at 175 °C (AF 4.5 of the Appendix), which indicated an increase in the minimum separation of the molecules from the surface, due to the greater entropy of the molecules. The weak H-bonding interaction between 2MBuOH and surface oxygen atoms was no longer evident at 175°C (Figure 4.9b). Likewise, H^{molec}- O^{molec} intermolecular RDFs reveal that H-bonding interactions between molecules in the 2MBuOH (Figure 4.9c) and 3HexOH (AF 4.6 of the Appendix) are weaker (g (r) < 0.3) at the higher temperature, due to their greater kinetic energy.

At 175°C the 1-hexadecanol molecules were observed to remain close to the surface, and the concentration profile (Figure 4.9d) was similar to that obtained at 25°C.

However, the H-bonding interaction between H^{molec}- O^{surf} was substantially weaker (g (r) < 0.3) at the higher temperature (Figure 4.9e). In comparison, there was an increase in the intensity of the first peak of the H^{molec}- O^{molec} intermolecular RDF (Figure 4.9f) suggesting a distinct orientation of the molecules on the quartz surface, which has also been proposed by Shevchenko and Bailey (1998). Similar behaviour was also evident with palmitic acid at the higher temperature (AF 4.7 of the Appendix). The molecules had greater kinetic energy at higher temperatures, and this led to an expansion of the volume of the organic layer. Consequently, there was a reduction in the density of the organic layer. As shown by the Hamaker relationship, a decrease in the density leads to a reduction of the van der Waals attraction between the layers and a decrease in E_{int}. Therefore, the E_{int}s for all organic layers at 175°C were reduced (~20 to 30%) compared to the corresponding layers at 25°C. Nevertheless, the 1-hexadecanol and palmitic acid layers maintained a greater packing efficiency and higher density of molecules at 175°C compared with the BVOCs. Therefore, the long-chain molecules continued to experience stronger van der Waals interaction with the quartz surface and have higher E_{int}s than the BVOCs.

The main implication of this finding is that during a low-temperature vegetation fire (175°C) the long chain molecules have insufficient energy to escape from the surface but sufficient energy to reorganize into a uniform layer. Furthermore, as small volatile molecules escape from the surface of soil particles, there will be a change in the relative composition, with the long-chain amphiphilic molecules representing a larger proportion of the remaining material. Consequently, at this temperature range, there should be an increase in SWR, which is consistent with previous field and experimental studies (Mainwaring et al. 2013). In addition to these physical effects, higher temperatures could also lead to pyrolysis of organic materials, resulting in the formation

of highly reactive species that can potentially chemically bond to mineral surfaces and further alter the SWR of the soil. However, the contribution of pyrolytic species is beyond the scope of the present study.

4.4   Conclusions

It was found that BVOCs derived from vegetation fire had a very insignificant role in inducing SWR on AWS, despite considerable variations in chain length, boiling point and functional groups. In comparison, palmitic acid was effective in inducing SWR on AWS in laboratory experiments, even at low loading ranges (1×10^{-6} mol g^{-1}). Heating samples to 105°C caused an increase in SWR for palmitic acid, but no change for the BVOCs investigated.

Molecular dynamics simulations provided insight into the molecular level interactions on sand particle surfaces. The simulations revealed that at 25°C, the molecules remain close to the quartz surface and formed layers as the concentration of molecules was increased. Long chain hydrophobic compounds covered the whole surface and were closely packed at higher concentrations. In comparison, the BVOCs appeared to be scattered on the surface. Hydrogen bond formation between molecules in the cis-3-hexen-1-ol and 2-methyl-3-buten-2-ol organic layers was stronger than the interactions towards the surface. The weaker interaction of BVOCs with the surface can also in part be attributed to the less efficient packing of the molecules on the surface that led to a lower density layer and hence a weaker vdW interaction. At 175°C, the BVOC molecules were found to be more randomly scattered, with higher separation distances from the surface and weaker intermolecular H-bonding interactions.

The long chain molecules (1-hexadecanol and palmitic acid) form more ordered and denser layers at 25°C than the BVOCs. Consequently, there was a stronger van der

Waals attraction between the long-chain molecules and the quartz surface. Furthermore, the long-chain molecules were found to have stronger H-bond interactions with the surface. The combination of these interactions led to the formation of a stable hydrophobic layer that induced SWR. At 175°C there was a decrease in the density of the layers composed of long-chain molecules and a decrease in the interaction energy; however, the layers remain intact. Therefore, the conclusion of this study is that fire-induced increases in SWR are mainly due to the reorganization of the long-chain aliphatic molecules already present in the soil, rather than the addition of fire derived BVOCs.

5 Physicochemical interaction of long-chain hydrophobic compounds in the soil environment - an experimental and molecular dynamics approach

5.1 Introduction

Soil water repellency (SWR) is mostly caused by organic compounds with extensive polymethylene chains (Doerr et al., 2000; Ma'Shum et al., 1988). However, the changes in the severity of repellency are attributed to changes in the molecular conformation of hydrophobic coatings on soil particles (Ma'shum & Farmer, 1985; Wallis & Horne, 1992). The compounds are usually incorporated into the soil, originating from plant and cuticular waxes (Hansel et al., 2008). The main components of these waxes are branched and unbranched C_{16}-C_{36} fatty acids and their esters as well as alkanes, phytanols, phytanes and sterols (Atanassova & Doerr, 2010; Doerr et al., 2005; Mainwaring et al., 2013; McKissock et al., 2003). It has been proposed that amphiphilic organic compounds such as fatty acids, contribute to hydrophobic coatings through the interaction of their hydrophilic head groups with sand particle surfaces (Cheng et al., 2010; Morley et al., 2005). This orientation should result in the hydrophobic tail of the fatty acids projecting from the surfaces of the soil particles, which can create a hydrophobic barrier at some surface densities (Walden et al., 2015).

Soil mineral surfaces have also been widely recognized as a crucial factor in SWR induction (Doerr et al., 2000). Coarser particles are usually more susceptible to becoming coated with hydrophobic compounds due to their smaller surface area per unit volume (Giovannini & Lucchesi, 1983). In fact, soil surface area and soil organic carbon content account for up to 63% of the variation in SWR (Harper et al., 2000).

Analysis of the amount of organic material present in water repellent soils suggests that their maximum SWR also depends on its distribution and may be sufficient for formation of multiple layers (Mainwaring et al., 2013; McKissock et al., 2003). It has been proposed that these layers may be of different forms including intimately packed films with steeply oriented molecules, largely expanded films or randomly separated films (Shaw & Costello, 1993). For instance, the loading required for a closely packed monolayer film of straight chain fatty acids can be estimated from the limiting area of 4.76 molecules nm^{-2} (Moore, 1972). Wax molecules can also be found in a two layer arrangement even at a relatively low surface coverage of 2.35 molecules nm^{-2} (Walden et al., 2015).

The chemistry of organo-mineral interfaces can also significantly influence the arrangement and stabilization of organic compounds in soils (Petridis et al., 2013). The presence of surface OH groups induces hydrophilicity of silica and kaolinite surfaces and provides a poor substrate for hydrophobic hydrocarbons (Nalaskowski et al., 2003; Tschapek, 1984). However, polar compounds can interact through their hydrophilic head groups with the OH groups of the polar surface through hydrogen bonding. Rigid flat crystalline quartz surfaces are less hydrophilic than silica and kaolinite (Zhuravlev, 2000). Hence, interfacial interactions have a significant role in the layering and packing of wax molecules on soil surfaces (Walden et al., 2015). The affinity of the organic molecules with mineral surfaces depends on hydrogen bonding and/or van der Waal's interactions (Horne & McIntosh, 2000; Ma'shum & Farmer, 1985; Wu et al., 2013). Morphological features including cavities and roughness on soil surfaces can also influence the arrangement and structure of monolayers (Miller et al., 2007; Tunega et al., 2004). Teppen et al. (1998) suggested at least three distinct mechanisms coexist for

the interaction of organic molecules on clay minerals in the environment: (i) full molecular contact, (ii) contact through a single atom and (iii) indirect contact.

Understanding both the chemical nature of the hydrophobic coating and its physical interaction with the soil surface is crucial to having an insightful understanding of SWR. However, soils are complex mixtures containing a wide range of organic components. In particular, we investigate the interaction of single component and mixtures of long chain hydrophobic/amphiphilic molecules on different simulated soils. Although analysis of soil solvent extracts can identify the relative amounts of individual compounds, it is often difficult to determine the relative importance of all components. It is even more difficult to identify synergistic effects from combinations of components. Experimental studies provide a broad understanding of the bulk effects of hydrophobic molecular coatings but do not provide a molecular level understanding of the coating structure or of its kinetic and/or thermodynamic stability. Considering this research gap we perform an experimental study and validate with a molecular dynamics simulation to investigate the physical interactions of the applied molecules with model mineral surfaces.

5.2 *Material and methods*

5.2.1 *Selection of organic compounds for application*

The organic compounds selected for this study have commonly been identified in hydrophobic soils (Atanassova & Doerr, 2011; Doerr et al., 2005; Franco et al., 2000b; Mainwaring et al., 2013; Morley et al., 2005). We have already investigated the loading effect of palmitic acid (PA) ($C_{16}H_{31}O_2H$) onto acid washed sand (AWS) (Uddin et al., 2017). In this study, we investigate a few additional soil organic components namely, a long-chain alcohol (1-docosanol, $C_{22}H_{45}OH$), a long-chain alkane (hexadecane, $C_{16}H_{34}$)

and a long-chain ester (isopropyl myristate, $C_{14}H_{27}O_2C_3H_7$) onto AWS and AWS with 5% kaolinite (KL). We also investigate mixtures of components including PA and hexadecane, PA and ester, 1-docosanol and hexadecane, 1-docosanol and ester, PA and 1-docosanol to identify if any synergistic relationships occur between these species.

5.2.2 Application of selected organic compounds

Organic compounds were applied directly on soil or mineral substrates at different loading ranges ($(0.25 -20) \times 10^{-6}$ mol g^{-1}) commensurate with previous studies (Mainwaring et al., 2013). The standard procedure involved preparing a solution of the mixture of selected compounds in tetrahydrofuran (THF) in a 50ml volumetric flask to achieve specific loadings. The solutions (50 mL) were then applied to AWS (40 g) as well as AWS with 5% kaolinite (19:1 by mass) and thoroughly mixed for 10 minutes. The solvent was then removed in a rotary evaporator at 45°C under reduced pressure.

5.2.3 Water repellency (SWR) assessment

The severity of SWR of each of the loaded samples was assessed using the molarity of ethanol droplet (MED) test (King, 1981). A stock solution of 4M ethanol was prepared, and a number of solutions were made at concentrations between 0 and 4M with increments of 0.2M. In each experiment, ~ 20g of AWS with loaded compounds was placed in a petri dish (50 × 10-mm) and put into a desiccator for around four hours following rotary evaporation, in order to make the sample free from humidity. A second sample with the same loading of the compound was placed in an oven at 105°C for 24 hours. The oven dried sample was then cooled to room temperature in a desiccator. The surface of the samples was leveled by gentle tapping on the bench, and in some cases, a light pressure was applied to the flat bottom of a beaker to make the surface smooth and uniform. Droplets (50-µl) of the prepared ethanol solutions were then applied to the

surface of the samples from 5-mm height, starting with the lowest ethanol concentration. The time required for each drop to penetrate the surface was recorded. The lowest concentration for which the infiltration time was <10 s was considered as the MED value for that sample (Walden et al., 2015).

5.2.4 Computational models

The modeling framework for both the surface and molecules was developed using Materials Studio v 7.0 (Accelrys, 2013). The surface of a sand particle was represented by a cleaved quartz surface while hydroxylated amorphous silica was used to represent a weathered sand particle surface. Clay particle surfaces were modeled by the gibbsite-like surface of kaolinite. Models of individual hydrophobic compounds included hexadecane (hexD), tridecanoic acid, 1-methylethyl ester (Td1Me) and mixtures of compounds (palmitic acid (PA) and hexD), (PA and Td1Me), (PA and 1-hexadecanol) were also investigated. Models of 1-hexadecanol (1-Hex-OH) and tridecanoic acid, 1-methylethyl ester (Td1Me) were used in the modeling studies rather than 1-docosanol and isopropyl myristate (IsoM), respectively to simplify the calculations. Different concentrations of compounds (0.1-5.0 molecules nm^{-2}) were achieved by placing different numbers of molecules on the built model surfaces. Each system was placed in a unit cell with dimensions 30.7 x 37.3 x 70.0 Å for quartz, 28.5 x 28.5 x 100.0 Å for silica and 30.9 x 35.7 x 140.0 Å for kaolinite. The large z-dimension ensures that adjacent cells do not interact along the z-axis when periodic boundary conditions are applied, resulting in a quasi-2D interface.

The potential energy for each system was calculated using the COMPASS force field (Sun, 1998), which has previously been shown to perform well for describing the interactions between condensed hydrophilic and hydrophobic surfaces (Henry et al.,

2006; Henry et al., 2005; Shaw et al., 2013). Electrostatic interactions were calculated using the Ewald procedure, while van der Waals interactions were calculated with an atom-based procedure using a 12.50 Å cutoff, a spline width of 1.00 Å, a buffer of 0.50 Å and a long-range tail correction. The modeled interfaces were initially energy minimized using the conjugate gradient procedure with a convergence criterion of 0.04 kJ mol^{-1}. Molecular dynamics simulations were performed in the canonical ensemble (NVT, constant number of atoms (N), volume (V) and temperature (T)), equilibrated for 500 ps followed by data acquisition for 4500 ps, using 1.0 fs time steps. The temperature was maintained at 298 K using the Andersen thermostat (Andersen, 1980) with a collision ratio of 1.0.

Concentration profiles of the mineral and selected compounds at the interfaces were found by averaging the number of atoms in strips (parallel to the x-y plane) in the molecular dynamics simulations. The profiles of individual components (surface and compounds) that comprise each system as a function of z position were included. The interface region of each system is arbitrarily considered as the region of coexistence of the two components (surface/compounds) and was found to be quite narrow (~0.05 Å) on the quartz surface due to the rigidity of the mineral.

5.3 Results and discussion

5.3.1 Experimental SWR assessment

The pure long chain hydrophobic molecules were applied onto acid washed sand (AWS) and AWS with 5% kaolinite (KL) with loadings ranging from (0.25 to 20) $\times 10^{-6}$ mole g^{-1}. Palmitic acid (PA) was found to induce SWR on AWS (0.33 and 1.27M) after drying at 24 °C and at 105 °C, respectively, even at a low loading level (0.50 x 10^{-6} mol g^{-1}) (Uddin et al., 2017). However, this loading level produced insignificant SWR on AWS

with 5% KL. The induced repellency is consistent with the study of Mainwaring et al. (2013), that octadecanoic acid induced SWR on AWS at loadings of $< 1 \times 10^{-6}$ mol g^{-1}. Generally, after heating (105°C) the severity of SWR increased. It is assumed that the higher temperature provides sufficient energy for the molecules to reorganize into a uniform layer that provides a greater barrier to water. It has been proposed that molecules with polar end groups such as fatty acids adsorb onto the charged hydrophilic surfaces of silicate particles through hydrogen bonding and/or dipole-dipole interactions leaving hydrophobic alkyl chains exposed (Ma'shum & Farmer, 1985). In comparison, the non-polar alkane hexadecane was found to not induce SWR on AWS even after heating (105°C) at any loading level, consistent with the reported results for octadecane at 20°C (Mainwaring et al., 2013). Pure 1-docosanol (1-Doco) was found to induce SWR on AWS both at 24 °C (1.87 M) and after heating to105 °C (4.0M) with a loading of 1×10^{-6} mol g^{-1}. On AWS with 5% KL, the same loading was found to induce a lower level of SWR (0.2 M and 2.33 M) after drying at both 24°C and 105°C, respectively. The level of SWR is in agreement with observations from field samples that clay reduces the severity of SWR (Walden et al., 2015). Isopropyl Myristate (IsoM) did not induce SWR on AWS or AWS with 5% KL even after heating, which compares well with an earlier study of Mainwaring et al. (2013).

As noted in the introduction, soils are complex mixtures of minerals, organic and inorganic molecules. Although single component experiments provide a measure of the efficacy of these compounds for inducing SWR, they are far removed from natural environmental systems. The first step in improving these models is to look at binary systems of key compounds. Thus, mixtures of PA and hexadecane were applied to AWS and 5% kaolinite to determine the effect of these compounds in combination.
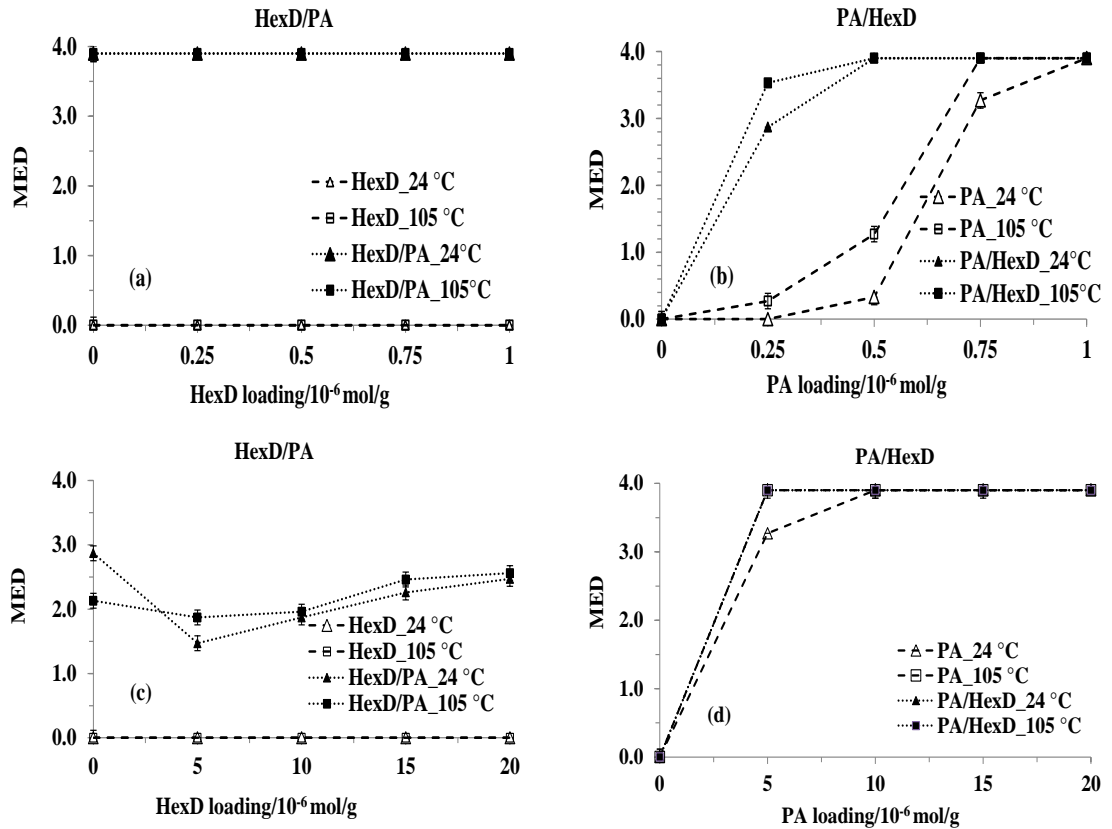
Figure 5.1   Effect of palmitic acid and hexadecane in different ratios (a) PA (fixed, 1×10^{-6} mole g^{-1}) and hexadecane on AWS (b) PA and hexadecane (fixed, 1×10^{-6} mole g^{-1}) on AWS (c) PA (fixed, 1×10^{-6} mole g^{-1}) and hexadecane on AWS with 5% KL (d) PA and hexadecane (fixed, 1×10^{-6} mole g^{-1}) on AWS with 5% KL.

As noted above, loading of 1×10^{-6} mole g^{-1} PA on AWS leads to an MED of 4.0 (Uddin et al., 2017), which is consistent with a previous study (Morley et al., 2005) that loadings equivalent to the total natural acid content of water repellent soils is able to induce the onset of strong SWR. When PA was applied to AWS with 5% KL at a loading of 1×10^{-6} mole g^{-1}, this leads to a MED of 2.87M, which demonstrates that the clay content lowers the non-wetting impacts of PA. In fact, long chain organic acids appear to be the most effective components for inducing SWR on sand/quartz substrates. The addition of increasing amount of hexadecane to the fixed loading of PA (1×10^{-6} mole g^{-1}) did not

129

lead to any change in MED relative to PA alone (Figure 5.1a). Alternately, when hexadecane content was fixed at 1×10^{-6} mole g^{-1}, and PA was added, the SWR value sharply increased for additions of 0.25×10^{-6} mole g^{-1} or greater of PA (Figure 5.1b). Notably, the SWR of those mixed loading samples is much higher than samples of the corresponding pure PA samples. The severity of SWR indicates that hexadecane can enhance the SWR effects of low levels of PA. On AWS with 5% kaolinite, it was found that addition of hexadecane to a PA, initially leads to a decrease in SWR, relative to a pure PA loading (Figure 5.1c). However, as the hexadecane content was increased above 5×10^{-6} mole g^{-1}, the SWR of the sample also increased back towards the levels for pure PA. For a fixed loading of hexadecane and a gradual increase of PA on AWS, the MED value abruptly increased. The addition of hexadecane is also found to enhance the WR effect of low levels of PA on AWS with 5% KL (Figure 5.1d).

As noted in the Methods section, each of the samples were also heated to 105 °C for 24 hours and cooled down in the desiccator following MED measurement. There is generally an increase in SWR following heating, consistent with the observations for pure PA loadings (Figure 5.1a-d). Enhanced SWR of laboratory samples after heating has previously been attributed to thermal rearrangement of organic molecules on the soil particle surfaces leading to more ordered hydrophobic layers (Mainwaring et al., 2013). Thermal energy input has also previously been found to induce increases in SWR, as measured by the water drop penetration time (WDPT) test in sandy forest soils from Slovakia (Dlapa et al., 2008). Savage et al. (1972) proposed that heating facilitates the movement of organic compounds "fixing" some of the more polar hydrophobic substances and revolatilizing the less polar substances, thereby broadening the water-repellent layer. Heating may also have melted the long chain compounds resulting in a better coating on the surfaces.
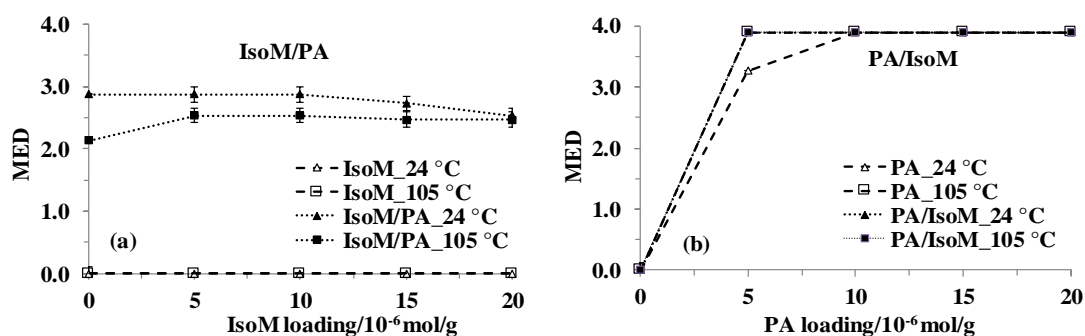
Figure 5.2   Effect of palmitic acid (PA) and isopropyl myristate (IsoM) in different ratios (a) PA (fixed, 1×10^{-6} mole g^{-1}) and IsoM on AWS with 5% KL (b) PA and IsoM (fixed, 1×10^{-6} mole g^{-1}) on AWS with 5% KL.

As noted earlier IsoM was found to have no effect in inducing SWR on AWS or AWS with 5% KL at any loading from $(0 - 20) \times 10^{-6}$ mole g^{-1}. Mixtures of PA and IsoM were applied on AWS, and it was revealed that for a fixed loading of PA (1×10^{-6} mole g^{-1}) and a gradual increase of IsoM loading, there was not any change in MED relative to PA alone. Likewise, for a fixed loading of IsoM (1×10^{-6} mole g^{-1}) and with a gradual increase of PA, the change in MED was identical to the corresponding pure PA systems. Therefore, IsoM was found to neither add to or detract from the WR effect of PA. When mixtures of PA (1×10^{-6} mole g^{-1}) and IsoM ($0 - 20 \times 10^{-6}$ mole g^{-1}) were applied onto AWS with 5% KL, it was found that severity of repellence slightly decreased with the increase of IsoM ($0 - 20 \times 10^{-6}$ mole g^{-1}) (Figure 5.2a). The severity of SWR was slightly lower following heating at 105 °C, indicating IsoM can have a reducing effect of SWR on the sample investigated (Figure 5.2a). For a fixed loading of IsoM and with a gradual increase of PA, the IsoM enhances the WR effects of PA at a loading of 5×10^{-6} mole g^{-1} (Figure 5.2b).
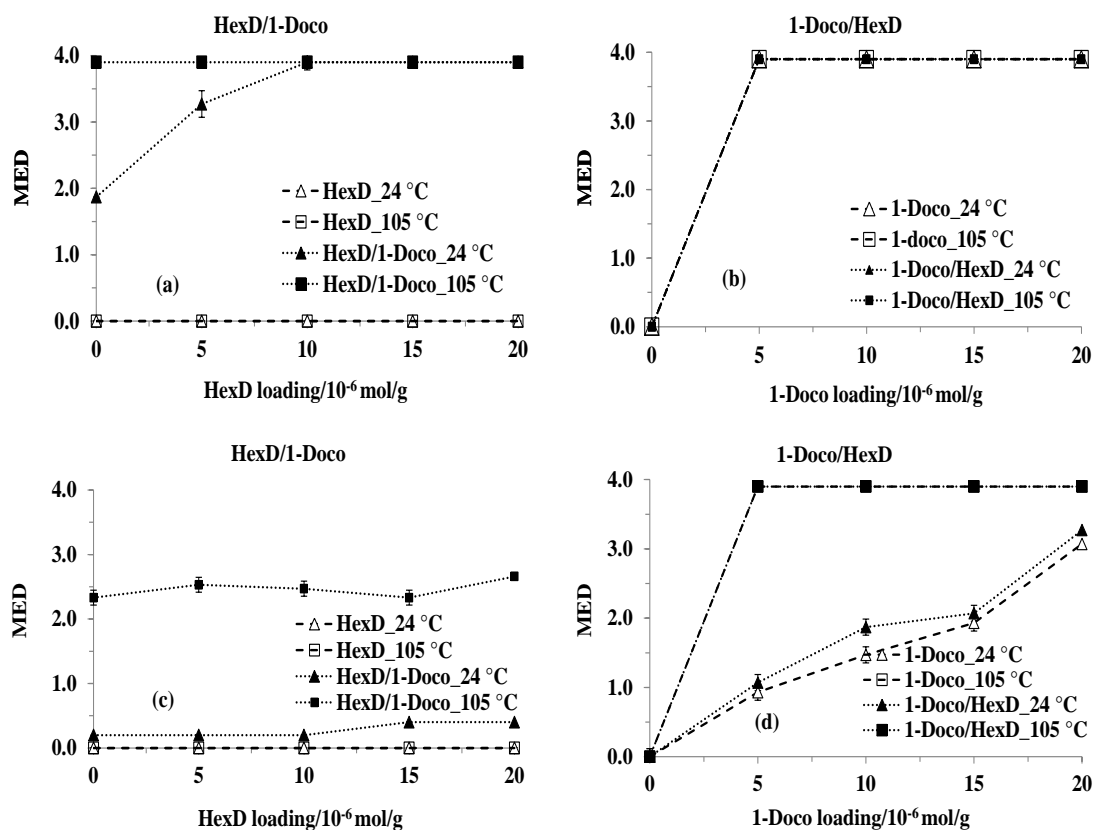
Figure 5.3   Effect of 1-docosanol and hexadecane in different ratios (a) 1-docosanol (fixed,1×10^{-6} mole g^{-1}) and hexadecane on AWS (b) 1-docosanol and hexadecane (fixed,1×10^{-6} mole g^{-1}) on AWS (c) 1-docosanol (fixed,1×10^{-6} mole g^{-1}) and hexadecane on AWS with 5% KL (d) 1-docosanol and hexadecane (fixed,1×10^{-6} mole g^{-1}) on AWS with 5% KL.

When 1-docosanol (1-Doco) (1×10^{-6} mole g^{-1}) alone was applied to AWS, it induced SWR (1.87M). However, with a gradual increase of hexD, the mixture leads to a sharp increase in the severity of SWR (Figure 5.3a). The increase of SWR suggests hexD has a cooperative effect with 1-Doco. Interestingly, 1-Doco was found to significantly induce SWR both on AWS as well as AWS with 5% KL (Figure 5.3b, d). The addition of a constant loading of hexadecane to 1-Doco did not affect SWR relative to 1-Doco alone (Figure 5.3b). When the mixture of 1-Doco and hexD were applied onto AWS

with 5% KL, it was revealed that for a gradual increase of hexadecane with fixed 1-Doco (1×10^{-6} mole g^{-1}), the MED value slightly increased. At the highest loading of 20×10^{-6} mole g^{-1} it was evident that hexD had an effect relative to 1-Doco alone (Figure 5.3c). Interestingly, when hexD concentration was fixed at 1×10^{-6} mole g^{-1}, the gradual increase of 1-Doco increased the severity of repellence on AWS with 5% KL slightly compared with 1-Doco alone (Figure 5.3d). It has been proposed that interaction of hydrogen donor atoms of amphiphilic molecules leads to the strong attachment to the surface of the mineral particles combined with the alignment of the long non-polar tails to give a hydrophobic condensed film (Shaw & Costello, 1993). After heating to 105°C the severity of SWR was increased for all mixtures on both mineral substrates. It was assumed that at higher temperature the molecules had sufficient kinetic energy to reorganize themselves on the surfaces investigated.
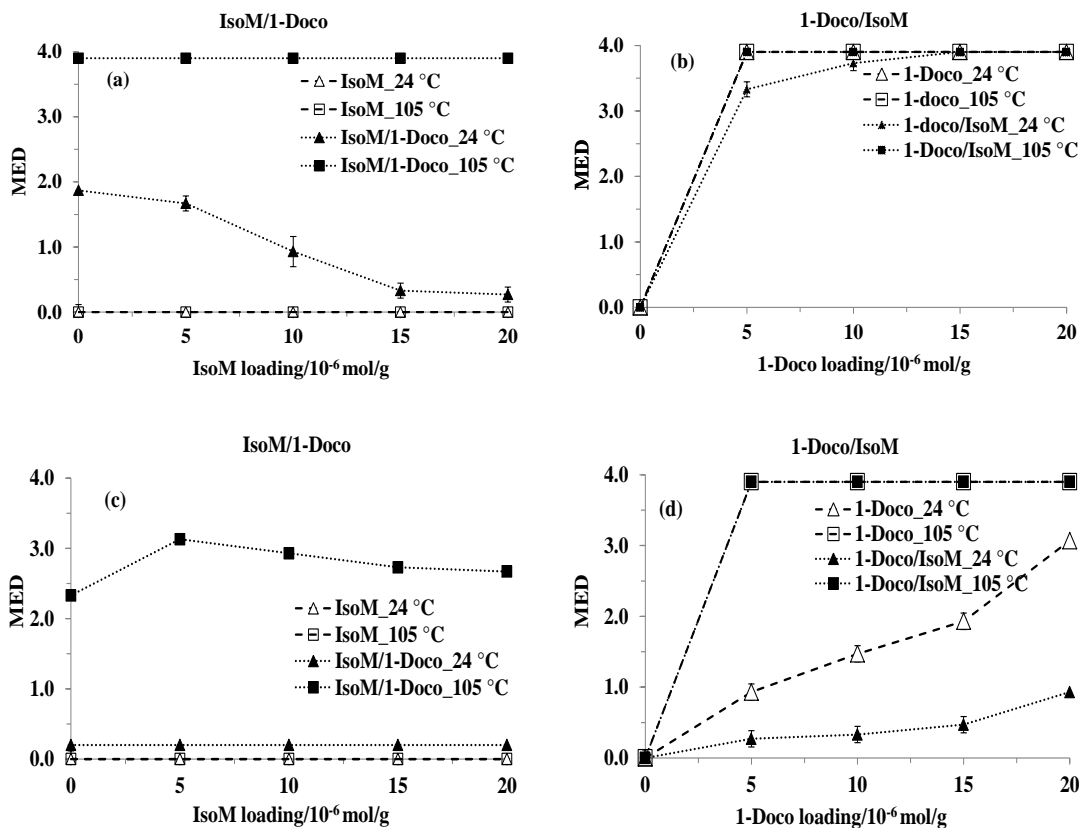
Figure 5.4   Effect of 1-docosanol and IsoM in different ratios (a) 1-docosanol (fixed,1×10^{-6} mole g^{-1}) and IsoM on AWS (b) 1-docosanol and IsoM (fixed,1×10^{-6} mole g^{-1}) on AWS (c) 1-docosanol (fixed,1×10^{-6} mole g^{-1}) and IsoM on AWS with 5% KL (d) 1-docosanol and IsoM (fixed,1×10^{-6} mole g^{-1}) on AWS with 5% KL.

Binary mixtures of 1-Doco and IsoM were applied onto AWS and AWS with 5% KL to determine their combined effect. It was revealed that for a gradual increase of the concentration of IsoM on AWS with a fixed loading of 1-Doco (1×10^{-6} mole g^{-1}), the severity of SWR decreased at 24°C (Figure 5.4a). However, with a steady increase of 1-Doco concentration with fixed loading of IsoM (1×10^{-6} mole g^{-1}), the severity of SWR sharply increased but was slightly lower than 1-Doco alone (Figure 5.4b).
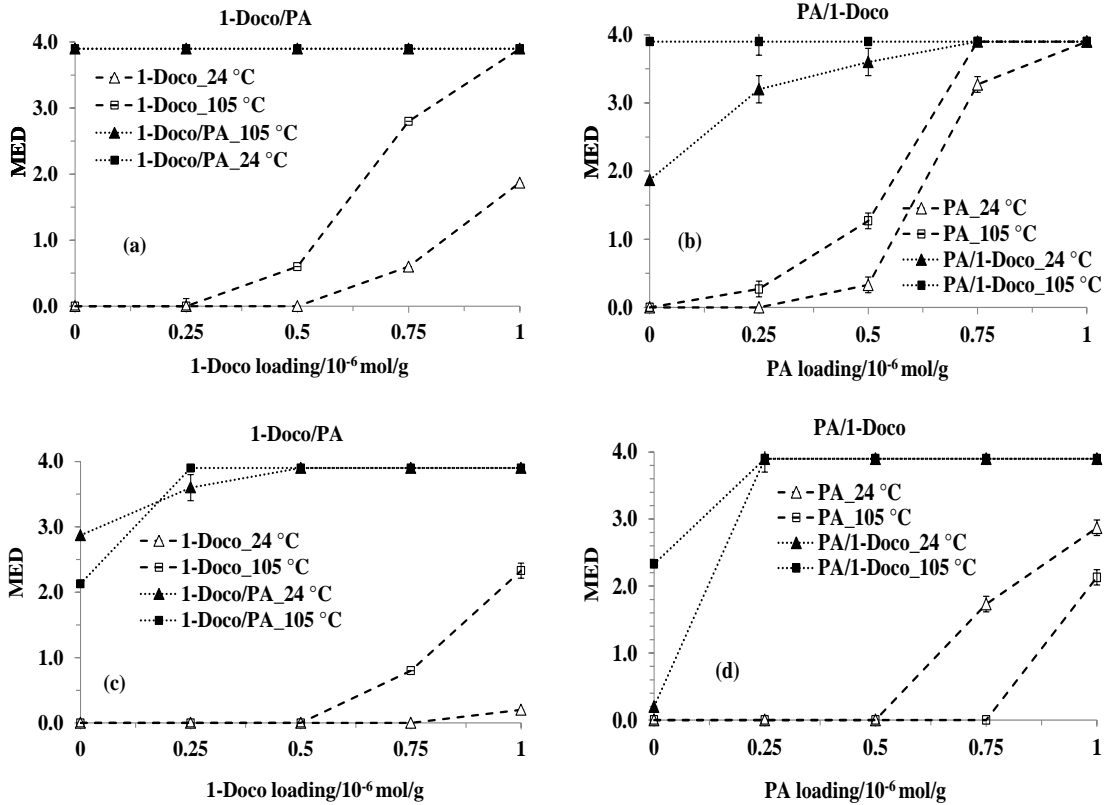
Figure 5.5　　　Effect of palmitic acid and 1-docosanol in different ratios (a) PA (fixed,1×10^{-6} mole g^{-1}) and 1-docosanol on AWS (b) PA and 1-docosanol (fixed,1×10^{-6} mole g^{-1}) on AWS (c) PA (fixed,1×10^{-6} mole g^{-1}) and 1-docosanol on AWS with 5% KL (d) PA and 1-docosanol (fixed,1×10^{-6} mole g^{-1}) on AWS with 5% KL.

Furthermore, when the mixture was applied on AWS with 5% KL, it was found that at a gradual increase of IsoM, did not affect the low level background SWR from 1-Doco. However, after heating to 105°C, IsoM leads to an initial increase in MED, but at higher concentrations, the MED begins to drop back towards 1-Doco value (Figure 5.4c). A gradual increase of 1-Doco concentration on AWS with 5% KL led to increased SWR at 24°C. However, adding a fixed loading of IsoM (1×10^{-6} mole g^{-1}), lowered SWR relative to 1-Doco alone (Figure 5.4d). Once again, the severity of SWR was substantially enhanced, following heating to 105 °C even for lower concentrations of different ratios of the applied binary mixtures of 1-Doco and IsoM.

As noted previously, PA and 1-Doco were individually found to induce SWR significantly. However, it is also of interest to consider the effect of these compounds in combination. Figure 5.5a reveals that a background level of 1×10^{-6} mole g^{-1} of PA is sufficient to induce severe SWR regardless of the level of 1-Doco loading. When 1-Doco concentration was constant at 1.0×10^{-6} mole g^{-1}, and PA was gradually increased, the SWR was sharply increased in combination with 0.25×10^{-6} mole g^{-1} PA (Figure 5.5b).

1-Doco only induces slight SWR on AWS with 5% KL at 24°C with loadings of greater than 0.75×10^{-6} mole g^{-1}. However, if a background level (1×10^{-6} mole g^{-1}) of PA is present its effect is dominant and severe SWR is induced in combination with 0.25×10^{-6} mole g^{-1} 1-Doco (Figure 5.5c).

PA induces SWR on AWS with 5% KL only at loadings of $>0.5 \times 10^{-6}$ mole g^{-1}. The synergistic effect of the two compounds is revealed when PA is combined with a background loading (1.0×10^{-6} mole g^{-1}) of 1-Doco. In this case, severe SWR is reached at 0.25×10^{-6} mole g^{-1} of PA (Figure 5.5d). The severity of SWR was enhanced following heating at 105 °C for all the above systems investigated (Figure 5.5a-d).

The differences in SWR of corresponding loadings on AWS and AWS with 5% KL may be due to the presence of particles with different sizes. For example, Ma'Shum et al. (1988) found particle size is inversely related to the degree of induced SWR. The differences in SWR of all the systems investigated might imply differences in the molecular level interactions with the mineral particle surfaces. Therefore, molecular dynamics simulations were performed to explore the nature of these interactions for a selection of these systems.

5.3.2 *Computational modeling*

At the lowest surface coverage, only a single molecule of hexadecane is placed on each of the surfaces for the molecular dynamics simulations. Consequently, the molecules have a high degree of conformational freedom. The length distribution profile clearly demonstrates the conformation on silica which ranges from ~4-18 Å (Figure 5.6a). However, for the kaolinite and quartz systems, the length distribution for hexadecane is concentrated between ~15-19 Å indicating the molecule adopts quite an extended conformation on these surfaces.
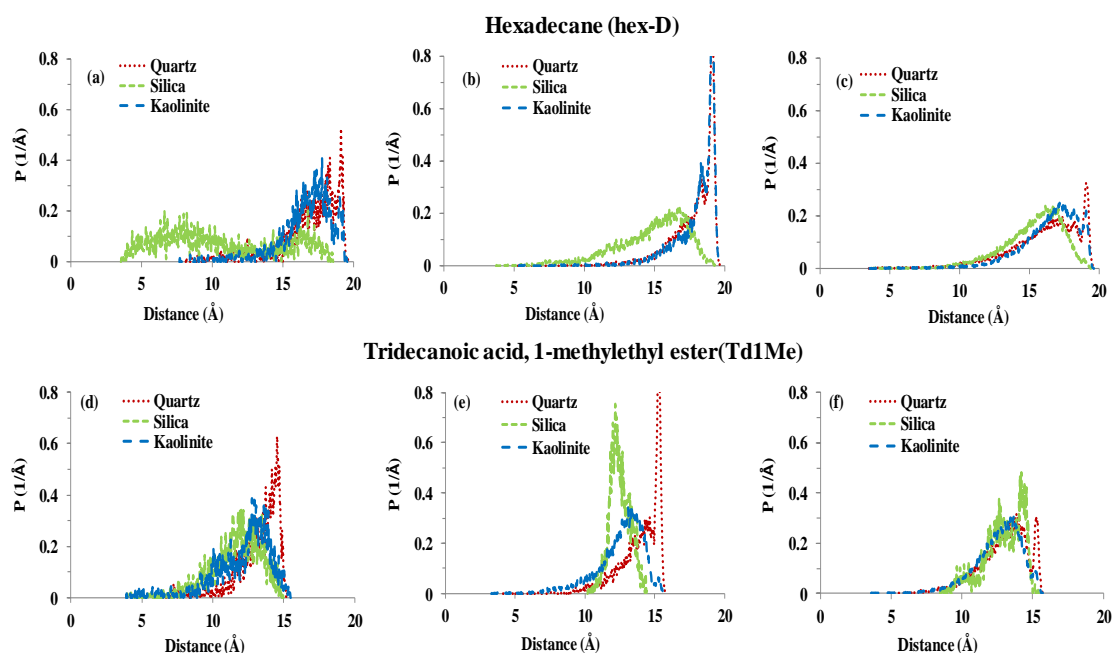
Figure 5.6   Chain length distribution of hexadecane and tridecanoic acid, 1-methylethyl ester (Td1Me) on cleaved model surfaces at a, d) 0.1 molec nm^{-2} b, e) 1.0 molecs nm^{-2} and c, f) 2.3 molecs nm^{-2}.

As the surface density of molecules increases (1.0 molecs nm^{-2}), there is less conformational freedom and the molecules spend more time in extended (-trans) conformations. This is particularly true for the quartz and kaolinite systems where the

molecules can align with the flat mineral surfaces (Figure 5.6b). However, the irregular surface of silica disrupts the alignment of the hexadecane molecules so that a substantial population of all-trans conformers is only observed at the highest surface coverage investigated (Figure 5.6c). Moreover, the length distribution for Tridecanoic acid, 1-methylethyl ester(Td1Me) was concentrated <15Å for silica and kaolinite (Figure 5.6d-f) at different surface densities. The conformational freedom for Td1Me is found minimum on silica (~7-15Å) (Figure 5.6d) even at the lower surface density (0.1 molecs nm^{-2}). However, a substantial population of extended conformers is exhibited on quartz at the higher surface densities (Figure 5.6e-f).

The interface region (the region of overlap) varies across the surfaces investigated due to their morphological features. When a single molecule of hexadecane is placed on each of the surfaces, it exhibits dynamic freedom and migrates randomly across the mineral surfaces. At a surface density of 1.0 molecs nm^{-2}, the molecules scatter randomly across the surface to initially form a monolayer. The layer is evident on quartz by the presence of a sharp peak at1.0 molecs nm^{-2}, and a shoulder on it indicates the initial stages of formation of the second lateral layer (Figure 5.7a).

Hexadecane (hex-D)

Tridecanoic acid, 1-methylethyl ester (Td1Me)
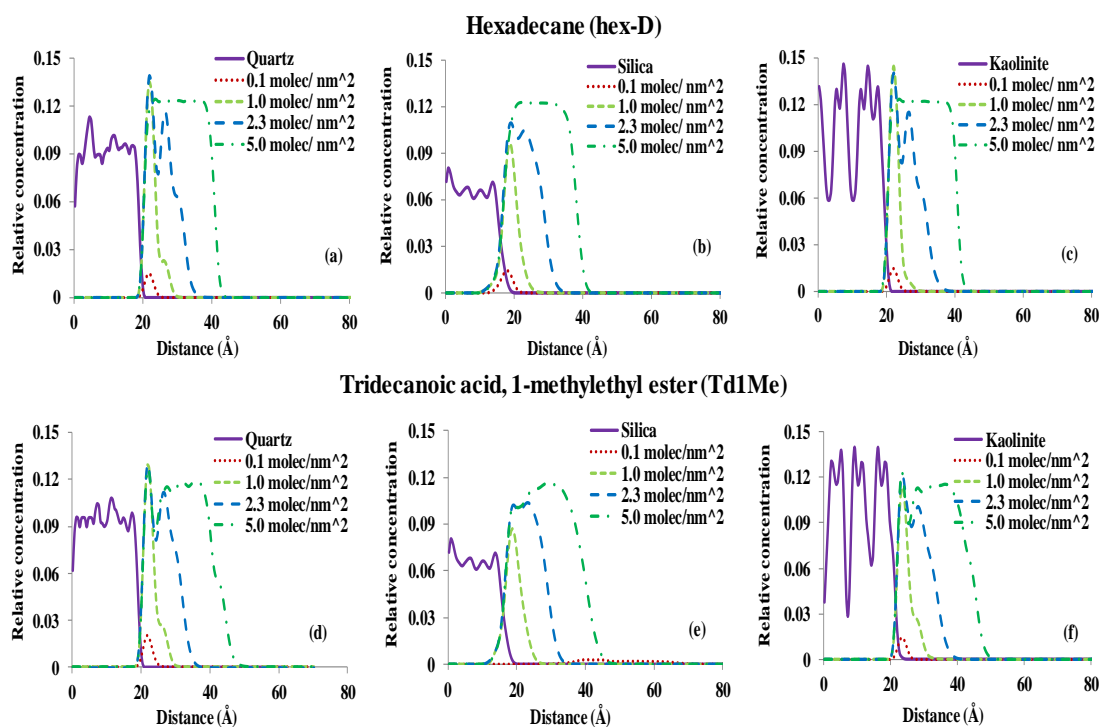
Figure 5.7   Concentration profiles of hexadecane and tridecanoic acid, 1-methylethyl ester (Td1Me) at different surface densities on cleaved model surfaces for a, d) quartz b, e) silica and c, f) kaolinite.

Further increases in the surface density (2.3 and 5.0 molecs nm^{-2}) leads to the formation of layering of molecules on quartz and kaolinite surfaces (Figure 5.7a, c, d and f). Layering also occurs on silica, but the irregular surface profile means that the organic layer is less uniform. The concentration profile reveals that a second layer is fully formed and a third lateral layer has already begun to form at a surface coverage at 2.3 molecs nm^{-2}, and this is consistent with the molecular conformation of wax molecules on quartz (Walden et al., 2015). The broader peak on the surfaces at the higher surface density (5.0 molecs nm^{-2}) denotes extended conformation of molecules on them (Figure 5.7a-f). The hexadecane molecules in these systems are well aligned compared to Td1Me with the mineral surface.

a) Hexadecane

quartz silica kaolinite

b) Tridecanoic acid, 1-methylethyl ester
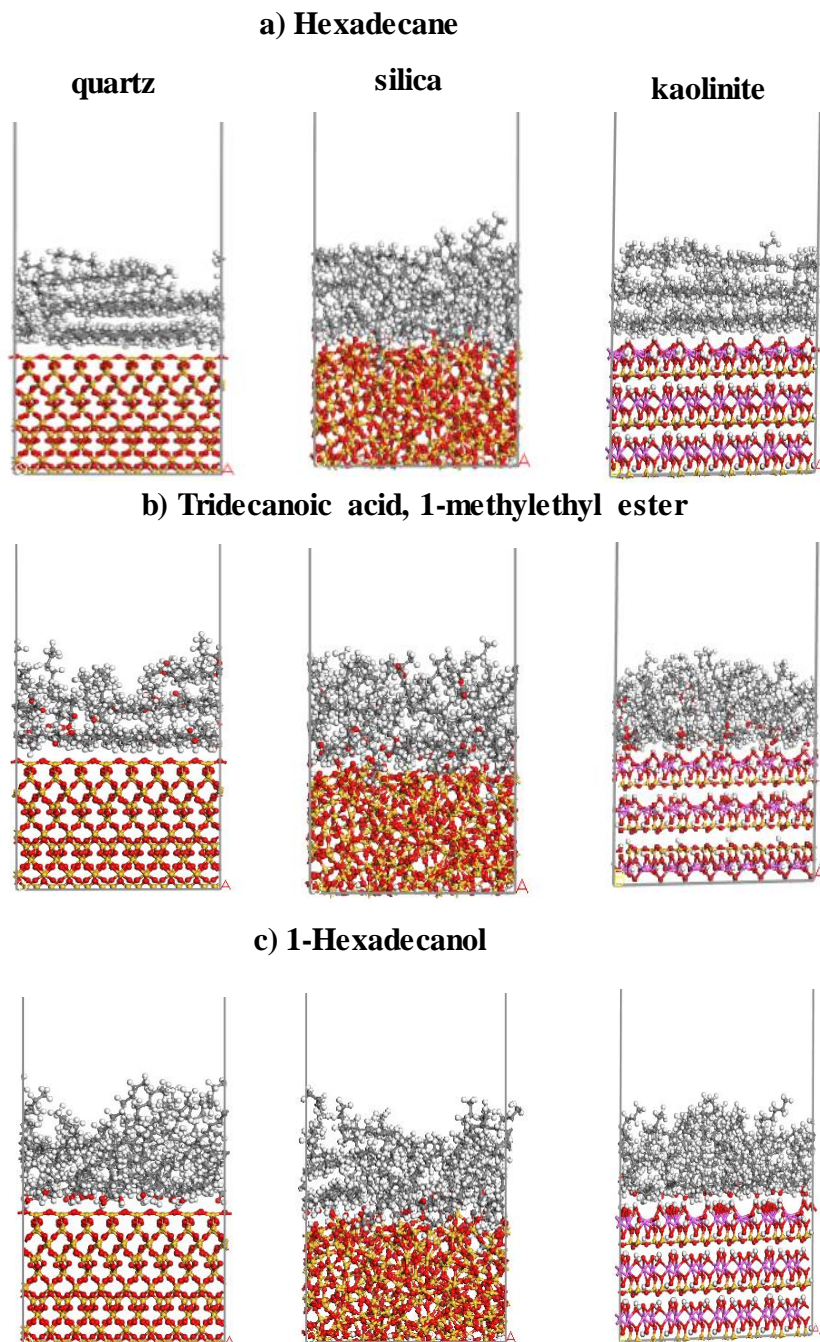
c) 1-Hexadecanol

Figure 5.8   Cross section of a) hexadecane, b) tridecanoic acid, 1-methylethyl ester (Td1Me) and c) 1-hexadecanol on cleaved model surfaces at 2.3 molecs nm^{-2} after equilibration.

However, the earlier studies of amphiphilic molecules on kaolinite indicated that a transition from lateral to tilted arrangement began at a surface density of ~2.3 molecs

nm^{-2}. The arrangement of molecules was attributed to H-bonding interaction of the polar head groups of the molecules with the OH$^-$ groups of the surface. Hexadecane does not contain a polar functional group, and therefore there is no specific interaction driving a transition from lateral to tilted alignment. Therefore, increasing the surface density of hexadecane molecules only leads to an increase in the number of lateral layers formed.

Hexadecane molecules are evident as laterally aligned on the quartz and kaolinite surfaces (Figure 5.8a). However, due to the presence of OH$^-$ groups on the kaolinite surface there is hydrogen bonding with Td1Me (ester), which facilitate a transition from lateral to tilted alignment at a surface density of ~2.3 molecules nm^{-2} (Figure 5.8b). The Td1Me molecules in the second lateral layer on quartz surface are not as well aligned as hexadecane molecules (Figure 5.8a, b). The alignment of molecules on the surface can be explained by reduced packing efficiency due to the bulkier head of Td1Me, which reduces cohesion between the hydrocarbon chains. This packing arrangement is consistent with our experimental finding that for a gradual increase of Isopropyl Myristate (IsoM) content on AWS with a fixed loading of 1-docosanol, the severity of SWR decreased. Mainwaring et al. (2013) noted that butyl tetradecanoate does not induce SWR over the loading range of $(0-20) \times 10^{-6}$ mole g^{-1}. Interestingly, on the rough surface of silica Td1Me exhibits meandering alignment of the molecules (Figure 5.8b). Hexadecane and 1-hexadecanol molecules were also not well aligned on the surface (Figure 5.8a, c). Moreover, 1-hexadecanol molecules on the quartz and kaolinite surfaces were observed to be in transition from lateral to extended conformation at this surface density (Figure 5.8c).

Simulations performed at the highest surface coverage (5.0 molecules nm^{-2}) of hexadecane, Td1Me and 1-hexadecanol (Figure 5.9a-c), started with a vertically aligned

monolayer similar to a Langmuir monolayer arrangement suggesting that the molecules sorb to mineral surface in a discrete zonal structure as proposed by Kleber et al. (2007). However, at this surface density Td1Me molecules are not as well aligned with the mineral surfaces as that of hexadecane and 1-hexadecanol (Figure 5.9a-c). The arrangement corresponds to a uniform monolayer of molecules with extended (trans) conformations consistent with the predictions of Zisman (1964). However, a close-packed monolayer is required before measurable hydrophobicity can be detected (Ma'Shum et al., 1988).

a) Hexadecane

quartz	silica	kaolinite

b) Tridecanoic acid, 1-methylethyl ester
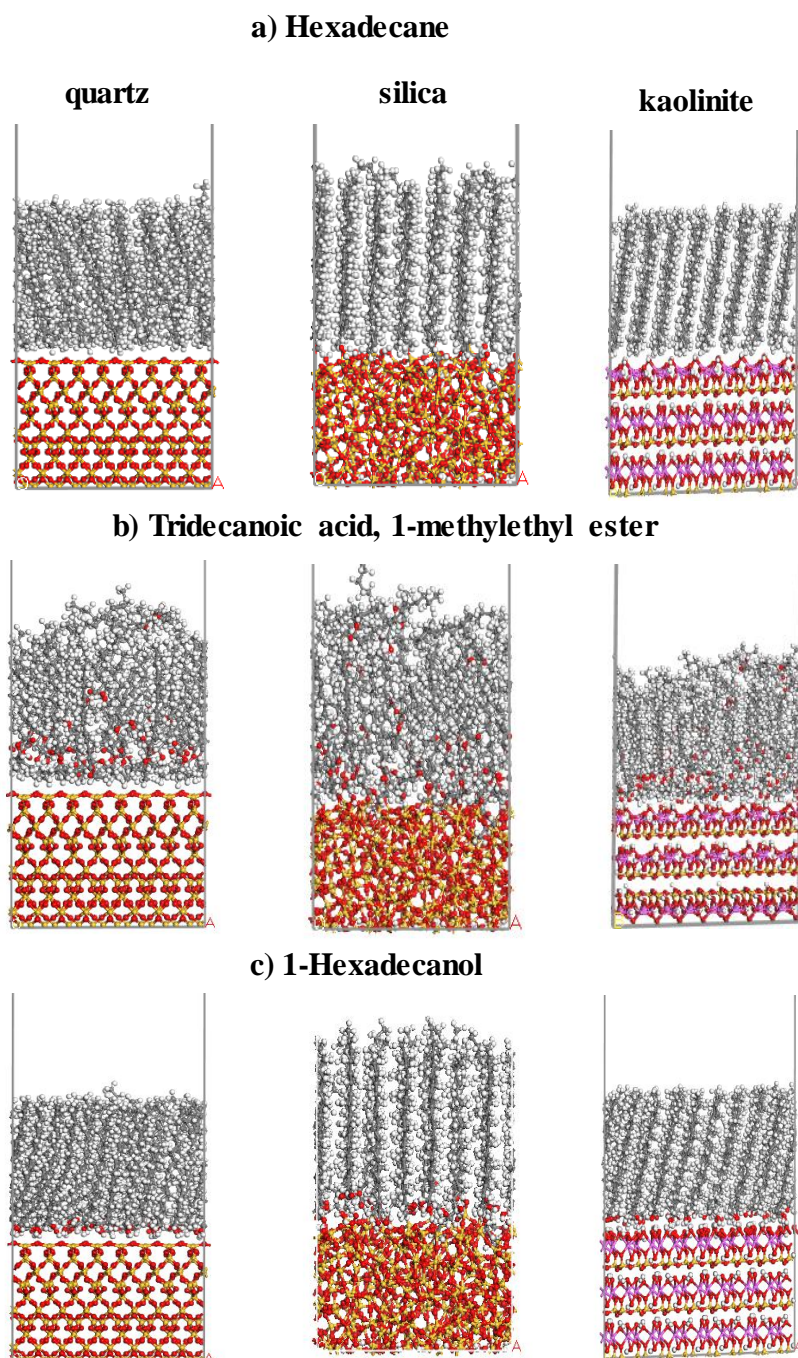
c) 1-Hexadecanol

Figure 5.9   Cross section of a) hexadecane, b) tridecanoic acid, 1-methylethyl ester (Td1Me) and c) 1-hexadecanol on cleaved model surfaces at 5.0 molecs nm^{-2} after equilibration.
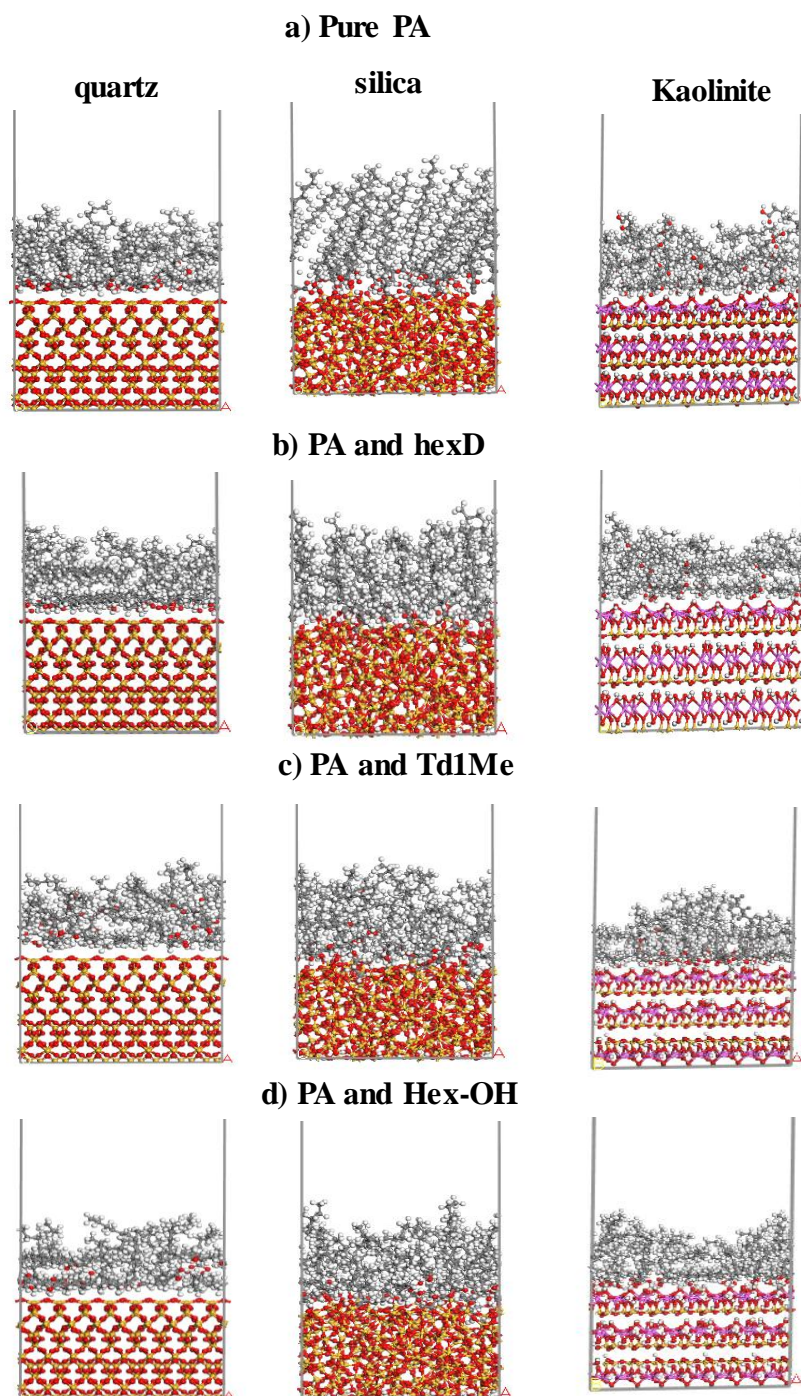
Figure 5.10   Cross section of a) pure palmitic acid (PA) b) PA and hexadecane (hex-D) c) PA and tridecanoic acid, 1-methylethyl ester (Td1Me) and d) PA and 1-hexadecanol (Hex-OH) of 2.3 molecs nm^{-2} after equilibration.

As the experimental loading experiments demonstrated, PA and 1-Doco coatings are very effective at inducing SWR, even at low concentrations. However, the presence of a hexadecane or tridecanoic acid, 1-methylethyl ester (Td1Me) can have a modulating effect on the non-wetting character of the coatings. To better understand this effect at a molecular level we investigated the binary mixtures of compounds on each of the mineral surfaces at a total surface density of 2.3 molecs nm^{-2}. It was evident that molecular arrangement of the binary mixtures on the surfaces was different between each other and even different with the PA on its own at the same surface density (Figure 5.10a-d).

Physicochemical interactions between a mineral and organic molecules of contrasting hydrophobicity determine the spatial order of compounds in a distinct zonal structure (Petridis et al., 2013). Interactions between surface atoms and all the pure lipidic compounds and their binary mixtures (PA, hexadecane, Td1Me, PA and hexadecane, PA and Td1Me, PA and 1-hexadecanol) were investigated using radial distribution functions (RDFs) ($g(r)$). In particular, the C^{molecs}- O^{surf} RDFs indicate that the minimum separation between the molecular chains and the surface is ~3.0Å and does not exhibit strong correlations for any of the individual compounds or mixtures studied (Figure 5.11a-d). However, the interaction between C^{molecs} – O^{surf} for the pure PA exhibited broader peaks on the surafces (Figure 5.11a). The similarity in the C^{molecs} – O^{surf} and C^{molecs}- Si^{surf} RDF for the mixtures on the surfaces reveals that the principal interaction between the hydrophobic tails and with the surface is van der Waals (vdW) forces. Wu et al. (2013) noted vdW as the main contribution of interaction of the molecular components of heavy crude oil on quartz surface. Moreover, the intermolecular C^{molecs} – C^{molecs} RDFs were exhibited with sharp peaks for the individual compounds or mixtures studied (Figure 5.11e-h). The complementary molecular dynamics simulation

also demonstrates that non-ionisable compounds may have a relatively low affinity for a mineral surface because they cannot form cation bridges (Shevchenko & Bailey, 1998).
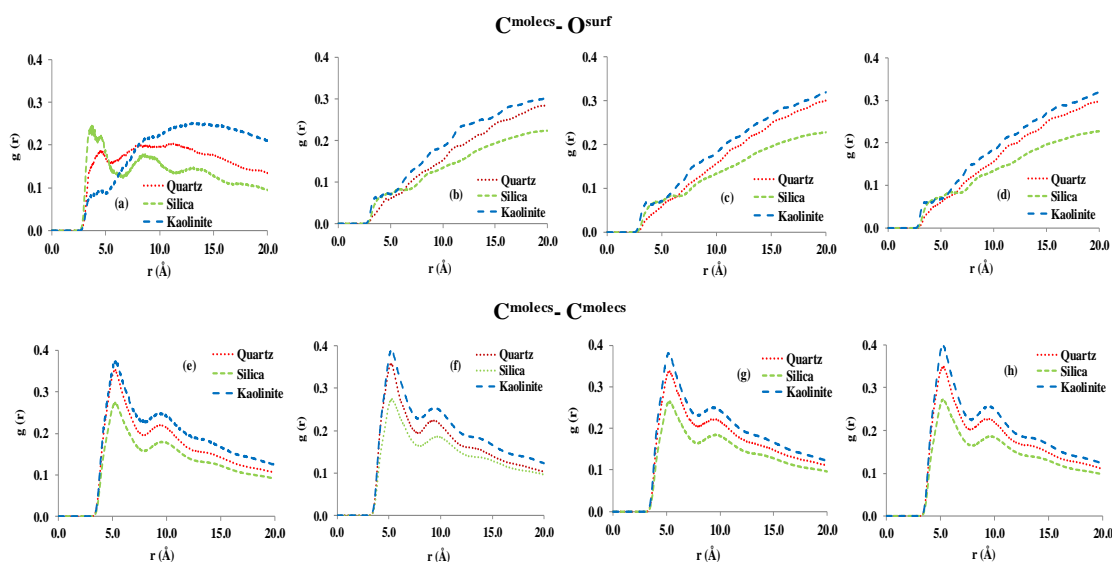
Figure 5.11 C^{molecs}- O^{surf} and C^{molecs}- C^{molecs} for 2.3 molecs nm^{-2} of PA (a, e), PA and hexD (b, f), PA and Td1Me (c, g) PA and Hex-OH (d, h) on the surfaces.

The specific atomic interactions in the molecular dynamics study are shown in Figure 5.12. The interactions between the acidic hydrogen of PA (H^{PA}) and oxygen atoms of the surfaces (O^{surf}) are investigated, and found with strong interactions (~1.4Å) for pure PA both on the quartz and silica surfaces (Figure 5.13a). The RDFs for H^{PA}-O^{surf} of the mixture of PA and hexD reveal that there are also strong hydrogen bond donor interactions with the quartz and silica similar to that of PA alone (Figure 5.13b). However, there is negligible H- bonding with the polar kaolinite surface that might be due to the presence of lateral molecular layer adjacent to the surface.
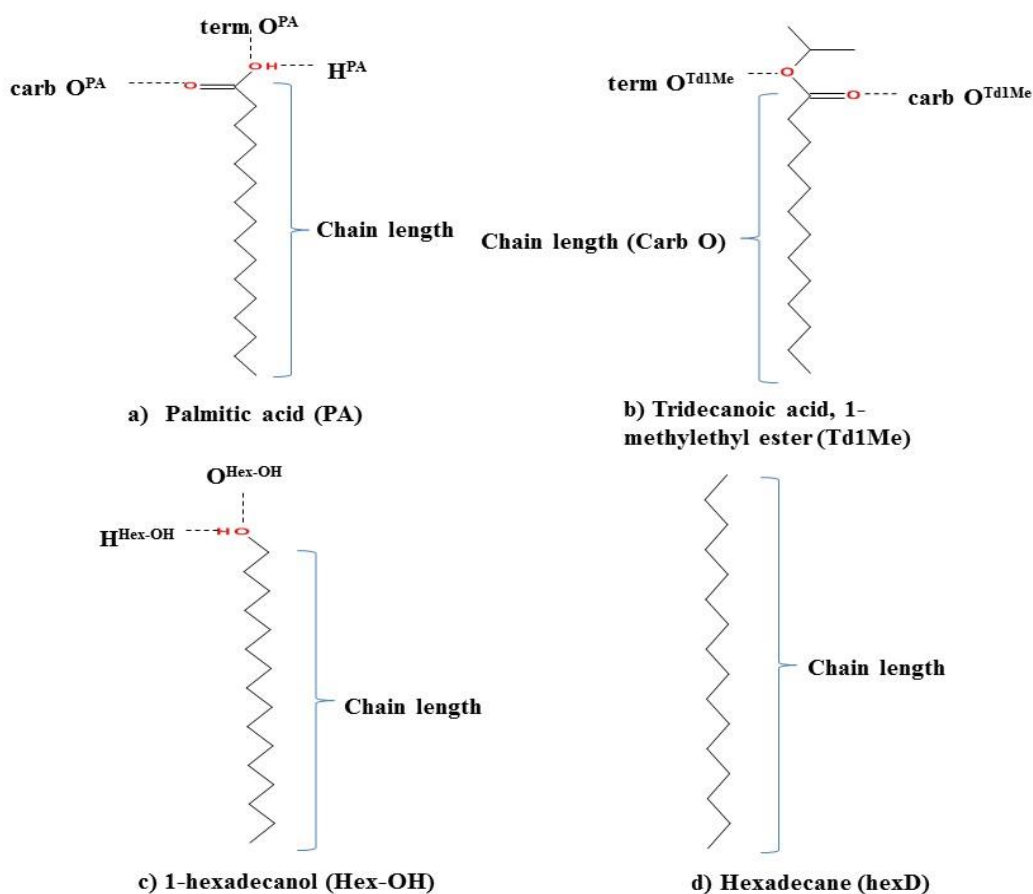
Figure 5.12   Molecular interactions studied based on particular atoms on the mineral surfaces a) palmitic acid b) tridecanoic acid, 1-methylethyl ester (Td1Me) c) 1-hexadecanol and d) Hexadceane.

The H^{PA} – O^{surf} RDF for the mixture of PA and Td1Me system has a sharp peak at ~1.5 Å on both silica and kaolinite surfaces while on the quartz surface it was found with a weaker interaction. This once again suggests the importance of interactions with OH^- groups of the mineral surfaces in influencing the molecular conformation on soil particle surfaces (Figure 5.13c). Moreover, the RDFs (H^{PA}-O^{surf}) for the mixture of PA and Hex-OH reveal that acidic and alcoholic - H atoms have very strong H-donor interactions with the oxygen atoms of kaolinite and silica surfaces (Figure 5.13d). However, the interaction with quartz was found to be weaker in comparison with the

other surfaces. This once again emphasizes the importance of polar (OH⁻) groups within

molecules and surfaces in stabilizing the interactions through hydrogen bonding.
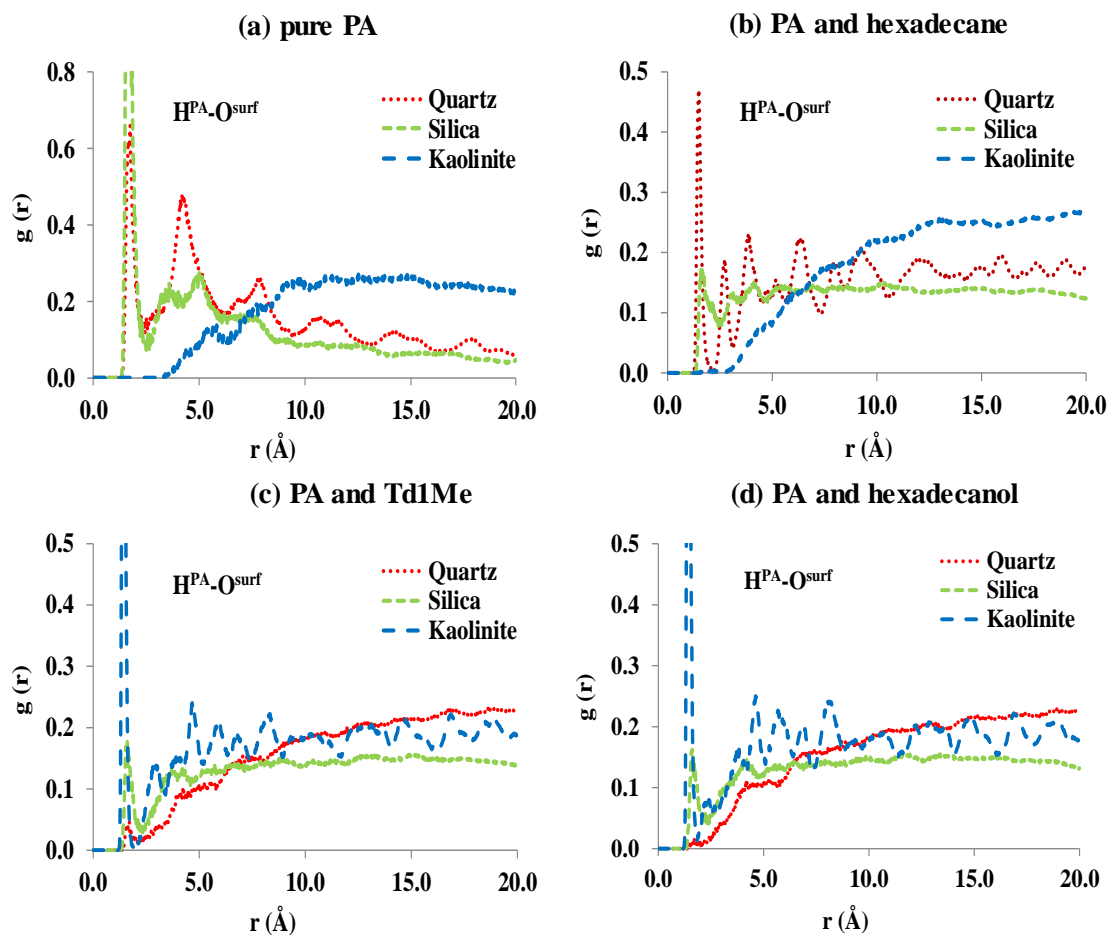
Figure 5.13 H^{PA}-O^{surf} RDFs at 2.3 molecs nm^{-2} for the mixture of a) pure PA, (b)PA

and hexadecane, (c) PA and Td1Me, and (d) PA and hexadecanol.

Sandy soils dominate most water repellent soil and thus we investigated and compared molecular level interaction of the individual and mixture of compounds on the model quartz surface. The interaction between the acidic hydrogen of PA and oxygen atoms of the surface (H^{PA}- O^{surf}) reveals that pure PA and mixture of PA and hexadecane generates sharp peaks at ~1.7Å and ~1.5 Å, respectively, indicating strong H-bonding between molecules and the surface (Figure 5.14a). In comparison, the intensity of interaction between PA and the surface is greatly reduced by the addition of Td1Me. The weaker interaction is consistent with our experimental result that for a gradual increase of the concentration of isopropyl myristate (IsoM) with a fixed loading of palmitic caid on AWS, the severity of SWR decreased.
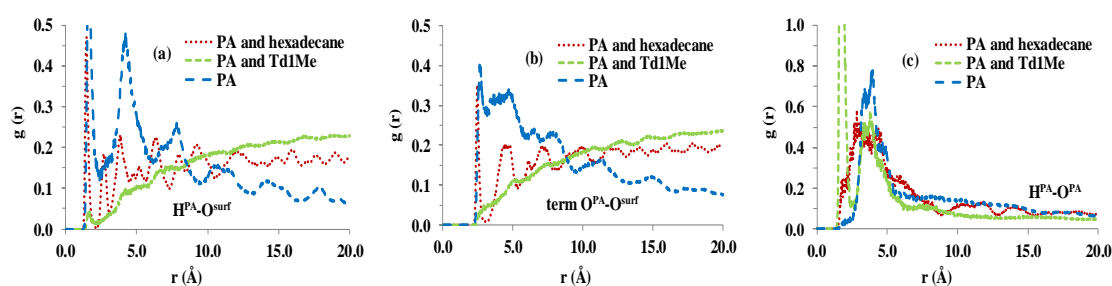
Figure 5.14   RDFs for a) H^{PA}- O^{surf} b)term O^{PA}- O^{surf} and c) H^{PA}- O^{PA} of the pure PA and combination of compounds on the quartz surface.

The termO^{PA}- O^{surf} RDFs reveal that both the pure PA and mixture of PA and hexadecane have a very sharp peak at ~2.5 Å (Figure 5.14b). Again, a combination of PA and Td1Me indicates a much weaker interaction. The intermolecular RDFs between acidic hydrogen and oxygen atoms of PA (H^{PA}- O^{PA}) show that the mixture of PA and Td1Me generates very sharp peak at ~1.6 Å while pure PA and mixture of PA and hexadecane reveal moderate peaks at ~3.3 and 2.8Å, respectively (Figure 5.14c). The strong H^{PA}- O^{PA} RDF for the mixture of PA and Td1Me inversely correlates with weaker interactions of the mixture with the surface.
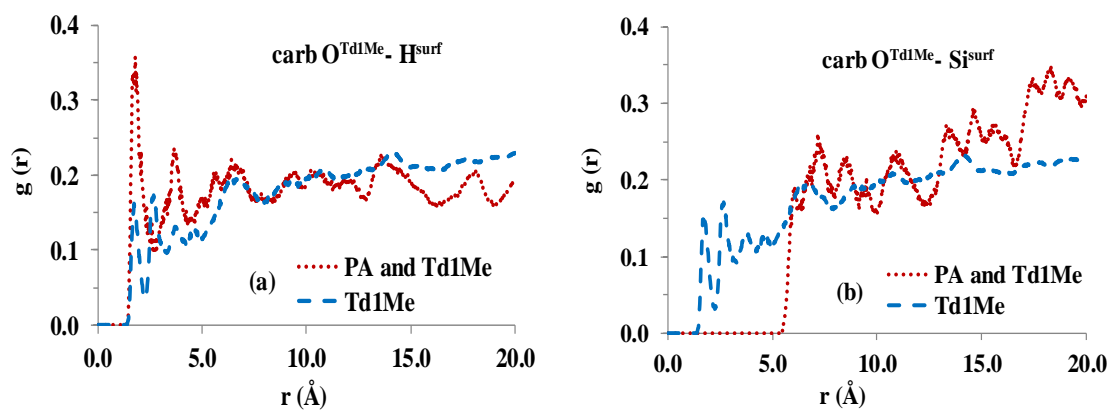
Figure 5.15   RDFs of a) carb O^{Td1Me} - H^{surf} and b) carb O^{Td1Me} - Si^{surf} for pure Td1Me and a mixture of PA and Td1Me on model kaolinite surface.

As mentioned in the previous section kaolinite is a highly polar surface and actively participates in influencing molecular arrangement. Accordingly pure Td1Me and a mixture of PA and Td1Me were applied to determine their molecular level interaction with the surface. The interaction between carbonyl oxygen of pure Td1Me (carb O^{Td1Me}) and hydrogen atoms of the kaolinite surface, RDF (carb O^{Td1Me} - H^{surf}) reveal a sharp primary peak at ~1.7Å. Interestingly, the RDF (carb O^{Td1Me}- H^{surf}) for the mixture of PA and Td1Me shows the first peak at ~2.0Å that could be due to the reduced packing efficiency of Td1Me (Figure 5.15a). The difference in packing efficiency suggests conformation of molecules varies between pure compounds and the mixtures, which ultimately affect the severity of SWR. Franco et al. (1995) found enhanced severity of SWR with compound loading on a surface precoated with an initial hydrophobic layer. Furthermore, (carb O^{Td1Me} - Si^{surf}) RDFs exhibits a sharp peak at ~1.7Å for Td1Me alone while the combination of PA and Td1Me generates the primary peak at ~6.0Å (Figure 5.15b).
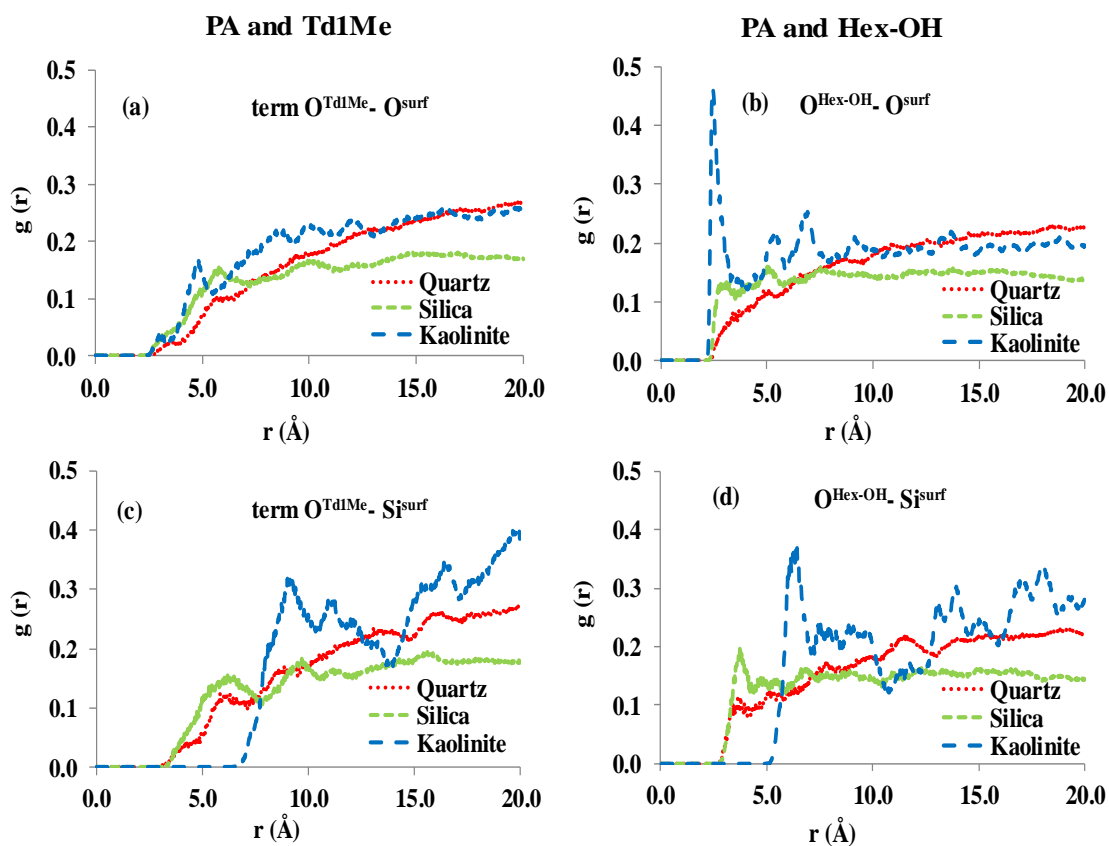
Figure 5.16   RDFs of term O^{molecs}- O^{surf} and term O^{molecs}- Si^{surf} for the mixture of PA and Td1Me (a, c) and a mixture of PA and Hex-OH (b, d) on model surfaces.

The RDFs of term O^{Td1Me} - O^{surf} reveals moderate interaction between the ester and kaolinite surface that is observed through a dominant peak at ~4.7Å. The small peak at shorter distance denotes the molecules in the mixture are not entirely well aligned with polar kaolinite surface. In addition, moderate peaks on quartz and silica are found at ~5.3Å and ~5.5Å, respectively (Figure 5.16a). In comparison, the interaction between the oxygen atom of hexadecanol and surface oxygen atoms, RDFs (O^{Hex-OH}- O^{surf}) reveals stronger interactions that exhibit sharp peak at ~2.4Å on kaolinite. A moderate interaction occurs on silica with a peak at ~2.7Å while on quartz the interaction was found to be insignificant (Figure 5.16b).

151

The RDFs between terminal oxygen atoms of Td1Me and the surface silicon (term O^{Td1Me} - Si^{surf}) reveal a moderate peak at ~5.8Å and ~6.0Å on both quartz and silica surfaces, respectively. However, a sharp peak is found at ~9.0Å on kaolinite surface (Figure 5.16c). Alternatively, the interaction between O^{Hex-OH}- Si^{surf} shows a moderate interaction with a closer approach to the alcohol exists on both quartz and silica surfaces, which is evident through the peak at ~3.3Å and ~3.6Å, respectively (Figure 5.16d). However, the primary peak on kaolinite surface is evident at ~6.0Å, which suggests a weaker interaction between these atom types. Besides, the RDFs for the mixture PA and Hex-OH suggest greater packing efficiency on the kaolinite surface in the lateral arrangement (2.3 molecules nm^{-2}).
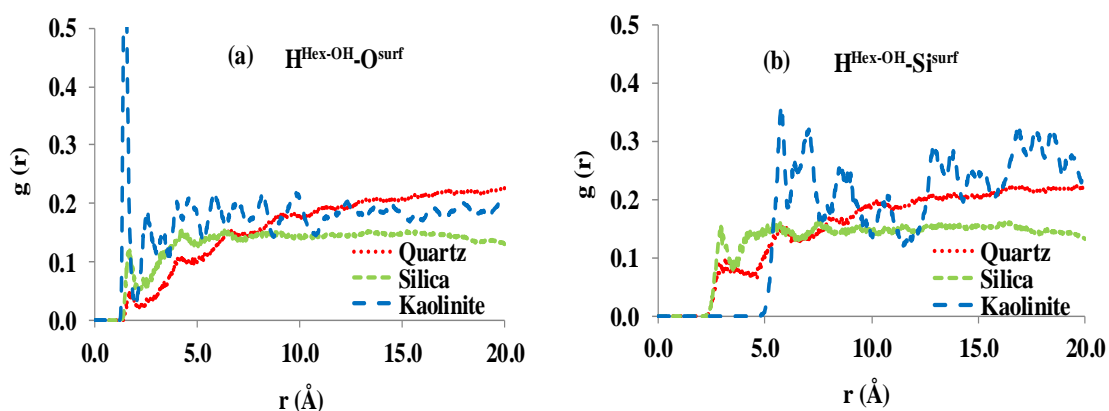
Figure 5.17   RDFs for a) H^{Hex-OH}-O^{surf} and b) H^{Hex-OH}-Si^{surf} of the mixture of PA and Hex-OH on surfaces.

The H^{Hex-OH}-O^{surf} RDFs in the mixture of PA and Hex-OH reveal strong interactions in the order of K> Si> Q at ~1.4Å (Figure 5.17a) while in the study of Uddin et al. (2017), the interaction on quartz was found at ~1.8Å with Hex-OH alone. However, H^{Hex-OH}-Si^{surf} RDFs are found with a moderate interaction at ~3.0Å (Figure 5.17b) on both quartz and silica surfaces. The interaction on the kaolinite surface is apparent at ~5.7Å due to the morphological structure of the mineral.

PA and Td1Me

(a) H^{PA}-term O^{Td1Me}

(c) carb O^{PA}- term O^{Td1Me}

(e) term O^{PA}-term O^{Td1Me}

PA and Hex-OH

(b) H^{PA}-term O^{Hex-OH}

(d) carb O^{PA}-term O^{Hex-OH}

(f) term O^{PA}-term O^{Hex-OH}
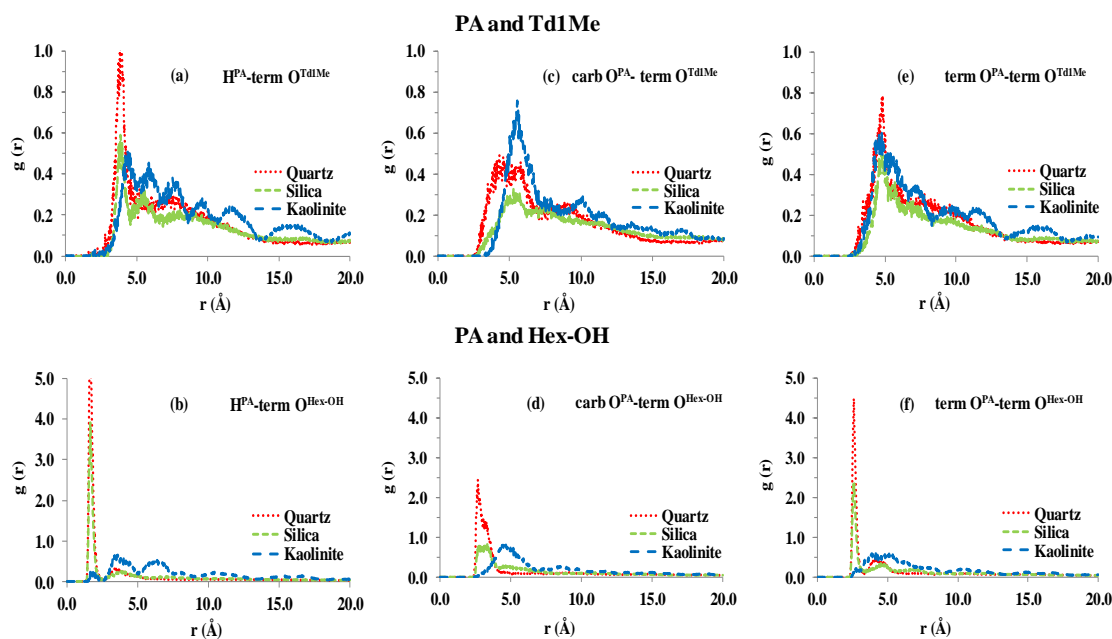
Figure 5.18   Intermolecular H^{PA}- term O^{molecs} (a, b), carb O^{PA}- term O^{molecs} (c, d), term O^{PA}- term O^{molecs} (e, f) RDFs for the mixture of PA and Td1Me, and PA and Hex-OH.

The radial distribution function for intermolecular interactions reflects the distance between molecular chains of the mixture of PA and Td1Me and PA and Hex-OH. The RDFs for terminal oxygen atoms of Td1Me (term O^{Td1Me}) with acidic hydrogen of PA (H^{PA}- term O^{Td1Me}) shows that there are weak H-bond type interactions between the molecules (Figure 5.18a). A sharp primary peak is observed at ~3.8Å for both quartz and silica surfaces. Secondary peaks correspond with the formation of the second lateral layer on quartz while the broad nature of the third peak on silica suggests that there are no specific long range interactions in the layers formed from these molecules. The primary peak shows weaker intermolecular H-bonding between PA and Td1Me on kaolinite at ~4.3Å, and secondary peaks at ~5.7 Å, ~7.3 Å and beyond suggest much greater packing order of the molecules (Figure 5.18a). Alternately, H^{PA}- term O^{Hex-OH} RDFs reveal that there are strong interactions (~1.7Å) between PA and Hex-OH on both

153

quartz and silica surfaces (Figure 5.18b) while a smaller peak is observed on kaolinite surface at a distance of ~1.5Å. The smaller primary peak on kaolinite again inversely correlates with the stronger interaction of amphiphilic molecules with the surface.

The RDFs for carbonyl oxygen atoms of PA (carb O^{PA}) with terminal oxygen atoms of Td1Me (carb O^{PA}- term O^{Td1Me}) exhibit two peaks on quartz surface at ~4.0 Å and ~5.0 Å, respectively (Figure 5.18c). This corresponds to the lateral layer formation of molecules on the quartz surface. A sharp peak observed at ~5.5 Å on kaolinite suggest a greater spacing of the head groups on this surface. Interestingly, a broad peak at ~5.3 Å on silica denotes that there is no specific packing arrangement. Interchangeably, the RDF between carb O^{PA}- term O^{Hex-OH} indicates strong attraction between PA and Hex-OH on quartz (~1.7Å) (Figure 5.18d). The structure of the molecules and size of their head groups have important implications for the packing and cohesion of the hydrocarbon chains. This is consistent with the concept that saturated palmitic acid increases the cohesion between the hydrocarbon chains relative to unsaturated double bond elaidic acid, thereby increasing the packing efficiency of the saturated acid (Mainwaring et al., 2013; Shaw & Costello, 1993). Moreover, the single dominant peak (at ~4.3 Å) on kaolinite suggests that the smaller head groups of Hex-OH are intimately aligned with an acid group of PA. The term O^{PA}- term O^{Td1Me} RDFs reveal a sharp peak on quartz at ~4.8Å (Figure 5.18e) that indicates a longer range intermolecular interaction between PA and Td1Me due to the bulkier head group of Td1Me (ester). This longer range interaction was also evident at ~4.4 and ~4.6Å on silica and kaolinite surfaces, respectively. The peak intensity on kaolinite indicates that the alignment of molecules is not lateral and uniformly packed on the surface. Alternately, the term O^{PA}- term O^{Hex-OH} RDFs shows that there are strong intermolecular interactions between PA and Hex-OH on both quartz and silica surfaces whereas, on the kaolinite surface the

RDF was found with a small peak at the same distance (Figure 5.18f). The intensity of intermolecular interaction again inversely correlates the stronger interactions of the molecules with the surface. Furthermore, the intermolecular H^{PA}- carb O^{Td1Me}, carb O^{PA}- carb O^{Td1Me} and term O^{PA}- carb O^{Td1Me} RDFs reveal stronger interactions on the quartz followed by silica and kaolinite surfaces for the mixture of PA and Td1Me on the surfaces (Figure 5.19).
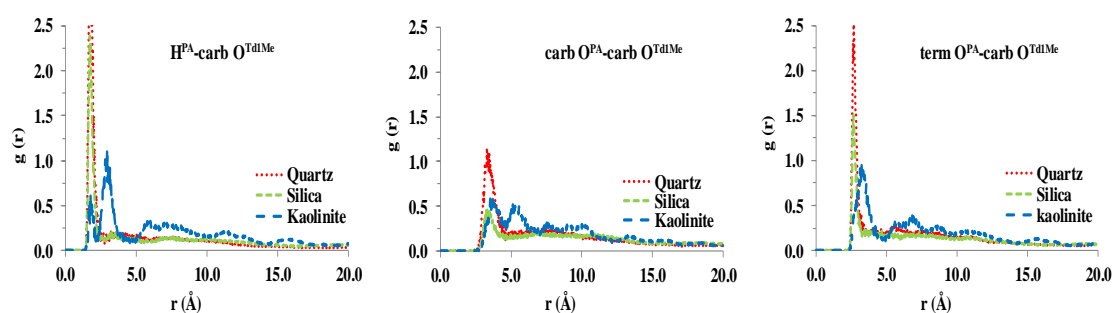
Figure 5.19   RDFs for H^{PA}- carb O^{Td1Me}, carb O^{PA}- carb O^{Td1Me}, term O^{PA}- carb O^{Td1Me} of PA and Td1Me.

The intermolecular interaction between acidic hydrogen and oxygen atoms of palmitic acid (H^{PA}- O^{PA}) in the mixture was also investigated. The H^{PA}- O^{PA} RDF for the pure PA revealed weaker intermolecular interaction that is exhibited from peaks at ~3.8 Å on the surfaces (Figure 5.20a). Applying PA and hexD on quartz surface it is found that a moderate interaction is evident from peaks at ~2.6 and ~3.6Å, respectively, that suggest the hexD molecules disrupt the H-bonding between PA molecules on this surface (Figure 5.20b). Sharp peaks on silica and kaolinite surfaces at ~1.8Å revealed stronger interactions between the acid groups due to interaction with OH⁻ groups of the surfaces.
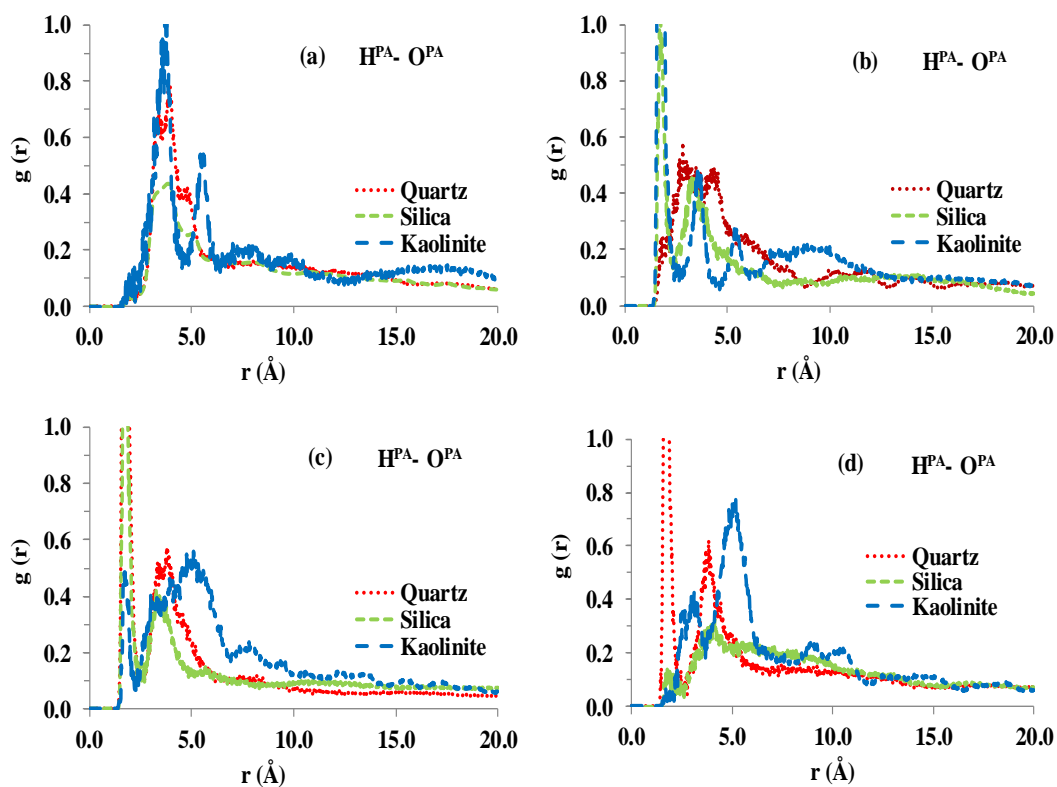
Figure 5.20   RDFs of H^{PA}- O^{PA} for the mixture of (a) pure PA (b) PA and hexD (c) PA and Td1Me (d) PA and Hex-OH on model surfaces.

The H^{PA}- O^{PA} RDF for the mixture of PA and Td1Me reveals strong interactions at ~1.6Å on both quartz and silica surfaces while a moderate interaction is apparent on kaolinite surface (Figure 5.20c). The moderate interaction on the kaolinite surface is again inversely correlated with H^{PA}- O^{surf} RDF on the surface as noted in the previous section. The bulky head groups of Td1Me may prohibit intimate packing on the surfaces that facilitate polar head groups to interact each other. The poorly aligned conformation of the mixture is evident through the cross section of the systems as shown in the previous figure. However, a moderate interaction on kaolinite emphasizes the contribution of surface OH- groups in the intermolecular H^{PA}- O^{PA} interactions. The H^{PA}- O^{PA} RDF for the PA and Hex-OH mixture shows, a very strong interaction is evident on quartz surface at ~1.7Å (Figure 5.20d) that suggests a uniform lateral layer

has developed. A weaker interaction was observed on both silica and kaolinite surfaces for the mixture of PA and Hex-OH.
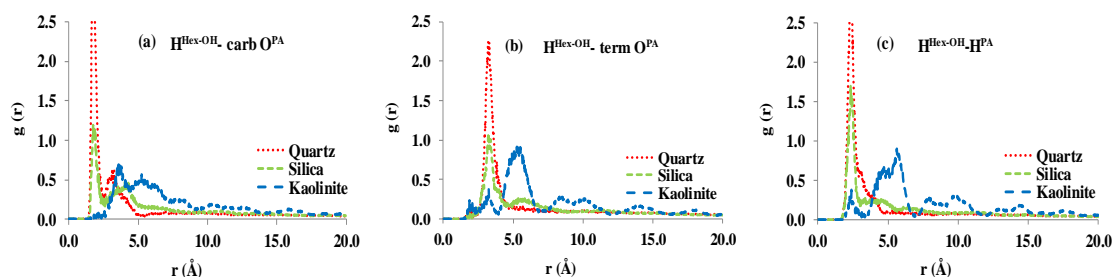
Figure 5.21   Intermolecular RDFs for H^{Hex-OH}- carb O^{PA}, H^{Hex-OH}- term O^{PA}, H^{Hex-OH}-H^{PA} of the mixture of PA and Hex-OH on model surfaces.

The intermolecular RDF for alcoholic hydrogen of Hex-OH and carbonyl oxygen of PA (H^{Hex-OH}- carb O^{PA}) revealed strong interactions at ~1.8Å (Figure 5.21a) on both quartz and silica surfaces while a moderate interaction was evident at ~3.5Å on kaolinite. This suggests a uniform arrangement of molecules in the lateral layers on these surfaces. The sharp primary peak and consequent broader peaks on kaolinite suggested less interaction on this surface. Furthermore, H^{Hex-OH}- term O^{PA} RDF revealed that a very small interaction is apparent on kaolinite at ~1.8Å and was evident at ~3.2Å on both quartz and silica surfaces (Figure 5.21b). Interestingly, the H^{Hex-OH}-H^{PA} RDF is apparently visible at ~2.2Å on the quartz, silica and kaolinite surfaces in the range of Q> Si> K (Figure 5.21c). The gradual peaks of primary, secondary and beyond on kaolinite surface suggest distinct orientation of the molecules as proposed by Shevchenko and Bailey (1998).

157

5.4 Conclusions

Individual and mixtures of compounds were applied to acid washed sand (AWS) and AWS with 5% kaolinite to investigate different molecular interactions with the mineral surfaces. For example, molecules with acidic and alcoholic hydrogen atoms were found to have strong hydrogen donor bond interactions with the surfaces. Experimental results revealed that a mixture of PA and hexadecane had strong potential for inducing SWR in comparison with pure PA or pure hexadecane. PA was found very effective in inducing SWR on AWS and AWS with 5% kaolinite even at the lower loading ranges. Hexadecane (hexD) alone does not induce SWR. However, hexD was found to enhance the effect of SWR of other compounds like PA and 1-docosanol. Moreover, heating the samples to 105°C for 24h increased the severity of SWR in almost all of the samples. However, the level SWR was different between AWS and AWS with 5% kaolinite.

Isopropyl Myristate (IsoM) was found to be insignificant in inducing SWR both on AWS and AWS with 5% kaolinite even though it has a polar ester group. It was also found to reduce the effect of 1-docosanol when combined in a mixture. In particular, for a gradual increase of ester (Td1Me) concentration, the severity of SWR was slowly decreased on AWS with 5% kaolinite. However, IsoM was found to neither add to or detract from the SWR effect of PA on AWS.

Mixtures of 1-docosanol (1-Doco) with hexadecane or IsoM gave similar behavior to the combinations with PA. For example, when 1-docosanol was mixed with hexadecane the severity of repellence was increased. On the contrary, mixing 1-Doco with IsoM, reduced the severity of SWR. However, a mixture of 1-Doco and PA was found to have enhanced severity of SWR relative to the individual components. This could be due to

158

the strong H-donor atoms of their OH$^-$ and –COOH groups which should lead to favorable intermolecular and surface interactions.

In the computational analysis, a gradual increase of the surface density (0.1 and 1.0 molecs nm$^-2$) of molecules (e.g. hexadecane, Td1Me) led to a layering of the molecules both on quartz and kaolinite surfaces. However, with the surface density of 2.3 molecs nm^{-2}, the amphiphilic molecules (PA and Hex-OH) were found tilted on the kaolinite surface. Furthermore, at the highest surface coverage of 5.0 molecs nm^{-2}, they maintained a vertically aligned monolayer. However, the irregular surface of silica disrupted the alignment of the hexadecane molecules so that a substantial population of all-trans conformers was only observed at the highest surface coverage investigated.

Hydrogen donor atoms of PA were found to have a strong interaction with the surface oxygen atoms on both quartz and silica surfaces when it was applied in combination with hexadecane. Moreover, when PA was combined with pure Td1Me or Hex-OH, it was found that H^{PA} had stronger interactions with the polar kaolinite surface. However, the intensity of interactions varied between the mixtures that could be due to the reduced packing efficiency and lack of cohesion between hydrocarbon chains.

Interactions of the polarized acid atoms (H^{PA}- O^{surf} and term O^{PA}- O^{surf}) for both pure PA layers and layers of PA and hexadecane were found to have strong interactions on quartz compared with that of a PA and Td1Me mixture. The bulky head group of Td1Me reduces the cohesion and packing efficiency between the hydrocarbon chains, which contributes to the weaker interaction. Interestingly, carb O^{Td1Me}- O^{surf} and carb O^{Td1Me}- Si^{surf} RDFs indicated the Td1Me molecules approach closer to the kaolinite surface for a pure layer compared with that of the combination layer of PA and Td1Me.

The variations in the calculated intermolecular interactions support our experimental findings that for a fixed loading of PA and gradual increase of IsoM content, the severity of SWR on AWS with 5% KL decreased. Furthermore, intermolecular H^{PA}- term O^{Hex-OH}, carb O^{PA}- term O^{Hex-OH}, term O^{PA}- term O^{Hex-OH} RDFs of the mixture of PA and Hex-OH revealed enhanced interactions, which corresponds to the enhanced SWR for PA/1-Doco mixtures.

 The H-bonding between PA molecules (H^{PA}- O^{PA} RDFs) in mixtures of PA and hexD, PA and Td1Me and PA and Hex-OH varied, due to changes in the organization and packing of the molecules on the simulated surfaces. This packing arrangement corresponds to the varying severity of SWR for the PA in combination with hexD, IsoM, and 1-Doco on the investigated substrates. Therefore, the conclusion of this study is that the severity of SWR depends on molecular conformation through their intermolecular and surface interactions.

6 Physicochemical interaction of long- chain hydrophobic compounds in an aqueous soil environment

6.1 Introduction

Organic materials responsible for SWR in soils are mostly hydrophobic and amphiphilic compounds in the soil profile, derived from the leachate of plant degradation products and lignin-carbohydrate complexes. Once these compounds are in the soil, they can interact with the soil mineral grains and are usually stabilized as aggregates bound together by weak bonding mechanisms, such as hydrogen bonding, π-bonding, van der Waals interactions and hydrophobic forces, resulting in micelle like or 'membrane like' structures (Wershaw, 1986). In fact, these ordered structures can constitute a separate phase in soil water systems (Wershaw, 1989). Amphiphilic compounds are believed to interact with mineral surfaces through their hydrophilic or polar head groups, which may include hydroxyl, carboxylic acid, carboxylate and amide functional groups. However, these polar head groups will also interact with water molecules when the soil is wet (Ma'shum & Farmer, 1985).
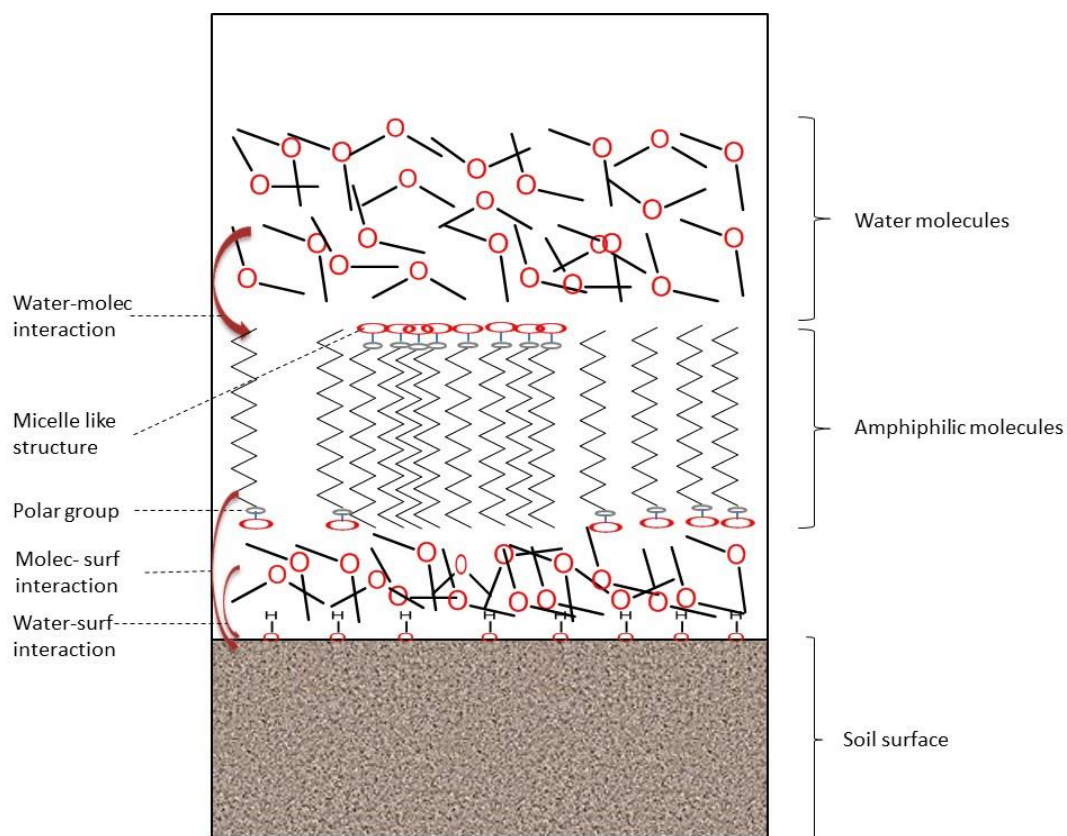
Figure 6.1   Organo-mineral interaction in an aqueous soil environment.

The complex nature of organo-mineral interfaces can significantly modify the extent of stabilization of organic compounds in soils (Petridis et al., 2013). Amphiphilic molecules in soil with high moisture content usually form ordered aggregates in which the hydrophobic parts of the molecules are in the interiors and the hydrophilic parts constitute the exterior surfaces (Tanford, 1980) as shown in Figure 6.1. The wettability of layered silicates is of widespread interest in biogeochemical contexts and is believed to be determined by their crystalline structure (Yin et al., 2012). For example, the octahedral and tetrahedral surfaces of the kaolinite layer are of different chemical nature and can be considered as hydrophilic and hydrophobic, respectively (Tunega et al., 2004). Furthermore, hydroxylation level on the mineral surface is of critical importance in determining hydrogen bonding interactions with the molecules (Zhuravlev, 2000). Three distinct mechanisms of organic compound adsorption to clay mineral surfaces are

found, including, (a) maximised contact area without water, (b) via a single functional group with low levels of water and (c) in a structured layer in the presence of high water content (Yu et al., 2003).

SWR is a dynamic phenomenon and changes with time, temperature and exposure to soil moisture. In this context, it is proposed that amphiphilic compounds that induce SWR, change their orientation and level of interactions with mineral surfaces in response to ambient soil moisture level (Figure 6.1). In principle, a close packed monolayer of amphiphilic molecules should be sufficient to render a soil particle water repellent but analysis of sandy soils suggests that there is often sufficient organic material for several layers (Ma'Shum et al., 1988). For example, 0.35 g of hydrophobic compounds in 1000 g of medium sized sand particles can induce severe SWR. A limiting area of 0.20-0.22 nm^2 molecule $^{-1}$ is estimated for formation of a monolayer, which is proposed as condensed films of straight chain fatty acids irrespective of chain length (Shaw & Costello, 1993). Mainwaring et al. (2013) reported that a loading of 0.1-0.2$\times10^{-6}$ mol g^{-1} is required for a monolayer coverage of octadecanoic acid on acid washed sand (AWS) with a specific surface associated with a particle size 200-300 cm^2g^{-1}. Furthermore, morphological features of different soil particles can influence the arrangement and structure of monolayers (Miller et al., 2007; Tunega et al., 2004). For example, a molecular dynamics study revealed that a low surface coverage of 2.35 molecules nm^{-2} of wax molecules was found to adopt a semi-ordered, tilted packing arrangement on the gibbsite like surface of kaolinite, whereas on quartz it leads to a two layer arrangement (Walden et al., 2015). This suggests strong hydrogen bonding or van der Waals dipole-dipole interactions affect the layering and packing of wax molecules on soil particles (Horne & McIntosh, 2000; Ma'shum & Farmer, 1985; Wu et al., 2013).

However, Wu et al. (2013) reported van der Waals intercations as the main contribution of adhesion of asphaltenes, resins, aromatics and saturates on quartz surfaces.

Understanding both the chemical properties of hydrophobic coatings and their physical interaction with mineral surfaces in an aqueous soil environment is necessary to improve our understanding of SWR. Experimental studies provide a broad understanding of the wetting behavior of soil or hydrological effects but do not provide a molecular level understanding of the interaction of molecules with water in a soil matrix or of its kinetic and thermodynamic stability. However, a detailed understanding of the mechanisms of the interaction is important in governing the fate of these hydrophobic compounds in the soil environment. Considering this research gap, we perform a simulation study to investigate the physical interactions of the applied organic compounds and water with the simulated soil particles. In particular, this study employs a molecular dynamics approach to investigate the interaction of both single compound layers and binary mixtures with mineral surfaces in the presence of water.

6.2   Computational models

The modeling framework for both the surface and molecules were developed using Materials Studio v 7.0 (Accelrys, 2013). The surface of a sand particle was represented by a cleaved quartz surface while hydroxylated amorphous silica was used to represent a weathered sand particle surface. A clay particle surface was modeled by the gibbsite like surface of kaolinite. Models of hydrophobic compounds included palmitic acid (PA), 1-hexadecanol (Hex-OH), and tridecanoic acid, 1-methylethyl ester (Td1Me). In addition to single compound monolayers, mixtures (50:50) of palmitic acid with tridecanoic acid, 1-methylethyl ester and palmitic acid with 1-hexadecanol were also investigated. Interfaces were wet with a water layer of ~20 Å thickness, comprising

~1200 water molecules. Different concentrations of compounds (0.1 – 5.0 molecules nm^{-2}) were achieved by placing different numbers of molecules on the built model surfaces. Periodic boundary conditions were used with unit cell with dimensions of 30.7 x 37.3 x 120.0 Å for quartz, 28.5 x 28.5 x 120.0 Å for silica and 30.9 x 35.7 x 180.0 Å for kaolinite. The large z-dimension ensures that adjacent cells do not interact along the z-axis when periodic boundary conditions are applied, resulting in a quasi-2D interface.

The potential energy for each system was calculated using the COMPASS force field (Sun, 1998), which has previously been shown to perform well for describing the interactions between condensed hydrophilic and hydrophobic surfaces (Henry et al., 2006; Henry et al., 2005; Shaw et al., 2013). Electrostatic interactions were calculated using the Ewald procedure, while van der Waals interactions were calculated with an atom-based procedure using a 12.50 Å cutoff, a spline width of 1.00 Å, a buffer of 0.50 Å and a long-range tail correction. The modeled interfaces were initially energy minimized using the conjugate gradient procedure with a convergence criterion of 0.04 kJ mol^{-1}. Molecular dynamics simulations were performed in the canonical ensemble (NVT, constant number of atoms (*N*), volume (*V*) and temperature (*T*)), equilibrated for 500 ps followed by data acquisition for 4500 ps, using 1.0 fs time steps. The temperature was maintained at 298 K using the Andersen thermostat (Andersen, 1980) with a collision ratio of 1.0.

Concentration profiles of the simulated soils and selected compounds were found by averaging the number of atoms in strips (parallel to the x-y plane) over the course of the molecular dynamics simulations. The profiles of individual components (surface and compounds) that comprise each system as a function of *z* position were included. The interface region of each system is arbitrarily considered as the region of coexistence of

the two components (surface/compounds) and is found to be quite narrow (~0.05 Å) on the quartz surface in comparison with other two mineral surfaces (silica and kaolinite), due to the morphology and rigidity of the mineral.

6.3   Results and Discussion

6.3.1   Concentration profile of the systems

When a single palmitic acid molecule was applied on either quartz and kaolinite, it adopted a lateral arrangement after equilibration, to maximize the interaction with the mineral surfaces (

Figure 6.2a). On silica the molecule conforms to the irregular shape of the mineral surface, often with the polar head group located in a cavity of the silica surface. Each of these three interfaces was then aquated with a layer of water molecules to investigate the effects of soil water. The silica - palmitic acid interface showed very little change with aquation (

Figure 6.2b). The palmitic acid molecule remained adhered to the quartz surface following aquation. However, the polar head group was drawn slightly away from the mineral surface due to the interaction with the water molecules (

Figure 6.2b). The kaolinite - palmitic acid interface exhibited the largest change following aquation. The water molecules completely wet the polar clay surface resulting in the release of the organic molecule to the air/water interface (

Figure 6.2b).

a) Dry system on surfaces

quartz   silica   kaolinite

b) Wet system on surfaces
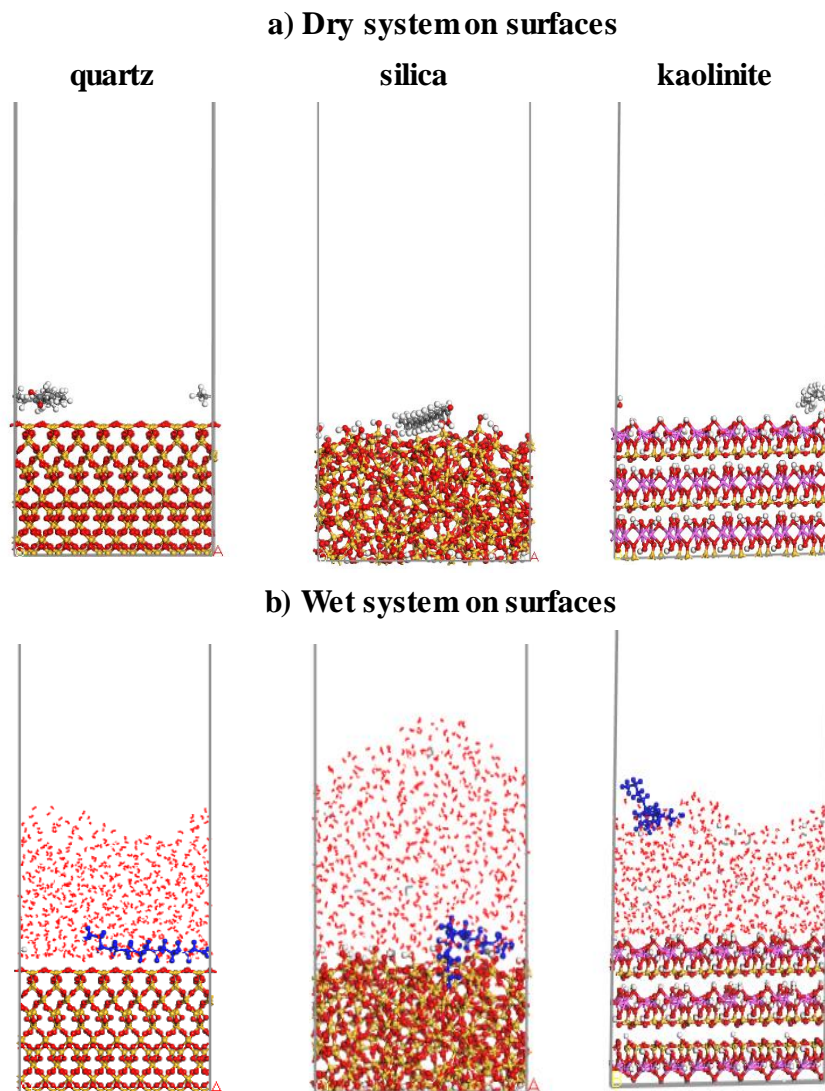
Figure 6.2   Cross section of PA/water simulation at 0.1 molec nm^{-2} both in the a) dry and b) wet systems after equilibration.

Importantly, when the surface density was increased to 1.0 molec/nm^2, the palmitic acid molecules arranged themselves in two lateral layers on quartz in the dry system while a single lateral layer was evident in the wet system (Figure 6.3a, b). Moreover, in the wet system, the polar head groups of some molecules were found at the top of the layer, suggesting a clear interaction between polar head groups and water molecules. Although mobility of the organic species is comparatively restricted on the silica surface, the polar head groups were found reoriented in the wet system compared with

the dry system. Interestingly, on kaolinite, the molecules were found clustered and attached to the point of the surface with polar head groups in the wet system while they were observed tilted on the thin lateral monolayer in the dry system.

a) Dry system on surfaces

| quartz | silica | kaolinite |

b) Wet system on surfaces
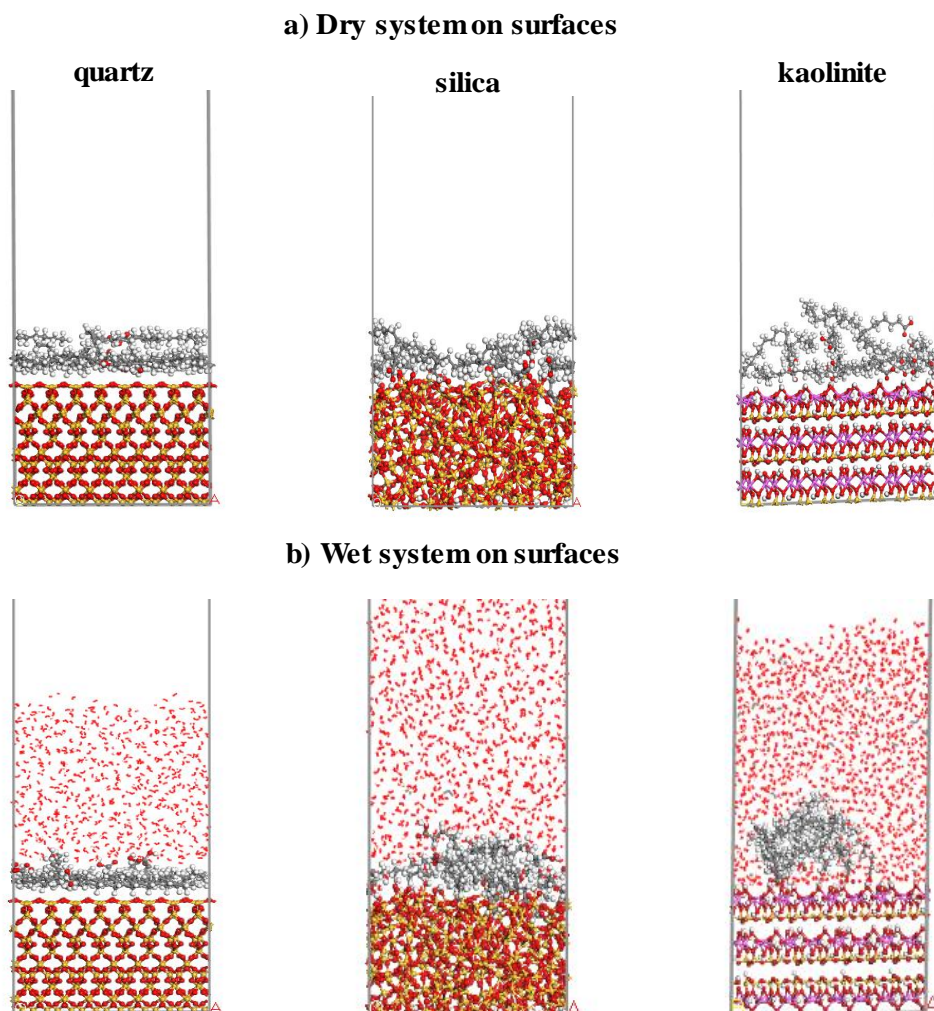
Figure 6.3   Cross section of PA of 1.0 molec/nm^2 both in the a) dry and b) wet systems after equilibration.

The interface regions (the region of overlap) of the concentration profiles were found varied across the surfaces investigated due to their morphological features (Figure 6.4). With a surface density of 1.0 molec nm^{-2}, the PA layer was found to occupy a narrow region in contact with the quartz providing little access for water to the mineral surface

(Figure 6.4a). However, the interface region was found wider between PA and water on both silica and kaolinite (Figure 6.4b, c), suggesting an intimate interaction of water molecules with the surfaces. The presence of hydroxyl groups on the polar kaolinite surface facilitated this closer interaction through H-bonding. The concentration profile on quartz surface also revealed an initial fully formed lateral layer and a small shoulder evident on it was presumably due to the presence of a couple of molecules on it.
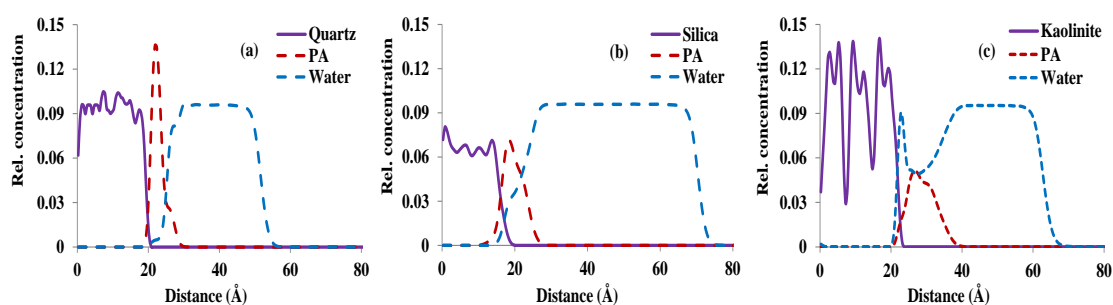
Figure 6.4   Concentration profiles of PA/water simulation at 1.0 molec nm^{-2} on a) quartz b) silica c) kaolinite.

6.3.2   Chain length distribution of the wet system

When a single molecule (0.1 molec nm^{-2}) of palmitic acid (PA) was placed on each of the surfaces in the wet system, the molecule was found to have a high degree of conformational freedom. The conformation is evident by the length distribution profile on silica (~11-18 Å) (Figure 6.5c). However, in the dry system, the length distribution was observed to be ~10-19 Å with the highest peak at ~17Å on this surface (Figure 6.5a). The mobility on the silica surface is restricted in part due to the amorphous nature of the substrate. However, on the kaolinite and quartz systems the length distribution for PA was concentrated between ~16-19 Å (Figure 6.5c) in the wet system, indicating the molecule adopts quite an extended conformation on these surfaces. The highest peak on kaolinite and quartz surfaces were observed at ~16 and ~18Å, respectively, in the dry system (Figure 6.5a).

At a surface density of 1.0 molec nm^{-2}, there is a substantial population of the molecules on silica in extended conformations in both of the systems (Figure 6.5b, d). The broader peak on kaolinite arises from the reorganization of the PA molecules away from the mineral into an aggregated micelle-like structure in the wet system. The highest peak on quartz in the wet system at ~17Å (Figure 6.5d) denotes the lateral distribution of a substantial population of molecules with the substrate. The dominant peaks on both the kaolinite (~17Å) and quartz (~18Å) surfaces in the dry system indicates lateral distribution of a large population of the molecules with the substrate.
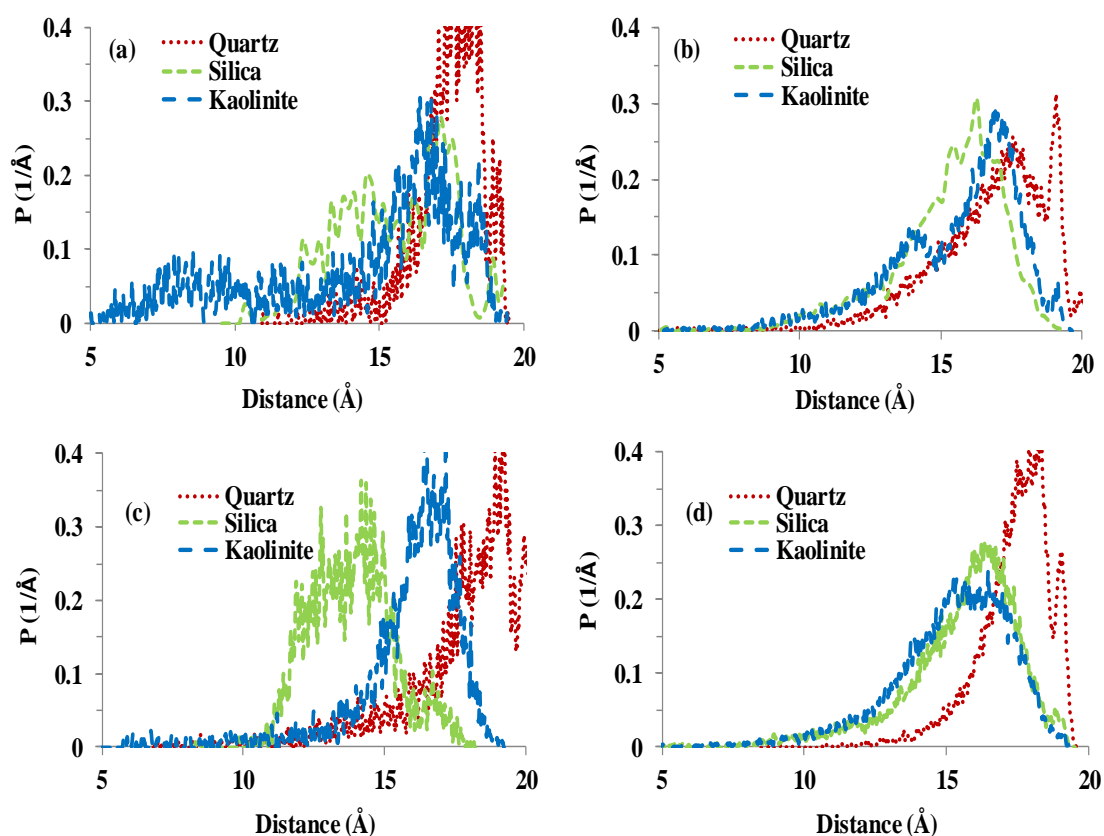
Figure 6.5   Chain length distribution for PA at 0.1 molec nm^{-2} (a, c) and 1.0 molec nm^{-2} (b, d) in the dry (a, b) and wet (c, d) systems.

When binary mixtures of PA and Td1Me, and PA and Hex-OH were placed on the surfaces at a surface density of 2.3 molec nm^{-2}, there was less conformational freedom

and the molecules spent more time in extended conformations (Figure 6.6a-d). This was particularly true for the quartz surface. As noted earlier, the irregular surface of silica was found to disrupt the alignment of the molecules. Therefore a substantial population of all extended conformers was only observed at the high surface densities for both pure PA and PA in combination with Td1ME or Hex-OH in the wet system. For example, the length distribution for PA in the mixtures was found to range from ~10-18Å on both the kaolinite and silica surfaces while on quartz it was observed to range from ~11-19Å (Figure 6.6a, b). Moreover, the chain length distributions of Td1Me or Hex-OH revealed that the molecules exhibit different conformational freedom in the mixed layers. This is consistent with findings in Chapter 4 that Td1Me and Hex-OH molecules can significantly modify the severity of SWR through molecular re-organization on soil particle surfaces. For example, Td1Me was found to be less extended than PA (~8-16.5Å) on all three surfaces (Figure 6.6c). The Hex-OH molecules had similar length distribution profile on silica but adopted less extended conformations on quartz and kaolinite (Figure 6.6d).
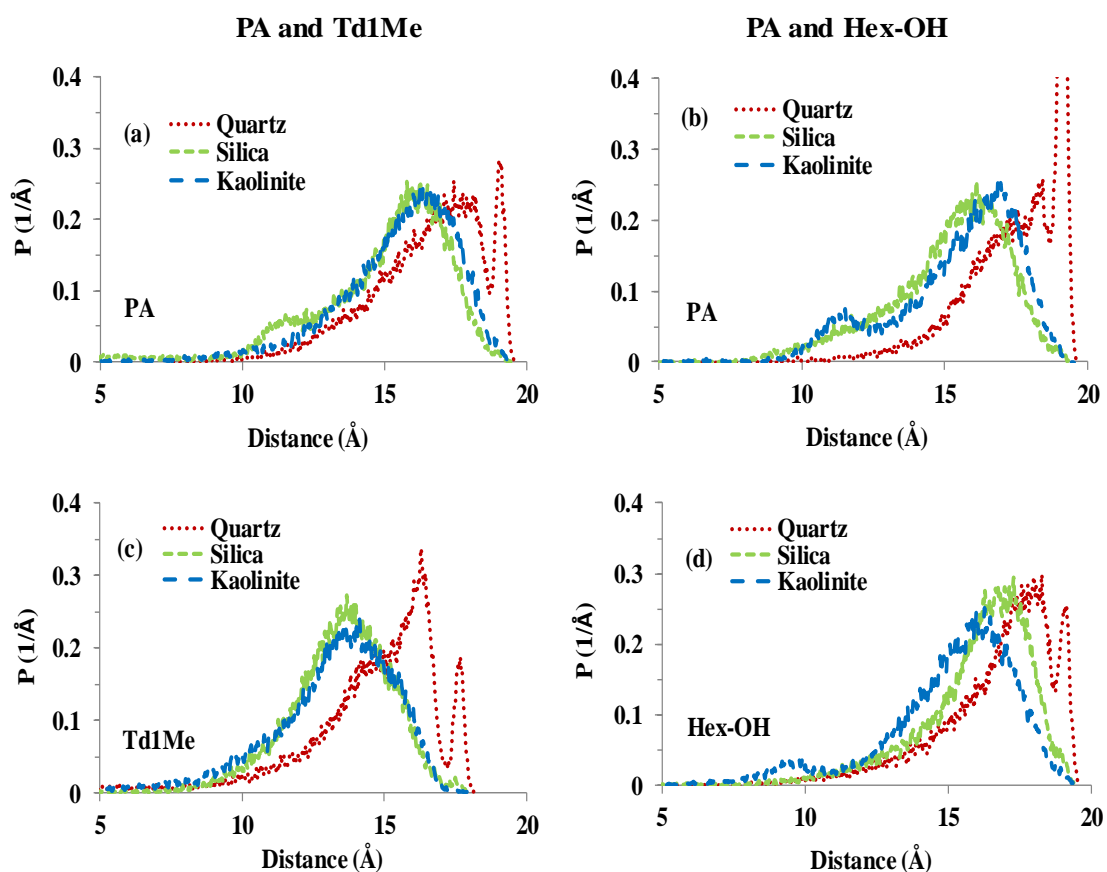
Figure 6.6   Chain length distribution of PA (a, b), Td1Me (c) and Hex-OH (d) for the mixture of PA and Td1Me, PA and Hex-OH in the wet system.

6.3.3   Conformation of PA on model soil surfaces

Interactions between organic molecules, water and the surfaces were investigated using radial distribution functions (RDFs) ($g(r)$). Palmitic acid (PA) molecules were found to have significant interaction with both the water molecules and polar surfaces. In particular, the interactions between acid hydrogen atoms (H^{PA}), carbonyl oxygen atoms (carb O^{PA}), terminal carboxylate oxygen atoms (term O^{PA}) and surface oxygen atoms (O^{surf}) were investigated. The interaction of acidic hydrogen of PA with water molecules was also examined. It was found that hydrogen and oxygen atoms of the polar head group of palmitic acid did not exhibit any specific interactions with the atoms of the quartz surface. In comparison, there were closer interactions between the polar head

groups and both the silica and kaolinite surfaces, due to hydrogen bonding. Sharp peaks were identified for the H^{PA}- O^{surf}, carb O^{PA}- O^{surf} and term O^{PA}- O^{surf} RDFs on kaolinite (~1.3 Å, ~3.0 Å and ~2.3 Å) and silica surfaces (~1.7 Å, ~3.2 Å and ~2.5 Å) (Figure 6.7a- c), indicating the importance of H-bonding in organo-mineral interactions. However, intermolecular interaction between PA and water was also evident through H^{PA}- O^{water}, carb O^{PA}- O^{water}, term O^{PA}- O^{water}, H^{PA}- H^{water}, carb O^{PA}- H^{water} and term O^{PA}- H^{water} RDFs on all the surfaces investigated (Figure 6.7d-i).
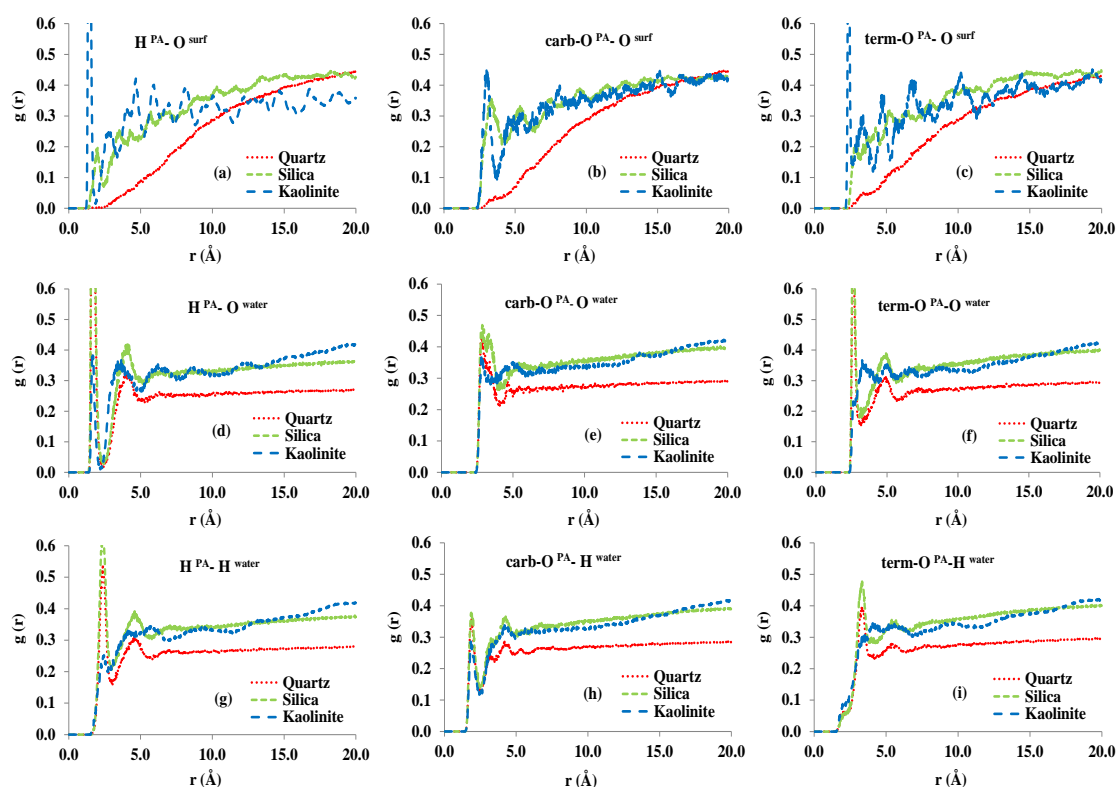
Figure 6.7   Molecs-surface (a-c) and molecs-water (d-i) interaction of 1.0 molec/nm² PA in the wet system.

The RDFs for H^{PA}- O^{water} and H^{PA}- H^{water} revealed sharp peaks at ~1.5 Å and ~2.3 Å, respectively, on all the surfaces, indicating H-bonding and specific orientation of water molecules around polar head groups. The intensity of these peaks for quartz and silica

surfaces was high while on kaolinite the peaks had lower intensity but at the same separation distance (Figure 6.7d, g). H-bond donation from water to the carbonyl oxygen of palmitic acid was also evident from the carb O^{PA}- O^{water} and carb O^{PA}- H^{water} RDFs (~2.8 Å and ~1.8 Å respectively) on all the surfaces (Figure 6.7e, h). The RDFs for term O^{PA}- O^{water} and term O^{PA}- H^{water} exhibited a peak at ~2.8 and ~3.2 Å, respectively, on both quartz and silica surfaces that indicate H-bond donation from water to the carboxylate oxygen atom of palmitic acid is weak (Figure 6.7f, i). The corresponding peak intensity on kaolinite surface was found to be even weaker. The weaker interaction of the carboxylate oxygen atom with water can be explained due to the stronger interaction with the surface compared to the carbonyl oxygen atom of palmitic acid.
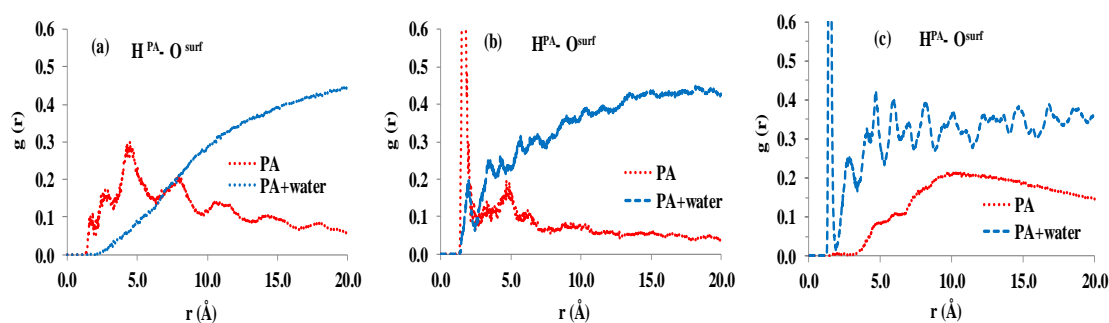
Figure 6.8 H^{PA} - O^{surf} RDF for pure PA (1.0 molec nm^{-2}) both in the wet and dry system on the surfaces of a) quartz b) silica and c) kaolinite

Moreover, when H^{PA}- O^{surf} RDF for PA (1.0 molec nm^{-2}) in the wet system was compared to the corresponding dry system, it was clearly evident that water molecules significantly modify the organo-mineral interaction (Figure 6.8). As noted in the previous section that a substantial population of PA is oriented in the dry system with their polar head groups towards the surface on quartz and silica surfaces (Figure 6.8a, b). However, the polar head groups were observed to turn away from the surfaces

following aquation. On kaolinite, the polar head groups were found to be attached in the clustered molecules following aquation. The interaction of the polar head groups of PA molecules with the kaolinite surface was found insignificant in the dry system (Figure 6.8c), suggesting a uniform lateral molecular layer with the surface, preventing rest of the molecules to interact. The weaker intensity peak on silica indicated the modulating effect of water in the organo-mineral interaction (Figure 6.8b).
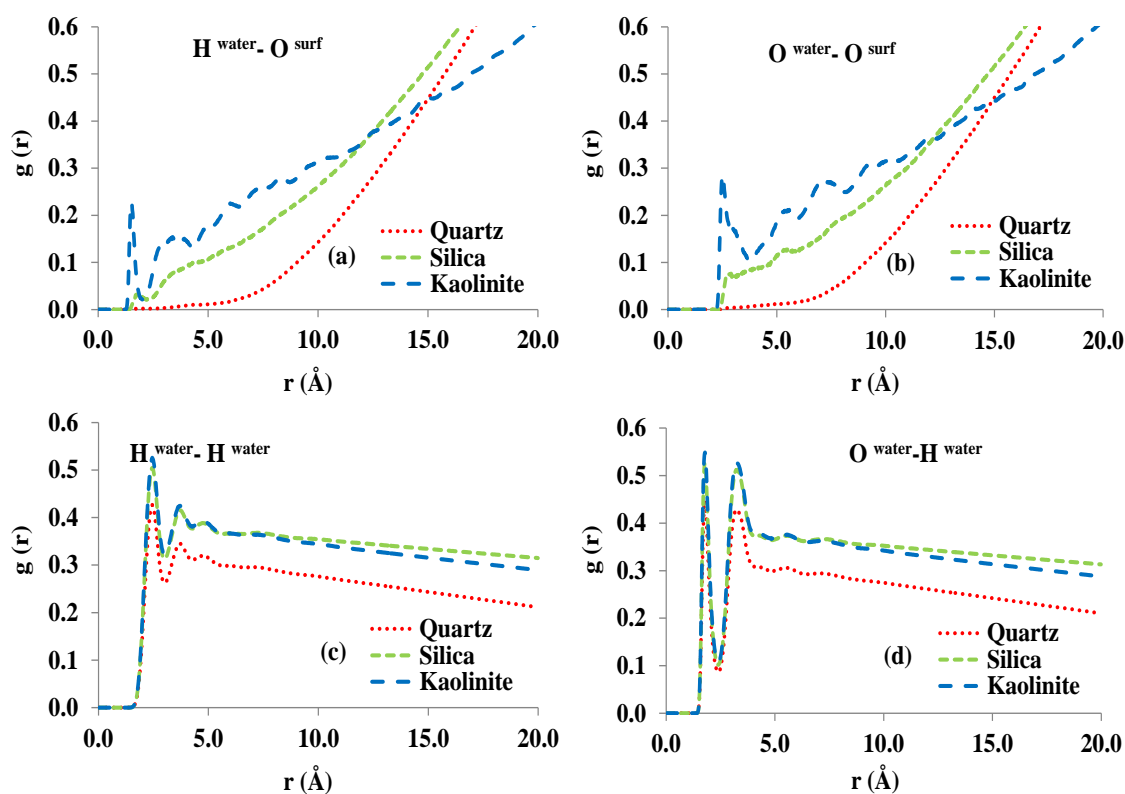
Figure 6.9   Water-surface (a-b) and intermolecular water (c-d) interactions of 1.0 molec/nm^2 for pure PA in the wet system.

Interactions between water molecules and the surfaces were investigated through H^{water}-O^{surf} and O^{water}-O^{surf} RDFs. It was found that water molecules have significant interactions with the kaolinite surface while on quartz it was found insignificant. For example, the peaks for H^{water}-O^{surf} and O^{water}-O^{surf} RDFs were found at ~1.6 and ~2.5 Å, respectively, on the kaolinite surface (Figure 6.9a, b). On silica, there was a weak

interaction that was evident from a very lower intensity peak. Intermolecular H^{water}-H^{water} and H^{water} - O^{water} RDFs revealed sharp peaks at ~2.3 and ~1.8 Å, respectively, that indicate a strong interaction between water molecules on all the surfaces investigated (Figure 6.9c, d).

6.3.4 *Conformation of molecules in the mixture of PA and Td1Me on mineral surfaces*

It was noted in Chapter 4 that a binary mixture of PA and Td1Me was not as effective at inducing SWR as that of PA alone. The conformation was attributed to zonal structure (Petridis et al., 2013). This spatial order of the molecules on the surfaces may change when the organo-mineral interface comes in contact with water. Therefore, simulations were performed to investigate how aquation of the organo-mineral interface affects the interactions of the compounds with the different mineral surfaces.

a) Pure PA (dry) system

quartz	silica	kaolinite

b) PA/Td1Me (dry) system

c) PA/Td1Me (wet) system
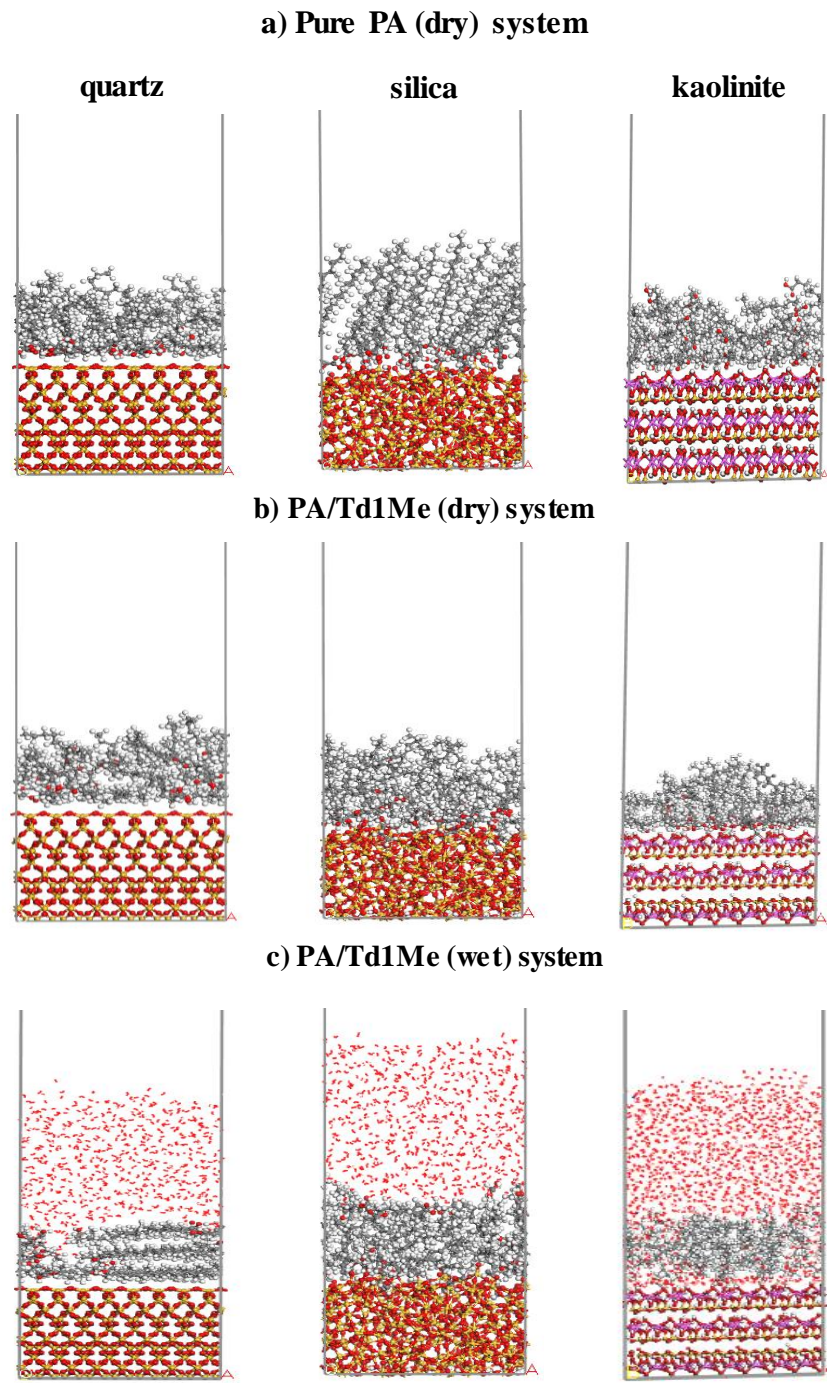
Figure 6.10   Cross section of a) pure PA (dry), b) mixture of PA and Td1Me (dry) and c) mixture of PA and Td1Me (wet) of 2.3 molec/nm^2 on the model surfaces after equilibration.

The organization of molecules on the different mineral surfaces changed following aquation. For the dry simulations, the arrangement of molecules at 2.3 molecs/nm^2 in

the pure PA and PA / Td1Me mixture on quartz was quite similar. However, aquation affects the molecular arrangement, leading to improved packing and alignment of the molecules into lateral layers (Figure 6.10c). Water is mostly excluded from the quartz surface by these layers, and this finding is consistent with the proposal of that Ma'Shum et al. (1988) an amount equivalent to that of several monolayers may be required to result in a complete cover on sandy surfaces. A pure layer of PA molecules on the silica exhibited a tilted arrangement, suggesting limited mobility of the molecules on the rough surface (Figure 6.10a). However, when PA was combined with Td1Me (50:50), it was observed that the layer was disordered, which may be due to the bulky head group of Td1Me preventing organization on the surface. The conformation of the molecules, particularly the arrangement of polar head groups on the silica surface was found to change following aquation. For example, a substantial population of the polar head groups was found at the interface between molecules and water in the wet system whereas, they were concentrated at the organo-mineral interface in the dry system (Figure 6.10b, c). In the mixture of PA and Td1Me on the kaolinite, the molecules form a disordered layer (Figure 6.10b) whereas, in the pure PA layer the molecules adopt either lateral or tilted conformation on the mineral surface (Figure 6.10a). The conformation is consistent with Walden et al. (2015) that at 2.35 molec/ nm^2 surface density, the waxy compounds form a tilted arrangement on the kaolinite surface. However, the molecules in the mixture were found combined on kaolinite following aquation (Figure 6.10c).
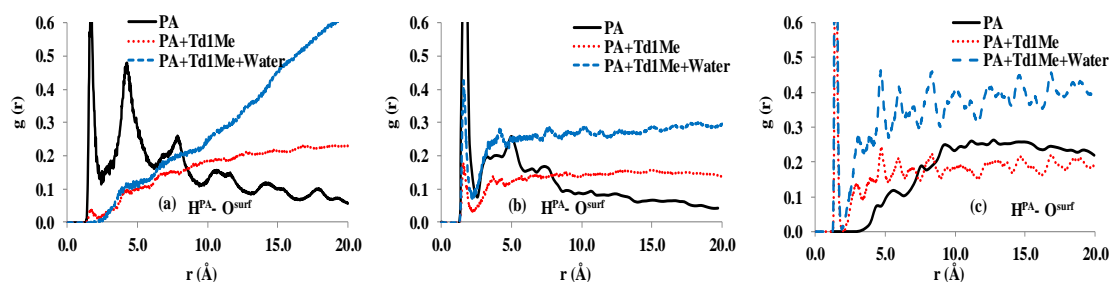
Figure 6.11   Comparison of pure PA (dry) and mixture of PA and Td1M (dry and wet) system at 2.3 molec/nm^2 on a) quartz b) silica c) kaolinite surfaces.

One means of characterizing the organo-mineral interaction is to analyze H-bonding between the acid group of PA and the oxygen atoms of the minerals using the H^{PA}- O^{surf} RDF. A strong interaction for pure PA on both the quartz and silica was evident with sharp peaks at ~1.6 Å. However, the interaction was found to be insignificant on kaolinite as shown by the higher separation distance (Figure 6.11). The H^{PA}- O^{surf} interaction was found to be weaker for the mixture of PA and Td1Me on quartz and silica compared to pure PA (Figure 6.11a, b). Aquation of the mixed layer on quartz leads to a further weakening of the H^{PA}- O^{surf} H-bonding. However, for silica and kaolinite, aquation enhances the H-bonding of the acids to the mineral surfaces. For example, the H^{PA}- O^{surf} RDF was evident at ~1.6 Å on kaolinite and silica in the wet system.
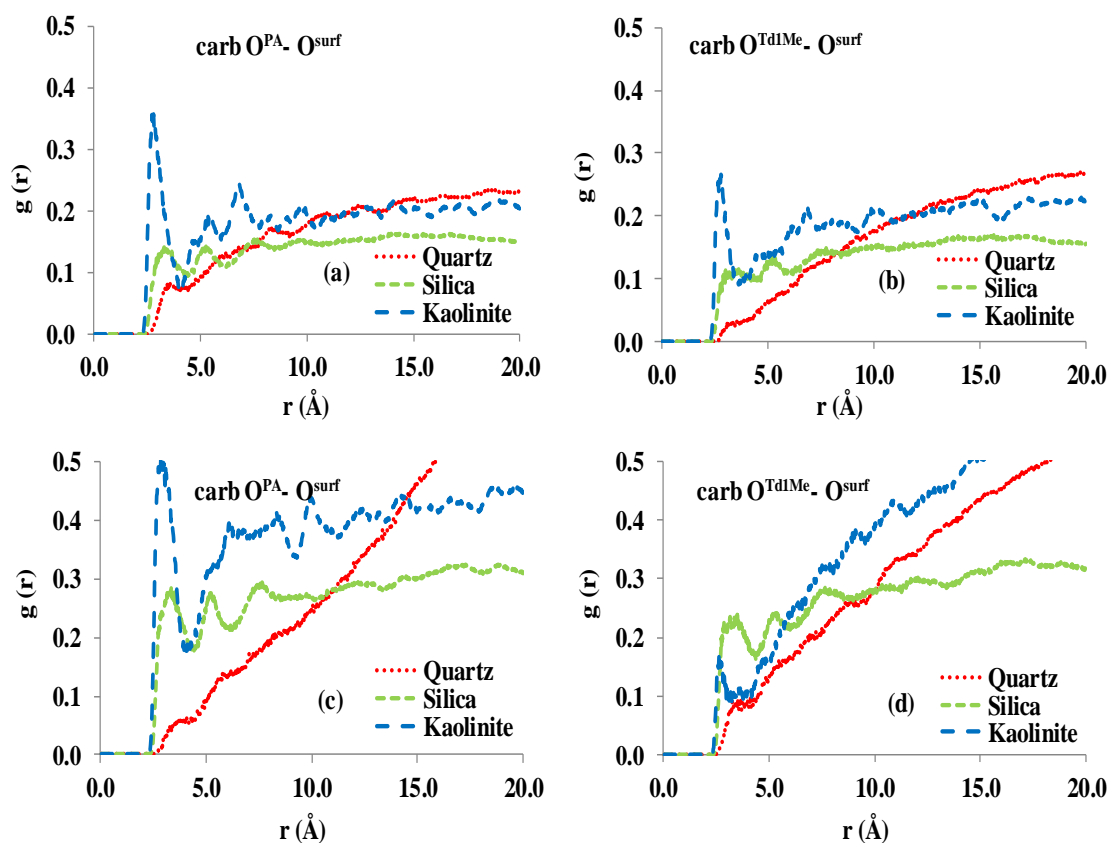
Figure 6.12   carb O^{PA}-O^{surf} and carb O^{Td1Me}-O^{surf} RDFs for the mixture of PA and Td1Me in dry (a, b) and wet (c, d) systems.

Analysis of the carb O^{PA}-O^{surf} and term O^{PA}-O^{surf} interactions can provide some insight to the orientation of the polar head groups on the mineral surfaces. The carb O^{PA}-O^{surf} RDF indicates only a weak interaction in the arrangement of these atom types on quartz with a peak at ~4.0 Å suggesting the carbonyl oxygen atom of PA is oriented away from the surface (Figure 6.12a). The alignment appears to also be true for the carbonyl oxygen of the Td1Me (carb O^{Td1Me}) (Figure 6.12b). The carb O^{PA}- O^{surf} and carb O^{Td1Me}-O^{surf} RDFs on the kaolinite (~2.7 and ~3.0 Å) and silica (~3.6 and ~3.4 Å) surfaces indicate that the carbonyl oxygen atoms of both PA and the Td1Me are in closer contact with these minerals than observed for quartz (Figure 6.12a, b). The positions of the peaks are essentially unchanged in the wet systems, but the intensity increases on silica and kaolinite for both molecules (Figure 6.12c, d).

The interactions between PA and Td1Me molecules with water were also examined through the H^{PA}- O^{water}, H^{PA}- H^{water}, carb O^{PA}- O^{water}, carb O^{PA}- H^{water}, carb O^{Td1Me} - O^{water} and carb O^{Td1Me} - H^{water} RDFs which exhibited sharp peaks at ~1.5, ~2.3, ~2.7, ~1.8 ~2.7 and ~1.8, Å respectively (Figure 6.13a-f). Significant hydrogen bonding was observed between the acidic hydrogen of PA and the oxygen atom of water, which was independent of the surface. The water molecules also clearly exhibit H-bonding to the carbonyl oxygen atoms of both PA and the Td1Me (ester). However, the interactions between carbonyl oxygen of PA and Td1Me with the water was found weaker on the silica surface (Figure 6.13b, c, e, f).
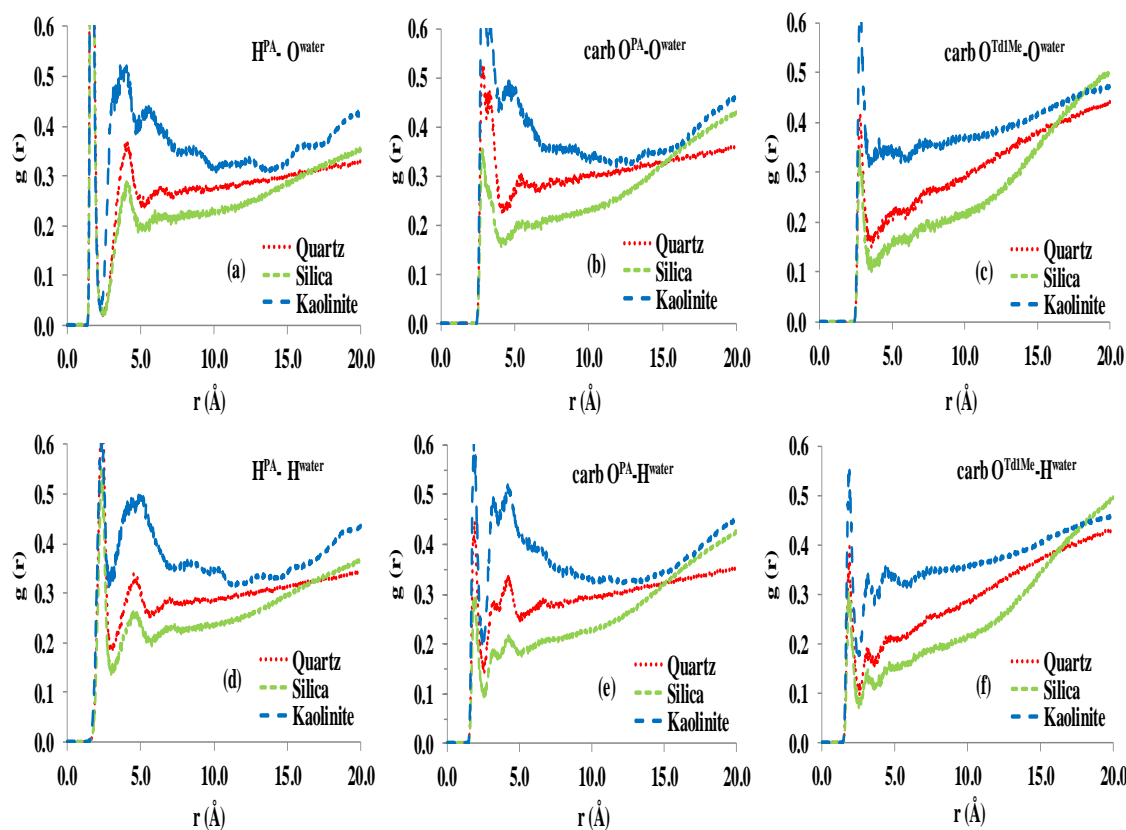
Figure 6.13   Molecs-water (a-f) interaction of the mixture of PA and Td1Me in the wet system on model soil particle surfaces.

The intermolecular interactions between the organic molecules in the layer (PA and Td1Me) were also investigated through H^{PA}-O^{PA} and H^{PA}-term O^{Td1Me} RDFs. The close interaction between PA molecules was evident from sharp peaks at ~1.6 Å on both quartz and silica surfaces in dry system whereas, on kaolinite, the interaction was found weaker (Figure 6.14a). However, the interaction was only evident at ~3.2 Å on kaolinite in the wet system while it was observed at ~1.9 Å both on quartz and silica surfaces (Figure 6.14c). The result indicates that H-bonding to water modulates the interaction between PA molecules of the layer so that the head groups are slightly more separated in the wet systems. The H^{PA}-term O^{Td1Me} RDF revealed that there is a longer range interaction between PA and Td1Me molecules than between PA molecules (Figure 6.14b). The strength of this interaction is greatest on quartz and weaker on silica. On

182

kaolinite, the interaction is elongated to ~4.5Å. The interaction was found even weaker in the wet system that was evident with the peaks at ~4.0, ~5.0 and ~6.0 Å on the quartz, silica and kaolinite surfaces, respectively (Figure 6.14d). The weaker interaction on the kaolinite and silica surfaces suggested that water molecules can significantly modify the conformation of amphiphilic molecules at the organo-mineral interfaces.
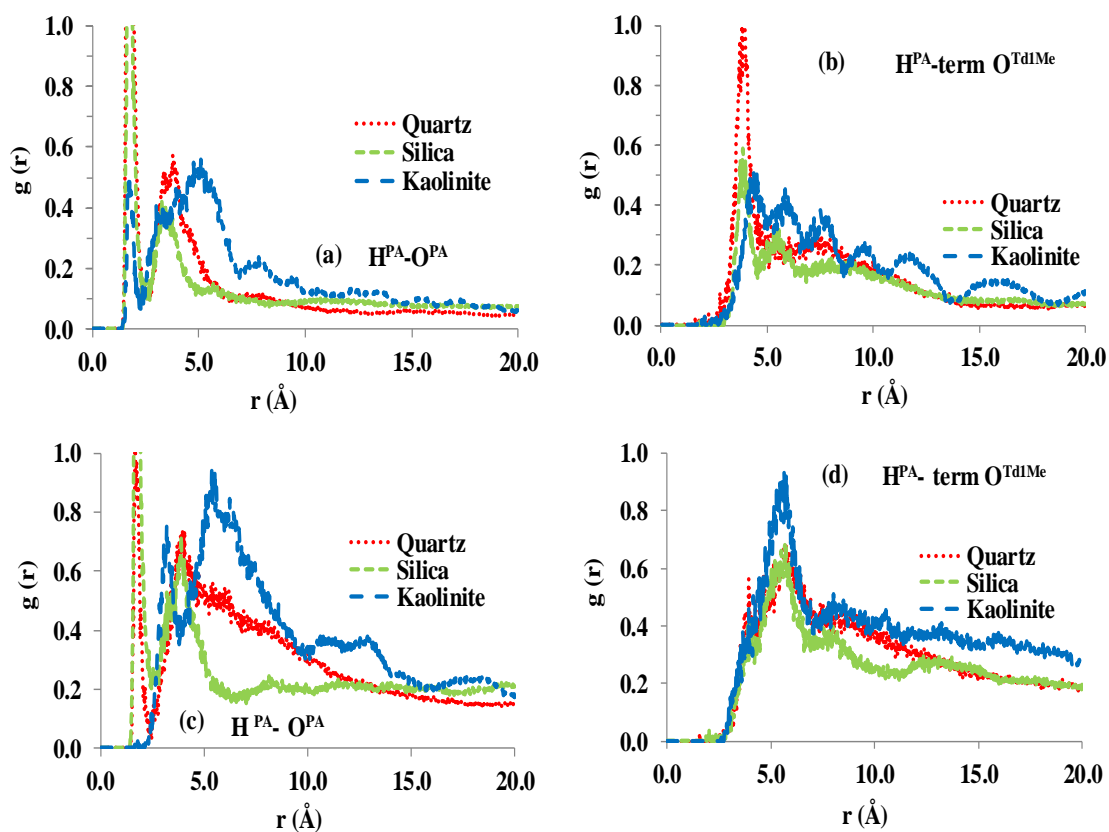
Figure 6.14 H^{PA}-O^{PA} (a, c) and H^{PA}-term O^{Td1Me} (b, d) RDFs for the mixture of PA and Td1Me in dry (a, b) and wet (c, d) systems.

Wesseling et al. (2009) reported that there is a close association between soil moisture and organic matter in the coarse textured soil that suggested an intimate interaction of the organic functional groups with the water molecules. The RDFs of H^{water}- term O^{PA} and O^{water}- term O^{PA} exhibited sharp peaks at ~2.9 and ~2.6 Å, respectively (Figure 6.15a, b). However, there was a smaller peak on kaolinite at ~2.2 Å. These results

indicate water has a closer interaction with the carbonyl oxygen than with the terminal carboxylate oxygen.
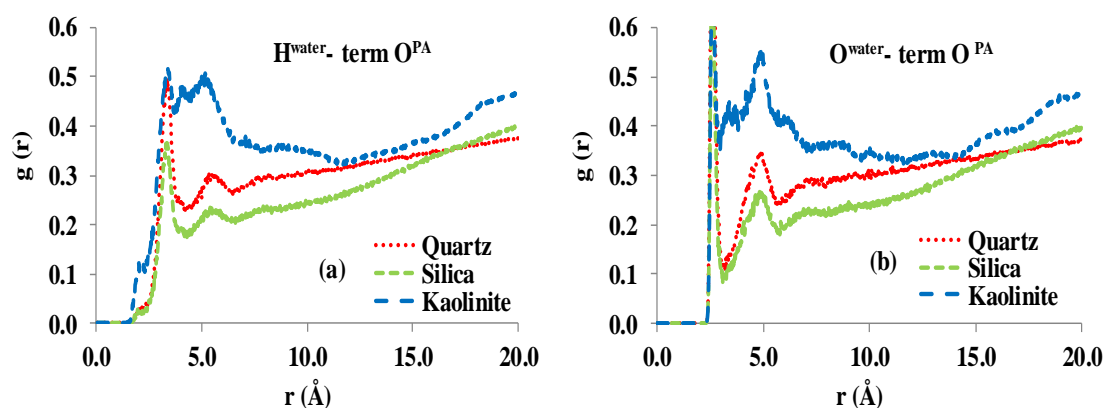
Figure 6.15   Water-molecs (a, b) interaction of PA in the mixture of PA and Td1Me on model soil surfaces in the wet system.

6.3.5   Conformation of molecules in the mixture of PA and Hex-OH on mineral surfaces

As noted in the previous section that aquation can significantly modify the conformation of organic molecules at organo-mineral interfaces and the conformation is varied on different mineral surfaces. The mixture of PA and Hex-OH (50:50) molecules in a dry system were found to organize into a lateral layer on the quartz surface. However, a substantial population of molecules exhibited extended conformations above the lateral layers at a surface density of 2.3 molecs/nm^2. In comparison, the molecules organized themselves in well-defined lateral layers following aquation on the surface. Furthermore, the polar head groups were found to orient themselves toward the organo-water interface (Figure 6.16a, b). On the silica surface aquation also reoriented a substantial population of polar head groups from the organo-mineral interface to organo-water interface, suggesting water molecules can significantly modify the conformation of organic molecules on the mineral surface. Moreover, the molecules of

184

the mixture on kaolinite were found aggregated and reoriented in extended conformations in the wet system compared with a lateral layer at the organo-mineral interface in the dry system. Interestingly, the molecules of the mixed PA/Hex-OH layer

a) PA/Hex-OH (dry) system

quartz	silica	kaolinite

b) PA/Hex-OH (wet) system
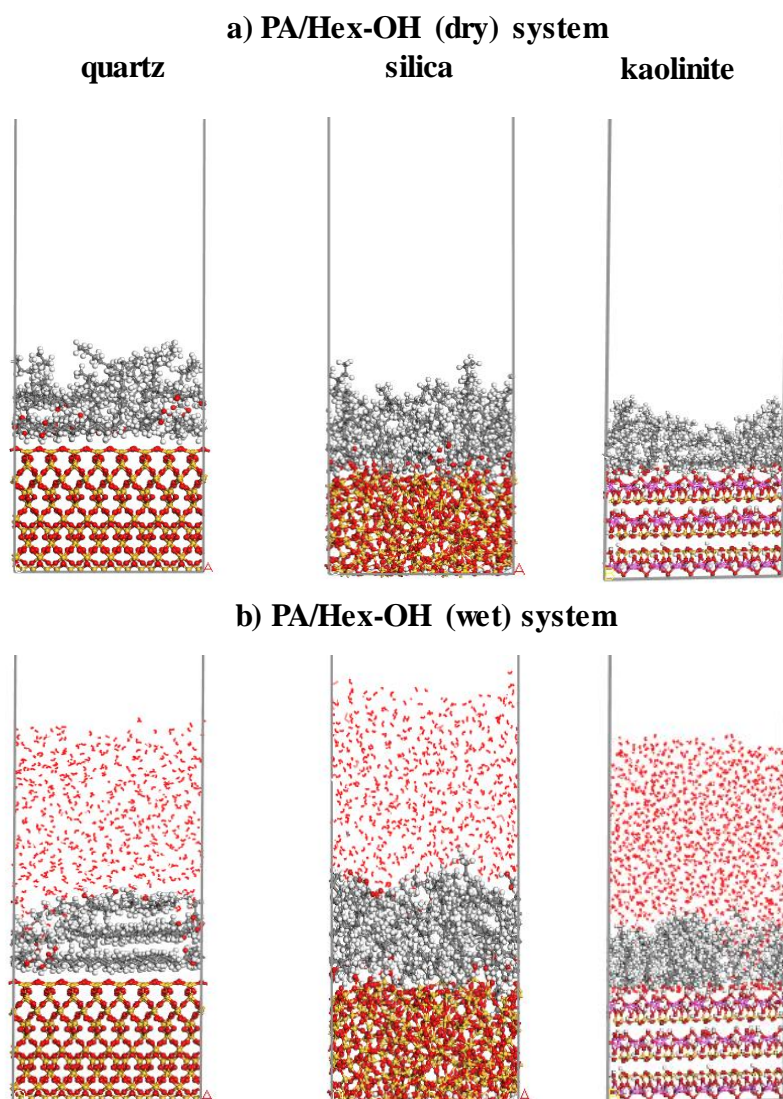
Figure 6.16   Cross section of the mixture of PA and Hex-OH (dry and wet) of 2.3 molec/nm^2 on surfaces.

were found more closely packed in the dry system than that of a pure PA layer on the three model soil particle surfaces shown in the previous section. The closely packed

organic layer is consistent with the earlier findings that a binary mixture of PA and Hex-OH is more effective in inducing SWR on the soil particles than PA alone (Chapter 4).
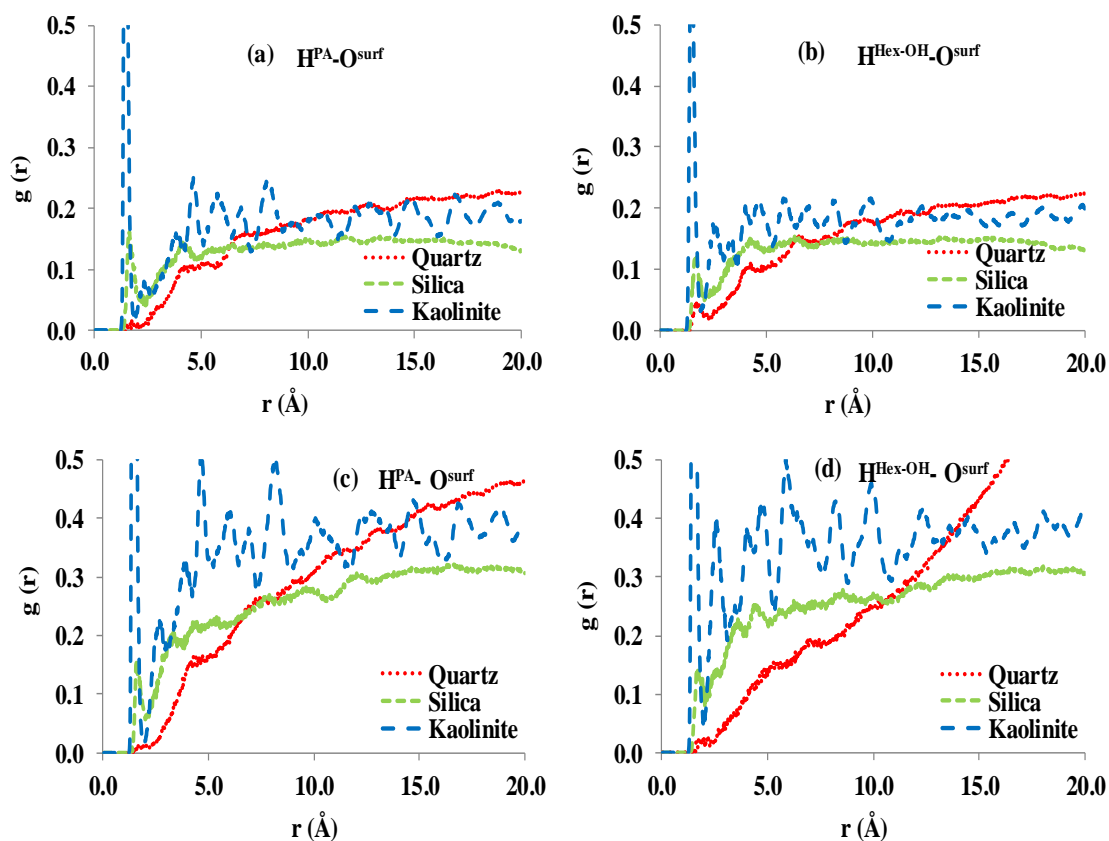
Figure 6.17 H^{PA}-O^{surf} and H^{Hex-OH}-O^{surf} RDFs for the mixture of PA and Hex-OH in dry (a, b) and wet (c, d) system.

The interactions of acidic hydrogen of PA and alcoholic hydrogen of Hex-OH with the quartz surface were found to be insignificant for both wet and dry systems (Figure 6.17b). Strong interactions on kaolinite were evident by the peaks in the RDFs of H^{PA}-O^{surf} and H^{Hex-OH}-O^{surf} at ~1.4Å in both wet and dry systems (Figure 6.17a-d). The interactions on silica were found weaker, which was evident from lower intensity peaks in the corresponding RDFs. However, the position of the peak shifts from ~1.6Å in the dry system to ~1.4Å following aquation. This finding is consistent with Doerr et al.

(2000) that amphiphilic molecules can reorganize themselves to the mineral surfaces with changes in soil moisture condition.

The intermolecular H^{PA}-O^{PA} RDF revealed in dry conditions a sharp peak at ~1.6Å (Figure 6.18a) on quartz providing evidence of close interaction of the acid molecules on this surface. Lower intensity peaks on silica and kaolinite in the dry systems suggest a weaker interaction between acid molecules due to competing interaction with the OH groups of these mineral surfaces (Figure 6.18a). The interaction was relatively unchanged (~1.6Å) on quartz and silica surfaces following aquation. However, a broader peak was evident on kaolinite at ~3.5Å suggesting increased spacing of the polar head groups due to the presence of water (Figure 6.18c). The H^{PA}-term $O^{Hex\text{-}OH}$ RDF exhibited a higher intensity peak at ~1.6Å on quartz and silica surfaces both in the dry and wet systems that indicate a closer interaction between acid and alcohol molecules than between neighbouring acid molecules. A lower intensity peak for the interaction was evident on kaolinite at ~1.7Å in the dry system and ~3.4Å following aquation (Figure 6.18b, d), indicating that the addition of water also leads to greater spacing between acid and alcohol functional groups on this surface.
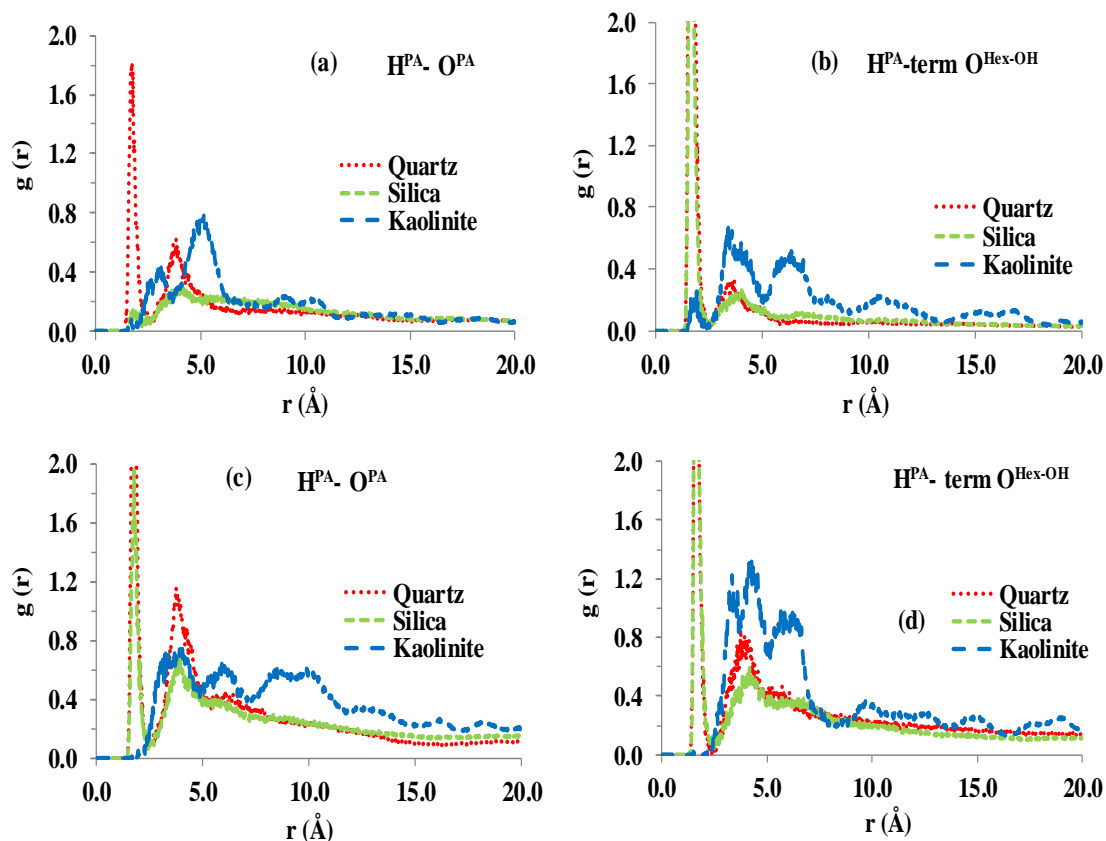
Figure 6.18 H^{PA}-O^{PA} (a, c) and H^{PA}-term O^{Hex-OH} (b, d) RDFs for the mixture of PA and Hex-OH in dry (a, b) and wet (c, d) systems.

The intermolecular interaction between organic molecules and water was examined, and it was revealed that there were strong interactions irrespective of surface characteristics. The RDFs of H^{PA}- O^{water}, H^{PA}- H^{water}, H^{Hex-OH}- O^{water} and H^{Hex-OH}- H^{water} exhibited peaks at ~1.6, ~2.2, ~1.6 and ~2.3 Å, respectively, on all the surfaces investigated (Figure 6.19a-d). Leighton-Boyce et al. (2005) observed soil moisture as the dominant variable in modifying water repellent soil under *Eucalyptus globulus* plantations in Portugal. The strong interactions between water and the polar head groups of PA and Hex-OH in the mixture inversely correlates with the organo-mineral interactions on quartz and silica surfaces as shown in Figure 6.17. Thus, hydrogen bonding can significantly modify the molecular conformation at organo-mineral interfaces following aquation.
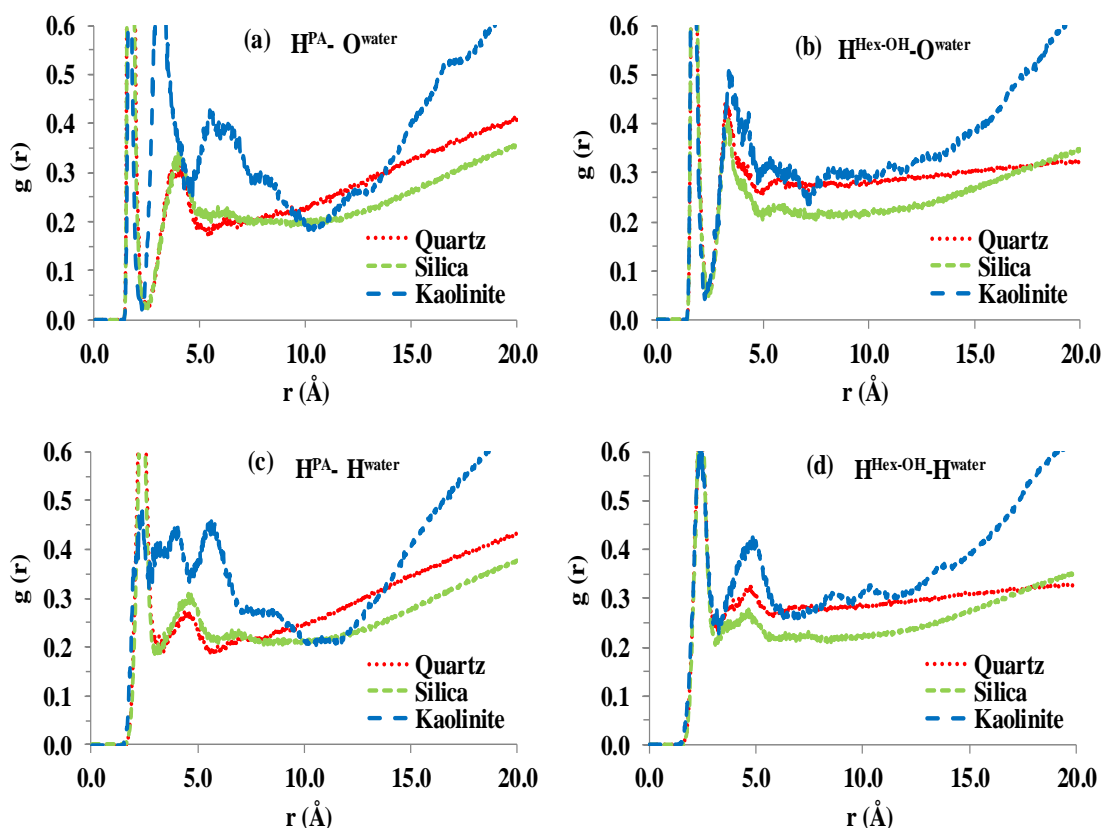
Figure 6.19   Molecs-water (a-d) interaction of the mixture PA and Hex-OH in the wet system.

The intermolecular interactions between water and Td1Me and Hex-OH were also investigated through H^{water}- term O^{Td1Me}, O^{water}- term O^{Td1Me}, H^{water}- term O^{Hex-OH} and O^{water}- term O^{Hex-OH} RDFs. The nearest approach on the surfaces was observed at ~2.8, ~3.0, ~1.5 and ~2.4 Å for H^{water}- term O^{Td1Me}, O^{water}- term O^{Td1Me}, H^{water}- term O^{Hex-OH} and O^{water}- term O^{Hex-OH} RDFs, respectively (Figure 6.20). It was clearly observed that the interaction of water with Td1Me is weaker than that of water with Hex-OH.
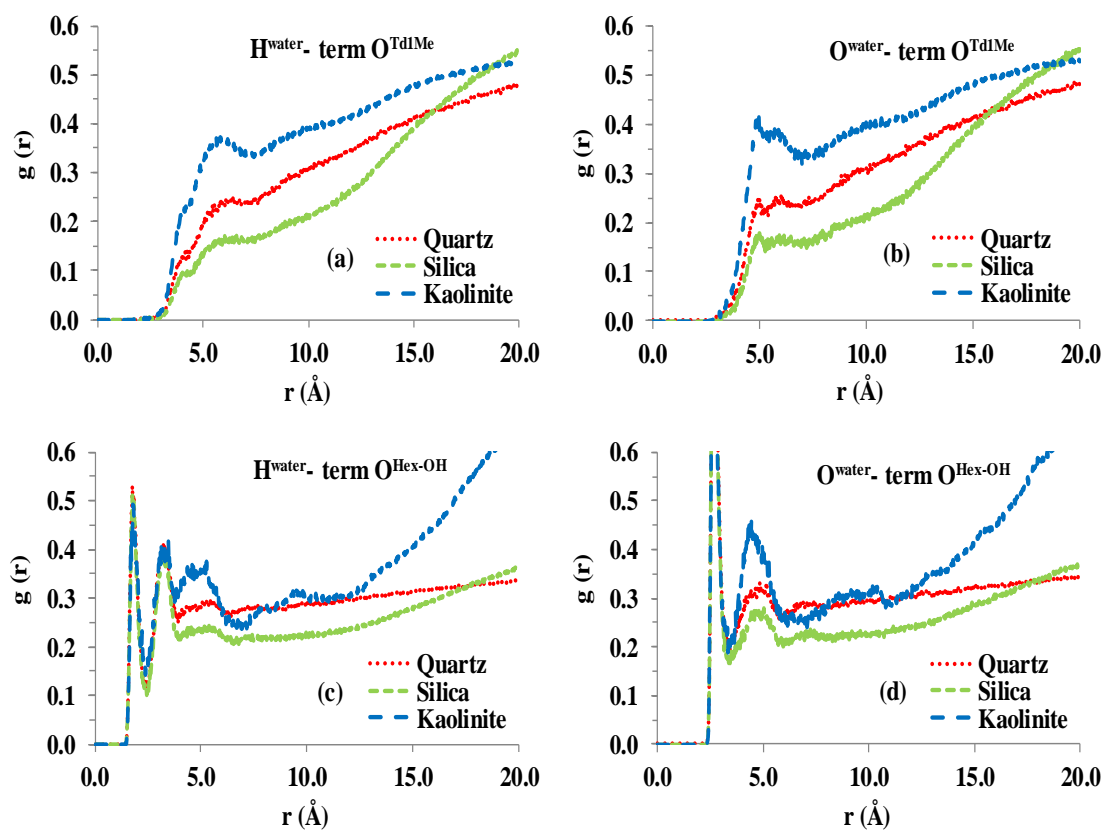
Figure 6.20   Water-molecs (a-d) interaction for the mixture of PA and Td1Me, PA and Hex-OH in the wet system.

Comparison between the dry and wet systems revealed that water molecules gradually weaken the organo-mineral interactions which were evident through H^{PA}- O^{surf} RDF of each system (Figure 6.21).
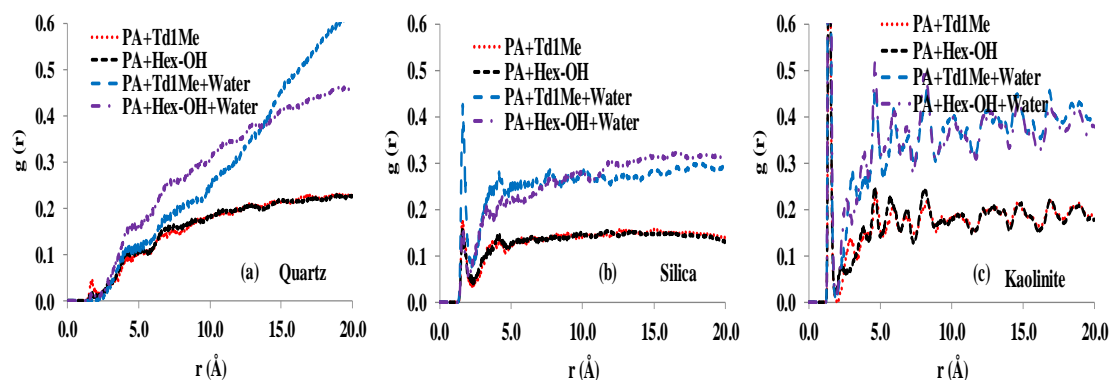
Figure 6.21   H^{PA}- O^{surf} RDFs (a-c) for the mixture of PA and Td1Me, PA and Hex-OH in the dry and wet systems.

6.3.6   *Organo-mineral interactions in both the dry and wet systems*

Radial distribution function analysis was used to determine if there was any affinity of the carbon atoms of the molecules (C^{molec}) for the oxygen (O^{surf}) and silicon (Si^{surf}) atoms of the model surfaces. The C^{molec} - O^{surf} RDF indicated that the minimum separation between the molecules and the surface was ~2.7Å (Figure 6.22a-f) and did not exhibit strong correlation between the dry and wet systems. However, overall the RDFs exhibited more distinct features in the wet system compared to dry system. In particular, both for the pure PA and mixtures, the slope of the curve is steeper in the wet system, indicating water molecules tend to uplift the polar head groups of the amphiphilic molecules. The C^{molec} - O^{surf} RDF was the representative of other molec-surf interaction of C^{molec} - Si^{surf} RDF and revealed that the principal interaction between the hydrophobic tails and the surface was vdW forces (Uddin et al., 2017). A previous study Shevchenko and Bailey (1998) demonstrated that molecular weight of organic molecules can significantly modify the affinity for mica surfaces.
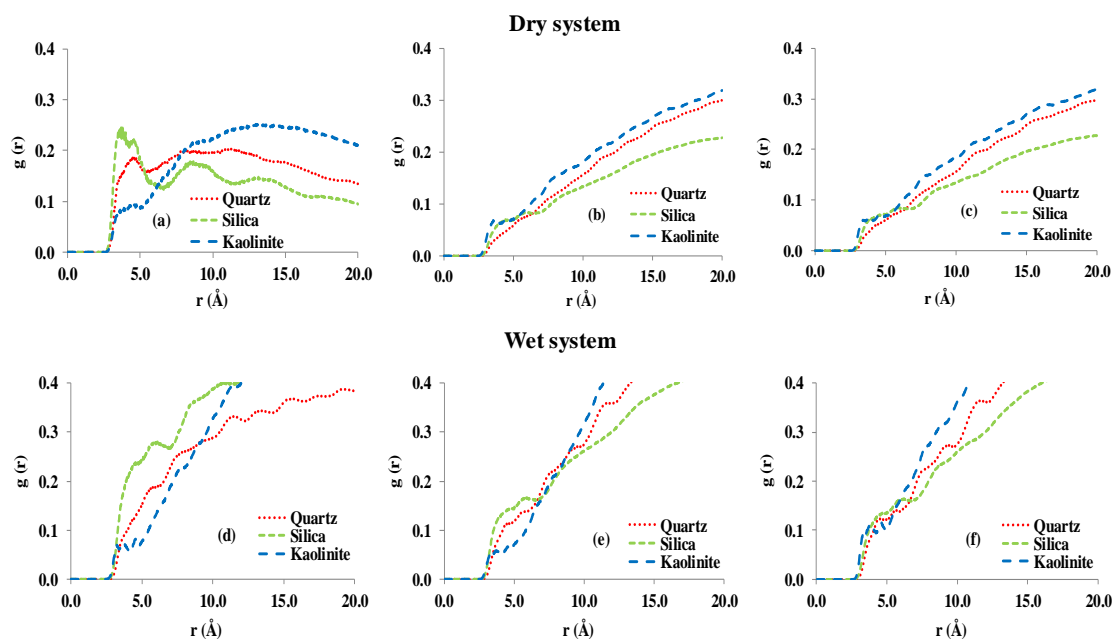
Figure 6.22 C^{molecs}- O^{surf} RDFs in PA (a, d), mixture of PA and Td1Me (b, e) and mixture of PA and Hex-OH (c, f) in the dry (a, b, c) and wet (d, e, f) systems at of 2.3 molecs nm^{-2}.

The stability of the surface monolayers is not only dependent on the interactions of the molecules with the surface but also on the interactions between the molecules in the layer. These interactions were investigated by analysing the intermolecular carbon-carbon RDFs (C^{molec} - C^{molec}). The C^{molec} - C^{molec} RDFs for the pure PA and mixtures were found with significant packing order of the long tail amphiphilic molecules, both in the dry and wet systems (Figure 6.23a-f), indicating a discrete zonal structure as proposed by Kleber et al. (2007). The higher intensity peaks in the wet systems suggested more orderly and aligned arrangement of molecules on the surfaces. These results indicate that the molecules form a structured layer in the presence of water, which is consistent with the findings of Yu et al. (2003).
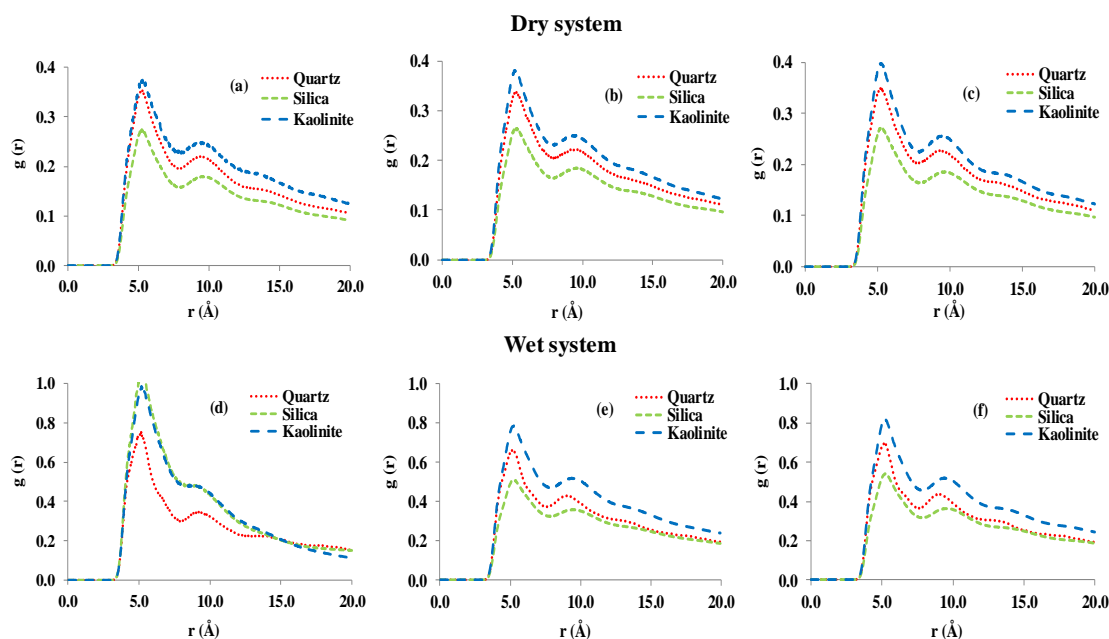
Figure 6.23 C^{molec}- C^{molec} RDFs in PA (a, d), mixture of PA and Td1Me (b, e) and mixture of PA and Hex-OH (c, f) in the dry (a, b, c) and wet (d, e, f) systems at of 2.3 molecs nm^{-2}.

6.4   Conclusions

The surface characteristics of the soil particles determine the level of organo-mineral interactions. However, the simulations performed in this study indicate that soil moisture can influence the conformation of molecules at the organo-mineral interfaces. The presence of hydroxyl groups on the polar surfaces (e.g., kaolinite) was found to intimately interact with both the amphiphilic molecules and water through hydrogen bonding. However, the conformation of the amphiphilic molecules on the surfaces was found to vary based on their density and functional groups. Intermolecular interactions between water and amphiphilic molecules were found to play a dominant role in the reorganization of organic molecules at the organo-mineral interface. For example, the acidic hydrogen group of PA and alcoholic hydrogen group of Hex-OH were found to exhibit strong H-bonding interactions both with the water and the polar surfaces.

At the lower surface density (0.1 molec nm^{-2}), the PA molecule remains adhered to the quartz surface following aquation whereas, the molecule was released from kaolinite to the air-water interface, reflecting differences in surface functionality. However, PA was also adhered to the irregular shape of silica even after aquation, suggesting the importance of morphological features of soil particles in the organo-mineral interaction.

At a higher surface density (1.0 molec nm^{-2}), the molecules conformed differently on the mineral surfaces following aquation. This conformation was due to the interactions both between amphiphilic molecules and interactions with the polar mineral surfaces and with water. The effect of water on the organic structure was evident from changes in the interface region at the different surfaces. For example, the interface region on quartz with water was found very narrow in comparison with polar like surfaces of silica and kaolinite. Furthermore, the surface density, chain length and composition of molecules in the organic layer were found to affect the molecular arrangement and conformation on soil particle surfaces.

Organo-mineral interactions determine the adhesion between amphiphilic molecules and mineral surfaces and thus the severity of SWR in the soil matrix. The equilibration or stability of this interaction is affected by soil moisture or the addition water molecules at the organo-mineral interface. The polar kaolinite and silica surfaces were found to easily wet-up following aquation which significantly modified the organo-mineral interaction. Hydrogen bonding was found to play a dominant role in the organo-mineral interaction. Hydrogen bond donation from water to kaolinite surface oxygen atoms (H^{water}- O^{surf}) was evident at ~1.6 Å. The intermolecular H^{PA}- O^{water} RDF revealed significant H-bonding between acidic hydrogen atoms and water molecules. The weaker intermolecular H^{PA}- O^{PA} interaction on kaolinite surface suggested an inverse relation

with organo-water attraction. Moreover, the C^{molecs}- O^{surf} and C^{molecs}- C^{molecs} RDFs revealed that van der Waals (vdW) force could play a dominant role in the organo-mineral interactions.

The effect of aquation on the structure of mixed organic layers was also investigated for pure PA and combination of PA with Td1Me (50:50) in both the dry and wet system at a surface density of 2.3 molecs/nm^{-2}. The lateral molecular layers of the mixture of PA and Td1Me on the quartz surface were more orderly and aligned following aquation. However, the interaction of the molecules was found to be weaker on the quartz surface following aquation, suggesting the importance of soil moisture in releasing amphiphilic molecules from the surface. The intensity of interactions of the carb O^{PA}- O^{surf} and carb O^{Td1Me}- O^{surf} RDFs on kaolinite and silica surfaces suggest, Td1Me molecules in the mixture are in similar contact with the surfaces in the dry and wet systems. Hydrogen bonding between the acidic hydrogen of PA and water plays a dominant role in the interactions between the organic molecules and water. Hydrogen bonding was also found to play a dominant role in the intermolecular interaction between neighboring PA molecules on the dry surfaces. However, the interaction was abruptly changed on kaolinite surface following aquation, suggesting water molecules can effectively change molecular arrangement at the organo-mineral interface.

The arrangement of molecules in the mixture of PA and Hex-OH was found more closely packed than that of pure PA on the mineral surfaces. The packed arrangement is consistent with our previous findings that combination of PA and Hex-OH enhances the severity of SWR compared with PA alone on the soil samples. However, the molecules were aggregated in extended conformation on kaolinite following aquation. The organo-mineral interaction through hydrogen bonding was evident in H^{PA}- O^{surf} and

H^{Hex-OH}- O^{surf} RDFs on kaolinite in both of the systems at ~1.4 Å. However, the intensity of interaction was weaker on silica, suggesting the number of hydroxyl groups on the mineral surface can influence the interaction both with amphiphilic molecules and water. Furthermore, the H^{PA}- O^{surf} RDF of pure PA (1.0 mole/nm^2) exhibited a sharp peak at ~1.3 and ~1.7 Å on kaolinite and silica surfaces, respectively, in the wet system, whereas, the interaction was insignificant on quartz.

Though the weaker intermolecular interaction was exhibited for H^{PA}-O^{PA} RDF on kaolinite at ~1.6Å in the dry system, it was found even more weaker with broader peak at ~3.5Å following aquation, suggesting re-orientation of polar head groups at the organo-mineral interface. The interaction of H^{PA}-term O^{Hex-OH} RDF was also weaker on kaolinite following aquation. The similar intermolecular interaction of H^{PA}-term O^{Hex-OH} RDF on silica indicated restricted mobility of the molecules on the surface. Hydrogen bond donation from PA and Hex-OH to water was clearly observed. The stronger interaction between water and organic molecules can be inversely correlated to organo-mineral interaction on soil particles.

7 General discussion

7.1 *Introduction*

Soil water repellency (SWR) has widely been recognized as a limiting factor in large tracts of agricultural and pasture land of Western Australia, having a significant impact on crop yield (Bond, 1972). It usually occurs in sandy top soils when plant-derived waxy substances coat the soil particles. As demonstrated in Ch. 2, native vegetation secretes exudates and releases these to the soil. However, soils are very complex and include different types of compounds. Thus, the relative contribution of the hydrophobic substances in inducing SWR is not straightforward. The outcomes of both experimental work and molecular dynamics simulations from this thesis have been described in Chapter 4 which has also been published (Uddin et al., 2017).

The interplay of research outcomes from this study helped to identify new details of SWR. The amounts and composition of plant exudates and soil extracts were characterized to identify the relative importance of particular organic compounds to SWR. The concentration of individual compounds can indicate their potential for inducing SWR. More detailed work was required to examine the effects of mixtures of compounds. Accordingly, both individual compounds and mixtures of compounds were applied onto acid washed sand (AWS) to assess their relative effectiveness in inducing SWR.

However, these experiments do not give a molecular level understanding of the interaction of the compounds with soil particle surfaces. Therefore, molecular dynamics simulations were employed to investigate the behavior of both individual and binary mixtures of compounds applied onto mineral surfaces to identify the conformation and

organization of the molecules on simulated soils. However, the organization of molecules at the organo-mineral interface might be different after adding a number of water molecules. Vegetation fire is also reported to play a role in the dynamics of SWR in dry land environment. However, until now there has not been an investigation on whether biogenic volatile organic compounds (BVOCs) emitted during vegetation fire play a substantial role in inducing SWR. Thus, by loading of BVOCs onto AWS and performing a molecular level investigation we can explore a new dimension of knowledge for this particular natural phenomenon.

7.2   Methodology

The first phase of this study involved the collection of plant exudates from different species. An improvised technique was used to capture the canopy derived exudates from native vegetation using mounted glass beakers. The collected exudates were extracted and separated using both nonpolar and polar solvents to identify the different fractions. Soils collected from under native species were air dried and sieved (2 mm). The dried samples were then extracted with IPA/NH_3 (70:30) solvent using a sonication technique. In the previous studies (Doerr et al., 2005; Franco et al., 2000b; Hansel et al., 2008; Morley et al., 2005), soil samples were extracted in a Soxhlet apparatus with the same solvent. The study conducted by Kitchens (2015) reported that the concentration of compounds extracted through sonication and Soxhlet apparatus were similar. However, care should be taken in the sonication technique so that organic compounds don't get broken down.

In order to discern the contribution of different carbon pools, soils were separated into coarse mineral materials and finer interstitial components using a winnowing technique. The impact of interstitial matter in inducing SWR was assessed by applying different

198

percentages (w/w) onto acid washed sand (AWS) and measuring the MED of the loaded samples. Likewise, the effect of individual organic compounds and combination of compounds (binary mixtures) was assessed by loading onto AWS and measuring the resulting MED. To understand the adhesion or molecular level interactions at the organo-mineral interface, a modeling framework for both the mineral surface and organic molecules was built using Materials Studio v 7.0. The interactions of the applied organic compounds with the simulated soil particles were then investigated by analyzing the fully atomistic molecular dynamics simulations.

7.3 *Implications of native species to SWR*

The two most prominent genera in Australia's woody plant communities are *Eucalyptus* and *Acacia*. Based on leaf texture they are broadly classified as sclerophyll vegetation. *Eucalyptus* species are also widely found outside of their native range in plantations on all vegetated continents of the world (Crous et al., 2013). Although eucalypts have been positively linked to SWR, a number of other dominant native species have only been anecdotally reported to be associated to SWR in Southwest Western Australia. Apart from forests and heathlands, the region supports areas of 'shrubby open-scrub' and 'grassy open-scrub' (Groves, 1994). Before extensive land development for agriculture, this area was covered in a range of xerophytic plants, such as *Eucalyptus marginata* (Dell et al., 1983). The leaves, fruits, and stems of many *Eucalyptus* species are very glaucous, which is evident during the juvenile period of growth (Horn et al., 1964; Pereira et al., 2005). Previous research on SWR in southern Australia and in Mediterranean plantations has focused on a small number of Australian native species namely, *E. globulus* (Doerr et al., 1996; Walden et al., 2015), *E. marginata* (Roberts & Carbon, 1972), *E. astringens* (McGhie & Posner, 1981), *Banksia speciosa* (Harper et al., 2000; Moore & Blackwell, 2004), *Pinus pinaster* (Doerr et al., 1996), and *Acacia*

mearnsii (Scott, 2000). Furthermore, several studies have identified induction of SWR following fire in eucalypt and other forests (Cawson et al., 2012; Doerr et al., 1996; Prosser & Williams, 1998; Shakesby, 2011). *Eucalyptus* waxes and oils are a complex mixture of monoterpenes, sesquiterpenes, aromatic phenols, oxides, ethers, alcohols, esters, fatty acids, aldehydes and ketones (Barton et al., 1989; Batish et al., 2008; Horn et al., 1964; Pereira et al., 2005). For example, ursolic acid is the common leaf wax constituent of the myrtaceous species (Courtney et al., 1983). The presence of waxy compounds in the soil is thought to contribute to the hydrophobic behavior in the undisturbed sandy soils under native Australian species. These waxes may originate from plant cuticles but are also added from different stages of plant degradation. For example, long chain fatty acids like substances are particularly difficult to degrade in the soil and may remain after other plant material has broken down (Hayes & Graham, 2000).

A range of hydrophobic compounds namely, long-chain alkanes, fatty acids, phytanols, amides, aldehyde, ketone, alkene, terpenoids, steroids and some ring containing compounds were detected in the canopy derived exudates of *Banksia menziesii*, *Eucalyptus marginata*, *Xanthorrhoea preissii* and, *Allocasuarina fraseriana*. Odd-numbered long-chain alkanes ($> C_{25}$) were detected similar to the study of Eglinton et al. (1962), where a major constituent of leaf waxes is odd-numbered alkanes. There was a predominance of an alkane with even-numbered carbon atoms ($> C_{24}$) in the soil samples, which is contrary to odd-numbered alkanes of exudates. This suggests that there was a microbial contribution to the size of soil carbon pools. Franco et al. (2000b) found the presence alkanes in the tree litter beneath the clumps of eucalyptus trees that are subjected to the decay or microbial or fungal attack (Morley et al., 2005). Soils are very complex and harbor a range of microbial communities. Some bacterial

communities are reported to degrade waxy compounds in the hydrophobic soil (Roper & Gupta, 2005). However, the effects are species dependent and are not consistent with the particular microbes (McGhie & Posner, 1981). The relative contribution of microbial communities to the size of carbon pools was beyond the scope of the present study.

A range of even-numbered (C_8-C_{26}) fatty acids were identified both in the exudates and soil. These fatty acids were also detected in previous studies of plant cuticles (Hayes, 1998) and hydrophobic soils (Franco et al., 1995; Horne & McIntosh, 2000; Ma'Shum et al., 1988). Similar chain-length distribution of fatty alcohol was also found both in the exudates and soil. Franco et al. (2000b) identified a long chain fatty alcohol (docosanol), significantly modifying the wetting properties of soil. Moreover, there was the presence of esters (C_8-C_{35}) both in the canopy exudates and soil. Mainwaring et al. (2013) found that methyl heptadecanoate (C_{18}) induced slight SWR onto acid washed sand. However, isopropyl myristate was found to have a reducing effect when it was combined with long chain amphiphilic molecules (Chapter 5). In the molecular dynamics study (Chapter 5), it was observed that tridecanoic acid, 1-methylethyl ester (Td1Me) had reduced packing efficiency on the mineral particles, due to their bulkier head groups.

The representative species of both the fatty acids (palmitic acid) (Uddin et al., 2017) and fatty alcohol (1-docosanol) (Chapter 5), significantly induced SWR on AWS. The difference in the amount and concentration of carbon pools at different periods of the study, supports the results found in Chapter 3 that heating can increase the severity of SWR most likely due to the distribution of compounds on the soil particles. However,

the smoke related compounds emitted during vegetation fire did not induce SWR onto the acid washed sand (Chapter 4).

The soil samples collected from under the native species of *Eucalyptus marginata, E. wandoo, Allocasuarina fraseriana, and Banksia menziesii* were also found to have similar hydrophobic compounds to those found in Chapter 2. Long chain fatty acids, phytols, phytanols, esters, sterols, alkanes, amides, acetates and aldehydes or ketones were also detected in the hydrophobic soil of previous studies (Franco et al., 1995; Horne & McIntosh, 2000; McKissock et al., 2003). However, long chain fatty acids and alcohols were not evident in the soil samples of *A. fraseriana*, whereas, they were identfied in the species of *E. marginata*, *E. wandoo* and *B. menziesii*. Hydrophobic soils are usually found to contain relatively long-chain carbon compounds as it was evident by Capriel et al. (1995).

SWR in soils is the outcome of the synergistic contribution of both the soil particles coated with hydrophobic substances and interstitial organic matter of the soil matrix. Thus, the severity of SWR is very dynamic due to the physical interaction of organic pools with different soil components. The variations in the concentration of carbon pools of the bulk soil with the separated coarse mineral materials and finer interstitial matter indicates particulate matter can significantly modify the incidence of SWR. Doerr et al. (2000) also reported that small amounts of hydrophobic particulate matter within the soil pores can change the severity of SWR. The reduction of the SWR through dilution of the bulk soils and coarse mineral materials indicated that the soil carbon pools can have a pivotal role in the incidence of SWR. For example, SWR was even observed for the diluted (with 75% AWS) samples of *E. marginata* and *E. wandoo* after heating at 105°C.

The severity of SWR sharply increased for *E. marginata*, *E. wandoo* and *B. menziesii* with increasing loadings of interstitial matter onto AWSs. Heating the samples at 105°C was also found to further increase SWR. Franco et al. (1995) reported that during heating, waxes from particulate organic matter migrate onto soil particle surfaces, thereby increasing severity of SWR. It has also been suggested that upon drying the amphiphilic molecules re-adopt a position in which their polar ends are attached to the mineral surface, and the nonpolar ends are oriented outwards (Doerr et al., 2000). Moreover, heating the mixture of acid washed sand loaded with interstitial matter (10%) at a range of temperatures, revealed increased SWR after heating at 150°C in all the samples, while following heating at 200°C it decreased. Apart from redistributing, heating can also improve the bonding of hydrophobic substances to soil particles (Savage et al., 1972).

Despite different carbon contents, the severity of SWR was similar between *E. marginata* and *E. wandoo*, suggesting finer fractions were dominating the soil matrix of *E. wandoo*. Moreover, the supply of hydrophobic materials under *E. wandoo* might be sufficiently high not only to cover the coarser, but also coat much of the fine-sized particles. Doerr et al. (1996) reported sufficient organic pools can increase the severity of SWR.

7.4   *Computer modelling to improve understanding of SWR*

The severity of SWR is thought to be associated with the molecular arrangement of the organic molecules on soil particles. Experimental studies provide a broad understanding of the bulk effects of hydrophobic films on soil particles but there is very little information on the coating structure or its kinetic and/or thermodynamic stability. By contrast, molecular dynamics simulations provide structural information and details of

physical interactions of applied hydrophobic molecules with the model mineral surfaces. For example, the simulations of long-chain amphiphilic molecules on the quartz surface reveal a balance between molecule-molecule and molecule-surface interactions (Uddin et al., 2017). Hydrophobic and amphiphilic molecules are found to organize themselves differently on different mineral surfaces (e.g., quartz, silica and kaolinite). It has been proposed that the differences in the molecular arrangement or conformation of the organic matter on soil particles correspond to the differences in the severity of SWR (Ma'shum & Farmer, 1985). The relative contribution of organic compounds to SWR depends on the particular head groups and their adsorption onto mineral surfaces. Moreover, fatty acid head groups can be complexed in the natural environment, at positively charged surfaces with cations and via divalent cation bridges at negatively charged surfaces with chains facing outward, rendering the surface hydrophobic (Graber et al., 2009; Kleber et al., 2007).

Heating (105°C for 24hours) of the soil samples loaded with pure organic compounds and their mixtures, redistributed them on the soil particle surfaces and thus changed the severity of SWR. The increased severity of SWR was even noted in Chapter 3, when interstitial matter was loaded onto acid washed sand at different rates. Temperature during vegetation fire and heating duration are reported as crucial factors in changing the severity of SWR (Doerr et al., 2004). Molecular dynamics simulations conducted at 175°C in Chapter 4 revealed that biogenic volatile organic compounds (BVOCs) had much greater kinetic energies and exhibited different molecular arrangement compared with the amphiphilic molecules on the quartz surface. The amphiphilic molecules were even found to be adhered to the surface at the higher temperature. However, the present study indicated an insignificant contribution of the smoke related compounds derived from vegetation fire in the incidence of SWR (Uddin et al., 2017).

The stability and longevity of organic films depend on the abundance and nature of fatty acids and other components at particle surfaces, the mineralogy of the substrate, and the chemistry of the soil solution (Graber et al., 2009). Molecular models can characterize the adsorption potential of hydrophobic films on mineral surfaces to indicate the potential for SWR or alternatively provide insights for amelioration strategies. For example, amphiphilic molecules with acidic and alcoholic hydrogen atoms were found to have strong hydrogen donor bond interactions with the surfaces as shown in Chapter 5 & 6. The result was consistent with the experimental loading of palmitic acid and 1-docosanol both on AWS and AWS with 5% kaolinite with stronger effect in inducing SWR. However, hexadecane was found to enhance the effect of SWR with the combination of palmitic acid and 1-docosanol. Molecular dynamics simulations also revealed that hydrogen donor atoms of PA not only have a strong interaction with the oxygen atoms of mineral surfaces on its own but also in combination with hexadecane, tridecanoic acid, 1-methylethyl ester (Td1Me) and 1-hexadecanol. Moreover, the interaction of hydrocarbon chains with the surfaces and between hydrocarbon chains revealed van der Waals (vdW) forces make a significant contribution to the organo-mineral interactions. Wu et al. (2013) also reported vdW force as the main contribution of interactions of the heavy crude oil on the quartz surface. The packing arrangement of palmitic acid and 1-docosanol was found in an orderly aligned and thus the cohesion between the hydrocarbon chains was increased. Reduced packing efficiency was reported for the double bond or branched chain organic compounds on sandy surfaces (Mainwaring et al., 2013; Shaw & Costello, 1993). Furthermore, isopropyl myristate (IsoM) was found to reduce the effect of 1-docosanol when combined in a mixture. However, IsoM was found to neither add to nor detract from the SWR effect of palmitic acid on AWS. The mixture of palmitic acid and 1-docosanol had a synergistic effect in

inducing SWR on AWS relative to the individual component. Molecular dynamics simulation again implies the difference in severity of SWR can be due to the molecular arrangement at the organo-mineral interface. The organo-mineral interactions were evident through differences in H-bonding between palmitic acid molecules when it was applied on its own and in combination with hexadecane, Td1Me and 1-hexadecanol. This is consistent with the findings of Ma'Shum et al. (1988) that a close-packed monolayer can only induce a significant level of SWR.

The simulations in this study also revealed that amphiphilic molecules closely interacted with the water molecules and organize themselves differently (Chapter 6) in comparison with the simulation conducted in the dry system in Chapter 5. In aqueous solution, the amphiphilic molecules are found to arrange themselves into micellar self-organization. However, although the components of a membrane-like organic layer may exchange more easily with the surrounding soil solution, they are retained on mineral surfaces with considerable force (Kleber et al., 2007).

Dissolved organic matter has also been reported to decrease the severity of SWR (Franco et al., 2000a). The results presented in Chapter 6 suggest further analysis is required to gain more insights on lifting of organic molecules away from the surfaces that could be investigated with enough water molecules and simulation time of the model mineral surfaces. The study suggests water molecules can completely remove or washing off hydrophobic substances from the soil particle surfaces and fresh input of hydrophobic substances may be required for the re-establishment of SWR in the natural environment. This is consistent with the findings of Doerr and Thomas (2000) that SWR did not reappear when the wet Portuguese sandy forest soils become dry.

7.5   *Final conclusions*

A range of hydrophobic compounds (polar and nonpolar) were detected in the canopy derived exudates and these imply a small contribution to the incidence of SWR in the soil. The number and concentration of characterized compounds was different between exudates and soil extracts. The compounds were also found with higher concentration in the autumn compared with the winter. The compounds were found to induce SWR when loaded onto acid washed sand (AWS) either singly or in mixtures. For example, pure palmitic acid and 1-docosanol were found to significantly induce SWR on AWS and AWS with 5% KL. Hexadecane in combination with the palmitic acid or 1-docosanol enhanced the severity of SWR. However, isopropyl myristate in the mixtures with palmitic acid and 1-docosanol was found to reduce SWR.

Along with the coating of hydrophobic compounds on soil particles, interstitial matter was found to significantly modify the severity of SWR. The concentration of different compounds in the bulk soil was found to be similar to the total concentration from the separated components, namely, coarse mineral materials and interstitial matter. Moreover, when interstitial matter was applied onto AWS at different percentages (w/w), it was found to significantly induce SWR. The severity of SWR was increased following heating at 105 °C. The molecular dynamics study in chapter 4 revealed that redistribution and reorganization of organic compounds on soil particle surfaces can play a substantial role in the variation of SWR.

Many of the biogenic volatile organic compounds (BVOCs) emitted during vegetation fire are amphiphilic compounds and the polar functional groups in these molecules should be attracted to mineral surfaces, with the nonpolar portion creating a hydrophobic layer that might be expected to induce SWR. However, these compounds

made no significant change to the wettability of AWS. Furthermore, palmitic acid (PA) was found to significantly induce SWR, even at low loading levels (1×10^{-6} mol g^{-1}). This is attributed to the strong attachment of the polar head groups (-COOH) to the surface of the sand particles, combined with alignment of the long nonpolar tails to give hydrophobic condensed films.

The physicochemical interactions of the organic molecules with the mineral surfaces were consistent both in the experimental and molecular dynamics study. For example, the severity of SWR of the applied amphiphilic compounds both on their own and in the mixtures, were different at different concentrations. The molecular dynamics study of the individual compounds and combinations also revealed different conformation of the organic layers at the organo-mineral interface. Long-chain amphiphilic molecules on the quartz surface revealed a balance between molecule-molecule and molecule-surface interactions and the molecules were found adhered to the surface. Moreover, the added water molecules on the mineral surface were found to reorganize the amphiphilic compounds in the form of micellar self-organization.

7.6   Future research directions

SWR is a perennial land management issue in southwestern Australia and other regions with a Mediterranean type climate. However, there is no straightforward pathway to address this natural phenomenon. It has an intricate relation with the type of soil particles, particular land use, and associated environmental factors. A number of hydrophobic and amphiphilic compounds were found in the canopy derived exudates from 4 native Australian species (*Eucalyptus marginata*, *Banksia menziesii*, *Xanthorrhoea preisii*, and *Allocasuarina fraseriana*) including long-chain alkane, fatty acids, fatty alcohols, esters, amides, and terpenoids. These compounds were also

208

detected in the extracts of the soil collected from the soil beneath these species. However, the composition and concentration of compounds were different in the soil extracts compared with the canopy exudates. The degree to which these differences correspond to different soil behaviors, including the fate of these compounds in the soil, changes in the run-off and infiltration dynamics await further investigation.

A key question arising from this study is whether the compounds derived from natural vegetation have any residual effects in the agricultural land. Much of the farmland was converted from natural vegetation in the last 50-100 years. For example, top-down exudates of hydrophobic compounds led to the development of SWR after 5-8 years of *E. globulus* establishment (Walden et al., 2015). Therefore, it is possible that the patterns of SWR in agricultural fields are related to pre-clearing natural vegetation. As seen in this thesis, and particularly in Chapters 2 and 3, there are marked differences in the induction of SWR by different species.

A key consideration in addressing SWR is to identify the amount of carbon pools in different soil components (e.g., coarser mineral materials and finer interstitial matter). However, the amount of carbon contained in the interstitial matter is unknown, and this will need to be quantified to clarify the thermal behavior (phase transition) of organic pools and their effect on the severity of SWR.

Higher temperatures were found to affect the molecular arrangement and interaction with the mineral surfaces. However, further research is required to gain insights into the intricate interactions between molecules and different soil components (e.g., interstitial matter, coatings). Moreover, the contribution of pyrolytic species in inducing SWR awaits further investigation.

Finally, SWR is closely associated to the organic carbon pools and their arrangement on the soil particles and interstices. A holistic approach based on soil types, land uses, existing organic carbon pools, concentration and arrangement of them in different soil components, and environmental parameters should be considered to address the incidence of SWR.

8 References

Accelrys. 2013. Accelrys Software Inc, BIOVIA, 5005 Waterridge Vista Drive, San Diego, CA 92121, USA.

Andersen, H.C. 1980. Molecular dynamics simulations at constant pressure and/or temperature. *The Journal of Chemical Physics*, **72**(4), 2384-2393.

Andreu, V., Imeson, A., Rubio, J.L. 2001. Temporal changes in soil aggregates and water erosion after a wildfire in a Mediterranean pine forest. *Catena*, **44**(1), 69-84.

Arcenegui, V., Mataix-Solera, J., Guerrero, C., Zornoza, R., Mayoral, A.M., Morales, J. 2007. Factors controlling the water repellency induced by fire in calcareous Mediterranean forest soils. *European Journal of Soil Science*, **58**(6), 1254-1259.

Atanassova, I., Doerr, S. 2010. Organic compounds of different extractability in total solvent extracts from soils of contrasting water repellency. *European Journal of Soil Science*, **61**(2), 298-313.

Atanassova, I., Doerr, S.H. 2011. Changes in soil organic compound composition associated with heat-induced increases in soil water repellency. *European Journal of Soil Science*, **62**(4), 516-532.

Baldock, J., Oades, J., Waters, A., Peng, X., Vassallo, A., Wilson, M. 1992. Aspects of the chemical structure of soil organic materials as revealed by solid-state 13 C NMR spectroscopy. *Biogeochemistry*, **16**(1), 1-42.

Barrett, G., Slaymaker, O. 1989. Identification, characterization, and hydrological implications of water repellency in mountain soils, southern British Columbia. *Catena*, **16**(4-5), 477-489.

Barton, A.F.M., Tjandra, J., Nicholas, P.G. 1989. Chemical evaluation of volatile oils in *Eucalyptus* species. *Journal of Agricultural and Food Chemistry*, **37**(5), 1253-1257.

Batish, D.R., Singh, H.P., Kohli, R.K., Kaur, S. 2008. *Eucalyptus* essential oil as a natural pesticide. *Forest Ecology and Management*, **256**(12), 2166-2174.

Bisdom, E.B.A., Dekker, L.W., Schoute, J.F.T. 1993. Water repellency of sieve fractions from sandy soils and relationships with organic material and soil structure. *Geoderma*, **56**(1–4), 105-118.

Blackwell, P.S. 2000. Management of water repellency in Australia, and risks associated with preferential flow, pesticide concentration and leaching. *Journal of Hydrology*, **231–232**(0), 384-395.

Bond, R.D. 1972. Germination and yield of barley when grown in a water-repellent sand. *Agronomy Journal*, **64**, 402-403.

Bond, R.D., Harris, J.R. 1964. The influence of the microflora on the physical properties of soils. I. Effects associated with filamentous algae and fungi. *Australian Journal of Soil Research*, **2**(1), 111-122.

Bond, W.J., Keeley, J.E. 2005. Fire as a global 'herbivore': the ecology and evolution of flammable ecosystems. *Trends in Ecology & Evolution*, **20**(7), 387-394.

Borken, W., Matzner, E. 2009. Reappraisal of drying and wetting effects on C and N mineralization and fluxes in soils. *Global Change Biology*, **15**(4), 808-824.

Buczko, U., Bens, O., Fischer, H., Hüttl, R.F. 2002. Water repellency in sandy Luvisols under different forest transformation stages in northeast Germany. *Geoderma*, **109**(1–2), 1-18.

Burch, G., Moore, I., Burns, J. 1989. Soil hydrophobic effects on infiltration and catchment runoff. *Hydrological Processes*, **3**(3), 211-222.

Capriel, P., Beck, T., Borchert, H., Gronholz, J., Zachmann, G. 1995. Hydrophobicity of the organic matter in arable soils. *Soil Biology and Biochemistry*, **27**(11), 1453-1458.

Cawson, J., Sheridan, G., Smith, H., Lane, P. 2012. Surface runoff and erosion after prescribed burning and the effect of different fire regimes in forests and shrublands: a review. *International Journal of Wildland Fire*, **21**(7), 857-872.

Cerdà, A., Doerr, S.H. 2007. Soil wettability, runoff and erodibility of major dry-Mediterranean land use types on calcareous soils. *Hydrological Processes*, **21**(17), 2325-2336.

Chandler, D. 1987. Introduction to modern statistical mechanics. *pp. 288. Foreword by David Chandler. Oxford University Press, Sep 1987. ISBN-10: 0195042778. ISBN-13: 9780195042771*, 288.

Chaves, M., Oliveira, M. 2004. Mechanisms underlying plant resilience to water deficits: prospects for water-saving agriculture. *Journal of Experimental Botany*, **55**(407), 2365-2384.

Chaves, N., Escudero, J.C., Gutierrez-Merino, C. 1997. Role of ecological variables in the seasonal variation of flavonoid content of *Cistus ladanifer* exudate. *Journal of Chemical Ecology*, **23**(3), 579-603.

Cheng, S., Doerr, S.H., Bryant, R., Wright, C.J. 2010. Effects of isopropanol/ammonia extraction on soil water repellency as determined by atomic force microscopy *Soil Science Society of America Journal*, **74**(5), 1541-1552.

Ciccioli, P., Centritto, M., Loreto, F. 2014. Biogenic volatile organic compound emissions from vegetation fires. *Plant, Cell & Environment*, **37**(8), 1810-1825.

Coelho, C.O.A., Laouina, A., Regaya, K., Ferreira, A.J.D., Carvalho, T.M.M., Chaker, M., Naafa, R., Naciri, R., Boulet, A.K., Keizer, J.J. 2005. The impact of soil water repellency on soil hydrological and erosional processes under *Eucalyptus* and evergreen *Quercus* forests in the Western Mediterranean. *Australian Journal of Soil Research*, **43**(3), 309-318.

Courtney, J.L., Lassak, E.V., Speirs, G.B. 1983. Leaf wax constituents of some myrtaceous species. *Phytochemistry*, **22**(4), 947-949.

Crockford, H., Topalidis, S., Richardson, D.P. 1991. Water repellency in a dry sclerophyll eucalypt forest — measurements and processes. *Hydrological Processes*, **5**(4), 405-420.

Crockford, R.H., Richardson, D.P. 1998. Litterfall, litter and associated chemistry in a dry sclerophyll eucalypt forest and a pine plantation in south-eastern Australia: 1. Litterfall and litter. *Hydrological Processes*, **12**(3), 365-384.

Crous, K.Y., Quentin, A.G., Lin, Y.-S., Medlyn, B.E., Williams, D.G., Barton, C.V.M., Ellsworth, D.S. 2013. Photosynthesis of temperate *Eucalyptus globulus* trees outside their native range has limited adjustment to elevated CO_2 and climate warming. *Global Change Biology*, **19**(12), 3790-3807.

de Blas, E., Rodríguez-Alleres, M., Almendros, G. 2010. Speciation of lipid and humic fractions in soils under pine and *Eucalyptus* forest in northwest Spain and its effect on water repellency. *Geoderma*, **155**(3–4), 242-248.

DeBano, L.F. 1991. The effect of fire on soil properties. *Proceedings-Management and productivity of western-Montane forest soils*. pp. 151-155.

DeBano, L.F. 2000. The role of fire and soil heating on water repellency in wildland environments: a review. *Journal of Hydrology*, **231**, 195-206.

DeBano, L.F. 1981. Water repellent soils: a state-of-the-art. *NASA STI/Recon Technical Report N*, **82**.

DeBano, L.F., Krammes, J. 1966. Water repellent soils and their relation to wildfire temperatures. *Hydrological Sciences Journal*, **11**(2), 14-19.

DeBano, L.F., Mann, L.D., Hamilton, D.A. 1970. Translocation of hydrophobic substances into soil by burning organic litter. *Soil Science Society of America Journal*, **34**(1), 130-133.

DeBano, L.F., Rice, R.M. 1973. Water repellent soils: Their implications in forestry. *Journal of Forestry*, **71**(4), 220-223.

Dekker, L.W., Doerr, S.H., Oostindie, K., Ziogas, A.K., Ritsema, C.J. 2001. Water repellency and critical soil water content in a dune sand. *Soil Science Society of America Journal*, **65**(6), 1667-1674.

Dekker, L.W., Ritsema, C.J. 1994. How water moves in a water repellent sandy soil: 1. Potential and actual water repellency. *Water Resources Research*, **30**(9), 2507-2517.

Dekker, L.W., Ritsema, C.J. 1996. Variation in water content and wetting patterns in Dutch water repellent peaty clay and clayey peat soils. *Catena*, **28**(1), 89-105.

Dekker, L.W., Ritsema, C.J. 2000. Wetting patterns and moisture variability in water repellent Dutch soils. *Journal of Hydrology*, **231–232**(0), 148-164.

Dekker, L.W., Ritsema, C.J., Oostindie, K. 2000. Extent and significance of water repellency in dunes along the Dutch coast. *Journal of Hydrology*, **231–232**(0), 112-125.

Dekker, L.W., Ritsema, C.J., Oostindie, K., Moore, D., Wesseling, J.G. 2009. Methods for determining soil water repellency on field-moist samples. *Water Resources Research*, **45**(4).

Dell, B., Bartle, J., Tacey, W. 1983. Root occupation and root channels of jarrah forest subsoils. *Australian Journal of Botany*, **31**(6), 615-627.

Dixon, K.W., Roche, S., Pate, J.S. 1995. The promotive effect of smoke derived from burnt native vegetation on seed germination of Western Australian plants. *Oecologia*, **101**(2), 185-192.

Dlapa, P., Simkovic, I., Doerr, S.H., Simkovic, I., Kanka, R., Mataix-Solera, J. 2008. Application of thermal analysis to elucidate water-repellency changes in heated soils *Soil Science Society of America Journal*, **72**(1), 1-10.

Doerr, S.H., Blake, W.H., Shakesby, R.A., Stagnitti, F., Vuurens, S.H., Humphreys, G.S., Wallbrink, P. 2004. Heating effects on water repellency in Australian eucalypt forest soils and their value in estimating wildfire soil temperatures. *International Journal of Wildland Fire*, **13**(2), 157-163.

Doerr, S.H., Llewellyn, C.T., Douglas, P., Morley, C.P., Mainwaring, K.A., Haskins, C., Johnsey, L., Ritsema, C.J., Stagnitti, F., Allinson, G., Ferreira, A.J.D., Keizer, J.J., Ziogas, A.K., Diamantis, J. 2005. Extraction of compounds associated with water repellency in sandy soils of different origin. *Australian Journal of Soil Research*, **43**(3), 225-237.

Doerr, S.H., Shakesby, R.A. 2006. Forest fire impacts on catchment hydrology: A critical review. *Forest Ecology and Management*, **234**, S161.

Doerr, S.H., Shakesby, R.A., Blake, W.H., Chafer, C.J., Humphreys, G.S., Wallbrink, P.J. 2006. Effects of differing wildfire severities on soil wettability and implications for hydrological response. *Journal of Hydrology*, **319**(1–4), 295-311.

Doerr, S.H., Shakesby, R.A., Walsh, R.P.D. 1996. Soil hydrophobicity variations with depth and particle size fraction in burned and unburned *Eucalyptus globulus* and *Pinus pinaster* forest terrain in the Águeda Basin, Portugal. *CATENA*, **27**(1), 25-47.

Doerr, S.H., Shakesby, R.A., Walsh, R.P.D. 2000. Soil water repellency: its causes, characteristics and hydro-geomorphological significance. *Earth-Science Reviews*, **51**(1–4), 33-65.

Doerr, S.H., Shakesby, R.A., Walsh, R.P.D. 1998. Spatial variability of soil hydrophobicity in fire-prone *Eucalyptus* and Pine forests, Portugal. *Soil Science*, **163**(4), 313-324.

Doerr, S.H., Thomas, A.D. 2000. The role of soil moisture in controlling water repellency: new evidence from forest soils in Portugal. *Journal of Hydrology*, **231–232**(0), 134-147.

Doerr, S.H., Woods, S.W., Martin, D.A., Casimiro, M. 2009. 'Natural background' soil water repellency in conifer forests of the north-western USA: Its prediction and relationship to wildfire occurrence. *Journal of Hydrology*, **371**(1–4), 12-21.

Eglinton, G., Gonzalez, A.G., Hamilton, R.J., Raphael, R.A. 1962. Hydrocarbon constituents of the wax coatings of plant leaves: A taxonomic survey. *Phytochemistry*, **1**(2), 89-102.

Ehrenfeld, J.G. 2003. Effects of exotic plant invasions on soil nutrient cycling processes. *Ecosystems*, **6**(6), 503-523.

Ellerbrock, R.H., Gerke, H.H., Bachmann, J., Goebel, M.-O. 2005. Composition of organic matter fractions for explaining wettability of three forest soils. *Soil Science Society of America Journal*, **69**(1), 57-66.

Ellies, A., Ramírez, C., Mac-Donald, R. 2005. Organic matter and wetting capacity distribution in aggregates of Chilean soils. *Catena*, **59**(1), 69-78.

Ferreira, A.J.D., Coelho, C.O.A., Walsh, R.P.D., Shakesby, R.A., Ceballos, A., Doerr, S.H. 2000. Hydrological implications of soil water-repellency in *Eucalyptus globulus* forests, north-central Portugal. *Journal of Hydrology*, **231–232**(0), 165-177.

Franco, C.M., Michelsen, P., Oades, J.M. 2000a. Amelioration of water repellency: application of slow-release fertilisers to stimulate microbial breakdown of waxes. *Journal of Hydrology*, **231**, 342-351.

Franco, C.M.M., Clarke, P.J., Tate, M.E., Oades, J.M. 2000b. Hydrophobic properties and chemical characterisation of natural water repellent materials in Australian sands. *Journal of Hydrology*, **231–232**(0), 47-58.

Franco, C.M.M., Tate, M.E., Oades, J.M. 1995. Studies on non-wetting sands. 1. The role of intrinsic particulate organic-matter in the development of water-repellency in non-wetting sands. *Australian Journal of Soil Research*, **33**(2), 253-263.

García, F.J.M., Dekker, L.W., Oostindie, K., Ritsema, C.J. 2005. Water repellency under natural conditions in sandy soils of southern Spain. *Australian Journal of Soil Research*, **43**(3), 291-296.

Garkaklis, M.J., Bradley, J., Wooller, R. 1998. The effects of woylie (*Bettongia penicillata*) foraging on soil water repellency and water infiltration in heavy textured soils in south-western Australia. *Australian Journal of Ecology*, **23**(5), 492-496.

Gerrits, A., Pfister, L., Savenije, H. 2010. Spatial and temporal variability of canopy and forest floor interception in a beech forest. *Hydrological Processes*, **24**(21), 3011-3025.

Ghadim, A.A. 2000. Water repellency: a whole-farm bio-economic perspective. *Journal of Hydrology*, **231**, 396-405.

Giovannini, G., Lucchesi, S. 1983. Effect of fire on hydrophobic and cementing substances of soil aggregates. *Soil Science*, **136**(4), 231-236.

Giovannini, G., Lucchesi, S. 1997. Modifications induced in soil physico-chemical parameters by experimental fires at different intensities. *Soil Science*, **162**(7), 479-486.

Goebel, M.-O., Bachmann, J., Reichstein, M., Janssens, I.A., Guggenberger, G. 2011. Soil water repellency and its implications for organic matter decomposition – is there a link to extreme climatic events? *Global Change Biology*, **17**(8), 2640-2656.

Goebel, M.-O., Bachmann, J., Woche, S.K., Fischer, W.R. 2005. Soil wettability, aggregate stability, and the decomposition of soil organic matter. *Geoderma*, **128**(1–2), 80-93.

Graber, E.R., Tagger, S., Wallach, R. 2009. Role of divalent fatty acid salts in soil water repellency *Soil Science Society of America Journal*, **73**(2), 541-549.

Greiffenhagen, A., Wessolek, G., Facklam, M., Renger, M., Stoffregen, H. 2006. Hydraulic functions and water repellency of forest floor horizons on sandy soils. *Geoderma*, **132**(1–2), 182-195.

Groves, R.H. 1994. *Australian Vegetation*. Cambridge University Press.

Hakola, H., Tarvainen, V., Laurila, T., Hiltunen, V., Hellén, H., Keronen, P. 2003. Seasonal variation of VOC concentrations above a boreal coniferous forest. *Atmospheric Environment*, **37**(12), 1623-1634.

Hallett, P.D., White, N.A., Ritz, K. 2006. Impact of basidiomycete fungi on the wettability of soil contaminated with a hydrophobic polycyclic aromatic hydrocarbon. *Biologia*, **61**(19), S334-S338.

Hamaker, H. 1937. The London—van der Waals attraction between spherical particles. *Physica*, **4**(10), 1058-1072.

Hansel, F.A., Aoki, C.T., Maia, C.M.B.F., Cunha Jr, A., Dedecek, R.A. 2008. Comparison of two alkaline treatments in the extraction of organic compounds associated with water repellency in soil under *Pinus taeda*. *Geoderma*, **148**(2), 167-172.

Harper, R.J., McKissock, I., Gilkes, R.J., Carter, D.J., Blackwell, P.S. 2000. A multivariate framework for interpreting the effects of soil properties, soil management and landuse on water repellency. *Journal of Hydrology*, **231–232**(0), 371-383.

Hayes, M. 1998. Humic substances: progress towards more realistic concepts of structures. *Special Publication-Royal Society of Chemistry*, **228**(1), 1-28.

Hayes, M.H., Graham, C.L. 2000. Procedures for the isolation and fractionation of humic substances. *Special Publication-Royal Society of Chemistry*, **259**, 91-110.

He, C., Murray, F., Lyons, T. 2000. Monoterpene and isoprene emissions from 15 *Eucalyptus* species in Australia. *Atmospheric Environment*, **34**(4), 645-655.

Heath, J.T., Chafer, C.J., Bishop, T.F., Van Ogtrop, F.F. 2015. Wildfire effects on soil carbon and water repellency under *Eucalyptus* forest in Eastern Australia. *Australian Journal of Soil Research*, **53**(1), 13-23.

Henry, D.J., Dewan, V.I., Prime, E.L., Qiao, G.G., Solomon, D.H., Yarovsky, I. 2010. Monolayer structure and evaporation resistance: a molecular dynamics study of octadecanol on water. *The Journal of Physical Chemistry B*, **114**(11), 3869-3878.

Henry, D.J., Evans, E., Yarovsky, I. 2006. Classical molecular dynamics study of [60] fullerene interactions with silica and polyester surfaces. *The Journal of Physical Chemistry B*, **110**(32), 15963-15972.

Henry, D.J., Lukey, C.A., Evans, E., Yarovsky, I. 2005. Theoretical study of adhesion between graphite, polyester and silica surfaces. *Molecular Simulation*, **31**(6-7), 449-455.

Hopper, S.D. 2009. OCBIL theory: towards an integrated understanding of the evolution, ecology and conservation of biodiversity on old, climatically buffered, infertile landscapes. *Plant and Soil*, **322**(1-2), 49-86.

Horn, D., Kranz, Z., Lamberton, J. 1964. The composition of *Eucalyptus* and some other leaf waxes. *Australian Journal of Chemistry*, **17**(4), 464-476.

Horne, D., McIntosh, J. 2000. Hydrophobic compounds in sands in New Zealand—extraction, characterisation and proposed mechanisms for repellency expression. *Journal of Hydrology*, **231**, 35-46.

Hunter, A., Chau, H., Si, B. 2011. Impact of tension infiltrometer disc size on measured soil water repellency index. *Canadian Journal of Soil Science*, **91**(1), 77-81.

Jiménez-Morillo, N.T., González-Pérez, J.A., Jordán, A., Zavala, L.M., Rosa, J.M., Jiménez-González, M.A., González-Vila, F.J. 2016. Organic matter fractions controlling soil water repellency in sandy soils from the Doñana National Park (south-western Spain). *Land Degradation & Development*, **27**(5), 1413-1423.

Jon, E.K., William, J.B., Ross, A.B., Juli, G.P., Philip, W.R. 2012. *Fire in Mediterranean ecosystems: Ecology, evolution and managemnt*. Cambridge University Press, Cambridge CB2 8RU, UK.

Jordán, A., Martínez-Zavala, L., Bellinfante, N. 2008. Heterogeneity in soil hydrological response from different land cover types in southern Spain. *CATENA*, **74**(2), 137-143.

Kamatou, G.P.P., Van Zyl, R.L., Van Vuuren, S.F., Figueiredo, A.C., Barroso, J.G., Pedro, L.G., Viljoen, A.M. 2008. Seasonal variation in essential oil composition, oil toxicity and the biological activity of solvent extracts of three South African Salvia species. *South African Journal of Botany*, **74**(2), 230-237.

Keizer, J., Coelho, C., Shakesby, R., Domingues, C., Malvar, M., Perez, I., Matias, M., Ferreira, A. 2005a. The role of soil water repellency in overland flow generation in pine and eucalypt forest stands in coastal Portugal. *Australian Journal of Soil Research*, **43**(3), 337-349.

Keizer, J.J., Coelho, C.O.A., Matias, M.J.S., Domingues, C.S.P., Ferreira, A.J.D. 2005b. Soil water repellency under dry and wet antecedent weather conditions for selected land-cover types in the coastal zone of central Portugal. *Australian Journal of Soil Research*, **43**(3), 297-308.

Keizer, J.J., Doerr, S.H., Malvar, M.C., Prats, S.A., Ferreira, R.S.V., Oñate, M.G., Coelho, C.O.A., Ferreira, A.J.D. 2008. Temporal variation in topsoil water repellency in two recently burnt eucalypt stands in north-central Portugal. *CATENA*, **74**(3), 192-204.

Kesselmeier, J., Bode, K., Hofmann, U., Müller, H., Schäfer, L., Wolf, A., Ciccioli, P., Brancaleoni, E., Cecinato, A., Frattoni, M. 1997. Emission of short chained organic acids, aldehydes and monoterpenes from *Quercus ilex* L. and *Pinus pinea* L. in relation to physiological activities, carbon budget and emission algorithms. *Atmospheric Environment*, **31**, 119-133.

Kim, J.-C., Kim, K.-J., Kim, D.-S., Han, J.-S. 2005. Seasonal variations of monoterpene emissions from coniferous trees of different ages in Korea. *Chemosphere*, **59**(11), 1685-1696.

King, C., Jacob, H.S., Berlandier, F. 2006. The influence of water deficiency on the relationship between canola (*Brassica napus* L.), and two aphid species (Hemiptera: Aphididae), *Lipaphis erysimi* (Kaltenbach) and *Brevicoryne brassicae* (L.). *Australian Journal of Agricultural Research*, **57**(4), 439-445.

King, P.M. 1981. Comparison of methods for measuring severity of water repellence of sandy soils and assessment of some factors that affect its measurement. *Australian Journal of Soil Research*, **19**(3), 275-285.

Kitchens, L. 2015. The Contribution of Western Australian native plant species to water repellency. *B Sc (Hons) Project in Chemistry, School of Engineering and Information Technology, Murdoch University, Murdoch-6150, Australia*, 105.

Kleber, M., Sollins, P., Sutton, R. 2007. A conceptual model of organo-mineral interactions in soils: self-assembly of organic molecular fragments into zonal structures on mineral surfaces. *Biogeochemistry*, **85**(1), 9-24.

Lambers, H., Brundrett, M.C., Raven, J.A., Hopper, S.D. 2010. Plant mineral nutrition in ancient landscapes: high plant species diversity on infertile soils is linked to functional diversity for nutritional strategies. *Plant and Soil*, **334**(1-2), 11-31.

Lambers, H., Chapin, F.S., Pons, T. 2008. Plant Water Relations. in: *Plant Physiological Ecology*, Springer New York, pp. 163-223.

Lambers, H., Mougel, C., Jaillard, B., Hinsinger, P. 2009. Plant-microbe-soil interactions in the rhizosphere: an evolutionary perspective. *Plant and Soil*, **321**(1-2), 83-115.

Lamparter, A., Bachmann, J., Woche, S. 2010. Determination of small-scale spatial heterogeneity of water repellency in sandy soils. *Soil Science Society of America Journal*, **74**(6).

Lebron, I., Robinson, D.A., Oatham, M., Wuddivira, M.N. 2012. Soil water repellency and pH soil change under tropical pine plantations compared with native tropical forest. *Journal of Hydrology*, **414–415**(0), 194-200.

Leighton-Boyce, G., Doerr, S.H., Shakesby, R.A., Walsh, R.P.D., Ferreira, A.J.D., Boulet, A., Coelho, C.O.A. 2005. Temporal dynamics of water repellency and soil moisture in eucalypt plantations, Portugal. *Australian Journal of Soil Research*, **43**(3), 269-280.

Letey, J. 1969. Measurement of contact angle, water drop penetration time, and critical surface tension. *In Proc. Symp. Water Rep. Soils, Univ. of California, Riverside, CA*, p. 43-47.

Lichner, L., Dlapa, P., Doerr, S.H., Mataix-Solera, J. 2006. Evaluation of different clay minerals as additives for soil water repellency alleviation. *Applied Clay Science*, **31**(3), 238-248.

Ma'shum, M., Farmer, V. 1985. Origin and assessment of water repellency of a sandy South Australian soil. *Australian Journal of Soil Research*, **23**(4), 623-626.

Ma'Shum, M., Tate, M.E., Jones, G.P., Oades, J.M. 1988. Extraction and characterization of water–repellent materials from Australian soils. *Journal of Soil Science*, **39**(1), 99-110.

Mainwaring, K., Hallin, I.L., Douglas, P., Doerr, S.H., Morley, C.P. 2013. The role of naturally occurring organic compounds in causing soil water repellency. *European Journal of Soil Science*, **64**(5), 667-680.

Maleknia, S.D., Bell, T.L., Adams, M.A. 2009. Eucalypt smoke and wildfires: temperature dependent emissions of biogenic volatile organic compounds. *International Journal of Mass Spectrometry*, **279**(2–3), 126-133.

Maleknia, S.D., Bell, T.L., Adams, M.A. 2007. PTR-MS analysis of reference and plant-emitted volatile organic compounds. *International Journal of Mass Spectrometry*, **262**(3), 203-210.

Mallik, A., Rahman, A. 1985. Soil water repellency in regularly burned Calluna heathlands: comparison of three measuring techniques. *Journal of Environmental Management*, **20**(3), 207-218.

Manalo, F.P., Kantzas, A., Langford, C.H. 2003. Soil wettability as determined from using low-field nuclear magnetic resonance. *Environmental Science & Technology*, **37**(12), 2701-2706.

Mao, J., Nierop, K.G., Rietkerk, M., Dekker, S.C. 2015. Predicting soil water repellency using hydrophobic organic compounds and their vegetation origin. *Soil*, **1**(1), 411.

Martínez-Zavala, L., Jordán-López, A. 2009. Influence of different plant species on water repellency in Mediterranean heathland soils. *CATENA*, **76**(3), 215-223.

Mataix-Solera, J., Arcenegui, V., Guerrero, C., Mayoral, A.M., Morales, J., González, J., García-Orenes, F., Gómez, I. 2007. Water repellency under different plant species in a calcareous forest soil in a semiarid Mediterranean environment. *Hydrological Processes*, **21**(17), 2300-2309.

Mataix-Solera, J., Doerr, S.H. 2004. Hydrophobicity and aggregate stability in calcareous topsoils from fire-affected pine forests in southeastern Spain. *Geoderma*, **118**(1–2), 77-88.

McArthur, W.M. 1991. *Reference soils of south-western Australia* Dept. of Agriculture, Western Australia on behalf of the Australian Society of Soil Science, Perth, W.A.

McCready, S., Slee, D., Birch, G., Taylor, S. 2000. The distribution of polycyclic aromatic hydrocarbons in surficial sediments of Sydney Harbour, Australia. *Marine Pollution Bulletin*, **40**(11), 999-1006.

McFarlane, D., Howell, M., Ryder, A., Orr, G. 1992. The effect of agricultural development on the physical and hydraulic properties of four Western Australian soils. *Australian Journal of Soil Research*, **30**(4), 517-532.

McGhie, D.A., Posner, A.M. 1981. The effect of plant top material on the water repellence of fired sands and water repellent soils. *Australian Journal of Agricultural Research*, **32**(4), 609-620.

McGhie, D.A., Posner, A.M. 1980. Water repellence of a heavy textured Western Australian surface soil. *Australian Journal of Soil Research*, **18**(3), 309-323.

McKissock, I., Gilkes, R., Harper, R., Carter, D. 1998. Relationships of water repellency to soil properties for different spatial scales of study. *Australian Journal of Soil Research*, **36**(3), 495-508.

McKissock, I., Gilkes, R., Van Bronswijk, W. 2003. The relationship of soil water repellency to aliphatic C and kaolin measured using DRIFT. *Australian Journal of Soil Research*, **41**(2), 251-265.

McKissock, I., Walker, E., Gilkes, R., Carter, D. 2000. The influence of clay type on reduction of water repellency by applied clays: a review of some West Australian work. *Journal of Hydrology*, **231**, 323-332.

Miller, J.D., Nalaskowski, J., Abdul, B., Du, H. 2007. Surface characteristics of kaolinite and other selected two layer silicate minerals. *The Canadian Journal of Chemical Engineering*, **85**(5), 617-624.

Moody, D.R., Schlossberg, M.J. 2010. Soil water repellency index prediction using the molarity of ethanol droplet test. *Vadose Zone Journal*, **9**(4), 1046-1051.

Moody, J.A., Ebel, B.A. 2012. Hyper-dry conditions provide new insights into the cause of extreme floods after wildfire. *CATENA*, **93**, 58-63.

Moore, G., Blackwell, P.S. 2004. Water Repellence. "Soil Guide' *Dept of Agriculture and Food, Western Australia Bulletin 4343. (Ed. G Moore); Department of Agriculture and Food, Perth, Western Australia.*, 53-94.

Moore, G.A. 2001. *Soilguide (Soil guide): a handbook for understanding and managing agricultural soils*. Department of Agriculture and Food, WA.

Moore, W. 1972. Physical Chemistry, 977 pp. *Prentic~ Hall, Englewood Cliffs, NJ*.

Morley, C.P., Mainwaring, K.A., Doerr, S.H., Douglas, P., Llewellyn, C.T., Dekker, L.W. 2005. Organic compounds at different depths in a sandy soil and their role in water repellency. *Australian Journal of Soil Research*, **43**(3), 239-249.

Muhr, J., Borken, W. 2009. Delayed recovery of soil respiration after wetting of dry soil further reduces C losses from a Norway spruce forest soil. *Journal of Geophysical Research: Biogeosciences (2005–2012)*, **114**(G4).

Murty, D., Kirschbaum, M.U.F., McMurtrie, R.E., McGilvray, H. 2002. Does conversion of forest to agricultural land change soil carbon and nitrogen? a review of the literature. *Global Change Biology*, **8**(2), 105-123.

Nalaskowski, J., Drelich, J., Hupka, J., Miller, J.D. 2003. Adhesion between hydrocarbon particles and silica surfaces with different degrees of hydration as determined by the AFM colloidal probe technique. *Langmuir*, **19**(13), 5311-5317.

Nyman, P., Smith, H.G., Sherwin, C.B., Langhans, C., Lane, P.N.J., Sheridan, G.J. 2015. Predicting sediment delivery from debris flows after wildfire. *Geomorphology*, **250**, 173-186.

Ogunwande, I.A., Olawore, N.O., Adeleke, K.A., Konig, W.A. 2003. Chemical composition of the essential oils from the leaves of three *Eucalyptus* species growing in Nigeria. *Journal of Essential Oil Research*, **15**(5), 297-301.

Owens, M.K., Lin, C.-D., Taylor, C.A., Whisenant, S.G. 1998. Seasonal patterns of plant flammability and monoterpenoid content in *Juniperus ashei*. *Journal of Chemical Ecology*, **24**(12), 2115-2129.

Pang, J., Wang, Y., Lambers, H., Tibbett, M., Siddique, K.H., Ryan, M.H. 2013. Commensalism in an agroecosystem: hydraulic redistribution by deep-rooted legumes improves survival of a droughted shallow-rooted legume companion. *Physiologia Plantarum*, **149**(1), 79-90.

Pate, J.S., Verboom, W.H. 2009. Contemporary biogenic formation of clay pavements by eucalypts: further support for the phytotarium concept. *Annals of Botany*, **103**(5), 673-685.

Pereira, S.I., Freire, C.S.R., Neto, C.P., Silvestre, A.J.D., Silva, A.M.S. 2005. Chemical composition of the epicuticular wax from the fruits of *Eucalyptus globulus*. *Phytochemical Analysis*, **16**(5), 364-369.

Petridis, L., Ambaye, H., Jagadamma, S., Kilbey, S.M., Lokitz, B.S., Lauter, V., Mayes, M.A. 2013. Spatial arrangement of organic compounds on a model mineral surface: implications for soil organic matter stabilization. *Environmental Science & Technology*, **48**(1), 79-84.

Pierson, F.B., Robichaud, P.R., Moffet, C.A., Spaeth, K.E., Williams, C.J., Hardegree, S.P., Clark, P.E. 2008. Soil water repellency and infiltration in coarse-textured soils of burned and unburned sagebrush ecosystems. *CATENA*, **74**(2), 98-108.

Plazzer, M.B., Henry, D.J., Yiapanis, G., Yarovsky, I. 2011. Comparative study of commonly used molecular dynamics force fields for modeling organic monolayers on water. *The Journal of Physical Chemistry B*, **115**(14), 3964-3971.

Prats, S.A., MacDonald, L.H., Monteiro, M., Ferreira, A.J.D., Coelho, C.O.A., Keizer, J.J. 2012. Effectiveness of forest residue mulching in reducing post-fire runoff and erosion in a pine and a eucalypt plantation in north-central Portugal. *Geoderma*, **191**(0), 115-124.

Prieto, I., Armas, C., Pugnaire, F.I. 2012. Water release through plant roots: new insights into its consequences at the plant and ecosystem level. *New Phytologist*, **193**(4), 830-841.

Prosser, I.P., Williams, L. 1998. The effect of wildfire on runoff and erosion in native *Eucalyptus* forest. *Hydrological Processes*, **12**(2), 251-265.

Rapparini, F., Baraldi, R., Facini, O. 2001. Seasonal variation of monoterpene emission from *Malus domestica* and *Prunus avium*. *Phytochemistry*, **57**(5), 681-687.

Rayment, G., Lyons, D. 2010. Soil chemical methods–Australasia. Australian soil and land survey handbooks series, CSIRO Publishing, Collingwood.

Ritsema, C.J., Dekker, L.W. 1994. How water moves in a water repellent sandy soil: 2. Dynamics of fingered flow. *Water Resources Research*, **30**(9), 2519-2531.

Roberts, F.J., Carbon, B.A. 1972. Water repellence in sandy soils of south-western Australia. II. Some chemical characteristics of the hydrophobic skins. *Australian Journal of Soil Research*, **10**(1), 35-42.

Rodríguez-Alleres, M., Benito, E. 2011. Spatial and temporal variability of surface water repellency in sandy loam soils of NW Spain under *Pinus pinaster* and *Eucalyptus globulus* plantations. *Hydrological Processes*, **25**(23), 3649-3658.

Roper, M.M. 2004. The isolation and characterisation of bacteria with the potential to degrade waxes that cause water repellency in sandy soils. *Australian Journal of Soil Research*, **42**, 427-434.

Roper, M.M. 2005. Managing soils to enhance the potential for bioremediation of water repellency. *Australian Journal of Soil Research*, **43**(7), 803-810.

Roper, M.M., Gupta, V.V.S.R. 2005. Enumeration of wax-degrading microorganisms in water repellent soils using a miniaturised most-probable-number method. *Australian Journal of Soil Research*, **43**, 171-177.

Rowell, D.L. 2014. *Soil science: Methods & applications*. Routledge, Long-man, Harlow. 350pp.

Roy, J.L., McGill, W.B. 2002. Assessing soil water repellency using the molarity of ethanol droplet (MED) test. *Soil Science*, **167**(2), 83-97.

Santos, J.M., Verheijen, F.G., Tavares Wahren, F., Wahren, A., Feger, K.H., Bernard-Jannin, L., Rial-Rivas, M.E., Keizer, J.J., Nunes, J.P. 2016. Soil water repellency dynamics in pine and eucalypt plantations in Portugal–a high-resolution time series. *Land Degradation & Development*, **27**(5), 1334-1343.

Savage, S. 1974. Mechanism of fire-induced water repellency in soil. *Soil Science Society of America Journal*, **38**(4), 652-657.

Savage, S., Osborn, J., Letey, J., Heaton, C. 1972. Substances contributing to fire-induced water repellency in soils. *Soil Science Society of America Journal*, **36**(4), 674-678.

Scott, D.F. 1993. The hydrological effects of fire in South African mountain catchments. *Journal of Hydrology*, **150**(2–4), 409-432.

Scott, D.F. 2000. Soil wettability in forested catchments in South Africa; as measured by different methods and as affected by vegetation cover and soil characteristics. *Journal of Hydrology*, **231–232**(0), 87-104.

Scott, D.F., Van Wyk, D.B. 1990. The effects of wildfire on soil wettability and hydrological behaviour of an afforested catchment. *Journal of Hydrology*, **121**(1–4), 239-256.

Senthil Nathan, S. 2007. The use of *Eucalyptus tereticornis* Sm. (Myrtaceae) oil (leaf extract) as a natural larvicidal agent against the malaria vector *Anopheles stephensi* Liston (Diptera: Culicidae). *Bioresource Technology*, **98**(9), 1856-1860.

Shakesby, R. 2011. Post-wildfire soil erosion in the Mediterranean: review and future research directions. *Earth-Science Reviews*, **105**(3), 71-100.

Shakesby, R.A., Boakes, D.J., Coelho, C.d.O.A., Gonçalves, A.J.B., Walsh, R.P.D. 1996. Limiting the soil degradational impacts of wildfire in pine and *Eucalyptus* forests in Portugal: A comparison of alternative post-fire management practices. *Applied Geography*, **16**(4), 337-355.

Shakesby, R.A., Chafer, C.J., Doerr, S.H., Blake, W.H., Wallbrink, P., Humphreys, G.S., Harrington, B.A. 2003. Fire severity, water repellency characteristics and hydrogeomorphological changes following the christmas 2001 Sydney forest fires. *Australian Geographer*, **34**(2), 147-175.

Shakesby, R.A., Wallbrink, P.J., Doerr, S.H., English, P.M., Chafer, C.J., Humphreys, G.S., Blake, W.H., Tomkins, K.M. 2007. Distinctiveness of wildfire effects on soil erosion in south-east Australian eucalypt forests assessed in a global context. *Forest Ecology and Management*, **238**(1–3), 347-364.

Shaw, D.J., Costello, B. 1993. Introduction to Colloid and Surface Chemistry: Butterworth-Heinemann, Oxford., Elsevier.

Shaw, L.A., Yiapanis, G., Henry, D.J., MacLaughlin, S., Evans, E., Yarovsky, I. 2013. Surface crosslinking effects on contamination resistance of functionalised polymers. *Soft Matter*, **9**(6), 1798-1806.

Sheridan, G.J., Lane, P.N.J., Noske, P.J. 2007. Quantification of hillslope runoff and erosion processes before and after wildfire in a wet *Eucalyptus* forest. *Journal of Hydrology*, **343**(1–2), 12-28.

Shevchenko, S.M., Bailey, G.W. 1998. Non-bonded organo-mineral interactions and sorption of organic compounds on soil surfaces: a model approach. *Journal of Molecular Structure: THEOCHEM*, **422**(1–3), 259-270.

Smith, R., Tanford, C. 1973. Hydrophobicity of long chain n-alkyl carboxylic acids, as measured by their distribution between heptane and aqueous solutions. *Proceedings of the National Academy of Sciences*, **70**(2), 289-293.

Soto, B., Díaz-Fierros, F. 1998. Runoff and soil erosion from areas of burnt scrub: comparison of experimental results with those predicted by the WEPP model. *Catena*, **31**(4), 257-270.

Sowerby, A., Emmett, B.A., Tietema, A., Beier, C. 2008. Contrasting effects of repeated summer drought on soil carbon efflux in hydric and mesic heathland soils. *Global Change Biology*, **14**(10), 2388-2404.

Spohn, M., Rillig, M.C. 2012. Temperature- and moisture-dependent soil water repellency induced by the basidiomycete *Agaricus bisporus*. *Pedobiologia*, **55**(1), 59-61.

Stoof, C.R., Moore, D., Ritsema, C.J., Dekker, L.W. 2011. Natural and fire-induced soil water repellency in a Portuguese shrubland. *Soil Science Society of America Journal*, **75**(6), 2283-2295.

Summers, R.N. 1987. The induction and severity of non-wetting in soils of the south coastal sandplain of Western Australia. *M Sc thesis, The University of Western Australia*, 130.

Sun, H. 1998. COMPASS: an ab initio force-field optimized for condensed-phase applications overview with details on alkane and benzene compounds. *The Journal of Physical Chemistry B*, **102**(38), 7338-7364.

Syphard, A.D., Radeloff, V.C., Hawbaker, T.J., Stewart, S.I. 2009. Conservation threats due to human-caused increases in fire frequency in Mediterranean-climate ecosystems. *Conservation Biology*, **23**(3), 758-769.

Takahashi, T., Kokubo, R., Sakaino, M. 2004. Antimicrobial activities of *Eucalyptus* leaf extracts and flavonoids from *Eucalyptus maculata*. *Letters in Applied Microbiology*, **39**(1), 60-64.

Tanford, C. 1980. *The Hydrophobic Effect: Formation of Micelles and Biological Membranes 2d Ed*. J. Wiley.

Teppen, B.J., Yu, C.-H., Miller, D.M., Schäfer, L. 1998. Molecular dynamics simulations of sorption of organic compounds at the clay mineral/aqueous solution interface. *Journal of Computational Chemistry*, **19**(2), 144-153.

Terry, J.P., Shakesby, R.A. 1993. Soil hydrophobicity effects on rainsplash: simulated rainfall and photographic evidence. *Earth Surface Processes and Landforms*, **18**(6), 519-525.

Tieu, A., Plummer, J.A., Dixon, K.A., Sivasithamparam, K., Sieler, I.M. 1999. Germination of four species of native Western Australian plants using plant-derived smoke. *Australian Journal of Botany*, **47**(2), 207-219.

Tschapek, M. 1984. Criteria for determining the hydrophilicity-hydrophobicity of soils. *Zeitschrift für Pflanzenernährung und Bodenkunde*, **147**(2), 137-149.

Tulloch, A. 1976. Chemistry of waxes of higher plants. in: *Chemistry and biochemistry of natural waxes*, Elsevier, pp. 235-287.

Tunega, D., Gerzabek, M.H., Lischka, H. 2004. Ab initio molecular dynamics study of a monomolecular water layer on octahedral and tetrahedral kaolinite surfaces. *The Journal of Physical Chemistry B*, **108**(19), 5930-5936.

Uddin, S.M.M., Daniel, N.R.R., Harper, R.J., Henry, D.J. 2017. Why do biogenic volatile organic compounds (BVOCs) derived from vegetation fire not induce soil water repellency? *Biogeochemistry*, **134**(1), 147-161.

Van Gool, D., Vernon, L., Runge, W. 2008. Land resources in the south-west agricultural region: a shire-based summary of land degradation and land capability. *Resource Management Technical Report*, **330**.

Walden, L.L., Harper, R.J., Mendham, D.S., Henry, D.J., Fontaine, J.B. 2015. Eucalyptus reforestation induces soil water repellency. *Soil Research*, **53**(2), 168-177.

Wallis, M.G., Horne, D.J. 1992. Soil Water Repellency. in: *Advances in Soil Science*, (Ed.) B.A. Stewart, Vol. 20, Springer New York, pp. 91-146.

Ward, P., Oades, J. 1993. Effect of clay mineralogy and exchangeable cations on water repellency in clay-amended sandy soils. *Australian Journal of Soil Research*, **31**(3), 351-364.

Watson, C.L., Letey, J. 1970. Indices for characterizing soil water repellency based upon contact angle-surface tension relationships. *Soil Science Society of America Journal*, **34**(6), 841-844.

Wershaw, R.L. 1989. Application of a membrane model to the sorptive interactions of humic substances. *Environmental Health Perspectives*, **83**, 191.

Wershaw, R.L. 1986. A new model for humic materials and their interactions with hydrophobic organic chemicals in soil-water or sediment-water systems. *Journal of Contaminant Hydrology*, **1**(1–2), 29-45.

Wesseling, J., Stoof, C., Ritsema, C., Oostindie, K., Dekker, L. 2009. The effect of soil texture and organic amendment on the hydrological behaviour of coarse-textured soils. *Soil Use and Management*, **25**(3), 274-283.

Woudt, B.D.v.t. 1959. Particle coatings affecting the wettability of soils. *Journal of Geophysical Research*, **64**(2), 263-267.

Wu, G., He, L., Chen, D. 2013. Sorption and distribution of asphaltene, resin, aromatic and saturate fractions of heavy crude oil on quartz surface: Molecular dynamic simulation. *Chemosphere*, **92**(11), 1465-1471.

Yang, B., Blackwell, P.S., Nicholson, D.F. 1996. A numerical model of heat and water movement in furrow-sown water repellent sandy soils. *Water Resources Research*, **32**(10), 3051-3061.

Yin, X., Gupta, V., Du, H., Wang, X., Miller, J.D. 2012. Surface charge and wetting characteristics of layered silicate minerals. *Advances in Colloid and Interface Science*, **179–182**, 43-50.

Yu, C.-H., Newton, S.Q., Norman, M.A., Schäfer, L., Miller, D.M. 2003. Molecular dynamics simulations of adsorption of organic compounds at the clay mineral/aqueous solution interface. *Structural Chemistry*, **14**(2), 175-185.

Zavala, L.M., González, F.A., Jordán, A. 2009a. Fire-induced soil water repellency under different vegetation types along the Atlantic dune coast-line in SW Spain. *CATENA*, **79**(2), 153-162.

Zavala, L.M., González, F.A., Jordán, A. 2009b. Intensity and persistence of water repellency in relation to vegetation types and soil parameters in Mediterranean SW Spain. *Geoderma*, **152**(3–4), 361-374.

Zhou, Q.Y., Shimada, J., Sato, A. 2002. Temporal variations of the three-dimensional rainfall infiltration process in heterogeneous soil. *Water Resources Research*, **38**(4), 1-1-1-15.

Zhuravlev, L. 2000. The surface chemistry of amorphous silica. Zhuravlev model. *Colloids and Surfaces A: Physicochemical and Engineering Aspects*, **173**(1), 1-38.

Zini, C.A., Augusto, F., Christensen, E., Smith, B.P., Caramão, E.B., Pawliszyn, J. 2001. Monitoring biogenic volatile compounds emitted by *Eucalyptus citriodora* using SPME. *Analytical Chemistry*, **73**(19), 4729-4735.

Zisman, W.A. 1964. Relation of the equilibrium contact angle to liquid and solid constitution. In: Gould, R. F. (Ed.), Contact Angle, Wettability, and Adhesion. American Chemical Society. Advances in Chemistry Series, Vol. 43. pp-1-51.

9 Appendix

CHAPTER 1 No tables and figures

CHAPTER 2

AT (Appendix Table) 2.1 Compounds extracted from soil using DCM/MeOH (2:1) solvents (colour codes indicate the concentration level ≥ 0.001 g/kg)

Class	Peak #	Formula	Assignment	Species			
				BM	EM	XP	AF
carbox. acids	5	$C_8H_{16}O_2$	Octanoic Acid		grey		
	15	$C_{10}H_{20}O_2$	n-Decanoic acid		grey		
	38	$C_{15}H_{30}O_2$	Pentadecanoic acid	grey			blue
	48	$C_{20}H_{40}O_2$	Eicosanoic acid	blue			
	69	$C_{22}H_{44}O_2$	Docosanoic acid	blue	blue	blue	
	72	$C_{24}H_{48}O_2$	Tetracosanoic acid			blue	
	74	$C_{26}H_{52}O_2$	Hexacosanoic acid	blue	blue	blue	
alcohols	10	$C_{10}H_{16}O$	1,5-Cyclohexadiene-1-methanol, 4-(1-methylethyl)-				grey
	13	$C_{10}H_{14}O$	Benzenemethanol, 4-(1-methylethyl)-	grey		grey	
	27	$C_{15}H_{26}O$	2-Naphthalenemethanol, decahydro	grey			
	36	$C_{15}H_{26}O$	2-Naphthalenemethanol, 2,3,4,4a,5,6,7,8-octahydro	grey			
	37	$C_{20}H_{40}O$	3,7,11,15-Tetramethyl-2-hexadecen-1-ol	grey	grey		grey
	43	$C_{16}H_{34}O$	1-hexadecanol	grey	blue	blue	
	49	$C_{22}H_{46}O$	1-Docosanol	blue	blue	blue	
	60	$C_{27}H_{56}O$	1-Heptacosanol				
alkane	44	$C_{24}H_{50}$	Tetracosane	grey	grey	grey	blue
	56	$C_{28}H_{58}$	Octacosane	blue	blue	grey	blue
	64	$C_{34}H_{70}$	Tertratriacontane	blue	blue	blue	
	67	$C_{36}H_{74}$	Hexatriacontane		blue	blue	blue
	75	$C_{44}H_{90}$	Tetratetracontane	blue	grey	blue	

Class	No.	Formula	Compound name	S1	S2	S3	S4
esters	6	$C_8H_8O_3$	Benzoic acid, 2-hydroxy-, methyl ester			gray	
	35	$C_{17}H_{34}O_2$	Isopropyl Myristate	gray	blue		blue
	40	$C_{21}H_{42}O_2$	Eicosanoic acid, methyl ester	gray	gray		
	42	$C_{17}H_{34}O_2$	Hexadecanoic acid, methyl ester		gray	blue	gray
	45	$C_{19}H_{38}O_2$	Isopropyl Palmitate	gray	gray	gray	
	46	$C_{16}H_{30}O_2$	Myristic acid vinyl ester	gray			
	52	$C_{21}H_{42}O_2$	Isopropyl stearate	blue	blue	gray	
	53	$C_{21}H_{40}O_2$	Elaidic acid, isopropyl ester	blue		gray	blue
	55	$C_{21}H_{42}O_2$	Hexanoic acid, pentadecyl ester		gray		
	63	$C_{17}H_{28}O_2$	Nerolidyl acetate	gray		blue	
	65	$C_{23}H_{46}O_2$	Docosanoic acid, methyl ester	gray		blue	gray
	66	$C_{24}H_{38}O_4$	1,2-Benzenedicarboxylic acid, diisooctyl ester		gray	gray	gray
	70	$C_{25}H_{50}O_2$	Tetracosanoic acid, methyl ester		gray		
	71	$C_{27}H_{54}O_2$	Hexacosanoic acid, methyl ester	gray		gray	
	77	$C_{28}H_{56}O_2$	Heptacosanoic acid, methyl ester	gray	blue		blue
	89	$C_{35}H_{62}O_3$	Benzenepropanoic acid, octadecyl ester	gray	gray	gray	gray
	90	$C_{31}H_{50}O_3$	Urs-12-en-28-oic acid, methyl ester		gray	gray	
amides	3	$C_6H_{13}NO$	Hexanamide	gray		gray	
	9	$C_7H_{15}NO$	Enanthamide	gray	gray	gray	
	16	C_7H_7NO	Benzamide				gray
	17	C_8H_9NO	Benzeneacetamide		gray	gray	gray
	33	$C_{12}H_{25}NO$	Dodecanamide	gray			
	47	$C_{14}H_{29}NO$	Tetradecanamide	blue		blue	gray
	51	$C_{16}H_{33}NO$	Hexadecanamide		blue	gray	blue
	54	$C_{18}H_{37}NO$	Octadecanamide		blue		blue
	62	$C_{18}H_{35}NO$	9-Octadecenamide, (Z)-		gray	gray	gray
	68	$C_{22}H_{43}NO$	13-Docosenamide, (Z)-	blue			blue
aldehyde	8	$C_{10}H_{12}O$	Benzaldehyde, 4-(1-methylethyl)-			gray	gray
ketone	24	$C_{12}H_{14}O_3$	4-Hydroxy-9-vinyladamantane-2,6-dione	gray			
	32	$C_{13}H_{22}O$	2-Butanone, 4-(2,6,6-trimethyl-1-cyclohexen-1-yl)-	gray	gray	gray	
	39	$C_{19}H_{38}O$	2-Nonadecanone			gray	gray
	41	$C_{18}H_{30}O$	5,9,13-Pentadecatrien-2-one, 6,10,14-trimethyl-,	gray	gray		
	57	$C_{18}H_{36}O$	2-Pentadecanone, 6,10,14-trimethyl-	blue			blue
	76	$C_{25}H_{50}O$	2-Pentacosanone	gray			gray
	78	$C_{27}H_{54}O$	2-Heptacosanone		gray		
pyranone	59	$C_{18}H_{34}O_2$	2H-Pyran-2-one, tetrahydro-6-tridecyl-	gray			
glyceride	2	$C_3H_8O_3$	Glycerin	gray	gray		
alkene	26	$C_{20}H_{40}$	9-Eicosene, (E)-			gray	gray

	No.	Formula	Name				
terpenoids	1	$C_{10}H_{14}$	Benzene, 1-methyl-2-(1-methylethyl)-		■		
	11	$C_{10}H_{16}O$	2-Caren-10-al		■	■	
	12	$C_{10}H_{14}O$	Phenol, 2-methyl-5-(1-methylethyl)-				■
	18	$C_{15}H_{24}$	.alpha.-Cubebene			■	■
	19	$C_{15}H_{24}$	(+)-Epi-bicyclosesquiphellandrene	■		■	■
	20	$C_{15}H_{22}$	Aromadendrene, dehydro-	■			
	22	$C_{15}H_{22}$	Cadala-1(10),3,8-triene		■	■	
	23	$C_{15}H_{24}$	Naphthalene, 1,2,3,4,4a,5,6,8a-octahydro-	■			
	25	$C_{15}H_{24}$	Caryophyllene	■	■		
	73	$C_{30}H_{50}$	Squalene			■	■
epoxide	29	$C_{15}H_{24}O$	cis-Z-.alpha.-Bisabolene epoxide	■		■	
	30	$C_{15}H_{24}O$	Aromadendrene oxide-(2)	■		■	
	31	$C_{15}H_{24}O$	Caryophyllene oxide	■	■	■	■
Ring cont. comps.	7	C_8H_8O	Benzofuran, 2,3-dihydro-			■	
	21	$C_{26}H_{52}$	Cyclopentane, heneicosyl-	■			
	28	$C_{15}H_{18}$	Naphthalene, 1,6-dimethyl-4-(1-methylethyl)-	■	■	■	■
	50	$C_{16}H_{30}O_2$	2(3H)-Furanone, 5-dodecyldihydro-		■		
	58	$C_{26}H_{52}$	Eicosane, 2-cyclohexyl-	■	▣	■	
	81	$C_{28}H_{48}O_2$	.gamma.-Tocopherol	■			
steroids	79	$C_{31}H_{50}O_2$	Stigmasta-5,22-dien-3-ol, acetate,	■			
	80	$C_{27}H_{44}O$	Cholesta-4,6-dien-3-ol, (3.beta.)-	■	■		
	82	$C_{31}H_{52}O_2$	.beta.-Sitosterol acetate	■	▣	■	■
	83	$C_{28}H_{46}O$	Ergosta-5,7-dien-3-ol, (3.beta.)-	■		■	■
	84	$C_{30}H_{52}O$	Lupeol	▣		▣	▣
	85	$C_{27}H_{42}O$	Cholesta-3,5-dien-7-one				■
	86	$C_{27}H_{42}O$	Cholesta-4,6-dien-3-one	■	▣		▣
	87	$C_{29}H_{48}O$	Stigmast-4-en-3-one	▣	■		
	88	$C_{32}H_{54}O_2$	9,19-Cyclolanostan-3-ol, acetate, (3.beta.)-	■			
unknown	14		Unknown			■	
	34		unknown				■
	61		unknown	▣	▣	▣	▣

AT 2.2 Compounds extracted from canopy derived exudates using nonpolar solvents

Class	Peak #	Formula	Assignment	Species			
				BM	EM	XP	AF
alkane	27	$C_{25}H_{52}$	Pentacosane	■	■	■	■
	33	$C_{29}H_{60}$	Nonacosane	■	■	■	■
	34	$C_{35}H_{72}$	Pentatriacontane	■	■	■	
	35	$C_{37}H_{76}$	Heptatriacontane	■	■	■	■
	37	$C_{55}H_{112}$	Pentapentacontane	■	■	■	
alkene	15	$C_{20}H_{40}$	9-Eicosene, (E)-			■	■
epoxide	20	$C_{15}H_{24}O$	cis-Z-.alpha.-Bisabolene epoxide	■		■	■
	21	$C_{15}H_{24}O$	Aromadendrene oxide-(2)	■		■	
	22	$C_{15}H_{24}O$	Caryophyllene oxide	■	■	■	■
lcohol	5	$C_{10}H_{18}O_2$	Bicyclo(3.1.1)heptane-2,3-diol			■	
	16	$C_{15}H_{24}O$	1H-Cycloprop[e]azulen-7-ol			■	
	17	$C_{15}H_{26}O$	2-Naphthalenemethanol, decahydro-			■	
	24	$C_{20}H_{40}O$	3,7,11,15-Tetramethyl-2-hexadecen-1-ol	■			■
ketone	13	$C_{12}H_{14}O_3$	4-Hydroxy-9-vinyladamantane-2,6-dione			■	
	23	$C_{13}H_{22}O$	2-Butanone	■	■	■	
	25	$C_{19}H_{38}O$	2-Nonadecanone			■	■
	26	$C_{18}H_{30}O$	5,9,13-Pentadecatrien-2-one	■			
	38	$C_{25}H_{50}O$	2-Pentacosanone	■			■
	39	$C_{27}H_{54}O$	2-Heptacosanone		■		
steroids	41	$C_{27}H_{42}O$	Cholesta-4,6-dien-3-one	■			■
	42	$C_{29}H_{48}O$	Stigmast-4-en-3-one		■		
triglyceride	2	$C_3H_8O_3$	Glycerine	■			
pyranone	30	$C_{18}H_{34}O_2$	2H-Pyran-2-one, tetrahydro-6-tridecyl	■		■	
amide	32	$C_{18}H_{35}NO$	9-Octadecenamide (Z)-		■		
Ring contain. compounds	10	$C_{26}H_{52}$	Cyclopentane, heneicosyl-	■	■		
	19	$C_{15}H_{18}$	Naphthalene, 1,6-dimethyl-4-	■	■		■
	28	$C_{16}H_{30}O_2$	2(3H)-Furanone				
	29	$C_{26}H_{52}$	Eicosane, 2-cyclohexyl-	■	■	■	■
	40	$C_{29}H_{48}O$	A'-Neogammacer-22(29)-ene			■	
phenol	4	$C_{10}H_{14}O$	Benzenemethanol, 4-(1-methylethyl)-	■			
aldehyde	18	$C_{10}H_{16}O$	3-Cyclopentene-1-acetaldehyde				■
unknown	31		unknown	■	■	■	■

terpenoids	1	$C_{10}H_{14}$	p-Cimene		▓		
	6	$C_{10}H_{16}O_2$	2-Cyclohexen-1-one			▓	
	7	$C_{15}H_{24}$	alpha-Cubebene			▓	▓
	8	$C_{15}H_{24}$	epi-bicyclosesquiphellandrene	▓		▓	▓
	9	$C_{15}H_{22}$	Aromadendrene, dehydro-	▓		▓	
	11	$C_{15}H_{22}$	Cadala-1(10),3,8-triene		▓	▓	
	12	$C_{15}H_{24}$	α-Selinene	▓		▓	▓
	14	$C_{15}H_{24}$	Caryophyllene	▓	▓		
	36	$C_{30}H_{50}$	Squalene			▓	

Class	Peak #	Formula	Assignment	BM	EM	XP	AF
carbox. acids	2	$C_8H_{16}O_2$	Octanoic acid		■		
	12	$C_{10}H_{20}O_2$	n-Decanoic acid		■		
	20	$C_{15}H_{30}O_2$	Pentadecanoic acid	■			■
	27	$C_{20}H_{40}O_2$	Eicosanoic acid	■			■
	40	$C_{22}H_{44}O_2$	Docosanoic acid	■	■	■	■
	43	$C_{24}H_{48}O_2$	Tetracosanoic acid			■	
	44	$C_{26}H_{52}O_2$	Hexacosanoic acid		■	■	
alcohols	19	$C_{15}H_{26}O$	2-Naphthalenemethanol, 2,3,4,4a,5,6,7,8-octahydro-	■		■	■
	23	$C_{16}H_{34}O$	1-hexadecanol	■	■		
	28	$C_{22}H_{46}O$	1-Docosanol	■		■	
	34	$C_{27}H_{56}O$	1-Heptacosanol		■	■	
esters	3	$C_8H_8O_3$	Benzoic acid, 2-hydroxy-, methyl ester			■	
	18	$C_{17}H_{34}O_2$	Isopropyl myristate	■	■		■
	21	$C_{21}H_{42}O_2$	Eicosanoic acid, methyl ester	■			
	22	$C_{17}H_{34}O_2$	Methyl hexadecanoate		■	■	■
	24	$C_{19}H_{38}O_2$	Isopropyl palmitate	■	■		
	25	$C_{16}H_{30}O_2$	Myristic acid vinyl ester	■			
	30	$C_{21}H_{42}O_2$	Isopropyl stearate	■	■	■	■
	31	$C_{21}H_{40}O_2$	Elaidic acid, isopropyl ester	■			
	38	$C_{23}H_{46}O_2$	Docosanoic acid, methyl ester	■	■		
	41	$C_{25}H_{50}O_2$	Tetracosanoic acid, methyl ester		■		
	42	$C_{27}H_{54}O_2$	Hexacosanoic acid, methyl ester	■		■	
	45	$C_{28}H_{56}O_2$	Heptacosanoic acid, methyl ester		■		■
	50	$C_{35}H_{62}O_3$	Benzenepropanoic acid, octadecyl ester			■	■
	51	$C_{31}H_{50}O_3$	aUrs-12-en-28-oic acid, 3-hydroxy-, methyl ester		■	■	■
	37	$C_{17}H_{28}O_2$	Nerolidyl acetate			■	
amides	1	$C_6H_{13}NO$	Hexanamide			■	
	6	$C_7H_{15}NO$	Enanthamide	■	■		
	13	C_8H_9NO	Benzeneacetamide			■	
	16	$C_{12}H_{25}NO$	Dodecanamide	■			
	26	$C_{14}H_{29}NO$	Tetradecanamide	■		■	■
	29	$C_{16}H_{33}NO$	Hexadecanamide		■	■	
	32	$C_{18}H_{37}NO$	Octadecanamide		■		
	36	$C_{18}H_{35}NO$	9-Octadecenamide, (Z)-		■	■	
	39	$C_{22}H_{43}NO$	13-Docosenamide	■			
Steroids	46	$C_{27}H_{44}O$	Cholesta-4,6-dien-3-ol, (3.beta.)-		■		
	47	$C_{31}H_{52}O_2$	.beta.-Sitosterol acetate	■	■	■	■
	48	$C_{28}H_{46}O$	Ergosta-5,7-dien-3-ol, (3.beta.)-	■		■	
	49	$C_{30}H_{52}O$	Lupeol	■			
Ketone	33	$C_{18}H_{36}O$	2-Pentadecanone, 6,10,14-trimethyl-	■			■

|							
aldehyde	5	$C_{10}H_{12}O$	Benzaldehyde, 4-(1-methylethyl)-			■	■
unknown	10		unknown			■	
	17		unknown	■	■	■	■
	35		unknown			■	
terpenoids	7	$C_{10}H_{16}O$	2-Caren-10-al		■	■	
	8	$C_{10}H_{14}O$	p-Cymene-2-ol				■
	9	$C_{10}H_{14}O$	Cuminol; p-Cymen-7-ol		■	■	
	14	$C_{15}H_{24}$	.alpha.-Cubebene			■	
phenol	11	$C_9H_{10}O_2$	2-Methoxy-4-vinylphenol			■	
ring con. comp.	4	C_8H_8O	Benzofuran, 2,3-dihydro-			■	

AT 3.1 Compounds extracted from soil using DCM/MeOH (2:1) solvents (coloured shades indicate the concentration level ≥ 0.001 g/kg)

Class	Peak #	Formula	Assignment	Species EM	EW	BM	AF
carbox. acids	6	$C_8H_{16}O_2$	Octanoic acid	grey			
	48	$C_{15}H_{30}O_2$	Pentadecanoic acid			grey	
	58	$C_{20}H_{40}O_2$	Eicosanoic acid		grey		
	61	$C_{18}H_{34}O_2$	Oleic acid		blue		
	80	$C_{22}H_{44}O_2$	Docosanoic acid	grey	grey		
	83	$C_{24}H_{48}O_2$	Tetracosanoic acid			grey	
	85	$C_{26}H_{52}O_2$	Hexacosanoic acid	blue	blue	blue	
alcohols	9	$C_{10}H_{22}O_2$	3,7-Dimethyl-1,7-octanediol	grey			
	11	$C_{10}H_{16}O$	1,5-Cyclohexadiene-1-methanol	grey			grey
	16	$C_{10}H_{14}O$	Benzenemethanol, 4-(1-methylethyl)-	blue			
	17	$C_{10}H_{18}O_2$	Bicyclo(3.1.1)heptane-2,3-diol,	grey			
	30	$C_{15}H_{26}O$	Epiglobulol		blue		
	34	$C_{10}H_{18}O$	3,3,6-Trimethyl-1,4-heptadien-6-ol		blue		
	36	$C_{15}H_{24}O$	Spathulenol	grey			
	37	$C_{15}H_{26}O$	2-Naphthalenemethanol, decahydro-			grey	
	46	$C_{15}H_{26}O$	2-Naphthalenemethanol, 2,3,4,4a,5,6,7,8-octahydro-				grey
	47	$C_{20}H_{40}O$	3,7,11,15-Tetramethyl-2-hexadecen-1-ol			grey	
	53	$C_{16}H_{34}O$	1-Hexadecanol		blue		
	59	$C_{22}H_{46}O$	1-Docosanol		blue	blue	
esters	7	$C_8H_8O_3$	Benzoic acid, 2-hydroxy-, methyl ester		grey		
	44	$C_{17}H_{34}O_2$	Isopropyl myristate	grey	blue		grey
	50	$C_{21}H_{42}O_2$	Eicosanoic acid, methyl ester			grey	
	52	$C_{17}H_{34}O_2$	Hexadecanoic acid, methyl ester	grey			grey
	55	$C_{19}H_{38}O_2$	Isopropyl palmitate	grey	blue	blue	
	56	$C_{16}H_{30}O_2$	Myristic acid vinyl ester				
	62	$C_{21}H_{42}O_2$	Isopropyl stearate	blue	blue	blue	blue
	63	$C_{21}H_{40}O_2$	Elaidic acid, isopropyl ester		blue		
	66	$C_{21}H_{42}O_2$	Hexanoic acid, pentadecyl ester	blue			
	73	$C_{17}H_{28}O_2$	Nerolidyl acetate			grey	
	76	$C_{23}H_{46}O_2$	Docosanoic acid, methyl ester	grey	grey	grey	grey
	77	$C_{24}H_{38}O_4$	1,2-Benzenedicarboxylic acid, diisooctyl ester	blue	blue		
	81	$C_{25}H_{50}O_2$	Tetracosanoic acid, methyl ester	grey			
	82	$C_{27}H_{54}O_2$	Hexacosanoic acid, methyl ester			grey	
	88	$C_{28}H_{56}O_2$	Heptacosanoic acid, methyl ester			blue	grey
	104	$C_{35}H_{62}O_3$	Benzenepropanoic acid, octadecyl ester	blue	blue	blue	grey

Class	No	Formula	Compound	1	2	3	4
steroids	90	$C_{31}H_{50}O_2$	Stigmasta-5,22-dien-3-ol, acetate,			G	
	91	$C_{27}H_{44}O$	Cholesta-4,6-dien-3-ol, (3.beta.)-	B	B	B	
	94	$C_{31}H_{52}O_2$	.beta.-Sitosterol acetate	B	G	B	G
	95	$C_{28}H_{46}O$	Ergosta-5,7-dien-3-ol, (3.beta.)-			G	
	98	$C_{30}H_{52}O$	Lupeol		B	B	B
	99	$C_{27}H_{42}O$	Cholesta-3,5-dien-7-one		B	B	
	100	$C_{32}H_{52}O_2$	9,19-Cyclolanost-24-en-3-ol, acetate,			B	
	101	$C_{27}H_{42}O$	Cholesta-4,6-dien-3-one	B	B	B	
	102	$C_{29}H_{48}O$	Stigmast-4-en-3-one			B	G
	103	$C_{32}H_{54}O_2$	9,19-Cyclolanostan-3-ol, acetate,			B	
ring contain. comps.	69	$C_{26}H_{52}$	Cyclohexane, eicosyl-		B		
	92	$C_{28}H_{48}O_2$	.gamma.-Tocopherol			G	G
	97	$C_{30}H_{50}$	A'-Neogammacer-22(29)-ene			B	G
alkanes	5	$C_{12}H_{32}$	Dodecane	B	B	B	B
	54	$C_{24}H_{50}$	Tetracosane		B	G	B
	67	$C_{28}H_{58}$	Octacosane	G	B	B	G
	74	$C_{29}H_{60}$	Nonacosane				B
	75	$C_{34}H_{70}$	Tetratriacontane	G	G	B	B
	78	$C_{36}H_{74}$	Hexatriacontane		G		
	86	$C_{44}H_{90}$	Tetratetracontane	B	B	G	G
alkene	35	$C_{20}H_{40}$	9-Eicosene, (E)-		B		
terpenoids	1	$C_{10}H_{14}$	Benzene, 1-methyl-2-(1-methylethyl)-	B			G
	12	$C_{10}H_{16}O$	1-Cyclohexene-1-carboxaldehyde, 4-(1-methylethyl)-	G			
	14	$C_{10}H_{16}O$	2-Caren-10-al	G			
	15	$C_{10}H_{14}O$	Phenol, 2-methyl-5-(1-methylethyl)-				G
	20	$C_{15}H_{24}$	ß-Gurjunene		G		
	21	$C_{10}H_{16}O_2$	2-Cyclohexen-1-one,	G			
	22	$C_{15}H_{24}$	.alpha.-Cubebene		G	G	
	24	$C_{15}H_{24}$	Epi-bicyclosesquiphellandrene			B	
	28	$C_{15}H_{22}$	Aromadendrene, dehydro-			G	
	31	$C_{15}H_{22}$	Cadala-1(10),3,8-triene				G
	32	$C_{15}H_{24}O$	Spathulenol		B		
	84	$C_{30}H_{50}$	Squalene		G	B	G
	96	$C_{30}H_{50}O$	Lanosterol			B	
ketones	33	$C_{12}H_{14}O_3$	4-Hydroxy-9-vinyladamantane-2,6-dione			B	
	41	$C_{13}H_{22}O$	2-Butanone, 4-(2,6,6-trimethyl-1-cyclohexen-1-yl)-				G
	49	$C_{19}H_{38}O$	2-Nonadecanone			G	
	51	$C_{18}H_{30}O$	5,9,13-Pentadecatrien-2-one, 6,10,14-trimethyl-,		G		
	68	$C_{18}H_{36}O$	2-Pentadecanone, 6,10,14-trimethyl-		B	B	G
	87	$C_{25}H_{50}O$	2-Pentacosanone	G			
	89	$C_{27}H_{54}O$	2-Heptacosanone	G			
	93	$C_{19}H_{38}O$	10-Nonadecanone				G

| Category	No.	Formula	Compound	S1	S2	S3	S4
amides	4	$C_6H_{13}NO$	Hexanamide		blue		
	10	$C_7H_{15}NO$	Enanthamide	gray	gray	gray	
	18	C_7H_7NO	Benzamide				gray
	19	C_8H_9NO	Benzeneacetamide				gray
	29	$C_9H_{11}NO$	Phenylpropanamide			blue	
	42	$C_{12}H_{25}NO$	Dodecanamide		blue	gray	gray
	57	$C_{14}H_{29}NO$	Tetradecanamide				blue
	60	$C_{16}H_{33}NO$	Hexadecanamide	gray		gray	blue
	65	$C_{18}H_{37}NO$	Octadecanamide	blue	blue		blue
	72	$C_{18}H_{35}NO$	9-Octadecenamide		blue	blue	
	79	$C_{22}H_{43}NO$	13-Docosenamide				blue
aldehyde	8	$C_{10}H_{12}O$	Benzaldehyde, 4-(1-methylethyl)-				gray
triglyceride	2	$C_3 H_8 O_3$	Glycerine	blue	gray	gray	blue
unknown	3		unknown	gray			
	13		unknown		gray		
	43		unknown			gray	
	45		unknown		blue		
	64		unknown	gray			
	71		unknown	gray			gray
phenols	23	$C_8H_{10}O_2$	Benzeneethanol, 4-hydroxy-(Tyrosol)			blue	
	25	$C_9H_{10}O_3$	Ethanone, 1-(4-hydroxy-3-methoxyphenyl)-	gray			
	26	$C_{14}H_{22}O$	Phenol, 2,4-bis(1,1-dimethylethyl)-		gray		gray
	27	$C_8H_{10}O_3$	Phenol, 3,5-dimethoxy-			gray	
epoxide	38	$C_{15}H_{24}O$	Aromadendrene oxide-(2)			gray	
	39	$C_{15}H_{24}O$	Caryophyllene oxide		blue		
	40	$C_{15}H_{24}O$	Isoaromadendrene epoxide	gray	gray		
pyranone	70	$C_{18}H_{34}O_2$	2H-Pyran-2-one, tetrahydro-6-tridecyl-				blue
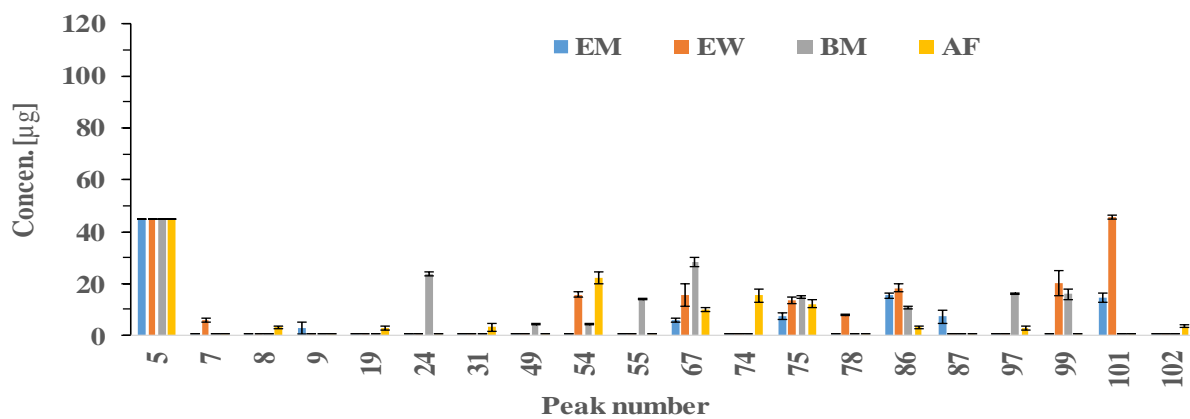
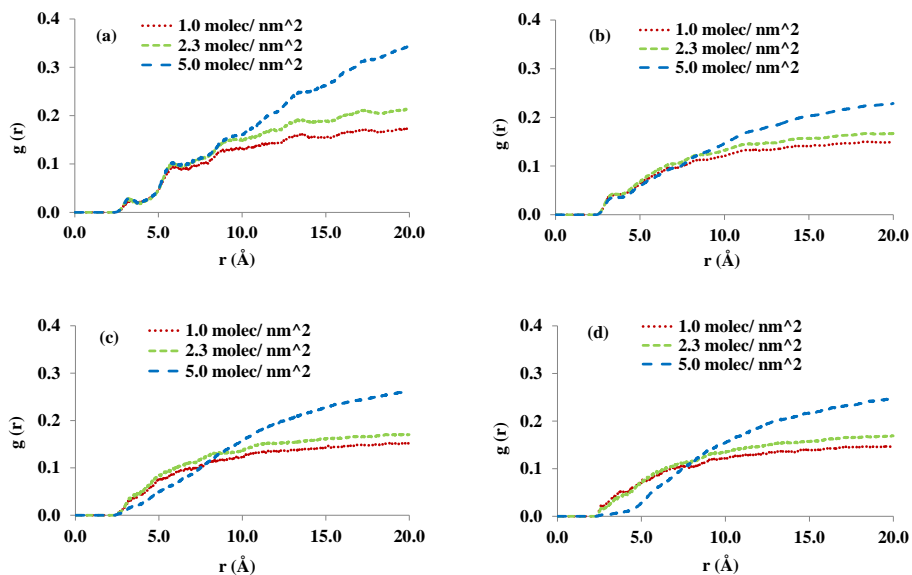AF (Appendix Figure) 3.1 Residual compounds after washing the winnowed coarse materials

CHAPTER 4
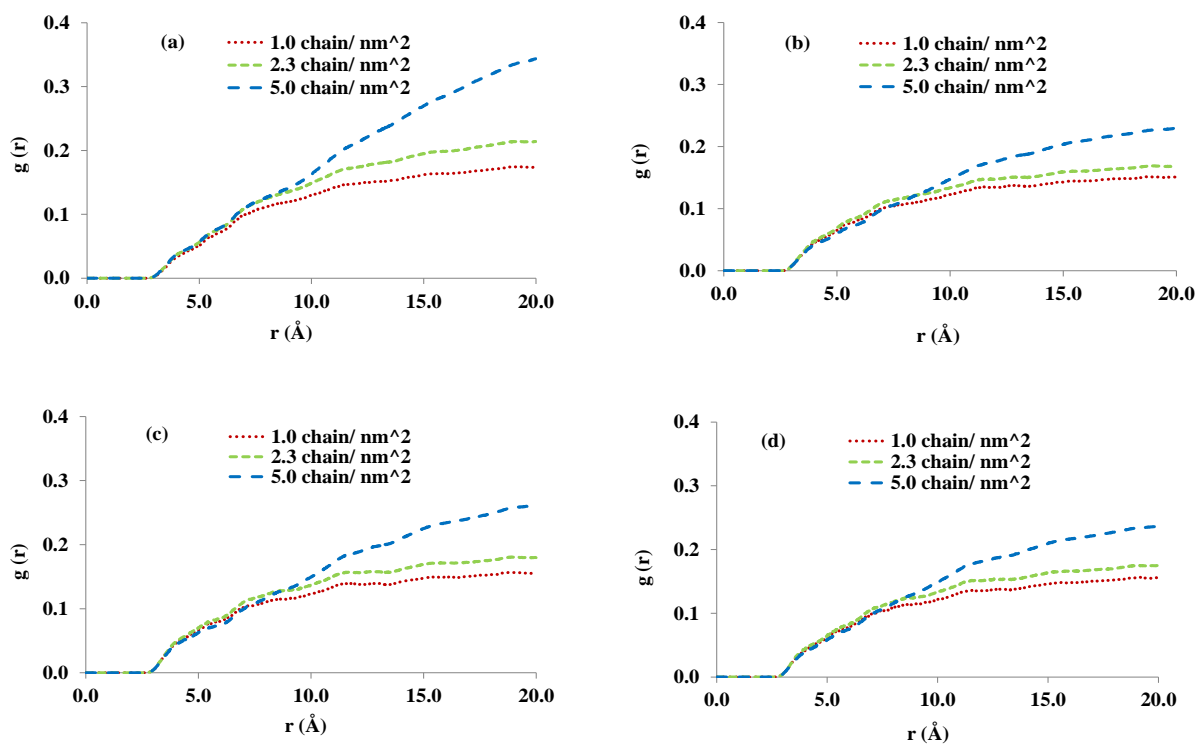
AF 4.1 C^{molec}-O^{surf} RDFs in a) cineole, b) levoglocosenone, c) cis-3-hexen-1-ol and d) 2-methyl-3-buten-2-ol/quartz systems.
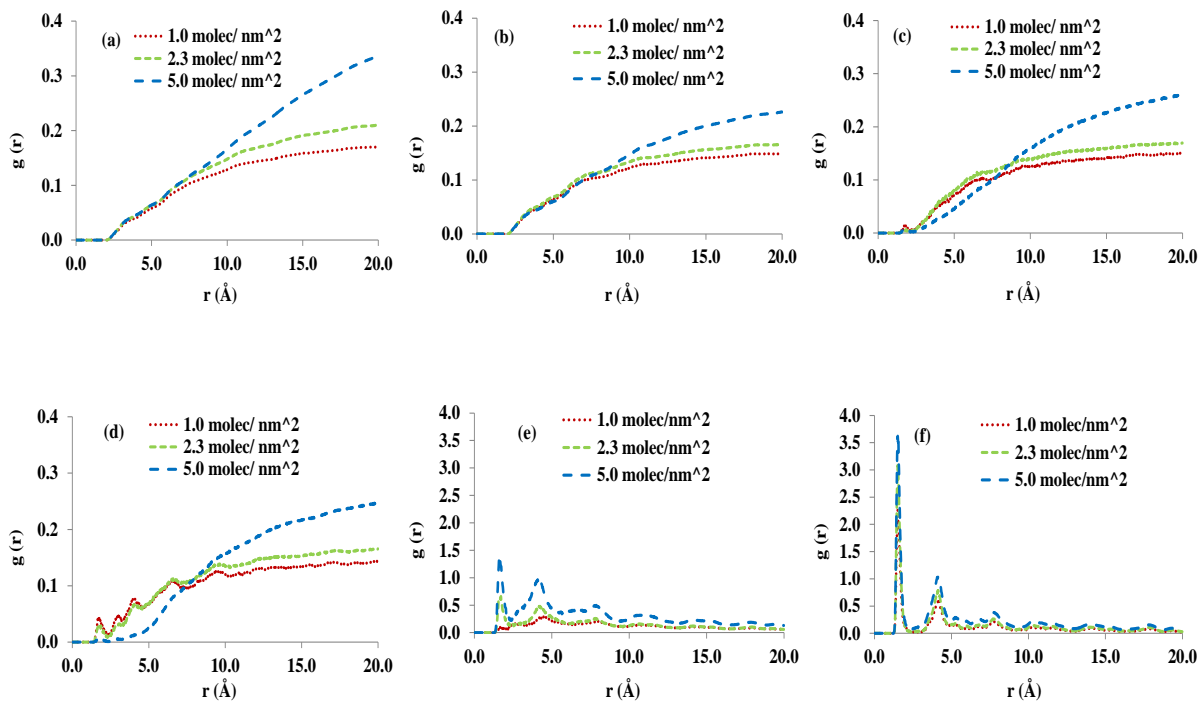
AF 4.2 H^{molec} - O^{surf} RDFs in a) cineole, b) levoglucosenone, c) cis-3-hexen-1-ol d) 2-methyl-3-buten-2-ol e) PA and f) 1-docosanol/quartz systems.

AF 4.3 O^{molec} - O^{surf} RDFs in a) cineole, b) levoglucosenone, c) cis-3-hexen-1-ol d) 2-methyl-3-buten-2-ol e) PA and f) 1-docosanol/quartz systems.
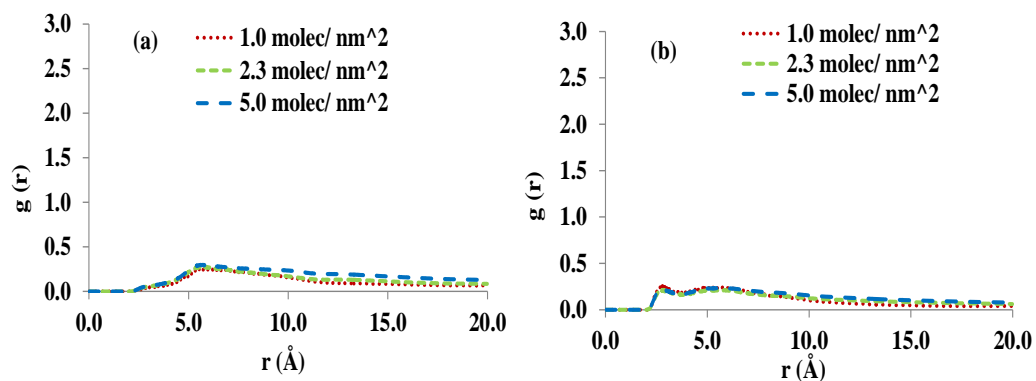
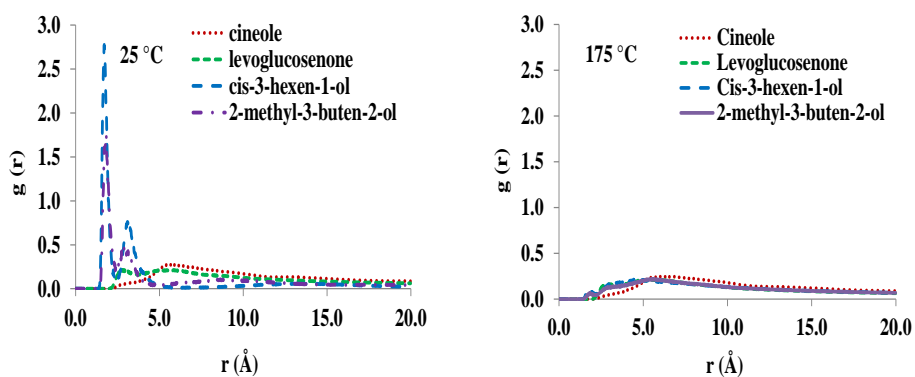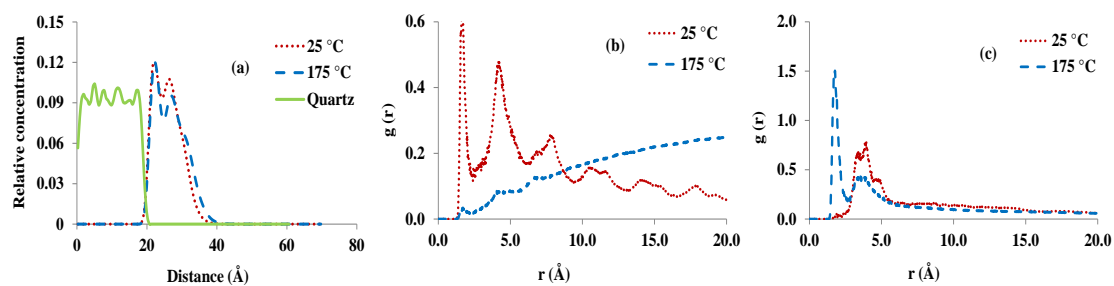AF 4.4 Radial distribution functions for O^{molec}- H^{molec} in a) cineole, b) levoglucosenone/quartz systems.
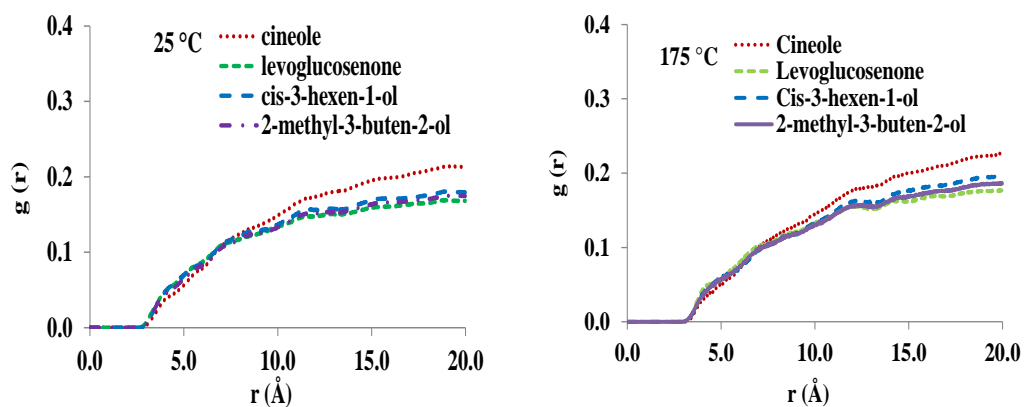
AF 4.5 C^{molec}- Si^{surf} RDFs at two different temperatures (25°C and 175°C)

AF 4.6 O^{molec}- H^{molec} RDFs at two different temperatures (25°C and 175°C)

AF 4.7 (a-c) a) Concentration profile, b) H^{molec}-O^{surf} RDF and c) H^{molec}-O^{molec} RDF of palmitic acid at two different temperatures of 25°C and 175°C

CHAPTER 5 No tables and figures

CHAPTER 6 No tables and figures

CHAPTER 7 No tables and figures